Department of Civil and Environmental Engineering

Modelling water flow and soil erosion in clayey, subsurface drained agricultural fields

Lassi Warsta

Aalto University

DOCTORAL DISSERTATIONS

Aalto University publication series
DOCTORAL DISSERTATIONS 82/2011

Modelling water flow and soil erosion in clayey, subsurface drained agricultural fields

Lassi Warsta

Doctoral dissertation for the degree of Doctor of Science in Technology to be presented with due permission of the School of Engineering for public examination and debate in Auditorium R1 at the Aalto University School of Engineering (Espoo, Finland) on the 11th of November 2011 at noon.

Aalto University
School of Engineering
Department of Civil and Environmental Engineering
Water Engineering

Supervisor
Prof. Harri Koivusalo

Instructors
Dr. Tuomo Karvonen
Dr. Antti Taskinen, Finnish Environment Institute
Prof. Emer. Pertti Vakkilainen

Preliminary examiners
Prof. Nicholas Jarvis, Swedish University of Agricultural Sciences, Sweden
Prof. Eila Turtola, MTT Agrifood Research Finland

Opponent
Prof. Jiří Šimůnek, University of California, Riverside, USA

Aalto University publication series
DOCTORAL DISSERTATIONS 82/2011

Cover photograph: © Pitopia, Peter Meurer, 2008

ISBN 978-952-60-4289-3 (pdf)
ISBN 978-952-60-4288-6 (printed)
ISSN-L 1799-4934
ISSN 1799-4942 (pdf)
ISSN 1799-4934 (printed)

Aalto Print
Helsinki 2011

Finland

The dissertation can be read at http://lib.tkk.fi/Diss/

Publication orders (printed book):
lassi@warsta.net

Author
Lassi Warsta

Name of the doctoral dissertation
Modelling water flow and soil erosion in clayey, subsurface drained agricultural fields

Publisher School of Engineering

Unit Department of Civil and Environmental Engineering

Series Aalto University publication series DOCTORAL DISSERTATIONS 82/2011

Field of research Water Resources Engineering

Manuscript submitted 16 May 2011 **Manuscript revised** 21 September 2011

Date of the defence 11 November 2011 **Language** English

☒ **Monograph** ☐ **Article dissertation (summary + original articles)**

Abstract

Soil erosion in clayey, subsurface drained agricultural fields in Finland can cause problems due to the export of suspended sediment and sediment-bound nutrients into nearby waterways. Suspended sediment is transported from the field via two main hydrological pathways: 1) surface runoff and 2) preferential flow in macropores to subsurface drains. In clayey fields especially, the sediment load via the subsurface drains can be a considerable part of the annual load. The mechanisms contributing to the sediment load during the growing season and the following autumn were quantified with a new numerical model (FLUSH) developed in the study, using sample data from two clayey, subsurface drained field sections in southern Finland.

The simulated field was computationally divided into two-dimensional overland and three-dimensional subsurface domains. Existing mechanistic approaches were applied to describe both surface and subsurface domain processes in the model. A dual-permeability model can simultaneously simulate flow in both soil matrix and macropore systems. The model supports simulation of suspended sediment transport in macropores, drainage systems, soil swelling and shrinkage processes and the effects of cropping and tillage operations on water and sediment yields. A new pentadiagonal matrix algorithm-based solution was developed to directly solve subsurface flow in both pore systems. A custom time integration method was derived to run the solution algorithms with different time steps in concurrent fashion. All the finite volume-based partial differential equation solution algorithms were parallelised with the OpenMP application interface. Computational grids, created with an automatic grid generation system, were used to test the effects of grid resolution on results.

The numerical model successfully described water flow and soil erosion in the study fields indicating that the hypothesised mechanisms for water flow and soil erosion were appropriate. The simulation results confirmed that preferential flow has a profound impact on field-scale hydrology. Runoff distribution between surface runoff and drainflow changed in the autumn due to tillage operations and soil swelling. Soil erosivity also increased after autumn tillage. In the simulations, hydraulic erosion was the primary process leading to high erosion rates in the Sjökulla field. In the Hovi field, lack of surface runoff notably lowered the sediment loads. Simulations with 1-D and 2-D grids indicated that the application of a 3-D model to undulating, clayey, subsurface drained fields was well justified. Tests with spatial variation of macroporosity presented evidence that the spatial variability of soil properties has a notable effect on runoff and sediment loads.

Keywords agricultural field, clay, drainage, erosion, overland flow, prefrential flow, dual-permeability model, soil shrinkage and swelling,e 3-D model, OpenMP, FLUSH

ISBN (printed) 978-952-60-4288-6 **ISBN (pdf)** 978-952-60-4289-3

ISSN-L 1799-4934 **ISSN (printed)** 1799-4934 **ISSN (pdf)** 1799-4942

Location of publisher Espoo **Location of printing** Helsinki **Year** 2011

Pages 209 **The dissertation can be read at** http://lib.tkk.fi/Diss/

A? Aalto-yliopisto

Tiivistelmä

Aalto-yliopisto, PL 11000, 00076 Aalto www.aalto.fi

Tekijä
Lassi Warsta

Väitöskirjan nimi
Veden virtauksen ja eroosion mallintaminen salaojitetuilla savipelloilla

Julkaisija Insinööritieteiden korkeakoulu

Yksikkö Yhdyskunta- ja ympäristötekniikan laitos

Sarja Aalto University publication series DOCTORAL DISSERTATIONS 82/2011

Tutkimusala Tekninen vesitalous

Käsikirjoituksen pvm 16.05.2011 **Korjatun käsikirjoituksen pvm** 21.09.2011

Väitöspäivä 11.11.2011 **Kieli** Englanti

☒ **Monografia** ☐ **Yhdistelmäväitöskirja (yhteenveto-osa + erillisartikkelit)**

Tiivistelmä

Salaojitetuilla savipelloilla tapahtuva eroosio voi aiheuttaa ongelmia vesistöissä pellolta kulkeutuvan kiintoaineen ja kiintoaineeseen sitoutuneiden ravinteiden takia. Kiintoaine kulkeutuu pelloilta pääasiassa pinta- ja salaojavalunnan mukana. Salaojiin kiintoaine kulkeutuu pellon muokkauskerroksesta makrohuokoskäytäviä pitkin. Etenkin savipelloilla salaojien kautta kulkeutuva kiintoainekuorma saattaa olla merkittävä osa vuotuisesta kokonaiskuormasta. Valuntaan ja kiintoainekuormaan vaikuttavia mekanismeja tutkittiin työssä kehitetyllä numeerisella laskentamallilla (FLUSH). Mallinnuksessa käytettiin apuna mittaustuloksia kahdelta suomalaiselta salaojitetulta savipellolta.

Simuloitava pelto jaetaan laskentamallissa kaksiulotteiseen pintaosaan ja kolmiulotteiseen maaperäosaan. Olemassa olevia teoreettisia menetelmiä käytettiin kuvaamaan virtaus- ja eroosioprosesseja pinta- ja maaperäosissa. Monihuokosmalli kuvaa virtausta erikseen maamatriisissa ja makrohuokosissa. Mallilla on myös mahdollista simuloida kiintoaineen kulkeutumista maan pinnalla ja makrohuokosten kautta salaojiin, samoin kuin saven kutistumista ja paisumista sekä viljelyn aiheuttamia muutoksia pellolla. Työssä kehitettiin uusi pentadiagonaaliseen matriisialgoritmiin perustuva menetelmä, jolla voidaan ratkaista suoraan maa- ja pohjavesivirtaus kahdessa huokossysteemissä. Kehitetty aikaintegrointimenetelmä maksimoi laskenta-algoritmien rinnakkaisen toiminnan. Kaikki osittaisdifferentiaaliyhtälöiden numeeriset ratkaisut on toteutettu kontrollitilavuusmentelmällä ja ne on hajautettu OpenMP ohjelmistorajapinnan avulla. Laskentaverkot luodaan järjestelmässä automaattisesti mikä helpottaa resoluution vaikutuksen arvioimista laskentatuloksissa.

Onnistuneet valunta- ja kiintoainesimulaatiot tutkimusalueilla vahvistavat käsitystä että malli sisältää tarvittavat veden virtausta ja eroosiota kuvaavat prosessit. Tuloksien mukaan oikovirtauksella oli suuri merkitys peltomittakaavan vesitaseeseen. Valunnan jakautuminen pinta- ja salaojavalunnan välille muuttui ja maan eroosioherkkyys kasvoi syksyllä kynnön jälkeen. Pintavirtailun aiheuttama hydraulinen eroosio oli tärkein syy suuriin kiintoainekuormiin Sjökullan pellolla. Pintavirtailun puute Hovin pellolla taas pienensi kiintoainekuormaa merkittävästi. Simulaatiot yksi-, kaksi- ja kolmiulotteisilla laskentaverkoilla osoittivat että kolmiulotteisen mallin käyttö kumpuilevilla, salaojitetuilla savipelloilla on perusteltua. Mallitulosten mukaan alueellisesti vaihtelevalla makrohuokoisuudella oli merkittävä vaikutus valuntaan ja kiintoainekuormaan.

Avainsanat pelto, savi, salaoja, eroosio, pintavirtailu, oikovirtaus, monihuokosmalli, kutistuminen ja paisuminen, 3-D malli, OpenMP, FLUSH

ISBN (painettu) 978-952-60-4288-6 **ISBN (pdf)** 978-952-60-4289-3

ISSN-L 1799-4934 **ISSN (painettu)** 1799-4934 **ISSN (pdf)** 1799-4942

Julkaisupaikka Espoo **Painopaikka** Helsinki **Vuosi** 2011

Sivumäärä 209 **Luettavissa verkossa osoitteessa** http://lib.tkk.fi/Diss/

Contribution by the author

The dissertation is partly derived from the Licentiate's thesis of the author (Warsta 2007). This thesis was fully rewritten and no duplicate text was used between the studies. The author is fully responsible for the manuscript and the research presented in it. The implementation of the presented model was developed by the author alone. Also, all the simulation results were calculated and analysed by the author. The dissertation is purely model oriented and no additional empirical measurements were conducted during the study, i.e. all the measurement data were acquired from previous studies.

The unpublished pentadiagonal matrix algorithm based solution was developed together with Dr. Tuomo Karvonen. Dr. Tuomo Karvonen also helped with the implementation of the analytical model by Tracy (2007). Otherwise, the role of the supervisor (Prof. Harri Koivusalo) and instructors (Dr. Tuomo Karvonen, Dr. Antti Taskinen and Prof. Emer. Pertti Vakkilainen) was to comment on the model development and the manuscript. In addition, Maija Paasonen-Kivekäs and Dr. Antti Taskinen helped with the compilation of data from the Sjökulla and Hovi experimental fields, respectively.

Lassi Warsta

21.09.2011 Espoo

Preface

I would like to thank the present and former supervisors of the thesis including Prof. Harri Koivusalo, Prof. Emer. Pertti Vakkilainen and Dr. Tuomo Karvonen for their help and support with the thesis. The instructor group, comprised of Prof. Harri Koivusalo, Dr. Tuomo Karvonen, Maija Paasonen-Kivekäs, Dr. Antti Taskinen and Prof. Emer. Pertti Vakkilainen, was indispensable to the author as a source of knowledge and support. In addition, Dr. Teemu Kokkonen gave comments on the manuscript. I was honored to have Prof. Nicholas Jarvis and Prof. Eila Turtola as pre-examiners of the manuscript of the thesis. I am grateful that Prof. Jiří Šimůnek accepted the invitation to act as my opponent at the public examination. Language of the thesis was examined by language consultant Katy Simmons.

I would like to thank the following organisations for funding this dissertation: Maa- ja vesitekniikan tuki ry (MVTT), the ENARCH Doctoral Programme of Aalto University, Salaojituksen tukisäätiö (Subsurface drainage foundation), Sven Hallinin tutkimussäätiö (Sven Hallin Research Foundation), the Doctoral Programme of the Built Environment (RYM-TK) of Aalto University and the Water Engineering research group of Aalto University. I have been fortunate that the executive manager of MVTT, Timo Maasilta has been so supportive and patient with the author.

I am thankful to the group of colleagues and institutes who provided me with an access to the datasets utilised in the thesis. The Sjökulla experimental field runoff data were collected by several persons including Maija Paasonen-Kivekäs at Helsinki University of Technology (Aalto University) and the research efforts in the field were initiated by Prof. Emer. Pertti Vakkilainen. The Hovi experimental field runoff measurements were conducted by Finnish Environment Institute and provided to me by Prof. Seppo Rekolainen. Additional data from the fields were kindly shared by Prof. Laura Alakukku (University of Helsinki), Finnish Meteorological Institute, and people from the MTT Agrifood Research Finland including Dr. Visa Nuutinen, Antti Ristolainen, Liisa Pesonen and Jere Kaivosoja.

I am grateful to all my colleagues in the Water Engineering group for creating an inspiring and pleasant working atmosphere. Finally, I would like to thank Tiia, my family and friends for their stellar support and understanding.

Lassi Warsta

21.09.2011 Espoo

Table of Contents

Abbreviations

1-D	One-dimensional
2-D	Two-dimensional
3-D	Three-dimensional
ADE	Advection-dispersion equation
AGGS	Automatic grid generation system
API	Application programming interface
DEM	Digital elevation model
ET	Actual evapotranspiration
FEI	Finnish Environment Institute
FEM	Finite element method
FVM	Finite volume method
GIS	Geographic information system
LAI	Leaf area index
MTT	MTT Agrifood Research Finland
MVG	Mualem-van Genuchten water retention model
N	Nitrogen
P	Phosphorus
PDE	Partial differential equation
PDMA	Pentadiagonal matrix algorithm
PE	Potential evaporation
PET	Potential evapotranspiration
REV	Representative elementary volume
PSDC	Particle size distribution curve
PT	Potential transpiration
SCS	Soil Conservation Service
SSCC	Soil shrinkage characteristic curve
TDMA	Tridiagonal matrix algorithm
TSS	Total suspended solids
USDA	United States Department of Agriculture
USLE	Universal Soil Loss Equation
WRC	Water retention curve

List of Symbols

α_F	[-]	Dimensionless stress factor (Feddes et al. 1978)
α_G	[L^{-1}]	Fitting parameter in Gardners WRC (Gardner 1958)
α_K	[-]	Soil shrinkage fitting parameter (Kim et al. 1992)
α_L	[L]	Longitudinal dispersivity
α_{MVG}	[L^{-1}]	Fitting parameter (van Genuchten 1980)
α_R	[-]	Empirical coefficient used to calculate M_R
α_T	[L]	Transverse dispersivity
α_W	[L^{-1} T^{-1}]	First order water exchange coefficient
β	[-]	Geometry coefficient in α_W
β_K	[-]	Soil shrinkage fitting parameter (Kim et al. 1992)
β_R	[-]	Empirical coefficient used to calculate M_R
Γ_S	[M L^{-3} T^{-1}]	Solute exchange rate between pore systems
Γ_W	[T^{-1}]	Water exchange rate between pore systems
γ_K	[-]	Soil shrinkage fitting parameter (Kim et al. 1992)
γ_S	[M L^{-2} T^{-2}]	Specific weight of sediment in fluid
γ_W	[-]	Scaling coefficient in α_W
Δt	[T]	Time step
Δt_{MAX}	[T]	Global time step
δ	[-]	Transport capacity equation parameter (Yalin 1963)
ε	[L^3 L^{-3}]	Soil porosity
ζ	[-]	Subsurface advective transport parameter
η	[-]	Simulation time step level
θ	[L^3 L^{-3}]	Volumetric water content
θ_A	[L^3 L^{-3}]	Volumetric water (Othmer et al. 1991)
θ_E	[L^3 L^{-3}]	Equilibrium water content (Ross and Smettem 2000)
θ_R	[L^3 L^{-3}]	Residual volumetric water content
θ_S	[L^3 L^{-3}]	Saturated volumetric water content
ϑ	[L^3 L^{-3}]	Soil moisture ratio
ϑ_A	[L^3 L^{-3}]	Soil moisture ratio threshold (Chertkov 2000, 2003)
ϑ_B	[L^3 L^{-3}]	Soil moisture ratio threshold (Chertkov 2000, 2003)
ϑ_L	[L^3 L^{-3}]	Soil moisture ratio threshold (Chertkov 2000, 2003)
ϑ_S	[L^3 L^{-3}]	Soil moisture ratio at the saturation point
ι	[T]	Equilibrium time constant (Ross and Smettem 2000)
κ	[-]	Exponent for the potential hydraulic erosion term
λ	[L^{-1}]	Fitting parameter (Mohanty et al 1997)
μ	[M T^{-1} L^{-1}]	Dynamic viscosity
Ξ	[-]	Parameter of the abscissa of Shields curve
Ω_D	[L]	Ditch entrance resistance
Ω_S	[L]	Subsurface drain entrance resistance
ρ_S	[M L^{-3}]	Sediment particle density
ρ_W	[M L^{-3}]	Density of water
ς	[-]	Parameter in the numerical solution of overland flow
σ	[L^3 L^{-3}]	Intercept of SSCC (Chertkov 2000, 2003)
τ	[M T^{-2} L^{-1}]	Shear stress
τ_C	[M T^{-2} L^{-1}]	Critical shear stress
υ	[L^2 T^{-1}]	Kinematic viscosity
φ	[-]	An empirical constant (Childs 1969)
χ	[-]	Local time step level of numerical submodel
ψ	[-]	Constant value used in the calculation of Y_{CR}
ω	[-]	Parameter of shrinkage curve (Chertkov 2000, 2003)
A	[L^2]	Area of overland cell or area of subsurface cell face
A_D	[L^2]	Ditch surface area against subsurface flow flux
A_S	[L^2]	Surface area of the subsurface drain
a_Y	[-]	Transport capacity equation parameter (Yalin 1963)
b	[L T^{-1}]	Conductance parameter (Beven and German 1985)
C	[M L^{-3}]	Sediment concentration in the overland water

C_C	[-]	Proportion of soil covered by canopy cover
C_G	[-]	Proportion of soil covered by ground cover
C_K	[L T^{-1}]	Kinematic wave velocity (Beven and German 1985)
C_W	[L^{-1}]	Differential water capacity
c	[M L^{-3}]	Sediment concentration in soil
D	[L^2 T^{-1}]	Dispersion coefficient
D^*	[L^2 T^{-1}]	Effective molecular diffusion
D_R	[m]	Median raindrop diameter (empirical equation)
D_S	[L]	Mean sediment particle diameter
D_W	[L T^{-1}]	Effective water diffusivity (Larsbo and Jarvis 2003)
d	[L]	Radius or half width of the matrix structure
d_A	[L]	Aggregate radii of pore systems (Othmer et al. 1992)
d_R	[L]	Half dimension of rock block (Duguid and Lee 1977)
d_S	[L]	Half dimension of soil block (Duguid and Lee 1977)
d_W	[L]	Crack width (Childs 1969)
E_{NS}	[-]	Nash-Sutcliffe model efficiency coefficient
e	[L^3 L^{-3}]	Soil void ratio
e_R	[L^3 L^{-3}]	Soil void ratio at the residual moisture point
e_S	[L^3 L^{-3}]	Soil void ratio at the saturation moisture point
F	[varies]	Generic flux between cells
F_W	[-]	Overland water depth correction factor
f_R	[-]	Empirical root distribution parameter
g	[L T^{-2}]	Acceleration due to gravity
g_H	[M L^{-2} T^{-1}]	Potential hydraulic erosion rate
g_R	[M L^{-2} T^{-1}]	Potential rain drop splash erosion rate
H	[L]	Hydraulic head
H_D	[L]	Hydraulic head in the ditch
H_S	[L]	Hydraulic head in the subsurface drain
h	[L]	Pressure head
h^*	[L]	Critical pressure head (Mohanty et al. 1997)
h_A	[L]	Pressure head in the matrix-macropore interface
h_D	[L]	Pressure head in the ditch
h_S	[L]	Pressure head in the subsurface drain
h_W	[L]	Effective overland water depth
$h_{W,THR}$	[L]	Overland flow threshold water depth
$h_{W,TOT}$	[L]	Total overland flow depth
I	[mm h^{-1}]	Rainfall intensity (empirical equation)
i	[-]	Horizontal cell index or pore system index
j	[-]	Horizontal cell index or pore system index
K	[L T^{-1}]	Unsaturated hydraulic conductivity
K^*	[L T^{-1}]	Critical hydraulic conductivity (Mohanty et al. 1997)
K_A	[L T^{-1}]	Hydraulic conductivity in the matrix-macropore interface
$K_{FS,MUL}$	[L T^{-1}]	Macropore saturated hydraulic conductivity multiplier
K_R	[L T^{-1}]	Relative hydraulic conductivity
K_S	[L T^{-1}]	Saturated hydraulic conductivity
k	[-]	Vertical cell index
k_H	[M L^{-2} T^{-1}]	Overland flow erodibility coefficient
k_R	[M^{-1} L^{-2}T^2]	Raindrop splash soil erodibility coefficient
L	[L]	Distance between subsurface cells or width of overland cell
L_S	[L]	Subsurface drain length
l	[-]	Kinematic wave exponent (Beven and German 1985)
l_{MVG}	[-]	Fitting parameter (van Genuchten 1980)
M_R	[M^2 T^{-3}]	Momentum squared for rain
m_{MVG}	[-]	Fitting parameter (van Genuchten 1980)
n	[-]	The Manning coefficient
n_I	[-]	Number of cells in a column in a computational grid
n_{MVG}	[-]	Fitting parameter (van Genuchten 1980)
Q	[L^2 T^{-1}]	Overland unit flow rate
Q_D	[L^3 T^{-1}]	Overland volumetric flux to ditch
Q_O	[L^3 T^{-1}]	Observed discharge

Q_S	[L^3 T^{-1}]	Simulated discharge
q	[L T^{-1}]	Soil fluid flux density
q_D	[L^3 T^{-1}]	Subsurface volumetric flux to ditch
q_{ET}	[L^3 T^{-1}]	Subsurface volumetric ET flux
q_{GW}	[L^3 T^{-1}]	Subsurface volumetric groundwater flux
q_I	[L^3 T^{-1}]	Subsurface volumetric infiltration flux
q_S	[L^3 T^{-1}]	Subsurface volumetric drain flux
R	[-]	Root distribution
Re	[-]	Reynolds number
R_S	[L]	Subsurface drain radius
r	[T^{-1}]	Macropore sorbance (Beven and German 1985)
r_S	[-]	Geometry factor for soil shrinkage and swelling
S	[T^{-1}]	Root uptake function (Feddes et al. 1978)
S_E	[L^3 L^{-3}]	Relative water content
S_G	[-]	Sediment specific gravity
S_O	[-]	Slope of the overland water surface
S_{OA}	[-]	Average slope of the overland water surface
S_S	[M L^{-3} T^{-1}]	Subsurface sediment source/sink term
S_W	[T^{-1}]	Subsurface water source/sink term
s_S	[M L^{-2} T^{-1}]	Overland sediment source/sink term
s_W	[L T^{-1}]	Overland water source/sink term
T	[-]	Number of time steps in the statistical tests
T_C	[M L^{-3}]	Sediment transport capacity of overland flow
T_M	[L T^{-1}]	Potential transpiration rate
t	[T]	Time
U	[L T^{-1}]	Overland flow velocity
U_R	[L T^{-1}]	Overland resultant flow velocity
U_S	[L T^{-1}]	Particle settling velocity
U_{SH}	[L T^{-1}]	Overland shear velocity
V	[L^3]	Subsurface cell volume
V_1	[L^3]	Soil layer volume before shrinkage (Bronswijk 1988)
V_2	[L^3]	Soil layer volume after shrinkage (Bronswijk 1988)
V_{CR}	[L^3]	Crack volume (Bronswijk 1988)
V_{DY}	[L^3 L^{-3}]	Dynamic crack volume fraction
V_M	[L^3 L^{-3}]	Soil matrix volume fraction
V_P	[L^3 L^{-3}]	Soil pore volume fraction
V_{SH}	[L^3 L^{-3}]	Volume fraction of overall matrix shrinkage
V_{SOL}	[L^3]	Volume of the solids
V_{ST}	[L^3 L^{-3}]	Volume fraction of static macropores
V_{SU}	[L^3 L^{-3}]	Volume fraction of subsidence shrinkage
V_V	[L^3]	Volume of voids
V_W	[L^3]	Volume of water
v	[L T^{-1}]	Subsurface flow velocity
w	[L^3 L^{-3}]	Relative volumetric proportion of the macropore system
w_S	[-]	Particle settling coefficient
x	[L]	Coordinate of the horizontal position
Y	[-]	Transport capacity equation parameter (Yalin 1963)
Y_{CR}	[-]	Ordinate of Shields diagram
y	[L]	Coordinate of the horizontal position
z	[L]	Coordinate of the vertical position
z_{CR}	[L]	Layer elevation (Bronswijk 1988)
z_L	[L]	Layer depth in saturated state (Bronswijk 1988)
z_R	[L]	Depth of the root zone
z_S	[L]	Soil surface elevation

There are variations of the above symbols with the letters *F*, *M*, *X*, *Y* and *Z* attached in the text. The *F* and *M* represent local variables of the same type in the soil macropore and matrix systems, respectively. *X*, *Y* and *Z* stand for directional components of the variables.

List of Figures

List of Tables

1. Introduction

Soil erosion is defined as loosening, dissolving and removal of earth or rock materials from any part of the surface (e.g. Aksoy and Kavvas 2005). Foster and Mayer (1972) describe erosion as a process of detachment and transport of soil materials by wind, rainfall, runoff and ice. In recent centuries, human population has increased exponentially, placing most of the suitable land under intensive cultivation and exposing the underlying top soil to the erosive forces of the elements. The problems caused by erosion vary geographically, and range from loss of available top soil for agriculture to sedimentation and eutrophication of waterways. Several different factors have an impact on erosion risk including climate, type of soil, topography, erosion prevention methods and crop types (Morgan 2005). The problem associated with soil erosion in northern Europe is usually not the actual soil loss itself, but the adverse effects of adsorbed nutrients, heavy metals and pesticides in surface waters (Kirkby 2006).

1.1 Background

In Finland, agriculture is concentrated in the southern and western parts of the country due to milder weather and more cultivable soils. In this region, clay soils are common in agricultural fields (e.g. Soinne 2002, Alakukku et al. 2010a). Although erosion occurs during peak runoff events in Finland, soil loss itself is not regionally a serious problem. Sediment loads vary between 0.03–3.3 t ha^{-1} a^{-1} in agricultural catchments while being considerably lower (0.02–0.2 t ha^{-1} a^{-1}) in forested catchments (Maasilta et al. 1980, Tattari and Rekolainen 2006). In clayey soils, most of the phosphorus (P) lost with surface runoff is adsorbed on sediment particles (Turtola and Paajanen 1995, Øygarden 1997, Uusitalo et al. 2001, 2007, Paasonen-Kivekäs et al. 2008). Of nitrogen (N) compounds, nitrate (NO_3^-) is water soluble while ammonium ions (NH_4^+) are adsorbed partly on soil particles. P load from agriculture is estimated to be 62% and N load 51% of the total human induced load to water courses (Nyroos et al. 2006).

About 90% of these losses are assumed to originate from field cultivation. Total annual load of N from arable land varies between 8 and 20 kg ha^{-1} a^{-1} and the total annual P load is between 0.9 and 1.8 kg ha^{-1} a^{-1} (Vuorenmaa 2002). P is considered to be the main cause of eutrophication in Finnish inland water bodies (e.g. Rekolainen et al. 2006).

Subsurface drains were installed in Finnish fields at the beginning of the 1920s to accelerate drainage and to facilitate crop cultivation on larger continuous fields (Aarrevaara 1993). Nowadays, 75 % of arable lands are subsurface drained in the southern and southwestern parts of the country (Finnish Field Drainage Association 2011). Several studies in Finland (e.g. Uusitalo et al. 2001, Turtola et al. 2007, Paasonen-Kivekäs et al. 2008, Vakkilainen et al. 2010) and in other Nordic countries (e.g. Ulén 1995, Øygarden et al. 1997, Laubel et al. 1999) on fine-textured soils suggest that considerable amounts of eroded soil can be transported from the fields via subsurface drains. According to future climate change scenarios, total particulate P losses will decrease in agricultural lands in Finland (Kallio et al. 1997, Puustinen et al. 2010). However, Vakkilainen et al. (2010) have reported that lack of frost, snow and vegetation during warm winters increases erosion and sediment load via subsurface drains. Initially, the sediment leaching via drains was attributed to deficient drainage workmanship and internal erosion in macropores (e.g. Øygarden et al. 1997). Cesium-137 measurements on clayey fields (Laubel et al. 1999, Uusitalo et al. 2001) indicate that most of the soil material transported through subsurface drains originates from the soil surface layer. In low permeable soils, suspended particles are assumed to move with preferential flow via macropores (McKay et al. 1993, Jacobsen et al. 1997, Øygarden et al. 1997) and drain trench backfill material down to the drain lines.

The Finnish Environment Institute (FEI) has prepared Water Protection Outlines for the Finnish Council of States up to the year 2015 (Finland's Environmental Administration 2007). According to this study, the current means, which include legislative, economic and educational measures, have not had the desired effect on the reduction of nutrient loads from agricultural fields (Aakkula et al. 2010, Väisänen and Puustinen 2010). Eutrophication is still the main concern of surface water protection. Farming subsidies should be directed to efficient protection measures in problem areas with the highest load potentials. The impact of conservation methods on loads are difficult to predict, as they have to be practised for several years before their effectiveness can be evaluated (e.g. Nyroos et al. 2006). The actual implementation of protective measures can be costly because some conservation methods, e.g. buffer zones and wetlands require extensive construction projects and reserve land from cultivation.

1.2 Research problem

In order to assess nutrient loads from clayey, subsurface drained agricultural fields, both water flow and soil erosion regimes have to be understood. Because N compounds are for the most part water soluble, transport of N depends on water movement in the field. P compounds, on the other hand, are partly in soluble and partly in adsorbed forms. Additional P is released from the adsorbed state as the concentration in the soil solution decreases. Thus, P load from fields depends on both flow and erosion processes. Two pathways were identified earlier for the sediment load: 1) surface runoff and 2) subsurface drains. Unfortunately, only limited tools are available to investigate the mechanisms of soil erosion and sediment loss via surface runoff and especially via subsurface drainflow. Thus, identification of risk areas and development of efficient conservation strategies remains difficult.

Runoff in clayey, subsurface drained agricultural fields is generated via three main pathways 1) surface runoff, 2) drainflow and 3) groundwater flow. In clayey fields surface runoff is generated either by Hortonian (Horton 1933) or Dunne type mechanisms (Dunne 1978). Hortonian surface runoff is triggered by the limited infiltration capacity of soils during precipitation events, while Dunne type mechanism is activated when the shallow groundwater table rises to the surface of the field and completely saturates the soil. Overland runoff is then initiated either by precipitation or soil water exfiltration. Subsurface drainflow is generated when the groundwater level rises above the drain level. Groundwater flow is governed by the pressure difference between the surrounding open ditch and water in the soil. It is also possible that in the underlying soil or rock there are permeable layers that conduct water away from the field as deep groundwater flow. Distribution of runoff between the three main components is difficult to predict due to the complex nature of clayey soils.

Clay particles are the most chemically and physically active soil fraction due to their high specific surface area and mineral composition (Hillel 1998). A leaf-like form is typical for clay minerals and they form slate-type structures when stacked together (Hillel 1998). Thinning of water film around clay soil particles increases aggregate formation and leads eventually to crack formation due to volume decrease of the clay soil matrix (e.g. Bronswijk 1991). The opposite, i.e. thickening of water film between clay particles, induces swelling of the matrix. Clay soil can lose structural integrity and liquefy under moist conditions, increasing susceptibility to erosion. The non-linear volumetric change can be measured in laboratory and represented as a soil shrinkage characteristic curve (SSCC). Three or

four different shrinkage stages can usually be identified including 1) structural shrinkage (not always present), 2) proportional shrinkage (or normal shrinkage), 3) residual shrinkage and 4) zero shrinkage (e.g. Bronswijk 1988, Peng and Horn 2005). Shrinkage cracks act as storage for water and pathways for preferential flow and solute transport. During dry seasons, cracks can reach to considerable depths; e.g. Alakukku (1996a, b) and Alakukku et al. (2010a) observed crack depths of at least 0.6–0.7 m in Finnish clayey fields. Because clay soil matrix conducts water poorly, cracking and swelling can markedly influence hydraulic conductivity of soil (Messing and Jarvis 1990). The most common clay minerals in Finnish clayey soils are mica, chlorite, vermiculite and some smectite (Sippola 1974). The shrinkage and swelling properties of Finnish clay soils are conservative (Rasa et al. 2009) compared to those of some other clay minerals, e.g. halloysite, montmorillonite and kaolinite (Hillel 1998).

Due to the low conductivity of the clay soil matrix, water percolation through the unsaturated soil layers to the groundwater table occurs in preferential flow paths including earthworm tunnels, plant root conduits, shrinkage cracks and drain trench backfill material (e.g. Bouma et al. 1977, Bouma and Dekker 1978, Bouma and Wösten 1979, Germann and Beven 1981a, Beven and Germann 1982, Booltink and Bouma 1991, Bronswijk et al. 1995, Nuutinen and Butt 2003, Alakukku et al. 2010a). Horizontal preferential flow can occur in the tillage layer above the compressed tillage pan (e.g. Beven and Germann 1982, Shipitalo et al. 2004). In preferential flow, water moves faster in certain parts of the soil profile resulting in an uneven wetting front. An important characteristic of preferential flow is the non-equilibrium nature of the flow. Water moving in the macropores does not have time to equilibrate with the slow moving water in the bulk of the soil matrix (Šimůnek et al. 2003).

Most of the annual sediment load in Finland is caused by spring snow melt and autumn rains. Soil erosion is mainly caused by 1) hydraulic shear forces of the overland flow acting on the particles on the field surface and by 2) impacts of rain drops. Flow erosion can be further partitioned into rill and interrill components. Another mechanism proposed by Aura et al. (2006) for clay soils is diffusion erosion that also occurs in standing water. Due to electrostatic and van der Waals' forces between individual clay particles, erodibility of clayey soil can be lower than expected from the particle size distribution (e.g. Soinne 2002, Klepsch et al. 2005). Cohesive soils are eroded in larger aggregates rather than in elementary particles (Meyer et al. 1980) and mechanistic approaches devised for larger particles may not function properly. However, there are no widely accepted alternative theories for describing clay soil erosion (Taskinen and Bruen

2007b). According to Laubel et al. (1999) and Uusitalo et al. (2001), most of the soil material in the drain water originates from the field surface. Suspended sediment is transported by preferential flow in soil macropores to subsurface drains (McKay et al. 1993 and Jacobsen et al. 1997). A certain amount of filtering may occur in the macropores (Turtola and Paajanen 1995, Jacobsen et al. 1997, Turtola et al. 2007). However, Turtola and Paajanen (1995), Uusitalo et al. (2001) and Paasonen-Kivekäs et al. (2008) found out that the sediment concentration in subsurface drainflow was approximately the same as in surface runoff.

Crop cultivation has a profound effect on both hydrology and erosion in agricultural fields. In Finland, almost half of the annual precipitation is used by crops through transpiration (Vakkilainen 1982). Crops decrease overland flow velocity by increasing surface roughness and increase infiltration rate by introducing additional macropores into the soil. The roots of typical crop species grown in Finland including, e.g. spring wheat, winter wheat and winter rye can reach down to depths of 0.75, 1.0 and 0.75 m, respectively (e.g. Linnér et al. 2006). Heavy machinery used in crop sowing, harvesting and tillage operations in the fields affects both water movement and soil erosion. Vakkilainen (1980), Aura (1983) and Alakukku (1996a, b) reported that compaction by heavy machines had long-term negative effects on macroporosity and hydraulic conductivity of soil. According to Alakukku (1996a, b), macropores are more sensitive to compaction in mineral soils than in organic soils. The effects of tillage on hydraulic conductivity and macroporosity of the profile are somewhat mixed. Results by Beven and Germann (1982), Ulén (1997), Kladivko (2001), Koskiaho et al. (2002) and Puustinen et al. (2005) indicated that conventional tillage can decrease conductivity of the soil profile. However, recent studies have presented evidence that conservation tilled fine-textured soils have lower hydraulic conductivity and infiltration rates compared to conventional tillage (Turtola et al. 2007). The variability of tillage effects on soil structure can be associated with differences in soil surface sealing, temporary water storage capacity and flow-active macropores made by fauna (Turtola et al. 2007).

The topography of the field can also have a large impact on the erosivity of the overland flow. In undulating fields, overland flow tends to converge into rills increasing erosivity of the flow compared to uniform, shallow, sheet-like flow (Morgan 2005). While overland flow and erosion are essentially two-dimensional (2-D) processes, subsurface flow and transport occur in three spatial dimensions (3-D). In contrast to the tillage layer flow, preferential flow via shrinkage cracks and biopores down to subsurface drains is essentially vertically one-dimensional (1-D). The funnelling type of

preferential flow in the soil layer over the compressed tillage pan is 2-D (Shipitalo et al. 2004). Description of the temporal dimension provides additional challenges. Overland flow and erosion, preferential flow and particle transport in macropores, and slow seepage in the clay soil matrix all occur in different time scales. Regardless of the differences between the time scales, the processes interact and are dependent on each other.

1.3 Research objectives, scope of the research and hypotheses

Simulation of water balance in clayey, subsurface drained agricultural fields is challenging due to preferential flow in macropores and the dynamic nature of the macropores themselves. The efforts of this study are concentrated on: 1) water balance and 2) soil erosion in clayey, subsurface drained fields. The first objective is to study and quantify specific hydrological processes including preferential flow, soil shrinkage and swelling and drainage systems. Also, the effect of spatial variation of topography and soil properties on the water balance is studied.

The second objective is to investigate the suitability of existing theoretical erosion models to describe and quantify transport of solids in clayey soils. The role of hydrology in the distribution of sediment load between surface runoff and drainflow is of special interest in this study. The transport of sediment to subsurface drains has been previously studied mainly by measuring sediment concentrations in the drainage waters. However, theoretical and quantitative analyses of the mechanisms responsible for the transport of sediment from the field surface to the drains are scarce. The effect of crop cultivation on hydrological and soil erosion processes is also included, albeit with a pragmatic approach. Different processes in the field are not investigated separately but are combined into a single holistic model of an agricultural field. The model describes the effects of different processes and interactions between them in field-scale rather than in plot or point scale. By basing the model on physical principles instead of empirical dependencies derived from data, the system can be applied to different problem areas with minimal modifications. The model is intended as a solid foundation for nutrient models.

Due to the complexity of nature, the scope of the study is narrowed in several places. While the nutrient loads are the main motivation to conduct the study, the study itself focuses only on the carrier media and processes associated with them, i.e. water flow and soil erosion. The lack of heat related processes in the model restricts the application of the model to periods when the temperature stays above 0.0 °C, i.e. soil freezing and thawing and snow processes are not included in the model. Transport of

gaseous substances is not considered either. It is thought that air can always escape from soil or re-enter when water pressure increases above or decreases below air entry point. Only a simplified description of evapotranspiration (ET) is adopted here. Potential evapotranspiration (PET) is approximated with the Penman-Monteith approach (Monteith 1981) and the Class-A evaporation pan results (Vakkilainen 1982).

The following formal hypotheses were formulated to condense the main directions of the research:

1. Preferential flow via macropores has a major impact on runoff dynamics and water balance in clayey, subsurface drained agricultural fields.
2. Mechanisms of preferential flow can be represented, and the related mass fluxes can be quantified using computational methods presented in the literature.
3. The sediment load via subsurface drains in the studied clayey fields can be simulated when the sediment load is assumed to originate from the tillage layer of the fields.
4. A distributed problem domain, including separate 2-D overland and 3-D subsurface domains with different process descriptions, is required for a holistic simulation of water flow and soil erosion in undulating, clayey, subsurface drained agricultural fields.

While there is empirical evidence available that supports hypotheses 1 and 3 (e.g. Uusitalo et al. 2001, Turtola et al. 2007, Paasonen-Kivekäs et al. 2008, Vakkilainen et al. 2010), no previous mechanistic models were found that could be used to describe the relevant processes at field-scale when both topography and soil properties vary. This implies that the process descriptions are not well known warranting further research. In erosion models, there seems to be a complete void regarding models that can simulate sediment transport in macropores to the subsurface drains. A model that is able to simulate these phenomena is presented in this thesis.

1.4 Research methods

Computational modelling is the primary tool used to investigate and quantify the problems outlined above. Simulation is a powerful tool to study complex systems with several interacting processes. A model contains a logical hypothesis for a phenomenon and cause and effect relationships that can be difficult to decipher from empirical data. The disadvantages are that models still need data for calibration and validation and the problems are

usually complex, excluding the possibility of simple direct answers. Hillel (1998) argued that the current holistic approach in environmental modelling calls for increasingly complex models, and when the complexity increases the models may become less comprehensible and harder to test. Zheng and Bennet (2002), on the other hand, defended the use of advanced models because the most important use of simulation models is not predictive calculation, but the investigative process itself. The authors noted that only simulation models provide a quantitative framework for integrating the expertise from a myriad of different fields together, which facilitates assessing whether data from the studied environmental system and the corresponding process descriptions support each other.

The approach to environmental modelling presented by Refsgaard and Henriksen (2004) has been adopted here. A model is divided into conceptual, numerical and computational parts. The conceptual model prescribes the characteristics and interactions of the processes constituting the system as well as the general mathematical equations describing each process. The numerical model encompasses numerical solutions to the mathematical representations. The computational model is the numerical model applied to a specific case study with data. Environmental models are inherently open because the systems contain many uncertainties and their true behavior cannot be fully confirmed (Refsgaard and Henriksen 2004). The new philosophy for modelling environmental systems rejects the idea that only one optimal model may be found for a given case, because universal verification and validation of the model in all temporal and spatial scales is impossible (Refsgaard and Henriksen 2004). Instead, models should be validated against data which is independent of the calibration data and model predictions should be associated with uncertainty assessments that take into account the uncertainty of the model structure and parameters (Beven and Binley 1992).

According to the problem definition, both processes in the field surface and below the surface have to be represented, including overland flow and erosion and subsurface flow and transport. Simulation of preferential flow and transport and soil shrinkage and swelling processes are also required. Several earlier studies demonstrate that models lacking preferential flow and transport processes are not well-suited for describing flow and solute transport in structured soils (e.g. Koivusalo et al. 1999, Vogel et al. 2000, Šimůnek et al. 2003, Gerke and Köhne 2004, Jauhiainen 2004, Gärdenäs et al. 2006, Räsänen 2009). All processes need not to be explicitly defined because some of them can readily be described with a suitable parameterisation, e.g. tillage layer flow. In addition, drainage, as well as the effect of crops and tillage operations needs to be taken into account.

Description of the Dunne type overland flow initiation mechanism requires the model to be continuous in time instead of being an event based model. Because of the inclusion of Dunne type overland flow initiation mechanism, the model must be dynamic and continuous instead of steady-state and single event-based. A literature review was conducted to assess the current state of available models (Section 2). The most important findings of these earlier studies are condensed below.

As the literature review shows, most of the recent field-scale erosion modelling in Finland has been conducted with the CREAMS model (Knisel 1980, in Finland, e.g. Kauppi 1982) or its derivatives GLEAMS (Leonard et al. 1987, in Finland, e.g. Knisel and Turtola 2000) and ICECREAM (e.g. Posch and Rekolainen 1993, Rekolainen and Posch 1993, Kallio et al. 1997, Rekolainen et al. 1999, Rankinen et al. 2001, Tattari and Bärlund 2001, Tattari et al. 2001, Bärlund et al. 2005, Yli-Halla et al. 2005, Kändler 2006, Nyholm 2006, Paasonen-Kivekäs et al. 2006, Schmieder 2008, Bärlund et al. 2009, Jaakkola 2009). A few process-based studies have also been published in Finland, e.g. Taskinen (2002) and Taskinen and Bruen (2007a, b). All the CREAMS model variants are based on empirical regression equations derived from data measured in the USA. However, Finnish soils and climate are different and this has caused problems in model applications in earlier studies (Kauppi 1982, Knisel and Turtola 2000, Tattari et al. 2001, Paasonen-Kivekäs et al. 2006). The most glaring problem with the CREAMS, GLEAMS and ICECREAM models is the lack of a proper description for subsurface drains. Only two previous conceptual erosion models were found that can simulate both overland erosion and suspended sediment transport to subsurface drains: a modified ICECREAM model by Larsson et al. (2007) and PSYCHIC by Davison et al. (2008). Approximately half of the reviewed field-scale, process-based models were event-based and thus unsuitable for the study. Some of the continuous process-based models including WEPP (USDA 1995), LISEM (De Roo et al. 1996a, b), SHESED (Wicks and Bathurst 1996, Abbot et al. 1986a, b) and the model by Sharda and Singh (1994) use integrated soil- and groundwater flow models to improve the prediction of overland flow initiation. However, there appeared to be no process-based models that have the preferential flow and transport simulation capabilities required in the current study.

A large body of research exists on preferential flow and transport phenomena and because they are an important part of the proposed system, an extensive part of the literature review (Section 2) is dedicated to the topic. The reviewed preferential flow models can be divided roughly into four groups according to how they treat the pore space in soil: 1) single pore system (e.g. Peters and Klavetter 1988, Mohanty et al. 1997, Ross and

Smettem 2000, Laine-Kaulio 2008), 2) dual-porosity (e.g. Coats and Smith 1964, Pruess et al. 1999, Šimůnek et al. 2006), 3) dual-permeability (e.g. Hoogmoed and Bouma 1980, Gerke and van Genuchten 1993a, Larsbo and Jarvis 2003, Karvonen and Paasonen-Kivekäs 2007) and 4) multi-permeability models (e.g. Steenhuis et al. 1990, Wilson et al. 1992, Gwo et al. 1995, Hendriks et al. 1999). Single pore system models simulate preferential flow and transport in one mobile pore system. Dual-porosity models divide the total pore space into mobile and immobile parts, while in dual- and multi-permeability models all the pore systems are mobile.

According to Šimůnek et al. (2003), single pore system models do not emulate true preferential flow well, while multi-permeability system approaches can be computationally demanding and difficult to parameterise (e.g. Ray et al. 1997, Schwarz et al. 2000). Dual-porosity approaches were shown to be less realistic than dual-permeability approaches by Gärdenäs et al. (2006). Dual-permeability models can be further divided into conceptual, gravity-based and Darcian approaches according to how preferential flow is simulated in the macropore system. The gravity-based approaches for preferential flow might be suitable for forest soils (e.g. Bronstert and Plate 1997) but in agricultural fields, subsurface drains create pressure-driven flow fields which have to be handled with Darcian approaches (e.g. Karvonen 1988, Aura 1995 and Köhne et al. 2006). Several authors argued in their studies that 1-D preferential flow and transport models were not robust enough to simulate subsurface flow and solute transport and recommended use of 2-D profile models or 3-D models (e.g. Bronstert and Plate 1997, Mohanty et al. 1998, Gerke and Köhne 2004, Köhne et al. 2006, Hintikka et al. 2008). However, for example Hintikka et al. (2008) lamented that there are very few 2-D and 3-D models available that support preferential flow and transport. Three 3-D soil and groundwater flow and substance transport models were found that could simulate preferential flow and transport including the HILLFLOW (Bronstert and Plate 1997), TOUGH2 (Pruess et al. 1999) and HYDRUS 3-D (e.g. Šimůnek et al. 2006) models. Preferential flow in the HILLFLOW model uses a gravity-based approach. The HYDRUS 3-D and TOUGH2 models use the dual-porosity concept.

While soil swelling and shrinkage models have been included in several earlier models, most notably in the FLOCR (Bronswijk 1988), MACRO (e.g. Larsbo and Jarvis 2003) and SWAP (e.g. Kroes et al. 2008) models, they are all restricted to 1-D simulations. Jussila (2007) presented a complex 2-D model that simulated deformation of a bentonite shell used to encase used fuel rods from nuclear reactors. Unfortunately, the scale of the model is not suitable for the larger environmental systems simulated here.

Previous studies that integrated soil shrinkage and swelling processes to a simulation model operating in three spatial dimensions were not found.

The reasoning behind the selection of numerical methods and model components is detailed below according to the presented literature review summary presented above (see the full literature review in Section 2). Even though no models were found that could be directly applied to the problem under study, it was evident from the review that a new custom model could be built based on the approaches used in earlier studies. Process-based models are usually based on partial differential equations (PDEs) representing governing flow and transport processes. Analytical solutions to PDEs are available only for special cases with simple domain geometry (e.g. Tracy 1995, 2007, 2008). General solutions applicable to any generic domain are derived with distributed numerical methods. According to the literature review, the most straightforward way is to divide the simulated field into separate 2-D overland and 3-D subsurface domains. This approach mirrors reality most accurately and the existing body of research in the two, somewhat separate, areas of research (soil erosion and subsurface flow and transport) can be applied as such.

According to the models reviewed, there are relatively established ways to simulate different flow and transport processes in the field. Description of overland flow is usually based on the Saint Venant equations (e.g. Nord and Esteves 2005) or one of their simplified forms (e.g. kinematic wave or diffuse wave approaches) (e.g. Smith and Woolhiser 1971, Smith et al. 1995, De Roo et al. 1996a, b, Taskinen and Bruen 2007a). The diffuse wave approach (e.g. by Johnson et al. 2000) takes both elevation and water depth components into account enabling water to fill up larger surface depressions. Bulk of the process-based erosion models are built around the sediment continuity equation coupled with erosion process descriptions. The most suitable theoretical model for subsurface flow and transport that includes preferential flow and transport processes seems to be the dual-permeability model (Schwarz et al. 2000, Gärdenäs et al. 2006, Köhne et al. 2006). For agricultural fields, the most popular approach to simulate subsurface flow is the Richards equation (Richards 1931). The equation supports gravity, capillary forces and pressure-driven flow in unsaturated and saturated soils. Transport of sediment in soils can be simulated with the advection-dispersion equation (ADE) (e.g. Bear 1979) by considering sediment as a solute. Finally, the SWAP model (e.g. Kroes et al. 2008) appears to have the most complete model for simulating shrinkage and swelling of clay soils.

A new simulation model is built using code and algorithms presented earlier in Karvonen (1988), Taskinen (2002) and Warsta (2005, 2007) as

guidelines. The results from the model are compared against theoretical cases and data from two subsurface drained, clayey agricultural fields in southern Finland. No new measurements were conducted in the study because there were several suitable data sets already available. A special concern is the computational burden of running simulations with this complex model. Different optimisation methods are investigated to keep the simulation times as short as possible. The objective is to use the model on desktop computers.

In addition to the hypotheses presented above, three research questions on computational modelling are formulated: 1) How can processes operating in different temporal scales be combined? 2) What is the effect of computational grid resolution on results and is it possible to achieve resolution-independent results? 3) Is it possible to accelerate the performance of the numerical model with special algorithms and hardware?

1.5 Structure of the study

The Introduction (Section 1) presents the motivation (Sections 1.1 and 1.2), the objectives and hypotheses (Section 1.3) and the outline of the proposed computational model (Section 1.4). The reasoning behind the selection of various model components (Section 1.4) is based on the Literature review (Section 2). Objective of the Literature review (Section 2) is to evaluate published models that are relevant for this study. Applied modelling studies or empirical studies are not considered in Section 2. The Model description section (Section 3) literally describes the proposed model. The presented algorithms are also theoretically tested in this section. However, to make Section 3 as clear and straightforward as possible the reasoning behind the component selection was presented already in Section 1.4. In the Model application section (Section 4), the model is tested with data from two clayey, subsurface drained agricultural fields in southern Finland. The Discussion section (Section 5) strives to analyse the results presented in Section 4 and to connect them to existing literature. Section 5 is organised around the hypotheses presented in Section 1.3. A separate Conclusions section (Section 6) lists the major findings and the thesis concludes with a brief summary section (Section 7).

2. Literature review

The literature review section provides an overview on computational methods for modelling water flow and soil erosion in clayey, subsurface drained agricultural fields. The main focus is on dynamic, 2-D and 3-D spatially distributed approaches. The studies are presented in a rough chronological order to illustrate the development of different methods. The review is divided into three parts: 1) Agrohydrological features, 2) Preferential flow and transport in soils and 3) Soil erosion. The literature about analytical models and specific numerical methods is presented alongside the numerical model in Section 3. The reasoning behind the selection of the different components in the developed model is presented in Section 1.4.

2.1 Agrohydrological features

Agrohydrological features section presents the basic elements required to model clayey, subsurface drained agricultural fields including 1) representation of water retention curves (WRC) and unsaturated hydraulic conductivity, 2) modelling soil swelling and shrinkage, 3) simulation of subsurface drains and 4) simulation of evapotranspiration.

Groundwater flow and solute transport modelling are relatively young research fields (Zheng and Bennet 2002). The fundamental law for saturated flow in porous media was derived by Darcy (1856) from sand column experiments performed in Dijon, France. Buckingham (1907 cited by Nimmo and Landa 2005) extended Darcy's law into unsaturated conditions by identifying the two main soil properties governing unsaturated flow: WRC and unsaturated hydraulic conductivity. Richards (1931) conducted experiments with unsaturated soils and discovered that unsaturated flow is driven by capillary forces. The origin of the advection-dispersion equation is more difficult to trace. Skopp and Warrick (1974) and van Genuchten and Wierenga (1976) noted that Lapidus and Amundsen (1952) had derived an analytical solution for advective and

effective diffusive transport and linear adsorption. The study of dispersion phenomenon continued intensively through the 1950s to 1970s (Bear 1979). In the 1970s, macroscopic heterogeneity of soil was identified as the primary cause for dispersion (e.g. Schwartz 1977).

2.1.1 Unsaturated hydraulic conductivity and WRC

After Buckingham (1907), several attempts were made to describe WRC and hydraulic conductivity of unsaturated soils. Mualem (1976) divided the methods into two groups. The first group is based on the assumption that relative hydraulic conductivity is a power function of effective saturation of soil and includes models, e.g. by Averjanov (1950), Irmay (1954), Brooks and Corey (1964) and Boreli and Vachaud (1966). The second group derives hydraulic conductivity in unsaturated soils from WRC and it includes models by, e.g. Childs and Collis-George (1950), Burdine (1953), Wyllie and Gardner (1958) and Farrel and Larson (1972). An early review of various models developed for predicting hydraulic conductivity in unsaturated soils was presented by Brutsaert (1967).

Andersson (1969) measured a large selection of WRCs and hydraulic conductivities of different soil types. Based on the texture of soil, an appropriate empirical representation of the curve can be selected. Mualem (1976) derived a compact general integral formula for WRC from the Childs and Collis-George (1950) model. The curve still had to be solved with numerical methods. Van Genuchten (1980) derived a closed-form equation to replace the general integral terms in Mualem's formula and thus created a simple analytical equation for WRC. Kosugi (1994, 1999) presented a closed-form formula for soils with log-normal pore size distribution. Jauhiainen (2004) developed a closed-form method for determining WRCs from particle size distribution curves (PSDC).

2.1.2 Soil swelling and shrinkage

Modelling flow of water and transport of solutes in swelling clay soils is complicated because hydraulic conductivity of soil changes according to the moisture state of the soil. The changes in hydraulic conductivity are caused by crack networks that form and disappear with soil moisture changes (e.g. Bronswijk 1991). The volume change of soil matrix as a function of soil moisture change can be represented with soil shrinkage characteristic curves (SSCC). The curves can be measured in laboratory with different methods as shown by, e.g. Lauritzen and Stewart (1941) and Berndt and Coughlan (1976). Similarly to parametric WRCs (e.g. van Genuchten 1980), several parametric SSCCs have been developed to represent void ratio of

soil as an analytical function of its moisture ratio. The void ratio e [L^3 L^{-3}] and the moisture ratio ϑ [L^3 L^{-3}] are defined as follows:

$$e = V_V V_{SOL}^{-1} \tag{1}$$

$$\vartheta = V_W V_{SOL}^{-1} \tag{2}$$

where V_V [L^3] is the volume of voids, V_{SOL} [L^3] is the volume of solids and V_W [L^3] is the volume of water. The volume changes are converted into 1-D, 2-D, or 3-D shrinkage or swelling using the geometry factor or the distribution factor for crack formation and subsidence (Bronswijk 1990). The soil shrinkage and swelling system is embedded, in turn, into a soil moisture flow model.

The soil swelling and shrinkage review section is divided into two parts: 1) Soil shrinkage characteristic curves and 2) Soil shrinkage systems in models. An earlier review of SSCCs was published by, e.g. Cornelis et al. (2006).

Soil shrinkage characteristic curves

Kim et al. (1992) derived a parametric SSCC for marine clay soils by combining linear and exponential functions. Proportional shrinkage is represented with a linear function, whereas the residual and zero shrinkage are described with an inverse of exponential function. The model does not consider structural shrinkage. The following equation was presented by the authors to represent SSCC:

$$e = \alpha_K \exp(-\beta_K \vartheta) + \gamma_K \vartheta, \qquad 0 < \vartheta < \vartheta_S \tag{3}$$

where α_K, β_K and γ_K [-] are fitting parameters and ϑ_S [L^3 L^{-3}] is the moisture ratio at the soil saturation point.

Chertkov (2000, 2003) proposed a model based on statistical analogy between crack networks (Chertkov and Ravina 1998) and the probabilistic microstructure of a matrix consisting solely of clay particles. The proportional shrinkage part was modified by Cornelis et al. (2006) for soils in general:

$$e = 2\omega(\vartheta_B - \vartheta_A)\vartheta + \sigma, \qquad \vartheta_B < \vartheta < \vartheta_L \tag{4}$$

where ω [-] is a model coefficient, ϑ_A [L^3 L^{-3}] is the moisture ratio corresponding to the end of residual shrinkage, ϑ_B [L^3 L^{-3}] is the moisture ratio at the air entry point and ϑ_L [L^3 L^{-3}] is the liquid limit point for clay soil. Parameter σ [L^3 L^{-3}] is the intercept of SSCC in the proportional zone:

$$\sigma = e_R - \omega(\vartheta_B - \vartheta_A)(\vartheta_B + \vartheta_A) \tag{5}$$

where e_R [L³ L⁻³] is the residual void ratio corresponding to moisture ratios below ϑ_A. The value of e equals ϑ above moisture ratio ϑ_B. SSCC (Eq. 4) was ranked best by Cornelis et al. (2006) in their review.

In their model, Peng and Horn (2005) took advantage of the fact that shrinkage curves have the same sigmoidal shape as WRC. SSCC was represented with an inverted Mualem-van Genuchten (MVG) WRC (Mualem 1976, van Genuchten 1980). A single equation is used to describe all the shrinkage zones including the structural shrinkage zone:

$$e = e_R + \frac{e_S - e_R}{\left[1 + \left(\frac{\alpha_{MVG}\vartheta}{e_S - \vartheta}\right)^{-n_{MVG}}\right]^{m_{MVG}}}, \qquad 0 < \vartheta < \vartheta_S \tag{6}$$

where e_S [L³ L⁻³] is the void ratio at saturation water content point and α_{MVG} [L⁻¹], n_{MVG} [-] and m_{MVG} [-] are MVG WRC parameters. The parameter α_{MVG} is related to the inverse of a characteristic pore radius and n_{MVG} to the pore size distribution (e.g. Gärdenäs et al. 2006). The Peng and Horn (2005) model raises hopes of a unified approach for representing WRC and SSCC. The WRC and SSCC pair could be further extended by including PSDC in the chain (PSDC->WRC->SSCC).

Soil shrinkage systems in models

The FLOCR model developed by Bronswijk (1988) and Oostindie and Bronswijk (1992), simulates water flow and dynamic crack formation in a 1-D soil column. The shrinkage parameters (moisture and void ratios) are presented in a table format as a function of pressure head. The volume change calculated with the shrinkage parameters is distributed with the geometry factor r_S [-] between the change of depth Δz_{CR} [L] and the change of crack volume ΔV_{CR} [L³] of the layer:

$$\Delta z_{CR} = z_L - \left[(V_2/V_1)^{1/r_S}\right] z_L \tag{7}$$

$$\Delta V_{CR} = (V_1 - V_2) - z_L^2 \Delta z_{CR} \tag{8}$$

where z_L [L] is the layer depth in saturated state and V_1 and V_2 [L³] are the volumes of the soil layers before and after shrinking or swelling.

Jarvis and Leeds-Harrison (1990) extended the model proposed by Jarvis and Leeds-Harrison (1987) and Jarvis (1989b) by adding swelling and shrinkage processes to the system. In the resulting CRACK model, the 1-D soil profile is divided into discrete layers each containing cube-shaped aggregates of equal size, separated by planar cracks. The crack porosity is calculated as a function of the bulk soil water status and the slope of SSCC. The crack width and aggregate surface area is calculated from the geometry when the crack porosity and aggregate size are known.

In the MACRO model (e.g. Larsbo and Jarvis 2003), the 1-D soil profile is treated as macroscopically rigid, i.e. the total porosity and the layer thickness are held constant. Macroporosity is calculated with a linear function of soil moisture in the matrix, i.e. SSCC is considered to be linear. Macroporosity value is used directly in the hydraulic conductivity function of the macropores.

Novák et al. (2000) extended the 1-D HYDRUS-ET model (Ŝimůnek et al. 1997) with the FRACTURE submodel. The crack porosity is calculated directly as a linear function of soil water content similar to the MACRO model. Additional parameters required are specific length of cracks per unit soil area and depth of cracks. The same assumptions are adopted about the rigidity of the soil layers as in the MACRO model.

Jussila (2007) presented a complex swelling model for bentonite clay cylinders used to encase spent fuel rods from nuclear reactors. The model features unsaturated moisture, heat and gas flows coupled to deformation of the medium.

The SWAP model (e.g. Kroes et al. 2008) includes several options regarding soil swelling and shrinkage modelling including combined simulation of dynamic macroporosity and static macroporosity. For clayey soils, the model uses the SSCC of Kim et al. (1992) and for peaty soils the model of Hendriks (2004).

2.1.3 Subsurface drains

The subsurface drain description is an integral part of models targeted at simulation of water flow in clayey fields. Different conceptual and steady-state approaches, as well as methods used in distributed systems are briefly reviewed. An extensive review on the topic was compiled earlier by Feddes (1988).

Development of steady-state equations to aid the design of parallel field drainage systems started in the first half of the 20th century. Hooghoudt (1940) presented a steady-state drainage equation for homogenous soils and soils with two distinct layers. In the latter case, the top layer is highly permeable while the bottom layer is poorly permeable. Ernst (1962) derived an equation for soils with a poorly permeable layer above a highly permeable substratum and a modified version for a case with two permeable layers below the drain level. Ernst (1975) combined the Hooghoudt (1940) and Ernst (1962) approaches into a single equation applicable to all the presented cases. van Beers (1976) has presented derivations and application examples for all three equations.

The Hooghoudt and Ernst's equations have been included in several conceptual and distributed models. The Hooghoudt equation is available,

e.g. in DRAINMOD (Skaggs 1980), WEPP (e.g. Savabi 1993), 2D-CROPWATN (Karvonen and Paasonen-Kivekäs 2007) and in models by Koivusalo et al. (1999) and Abbaspour et al. (2001). The Ernst equation is used in the FLOCR model (Bronswijk 1988, Oostindie and Bronswijk 1992, Hendriks et al. 1999). In the SWAP model (e.g. Kroes et al. 2008), the user can choose between Hooghoudt variants and Ernst equations according to the problem at hand. Subsurface drainflow in the MACRO model (e.g. Larsbo and Jarvis 2003) is calculated in two parts. Flux from the saturated layers above the drains is calculated with a seepage potential theory for layered soils (Youngs 1980, Leeds-Harrison et al. 1986). Flux to drains from below is calculated with the Hooghoudt equation. The seepage potential theory is also used in the CRACK-NP model (Armstrong et al. 2000).

In distributed models, drains are usually modelled in a more straightforward way than in steady-state approaches because the soil layers and pressure distributions are taken into account by the model. Fipps et al. (1986) tested four different methods for representing subsurface drains in a finite element-based numerical solution of the Richards equation: 1) multimode approach with model drain, 2) single node approach with specified flux, 3) the specified head approach and 4) the resistance adjustment approach. In the resistance adjustment method, the conductivity at the drains is adjusted by a factor determined from the ratio of the effective radius of the drain to the size of the elements surrounding the drain node. The problem with methods 1) and 3) is that a large amount of nodes is needed in the vicinity of the drain for realistic results, while methods 2) and 4) also worked with coarse grids. Fipps and Skaggs (1989) investigated the effect of slope and different boundary conditions on drainage of hillsides with the same model as Fipps et al. (1986). Small slopes (< 0.15) had little effect on drainflow rates and water table depths in the central region of the slope. The study confirmed that drainage theory developed for flat land applications can be applied to the interior drains on small slopes.

Karvonen (1988) made a thorough comparison between 1) a 2-D finite element-based approach with a progressively denser grid near the drain, 2) an analytical model and 3) a 1-D approximation. The author concluded that there are no major benefits to be gained from the more complicated modelling of the drain geometry compared to simpler approaches, due to uncertainty with available field data. Aura (1995) modelled subsurface drains in a 2-D finite element network by setting the node containing the drain and the surrounding gravel envelope nodes at constant atmospheric pressure. In the HYDRUS model (e.g. Šimůnek et al. 2006), the drains can

be simulated with a resistance adjustment or as seepage faces at the drain perimeter.

2.1.4 Evapotranspiration

Literature on modelling actual evapotranspiration (ET) is only presented briefly because it is not the main topic of the thesis. The process has a notable impact on the water balance during the growing season.

Penman (1948) presented an equation that described evaporation from an open water surface and lysimeters as a function of daily mean temperature, wind speed, relative humidity and solar radiation. Monteith (1965, 1981) extended the Penman (1948) model to estimate actual evaporation from vegetated areas. Other methods to calculate PET include, e.g. the Makkink (Makkink 1957), Haude (Haude 1958), Allen (e.g. Allen et al. 1994) and Mikkelsen-Olesen (Mikkelsen and Olesen 1991 cited by Christiansen et al. 2004) approaches. Tamm (2002) found out that both Penman-Monteith and Priestley-Taylor (Priestley and Taylor 1972) methods can be used to derive PET values in Estonian conditions. PET can also be approximated from the water loss measured from evaporation pans, although the results from the pans have to be corrected with experimental multipliers (Vakkilainen 1982).

In distributed simulation models, the calculated PET value is usually first divided into potential evaporation (PE) and potential transpiration (PT) with approaches based on leaf area index (LAI) or soil cover fraction. Methods for dividing PET into PE and PT components were presented by, e.g. Karvonen (1988), Larsbo and Jarvis (2003) and Kroes et al. (2008). The PT part is then divided into the root zone, uniformly or according to a root mass distribution. The root distribution R [-] can be modelled with an exponential function (Feddes et al. 1974, Gerwitz and Page 1974 cited by Jarvis 1989a):

$$R_i = f_R \left(\frac{\Delta z_i}{z_R} \right) \exp(-f_R \, z_i / z_R) \tag{9}$$

where f_R [-] is an empirical root distribution parameter, Δz_i [L] is the thickness of the layer i, z_R [L] is the depth of the root zone and z_i [L] is the depth of the layer i at its midpoint below the surface. The root mass distribution in the model by Karvonen (1988) is obtained from the crop growth model included in the system. In the HYDRUS model (e.g. Šimůnek et al. 2006), R_i is prescribed as an external input.

If soil is too dry or wet it is possible that the full PT value cannot be extracted by plants. Feddes et al. (1978) proposed a dimensionless stress factor α_F [-] that could be used in a root uptake function S [T^{-1}]:

$$S = \alpha_F T_M / z_R \quad (10)$$

where T_M [L T^{-1}] is the PT rate. The α_F factor is a piecewise linear function of pressure head h [L] (Fig. 1). Transpiration stops when h rises above the threshold pressure head h_1 or falls below the pressure head h_4 (wilting point)(Fig. 1).

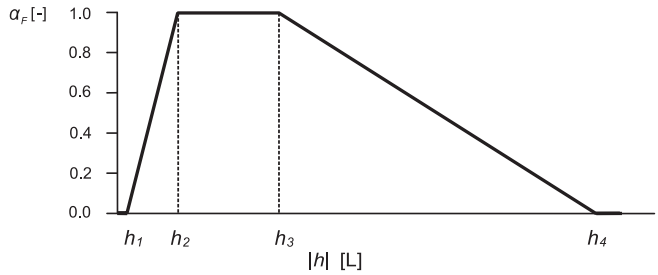

Figure 1. Dimensionless reduction factor α_F of potential transpiration as a function of absolute soil pressure head (Feddes et al. 1978).

The factor α_F by Feddes et al. (1978) has been widely used in models, e.g. in the model by Karvonen (1988), FLOCR (Hendriks et al. 1999), HYDRUS (e.g. Šimůnek et al. 2006) and SWAP (e.g. Kroes et al. 2008). The original FLOCR model takes transpiration only from the top layer of the profile and is thus suited only for plants with shallow root depths (Bronswijk 1988, Oostindie and Bronswijk 1992). Jarvis (1989a) presented a root water uptake model that allows stress-induced reductions in water uptake in one part of the root zone to be compensated by enhanced flow rates from other parts which still contain available water. Stress indices are calculated for each layer in the root zone with a threshold type function. The system is used in the MACRO model (e.g. Larsbo and Jarvis 2003).

Evaporation from the field surface is restricted by the moisture state of the soil. In the SWAP model (e.g. Kroes et al. 2008), Darcy's law is used to calculate the maximum evaporation rate. In Karvonen's (1988) model, evaporation is integrated into the top boundary condition. When the pressure head at the soil surface is below vapour pressure in the atmosphere, the surface is treated as a prescribed head boundary for evaporation. When the pressure head of the surface is above atmospheric equilibrium and below zero pressure, the surface is treated as a flux boundary for infiltration. The model does not consider higher pressure heads than zero at the surface, indicating that surface ponding is neglected. A similar method is used in the HYDRUS model (e.g. Šimůnek et al. 2006).

2.2 Preferential flow and transport in soils

Interest in the study of preferential flow has increased dramatically since the 1980s, as evidenced by the rapid growth in the number of papers published on the subject (Jarvis 2007). Both theoretical and numerical models, aimed at simulating preferential flow and solute transport in structured soils, are reviewed. The studies are divided here into three categories: 1) Single pore system models, 2) Dual-porosity models and 3) Dual- and multi-permeability models. The different mass exchange approaches used in the models to exchange water and solutes between pore systems are also reviewed. Earlier reviews have been published on the topic by, e.g. Beven and Germann (1982), van Genuchten and Dalton (1986), Brusseau and Rao (1990), Feyen et al. (1998), Nieber (2001), Šimůnek et al. (2003), Klepsch et al. (2005), Gerke (2006) and Clothier et al. (2008). A separate discussion section on the different preferential flow approaches is included at the end of the section.

2.2.1 Single pore system models

Several models adopt a single pore system concept but use different approaches to simulate preferential flow. Soil water flow is based on the Richards equation in all of the models presented in this section. Peters and Klavetter (1988) assumed that the pressure heads in the macropore and soil matrix systems are in instantaneous equilibrium, but the hydraulic properties of soil are the weighted average of both systems:

$$[wC_{WF} + (1-w)C_{WM}]\frac{\partial h}{\partial t} = \frac{\partial}{\partial z}\left\{[wK_F + (1-w)K_M]\left[\frac{\partial h}{\partial z} - 1\right]\right\} \qquad (11)$$

where w [L^3 L^{-3}] is the relative volumetric proportion of the macropore system, z [L] is the vertical coordinate, t is the time [T] and C_W [L^{-1}] and K [L T^{-1}] are the differential water capacities and unsaturated hydraulic conductivities, respectively, for matrix (M) and macropore systems (F).

Mohanty et al. (1997) devised a model which uses piecewise-continuous hydraulic functions that account for the rapid increase in the hydraulic conductivity near the saturation point:

$$K = K^* + K^*\{\exp[(h - h^*)\lambda] - 1\}, \qquad h^* < h \leq 0 \qquad (12)$$

where h^* [L] is the critical pressure head where the flow changes from capillary dominated flow to macropore flow, K^* [L T^{-1}] is the hydraulic conductivity corresponding to h^* and λ is a fitting parameter [L^{-1}].

In an approach by Ross and Smettem (2000), pressure head and water content are uncoupled and an additional equation is used to describe the

change of water content in soil. Pressure is then able to propagate more rapidly into soil, followed by rising water content.

$$\theta^{\eta+1} = \theta^{\eta} + \left(\theta_E^{\eta+1} - \theta^{\eta}\right)[1 - \exp(-\Delta t/\iota)] \quad (13)$$

where θ [L^3 L^{-3}] is the volumetric water content, the superscripts η and $\eta+1$ [-] are the new and old computation time steps, respectively, in the numerical time discretisation, θ_E [L^3 L^{-3}] is the equilibrium water content from the water retention function, Δt [T] is the time step and ι [T] is the equilibrium time constant.

2.2.2 Dual-porosity models

In dual-porosity models, the soil or rock matrix works as a reservoir and forms the immobile pore system. The actual flow and solute transport occurs in the macropore domain which forms the mobile pore system (Šimůnek et al. 2003). The matrix and macropore domains are connected with mass exchange functions for water and solutes with various formulations. The dual-porosity term is slightly ambiguous in the literature. For example, Gerke (2006) groups early models used in petroleum reservoirs and groundwater exploitation (e.g. Duguid and Lee 1977, Bibby 1981) to this group, even though they may have two conducting pore systems.

Discrete, gravity driven, macropore flow models

Theoretical models reviewed in this section use gravity-based approaches to describe flow in the mobile pore system consisting of one or several discrete macropores, such as cracks or wormholes. With the exception of CRACK-NP, the models do not support the computation of solute transport.

Edwards et al. (1979) developed a numerical model to simulate non-capillary infiltration through a circular, vertical macropore in the soil. Precipitation in the model is initially directed into the soil matrix as infiltration. Additional water is directed into the macropore or lost as surface runoff when the infiltration capacity of the macropore is exceeded. Infiltration into the soil matrix from macropore walls is calculated with the Richards equation which is solved numerically with a finite difference method in a cylindrical coordinate system. The authors found out that macropore diameter, depth and horizontal spacing had a strong influence on infiltration and runoff results.

Ruan and Illangesekare (1998) used a similar approach to simulate the effect of circular macropores on the generation of overland flow. They investigated the effect of hillslope and depression scale topography on

macropore flow activation. A rising water level in the analytically generated depressions activated new macropores. Water depths started to change at the hillslope scale after the depressions filled up and overland flow started. The sensitivity analysis showed that macropore and overland flow were more sensitive to the macroporosity of the soil and less sensitive to the microtopographic variations.

Léonard et al. (2001) developed and tested an event-based model to simulate the effect of spatially distributed large circular macropores on surface runoff. The modelling results showed that small heterogeneities, such as macropores or areas where the crust is destroyed, can have a high impact on runoff generation.

Jarvis and Leeds-Harrison (1987) extended a previously developed 1-D model of water movement in drained clay soil (Leeds-Harrison et al. 1986) with a crack flow component. Infiltration into the soil matrix is calculated with the Philip's (1957) equation. Water flow in parallel cracks is calculated with a modified version of Childs' (1969):

$$q = \frac{\rho_W g}{12\mu} d_W^2 S_E^{\varphi} \tag{14}$$

where q [L T^{-1}] is the soil fluid flux density, ρ_W [M L^{-3}] is the density of water, g [L T^{-2}] is the acceleration due to gravity, μ [M L^{-1} T^{-1}] is the dynamic viscosity of water, d_W [L] is the crack width, S_E [L^3 L^{-3}] is the relative water content (Eq. 43) in the cracks and ϕ [-] is an empirical constant. The authors emphasised that horizontal water uptake during fast descending crack flow was a major component of the water balance, unlike in the model by Hoogmoed and Bouma (1980) where the horizontal infiltration was not important.

Jarvis (1989b) and Jarvis and Leeds-Harrison (1990) extended the model by Jarvis and Leeds-Harrison (1987) with transpiration, continuous exchange of water between the pore systems and dynamic treatment of cracks. The resulting CRACK model was applied to a grass field site in Bedford, England. The authors concluded that water balance in clay soils may be predicted with accuracy from water uptake by roots and the rapid flow in the cracks. The CRACK model was extended later with leaching of nitrates and pesticides (CRACK-NP) by Armstrong et al. (2000).

Volume averaged flow and transport models

Theoretical models and applied modelling studies presented in this section use Darcy or the Richards equation for water flow and advection, dispersion, or a combination of the two processes for solute transport in the mobile pore system.

Coats and Smith (1964) presented a theoretical dual-porosity transport model using ADE to describe 1-D solute transport in the inter-aggregate space:

$$\theta_F \frac{\partial c_F}{\partial t} = \theta_F D_F \frac{\partial^2 c_F}{\partial z^2} - \theta_F v_F \frac{\partial c_F}{\partial z} - \Gamma_S \tag{15}$$

$$\theta_M \frac{\partial c_M}{\partial t} = \Gamma_S \tag{16}$$

where c [M L^{-3}] is the solute concentration in soil (F refers to the macropore and M to the matrix pore systems), D [L^2 T^{-1}] is the dispersion coefficient, v [L T^{-1}] is the subsurface flow velocity and Γ_S [M L^{-3} T^{-1}] is the solute exchange rate between the pore systems.

Skopp and Warrick (1974) described a dual-porosity solute transport model with advection as the only transport mechanism in the mobile region and molecular diffusion as the exchange mechanism between the mobile and immobile regions. The proposed equations were solved with an analytical approach. The model was used to describe breakthrough curves of calcium replacing magnesium and picloram herbicide displacement. The results of picloram simulations were not so successful, which was attributed to the complex adsorption properties of the organic compounds.

Van Genuchten and Wierenga (1976) extended the model of Coats and Smith (1964) to sorbing porous media. The analytical model derived by the authors reproduced the long tailing effect common with flow through unsaturated, aggregated, sorbing media and the early breakthrough of chemicals in the effluent.

Sudicky (1990) applied the finite element Laplace transform (FELT) method to solve transport of solutes in dual-porosity media including parallel slabs and spherical blocks. The solution is divided into three steps. First, a Laplace transform operator is applied to the dual-porosity transport equations (Eqs. 15 and 16). Finite element discretisation and solution is then used to obtain concentrations in the Laplace space (Gallo et al. 1996). Finally, an inversion of the solution in the Laplace domain is used to obtain concentrations in the time domain. The concentrations at any future time point can be obtained without the use of time disretisation with the approach. Analytical solutions were used to check the validity of the results. Gallo et al. (1996) noted that the FELT technique for solute transport is only applicable to problems with constant velocity and saturation fields.

The TOUGH2 model is capable of modelling 1-D, 2-D and 3-D saturated and unsaturated flow, as well as multi-phase and multi-component chemical transport in porous and fractured media (Pruess et al. 1999). The dual-porosity approach in the model is based on the classical Warren and

Root (1963) concept, i.e. water flows only in the fractures and the matrix blocks act as immobile reservoirs. However, it is possible to embed several matrix blocks inside each other to simulate the slow saturation of the blocks.

The HYDRUS software package is a commercial model for simulating 1-D, 2-D and 3-D movement of water, heat and multiple solutes in variably-saturated media (e.g. Vogel et al. 1996, Ŝimůnek et al. 1997, Šimůnek et al. 2006). The spatial components of the PDEs are solved implicitly with a finite element method, with options for several different 2-D and 3-D element shapes. Preferential flow is simulated with the dual-porosity concept, and the Richards equation and ADE are used to simulate water flow and solute transport in the mobile pore system. It is possible to simulate chemical reactions, e.g. nitrogen processes, with the reactive transport model (e.g. Räsänen 2009). Several different boundary conditions are supported including Dirichlet, Neumann and specified gradient-type boundary conditions.

2.2.3 Dual- and multi-permeability models

Dual- and multi-permeability models divide the total pore volume into two or more pore systems which all conduct water and solutes and exchange water according to a specified scheme.

Conceptual dual-permeability models

Conceptual dual-permeability models include two mobile pore systems of which at least one is described in a non-mechanistic way. Flow in the soil matrix is calculated with the Richards equation if not mentioned otherwise.

Hoogmoed and Bouma (1980) combined two existing models (van Keulen and van Beek 1971, van der Ploeg and Benecke 1974) to simulate the flow of water in cracked clayey soil. Data from heavy clay soils from the Netherlands reported by Bouma et al. (1978) were used to verify the dynamic simulations. Due to the short duration (< 1.0 d) of the experiment, the cracks were treated as static. Flow in the soil matrix is calculated with the Richards equation using a measured hydraulic conductivity-pressure relation. When the soil surface water depth exceeds a threshold of 2.0 mm the additional water is directed to the cracks. Water in the cracks is moved directly from the soil surface to a specified depth. The advantage of this simplified approach is that only a single set of hydraulic parameters is needed. Horizontal infiltration into crack walls is calculated with a simplified Richards equation with measured diffusivity-volumetric water

content relation. The wetted surface area in the cracks is also based on measurements.

Bronswijk (1988) and Oostindie and Bronswijk (1992) developed the FLOCR model by adding a dynamic cracking and subsidence model into the FLOWEX model (Wind and Van Doorne 1975). Data on clay soil from a Dutch basin were used to test the model. In the FLOWEX model, water starts to infiltrate laterally into crack walls only at the bottom of the crack and thus no infiltration into the matrix occurs during the rapid vertical flow. The model supports a maximum of five different soil types and 30 computational layers.

Novák et al. (2000) developed the FRACTURE submodel for the 1-D, single pore system HYDRUS-ET model and tested the system with several theoretical scenarios, using soil data from Trnava experimental site in Slovakia. Water flow into cracks is initiated after the surface water depth threshold (1.0 mm) is exceeded. Water that does not infiltrate into the soil matrix or does not fit into the cracks is considered surface runoff. Water infiltrating into the cracks is directly transferred to the saturated zone below. Novák et al. (2000) noted that the infiltration rate from the cracks into the soil matrix accelerated after the cracks started to fill up. This was due to the increased wetted surface area and pressure gradient. The infiltration capacity of soil without cracks was less than half of the infiltration capacity of soil with cracks.

Abbaspour et al. (2001) extended the SWMS_2D model (Simunek et al. 1994) by adding a macropore system and an additional Hooghoudt drain boundary condition. In the resulting M-2D model, overland water infiltrates first into the top surface cells. When the top cells fill up, the excess water is directed to the macropore cells. Flow in the macropore system is 1-D, non-capillary and laminar, and solute transport is purely advective. Solute transport in the soil matrix is calculated with ADE. The M-2D model was tested with data from a subsurface drained experimental site in Zurich, Switzerland. The macropore system and Hooghoudt drain boundary condition improved simulation of concentration peaks and water table level dynamics markedly.

The SWAP model is a free 1-D model for simulating water flow and transport of heat and solutes in the vadose zone (e.g. Kroes et al. 2008). Preferential flow is simulated with a conceptual approach. Water infiltrating into macropores is instantaneously added to the water storage at the bottom of the macropores. The structure of the macropore system is described by three properties: continuity, persistency and horizontal distribution. Macropores are divided into main bypass and internal catchment domains according to their vertical and horizontal continuity.

The main bypass flow domain forms a network of continuous macropores to subsurface drains, while the internal catchment domain is formed of disconnected macropores that end at different depths in the profile. Water can be exchanged between soil matrix and macropores via infiltration and exfiltration schemes. Different schemes are used for low soil moisture conditions and wet conditions.

Larsson et al. (2007) extended the ICECREAM model with several new processes including macropore flow, particle transport in macropores and a new description for particle detachment on the field surface. Infiltration into macropores is assumed to occur only if the water content of the two top layers exceeds an assigned threshold water content value. Water and suspended particles in macropores are channelled directly to the groundwater reservoir without interaction with the soil matrix. The flux of suspended particles is reduced by sieving processes such as mechanical trapping and sedimentation in the macropores. Subsurface drainflow is extracted from the groundwater reservoir.

Karvonen and Paasonen-Kivekäs (2007) presented the 2D-CROPWATN model that simulates water flow in a 2-D soil profile in a sloping field. The original CROPWATN model (Karvonen and Kleemola 1995) is loosely based on the DRAINMOD model (Skaggs 1980). In contrast to the DRAINMOD model, the profile in 2D-CROPWATN does not have to be in a hydraulic equilibrium. The model includes a non-equilibrium water storage that is filled up with excess water infiltrating into the soil matrix or macropores. Water from the storage can discharge to either pore system (matrix or macropores). Other differences are that the soil matrix and macropore systems are simulated separately, and soil moisture state can be calculated in two separate layers.

Gravity driven dual-permeability models

The models in this section use gravity-based approaches, e.g. the kinematic or diffuse wave approximations of the general shallow water equations to calculate flow in the macropore system. In the kinematic wave approximation, the Saint Venant equations are simplified by neglecting the local inertia, the convective inertia, the pressure gradient and the momentum source terms. In the diffuse wave approximation, the water pressure gradient is included in the momentum equation. Water movement in the soil matrix is calculated with the Richards equation if not stated otherwise.

Beven and Germann (1981) used the Childs (1969) approach with different macropore geometries to derive a general kinematic wave type model for flow in macropores. The model was applied to several theoretical

scenarios, including the relative effect of macropores in soils with different soil matrix hydraulic conductivities. The effect of macropore flow was greatest in soils with intermediate hydraulic conductivities. If the matrix conductivity was low diffusion from macropores to matrix was slow while the volume of the macropores was insignificant compared to the volume of precipitation. On the other hand, a matrix with high conductivity quickly masked out the effect of macropores.

Germann and Beven (1985) devised a kinematic wave type approach to model a single square pulse moving in an undisturbed block of soil. It was assumed that a uniform macropore system existed throughout the soil block in which the pulse can travel with a piston type movement.

$$\frac{\partial q}{\partial t} + C_K \frac{\partial q}{\partial z} + C_K r \theta_F = 0 \tag{17}$$

$$q = b\theta_F^l \tag{18}$$

$$C_K = \frac{\partial q}{\partial \theta_F} \tag{19}$$

where C_K [L T^{-1}] is the kinematic wave velocity, r [T^{-1}] is the macropore sorbance as a decrease of volume flux density per unit depth, b [L T^{-1}] is the macropore conductance parameter and l [-] is the kinematic wave exponent.

MIKE-SHE is a commercial modelling system developed by the Danish Hydraulic Institute (DHI). The model includes 1-D unsaturated and 3-D saturated subsurface flow simulation approaches. Solute transport processes are described with ADE. Preferential flow is provided as an optional add-on and is described with the kinematic wave simplification. Macropore flow is initiated when the prescribed pressure threshold in the soil matrix is exceeded. MIKE-SHE can be combined with the DAISY model (Abrahamsen and Hansen 2000) to include pesticides and crop-related processes in the model (Christiansen et al. 2004).

The MACRO model is a free 1-D model for simulation of water flow and solute transport in field soils (e.g. Jarvis 1994, Jarvis and Larsson 1998, Larsbo and Jarvis 2003). Vertical water movement in the macropore system is solved with the kinematic wave approach, i.e. capillarity is assumed to be negligible. Flow in the pore systems is separately treated in the numerical solution. The matrix system is solved with a fully implicit scheme while the macropore system is solved with an iterative implicit method called interval halving (Larsbo and Jarvis 2003).

Bronstert and Plate (1997) presented a comprehensive modelling system HILLFLOW for 2-D or 3-D simulation of runoff generation and soil

moisture dynamics in hillslopes and micro-catchments. In the HILLFLOW model, infiltration into the soil matrix at the surface is calculated with the method of Feddes et al. (1978). Matrix water dynamics are solved with etiher potential flow theory or with a quasi-explicit solution of the Richards equation. Infiltration into macropores is initiated when the soil matrix infiltration capacity is exceeded. Lateral macropore flow is called subsurface storm flow in the model and is calculated with the diffuse wave approximation. Subsurface storm flow is initiated when more water is infiltrating into macropores from the surface than is infiltrating from macropores to the soil matrix. The model was tested with data from several small forested catchments in Germany. The authors concluded that a realistic representation of the prevailing hydrological conditions requires that lateral fluxes are included in simulation models.

RZWQM or Root Zone Water Quality Model is a free 1-D water flow and agro-chemical transport model developed by the Agricultural Systems Research Unit of the United States Department of Agriculture (USDA) (e.g. RZWQM Team 1998). The flow in macropores is calculated using Poiseuille's law assuming gravity flow. Water infiltrates into macropores only from the field surface. However, water can be absorbed from macropores to the soil matrix. A dead end macropore system in the model can store water after the matrix system is saturated.

Darcian dual-permeability models

Darcian dual-permeability models include theoretical models and model applications which use volume averaged Darcy or Richards equations to model flow in both pore systems. Pure solute transport models using two ADEs to describe transport in soil matrix and macropores are also included in this category.

Skopp et al. (1981) constructed a 1-D dual-permeability model by coupling to ADEs together with an interaction coefficient. Total porosity of soil is divided between macro- or inter-aggregate and matrix or intra-aggregate porosities. The theoretical model is as follows:

$$\frac{\partial c_F}{\partial t} = D_F \frac{\partial^2 c_F}{\partial z^2} - v_F \frac{\partial c_F}{\partial z} - \Gamma_S \tag{20}$$

$$\frac{\partial c_M}{\partial t} = D_M \frac{\partial^2 c_M}{\partial z^2} - v_M \frac{\partial c_M}{\partial z} + \Gamma_S \tag{21}$$

Skopp et al. (1981) presented an analytical solution based on the regular perturbation theory for the equations for slow interactions and showed that for rapid interactions the model simplified into a single ADE. Gerke and van Genuchten (1993a) noted that the approach is still limited to steady-

state transport, while the analytical solution is only valid for relatively slow interaction between the pore systems.

Othmer et al. (1991) presented a 1-D, unsaturated water flow model using a set of two Richards equations coupled with a source/sink term. The measured WRC was split into two parts and the resulting bimodal model was used for the two pore systems. The theoretical model is as follows:

$$\frac{\partial \theta_F}{\partial t} = \frac{\partial}{\partial z}\left[K_F \frac{\partial (h_F - z)}{\partial z}\right] - \Gamma_W \tag{22}$$

$$\frac{\partial \theta_M}{\partial t} = \frac{\partial}{\partial z}\left[K_M \frac{\partial (h_M - z)}{\partial z}\right] + \Gamma_W \tag{23}$$

where Γ_W [T^{-1}] is the water exchange rate between the pore systems. The model was tested with soil samples from Neuenkirchen, Germany. The hydraulic functions have to be well defined in the wet range to accurately approximate the properties of the macropore system with this approach (Gerke and van Genuchten 1993a).

Gerke and van Genuchten (1993a) proposed a theoretical 1-D model for flow of water and solute transport in unsaturated soil or rock using the Richards equations and unsaturated ADEs for the soil matrix and macropore systems. Instead of using a bimodal WRC such as in Othmer et al. (1991), separate parameterisations were applied to both pore systems. The authors also presented a 1-D finite element-based numerical solution for the problem. The discretised flow equations of the soil matrix and macropore systems were solved simultaneously with Gaussian elimination using LU decomposition (seven-diagonal matrix) and back substitution (Gerke and van Genuchten 1993a). The authors noted that the simultaneous solution was more stable than iterating between the pore systems.

The dual-permeability model of Gerke and van Genuchten (1993a) was extended to two spatial dimensions by Ray et al. (1997). An element averaged fluid exchange term between the pore systems was introduced to balance the oscillatory behaviour encountered with high advective exchange rates in the original model. The model was used to evaluate the theoretical impacts of agricultural practices including conventional and conservation tillage on solute leaching. The macropore system was parameterised with the hydraulic properties of coarse sand.

Vogel et al. (2000) presented the theoretical model of Gerke and van Genuchten (1993a) in a general form and derived a 2-D, numerical, finite element-based solution to the equations. Five theoretical furrow irrigation scenarios were compared with the model: 1) a single pore system having

uniform hydraulic properties, 2) a single pore system with randomly distributed hydraulic conductivity, 3) a dual-permeability system with uniform hydraulic properties, 4) a dual-permeability system with randomly distributed fracture hydraulic conductivity and 5) a dual-permeability system with randomly distributed matrix hydraulic conductivities. The dual-permeability systems with spatial variability produced the most rapid solute leaching rates.

Novak et al. (2003) assessed metolachlor herbicide losses via subsurface drainflow in structured soil in France with the mechanistic, stochastic AgriFlux model (Banton et al. 1997). AgriFlux allows the use of statistical variability of the parameters using the Monte Carlo approach. Because of the stochastic approach, two physical domains can be juxtaposed to reflect the matrix and macropore systems. However, the method does not support exchange of water and solutes between the pore systems. Subsurface water flow is determined from the cubic approximation of the unsaturated hydraulic conductivity. The PDEs are solved numerically with the integrated finite difference method. The results suggested that the main factors involved in metolachlor transport in the field site were soil macroporosity and sorption kinetics.

Gärdenäs et al. (2006) compared several conceptually different ways to model preferential flow and transport of a pesticide into subsurface drains with the HYDRUS 2-D model. The models were applied to a strongly undulating, glacial till field site under cultivation in Sweden. The authors used four different model configurations: 1) an equilibrium flow model using the composite hydraulic conductivity function of Vogel and Císlerová (1988) and ADE for solute transport, 2) an equilibrium flow model and mobile-immobile solute transport model (van Genuchten and Wierenga 1976), 3) a dual-porosity model (e.g. Šimůnek et al. 2003) and 4) a dual-permeability model (a specially developed version of HYDRUS 2-D). The modelled 2-D field section was approximately 50 m wide and 3 m deep and contained three subsurface drains. The most interesting result was that none of the models captured the flow and transport processes very well with the measured and approximated soil properties. Dual-porosity and dual-permeability models were able to capture the dynamics of the measured pesticide concentration, while the models using equilibrium flow approaches produced too low concentration peaks, occurring too late.

Multi-permeability flow and transport models

Multi-permeability models have three or more pore systems that are either mobile or immobile. Steenhuis et al. (1990) developed a 1-D, preferential flow and transport model with an arbitrary number of pore

systems. The hydraulic conductivity in a pore system cell is calculated as a linear function of the water content. The hydraulic conductivity in each successive pore system is a constant integer multiple of the previous system. The value of hydraulic gradient between cells is assumed to remain constant near unity, while matric potential gradient is not considered. The time for water to travel the cell height in the pore system with the largest pores is the shortest time interval in the model and it is used as the basic computational time step. Solute transport inside a pore system and exchange between the pore systems are simulated with advection only. The model was tested against laboratory column data.

Wilson et al. (1992) extended the model by Smettem and Kirkby (1990) to a flow system consisting of micro-, meso- and macropore systems. WRC was modelled in a piece-wise manner across the pore systems. Fermi functions were used for the macropore system and a combination of Fermi functions with MVG model for the meso- and micropore systems. The model was fitted to data from A, B and C soil horizons from a forested site. When soil was saturated, flow occurred through all the three pore systems, but most rapidly through macropores. For soil conditions below saturation but above field capacity, flow occurred predominantly through meso- and micropores. For soil water conditions below field capacity, flow occurred only in the micropores. The division between macro- and mesopore systems was assumed to take place at 0.1 m suction.

Skopp and Gardner (1992) extended the solute transport model by Skopp et al. (1981) to handle continuous velocity distributions instead of two discrete velocities in two pore systems. Strictly speaking, the pore system model is continuous because the total porosity is not divided into discrete systems as in the other models presented here. The geometric model incorporates a distribution of velocities and the exchange of solutes across regions of differing velocities. The transport of solutes across velocity regions is assumed to behave as a diffusion-type process. The authors emphasised that to understand solute movement parallel to the average flow direction, an analysis of orthogonal transport across regions of varying velocities is needed.

Gwo et al. (1995) presented a theoretical, 1-D, multi-permeability model using three separate pore systems to simulate flow and transport in micro-, meso- and macropores extending the model by Wilson et al. (1992). The numerical models MURF and MURT were developed to simulate flow and transport in a laboratory setup where a tracer was injected into a soil column under steady flow conditions. The Richards equation and ADE were used in every pore system. The new model (Gwo et al. 1995) consistently fitted the data at least as well as the tested dual-porosity and single porosity

models. Results suggested that the pore systems behaved differently under different degrees of saturation, similar to the results published by Wilson et al. (1992).

Hendriks et al. (1999) combined the FLOCR model (Bronswijk 1988) with the ANIMO nutrient transport model (e.g. Rijtema and Kroes 1991) to simulate bromide and nitrogen transport in a clayey subsurface drained experimental plot. The FLOCR (v.3.0) model divides the macropore system into a maximum of five separate parts at different hierarchical levels. The states and fluxes of the macropore systems are lumped together into one system for ANIMO. Solute transport in ANIMO is simulated with ADE in both soil matrix and macropore systems. The model was tested only in wet, swollen conditions. The authors underlined that before drawing further conclusions, the model should be tested in both dry conditions with shrinkage cracks and wet conditions with only permanent macropores present.

Šimůnek and van Genuchten (2008) described different non-equilibrium flow and solute transport simulation methods in the HYDRUS 1-D software package. In addition to single porosity, dual-porosity and dual-permeability models, HYDRUS 1-D includes a dual-permeability model in which the soil matrix is further partitioned into mobile and immobile pore systems. This is accomplished by replacing the matrix pore system with a dual-porosity model. The software also includes additional non-equilibrium chemical models, but they are not further considered here.

2.2.4 Mass exchange between pore systems

Mass exchange formulations used to transfer water and solutes between pore systems are important parts of dual-porosity and dual- and multi-permeability flow and transport models. In most of the models, the exchange of water and solutes is described with a linear, time-independent mass exchange function. The exchange of water is usually based on pressure head or water content difference between the pore systems while the exchange of solutes depends on concentration differences coupled with advective solute transport.

The rate of mass exchange between the pore systems controls the non-equilibrium characteristics of the flow and transport phenomenon. A single ADE equation seems to represent well homogenous media or media composed of several interacting pore systems with high mass exchange rates (e.g. van Genuchten and Wierenga 1976). Skopp et al. (1981) noted that while high exchange rates between pore systems are the nature of homogenous soils, decreased exchange rates characterise structured soils. The authors postulated that decreased exchange rates may be due to

channelling of the flow or to the presence of low permeable clay skins on aggregates. Skopp and Gardner (1992) and Gwo et al. (1995) found out that intra-pore system dispersion became smaller than the overall dispersion of the medium in models with several pore systems, because part of the dispersion was due to the inter-pore system mass exchange. Thus, the studies suggest that mass exchange is one of the components of the macroscopic dispersion phenomenon.

Linear mass exchange approaches

Othmer et al. (1991) applied the following pressure head based formulation for exchange of water between pore systems:

$$\Gamma_W = K_A[\theta_A(h_A)]\frac{h_F - h_M}{d_A} \tag{24}$$

where K_A [L T^{-1}] is the hydraulic conductivity at the matrix-macropore interface and d_A [L] is the aggregate radii of both pore systems. K_A is a function of the water content θ_A [L^3 L^{-3}] and the pressure head h_A [L] in the interface. K_A is set equal to the lowest hydraulic conductivity of the two pore systems. Gerke and van Genuchten (1993a) derived a similar approach in their model:

$$\Gamma_W = \alpha_W(h_F - h_M) \tag{25}$$

where α_W [L^{-1} T^{-1}] is the first order water exchange coefficient. Gerke and van Genuchten (1993a) developed an expression for α_W with a scaling procedure:

$$\alpha_W = \frac{\beta}{d^2}K_A\gamma_W \tag{26}$$

where β [-] is the geometry coefficient, d [L] is the characteristic radius or half width of the matrix structure and γ_W [-] is the scaling coefficient. Macropore geometry coefficient β can be thought of as the ratio of the effective surface area of macropores to the volume of the soil matrix (Gerke and van Genuchten 1996). The first order approximate and the exact solution to the diffusion problem are matched together with γ_W (e.g. Eq. 26). In principal, values for the parameter β could be derived by measuring macropore shapes and sizes and applying the method presented by Gerke and van Genuchten (1996). The same applies to the parameter d. In practice, the parameters are commonly calibrated in model application studies. The method by Gerke and van Genuchten (1993a) (Eq. 26) is applied in several studies (e.g. Ray et al. 1997, Schwarzt et al. 2000, Vogel et al. 2000, Abbaspour et al. 2001, Haws et al. 2005). Gwo et al. (1996)

used the following approach to describe water exchange in their three pore system model:

$$\Gamma_{W,i} = -\sum_{\substack{j=1 \\ j \neq i}}^{3} \alpha_{W,i,j}\left(h_i - h_j\right) \tag{27}$$

where i and j [-] are pore system indices. The first order mass exchange coefficient α_W (Eq. 27) is based on the approach by Duguid and Lee (1977) defined as follows:

$$\alpha_{W,i,j} = \frac{4K_j\varepsilon_i}{\pi d_S d_R} \tag{28}$$

where ε [L^3 L^{-3}] is the porosity of the pore system i and d_S and d_R [L] are the half dimensions of soil and rock blocks, respectively. In the MACRO model, the exchange of water is based on the difference between the saturated and prevailing volumetric water contents of the soil matrix (Larsbo and Jarvis 2003):

$$\Gamma_W = \left(\frac{\beta D_W \gamma_W}{d^2}\right)(\theta_{SM} - \theta_M) \tag{29}$$

where D_W [$L\ T^{-1}$] is the effective water diffusivity and θ_S [L^3 L^{-3}] is the saturated water content. Šimůnek et al. (2001) adopted a similar approach but used effective volumetric water contents in soil matrix and macropores instead and a lumped α_W term. Other options to calculate exchange of water between macropores and soil matrix include the Green and Ampt (1911) model (e.g. Novák et al. 2000, Cameira et al. 2000) and Phillip's (1957) equation (e.g. Jarvis and Leeds-Harrison 1990, Hendriks et al. 1999).

Equivalent solute exchange functions exist for the presented water exchange functions. Van Genuchten and Wierenga (1976) and Skopp et al. (1981) applied diffusion based models to represent solute exchange. Gerke and van Genuchten (1993a) included both diffusive and advective exchange processes in their their dual-permeability transport model. Some authors, e.g. Sudicky (1990) and Hendriks et al. (1999) applied the Fick's law to calculate solute exchange between the pore systems. The solute exchange between the pore systems is not discussed further because sediment, which is represented as a solute in this thesis, is constrained into the macropore system and cannot enter the matrix system.

Non-linear mass exchange approaches

The principal difficulty in applying models with several interacting pore systems is the non-linear mass exchange at the wetting front and the tendency to over-predict solute adsorption equilibrium (Zimmerman et al.

1993). Fitted mass exchange coefficients seem to represent a lumped process resulting from the combined effects of intra-aggregate diffusion and local flow variations (Schwarz et al. 2000). According to Gerke and van Genuchten (1996), linear exchange terms yield relatively good approximations, except near the infiltration front. To overcome this limitation non-linear approaches have been developed, e.g. Dykhuizen (1990), Zimmerman et al. (1993) and Zimmerman et al. (1996).

2.2.5 Discussion on preferential flow models

Even though models with several pore systems seem to be able to describe preferential flow and transport in structured soils, a few new problems arise from this methodology.

Brusseau and Rao (1990) noted that in order to apply models with several pore systems, knowledge on the size and shape distributions of aggregates is required. Steenhuis et al. (1990) criticised that the division of pore space into only two systems is unrealistic. According to the author, this leads to arbitrarily defined parameters that are difficult to determine. Wilson et al. (1992) pointed out the arbitrariness of dividing soil pores into multiple pore regions when there are no clear boundaries. Gwo et al. (1995) argued that it is possible to divide the total soil porosity into systems according to measurable tension ranges, even though it would be better to associate the pore domains to geological features. However, Šimůnek et al. (2003) came to a conclusion that single pore system models cannot simulate true preferential flow.

One of the drawbacks of dual- and multi-region models is the number of parameters to be estimated from usually limited laboratory or field data (Gerke and van Genuchten 1993a). For non-reactive solutes, classical ADE requires three parameters, while a dual-porosity and a multi-region models require five and 13 parameters, respectively (Gwo et al. 1995). The large number of tunable parameters in dual-permeability and multi-region models enables better mathematical description of experimental data than low number of parameters in single-region models. However, e.g. Jarvis et al. (2008) decided that the model by van Genuchten and Wierenga (1976) was over-parameterised for their problem and opted to switch to a simpler empirical model. It is questionable whether the solutions of such complex models are unique and whether fitted model parameters actually reflect the effective transport processes in the soil (Schwarz et al. 2000). In addition, measuring hydraulic parameters for the macropore system (e.g. WRC) can be difficult (Wilson et al. 1992).

Yet another issue related to multi-region concepts is the difference between local-scale and field-scale, or small vs. large scale heterogeneities.

Representative elementary volume (REV) is used to describe material properties of porous media in volume averaged flow and transport models. The problem with the REV concept is that each soil parameter may have a unique temporal and spatial scale and the soil parameters may exhibit a systematic change in one direction or another (Hillel 1998). Due to the interaction between micro- and macropore domains, REV for micropores should be of the same order as that of the macropores (e.g. Beven and Germann 1981). However, large interblock cracks in clayey soils are objects with indefinite REV, at least in the vertical direction (Chertkov and Ravina 2002). Thus, large scale features of geological signature should be separated from small scale features applicable to dual- and multi-pore system approaches (Gwo et al. 1995).

A selected group of preferential flow models is presented in Table 1.

Table 1. Examples of reviewed preferential flow and transport models. Abbreviations used: Stor. rout. = storage routing, Concep. = conceptual and Diff. wave = Diffuse wave.

Model:	Dimensions:	Macropore flow:	Macropore transport:	Matrix flow:	Matrix transport:
2D-CROPWATN	2-D	Stor. rout.	-	Stor. rout.	-
AgriFlux	1-D	Richards	ADE	Richards	ADE
ANIMO	1-D	-	ADE	-	ADE
CRACK	1-D	Childs	-	Concep.	-
DUAL	1-D	Richards	ADE	Richards	ADE
FLOCR	1-D	Concep.	-	Richards	-
HILLFLOW	2/3-D	Diff. wave	-	Richards	-
HYDRUS 2/3-D	2/3-D	Richards	ADE	Storage	Storage
ICECREAM	1-D	Concep.	Concep.	Concep.	Concep.
M-2D	2-D	Concep.	Advection	Richards	ADE
MACRO	1-D	Kin. wave	ADE	Richards	ADE
MIKE SHE	3-D	Kin. wave	ADE	Richards	ADE
MURF/MURT	1-D	Richards	ADE	Richards	ADE
RZWQM	1-D	Poiseuille	ADE	Richards	ADE
SWAP	1-D	Concep.	Concep.	Richards	ADE
TOUGH2	3-D	Richards	ADE	Storage	Storage

2.3 Overland flow and erosion

In contrast to preferential water flow models, a large number of established erosion models are available for different scales that are based on physical principles. Several lumped and distributed field-scale models are reviewed here. The models are divided into two categories: 1) conceptual and universal soil loss equation (USLE)-based erosion models and 2) process-based, distributed erosion models. Models in the first group use regression or similar type equations derived from experimental data. USLE-based erosion models are important to this study because the bulk of the erosion modelling in Finland (Section 1.4) has been conducted with such models. The models in the second group are usually composed of a sediment continuity equation coupled to erosion processes including the effect of raindrops, flowing water, deposition of particles and transport

capacity of the flow. The models reviewed here include only advective sediment transport, i.e. dispersive transport is omitted. Detailed presentation of erosion equations is left out from this section (see textbooks by e.g. Foster 1982, Morgan 2005 for a review on the topic).

It is assumed here that overland flow is one of the main drivers of soil erosion and overland flow models are reviewed alongside the erosion models (see descriptions of runoff generation mechanisms in Section 1.2). In conceptual models, surface runoff is simulated with different approaches, e.g. the Soil Conservation Service (SCS) curve number method (USDA 1972), the unit hydrograph theory (Dooge 1959) and transfer functions (e.g. Koivusalo and Karvonen 1995). In distributed models, in turn, overland flow is simulated with the Saint Venant equations or with one of their simplified forms, such as kinematic wave or diffuse wave equations (Section 2.2.3.2). Infiltration is usually simulated with approaches such as Green and Ampt (1911), Philip (1957) or with a fully-fledged soil and groundwater flow model. Previous erosion model reviews were published, e.g. by Jetten et al. (1999), Aksoy and Kavvas (2005), Jetten and Favis-Mortlock (2006) and Borah et al. (2008).

2.3.1 USLE based and conceptual erosion models

CREAMS (Knisel 1980) is a conceptual, daily simulation model for estimating runoff, erosion and sediment transport and plant nutrient and pesticide loss from field-sized areas. A field is defined as a management unit having 1) single land use, 2) homogenous soils, 3) spatially uniform rainfall and 4) a single set of management practices. The field is structured from three basic elements: overland flow area, concentrated (channel) flow and impoundment (pond). Runoff is simulated either with the SCS curve number method or with an infiltration-model, depending on the time resolution of the precipitation data (daily or hourly). Water moving through soil layers is modelled with a simple capacity approach. The erosion model is based on USLE but it is extended with surface runoff transport capacity.

The GLEAMS model was developed as a management-oriented CREAMS model that incorporated a component for vertical flux of pesticides (Leonard et al. 1987). The soil erosion model is derived from the USLE equation with added rill and inter-rill processes, rain drop splash erosion and sediment transport capacity simulation. Sediment transport capacity is simulated with a modified Yalins equation (Yalin 1963). Knisel and Turtola (2000) applied an external model to approximate the sediment load via subsurface drains, with daily percolation values obtained from GLEAMS.

The ICECREAM model is another CREAMS variant modified to Nordic conditions by Rekolainen and Posch (1993, 1994) and Posch and

Rekolainen (1993). The authors added processes for snow accumulation, snowmelt and soil frost and modified the crop growth submodel. The USLE-based erosion model in ICECREAM includes the same erosion components as GLEAMS. The difference between the ICECREAM and GLEAMS models is that the former only considers surface response of phosphorus while the latter can be used to simulate subsurface processes as well. Larsson et al. (2007) presented a modified version of the ICECREAM model that also includes transport of sediment and phosphorus to subsurface drains via preferential flow paths.

PSYCHIC is a conceptual phosphorus and erosion model presented by Davison et al. (2008). The model was designed to work both with catchment and field-scales and uses a monthly time step. Hydrology in the model is simulated with the Mean Climate Drainage Model (MCDM, Anthony 2003) that simulates water balances for different UK land use types. Surface runoff is based on the Green and Ampt model, storm profile information and surface storage, which is calculated with the empirical method of Onstad (1984). Sediment loss is estimated roughly due to the monthly time step with a modified Morgan-Morgan-Finney model (Morgan 2001). The erosion model is comprised of raindrop splash erosion and surface runoff shear stress components. The effect of soil cohesivity on erosion can be approximated with the model. Sediment produced in the field is lost via surface runoff and subsurface drainflow when drains are present. A simple attenuation multiplier is introduced to simulate the filtering effect of soil on load via drains.

2.3.2 Distributed, process-based erosion models

The Water Erosion Prediction Project (WEPP) was initiated by USDA to develop a new process-oriented computer model that simulates plant growth, overland and subsurface hydrology, erosion and weather parameters in field-sized areas and hillslopes (USDA 1995). The WEPP model simulates the fluctuation of the groundwater table and can thus be used to simulate Dunne type saturation excess overland flow in poorly drained soils (Savabi 1993). The model includes processes for subsurface drainage following Skaggs (1980). Infiltration is calculated with the modified Green and Ampt model and overland flow is calculated with the kinematic wave approach. For erosion simulation, WEPP uses a steady state, 1-D sediment continuity equation coupled with rill and interrill processes. Soil detachment in interrill areas is modelled as a function of rainfall intensity and runoff rate, while delivery of interrill sediment to rills is a function of slope and surface roughness.

KINEROS2 is a dynamic and distributed event-based model that treats catchments as an assembly of 1-D rectilinear surfaces and channels. Overland flow is solved with the kinematic wave approach. Infiltration is simulated with a function combining the Green and Ampt and Smith and Parlange models (Smith et al. 1995). In addition, KINEROS2 includes a possibility to divide the soil profile into two layers to enable more complex infiltration schemes. The erosion model is composed of rainsplash and hydraulic erosion components. Transport capacity description is derived from the Engelund and Hansen method (Engelund and Hansen 1967). KINEROS2 (Smith et al. 1995) is an improved version of the original KINEROS model by Woolhiser et al. (1990). In particular, KINEROS2 features simulation of several particle sizes and has improved infiltration simulation capabilities compared with the older version.

The EUROSEM model was developed to improve erosion risk evaluation and the design of erosion control measures in European conditions (Morgan et al. 1998). EUROSEM is linked to the water and sediment routing structure of the KINEROS model (Smith et al. 1999) or the MIKE SHE model. In addition, EUROSEM includes explicit consideration of rill and interrill flow, improved simulation of plant cover effects, and takes into account the influence of rock fragments on infiltration. The erosion model includes hydraulic and splash erosion components and an empirical transport capacity approach derived from a large number of shallow water experimental flow observations. Rills are essentially presented as trapezoidal channels. The depth and width of the rills at each point are changed according to erosion and deposition processes. Deposition and erosion by flow and splash detachment can occur at any point on either the rill or interrill areas. Depression storage is calculated with a unique empirical regression equation as a function of ratio of line segment length drawn directly between two end points, and line segment drawn over all the microtopographic irregularities.

The LISEM model (De Roo et al. 1996a, b) is an event-based process model which is one of the first models to be completely incorporated into a GIS framework. Hydrological and hydraulic processes incorporated in the model include rainfall, interception, surface storage in micro depressions, 2-D overland flow and 1-D channel flow (the kinematic wave approximation), infiltration (the Richards equation and the Green and Ampt model options) and 1-D vertical movement of water in soil (the Richards equation). The time step lengths in the soil water model are adjusted according to the simulated pressure head changes and the equations are solved with the Thomas (tridiagonal matrix) algorithm. The MVG model or look-up tables are used for WRCs. Erosion processes include

soil detachment by rainfall and throughfall, detachment by overland flow and simulation of transport capacity of the flow. The raindrop splash detachment is calculated as a function of soil aggregate stability, rainfall kinetic energy and depth of overland water layer. The transport capacity of overland flow is modelled as a function of unit stream power. Flow detachment and deposition simulation in rill and interrill areas is similar to the EUROSEM model. LISEM also includes options for modelling subpixel features such as roads, wheel tracks and channels.

SHESED is a dynamic, continuous and 2-D distributed erosion model component (Wicks and Bathurst 1996) for the SHE hydrological modelling system (Abbot et al. 1986a, b). The model is also applicable to larger catchment areas (> 1.0 km^2). The SHE model includes simulation of overland, channel and subsurface water movement. Importantly, it is able to simulate overland flow produced by both Dunne and Hortonian mechanisms. SHESED includes simulation of raindrop impacts, leaf drip, sheet type hydraulic erosion (without rilling) and transport of eroded material by overland flow. The model can also simulate erosion of bed material, transport of sediment and entrainment of material in channels. The SHESED model contains an intricate raindrop splash erosion component that takes into account the controlling effects of rain intensity, water depth at the surface and overland shielding factors, such as canopy and ground cover.

EROSION 3D (Werner 1995) is an event-based, 2-D distributed erosion model for small watersheds that can be integrated into GIS systems such as ArcInfo, IDRISI or GRASS (Schmidt et al. 1999). A modified lowest neighbor routing algorithm (O'Callaghan and Mark 1984) is used to route overland flow and sediment load from upland areas towards the catchment outlet. Infiltration is calculated with the Green and Ampt model. The infiltration model is modified with a simple empirical correction factor to account for the effects of tillage practices and soil textures on erodivity of soil. The EROSION 3D model includes simulation of soil erosion by overland flow and rain drops, settling of particles and simulation of transport capacity. In spite of the model name, which is related to the 3-D visualisation tools included in the system, the model does not include subsurface internal erosion or transport of sediment to the subsurface drains components.

CASC2D-SED is an event-based, 2-D distributed erosion model for predicting soil erosion during single event storms (Johnson et al. 2000). The model can be interfaced with GIS software. Like SHESED, the CASC2D-SED model is also applicable to larger catchments (> 1.0 km^2). Water flow in the model is computed with the CASC2D model (Julien et al.

1995) which calculates 2-D overland flow and 1-D channel flow with the diffuse wave approximation. Infiltration is simulated with the Green and Ampt model. The CASC2D-SED model consists of empirical sediment transport capacity equations developed in the USA, coupled with a sediment continuity equation. Raindrop, rill and interrill erosion are simulated as a lumped process. The sediment transport equations use USLE parameters to account for the effects of soil erodibility, cultivation practices and erosion prevention methods. Upland erosion is divided into three particle size classes (sand, silt and clay).

Taskinen (2002) and Taskinen and Bruen (2007a, b) presented an erosion model that includes event-based, 2-D distributed, overland flow, soil erosion and phosphorus transport components. Overland flow is solved with the kinematic wave approximation. Infiltration is simulated either with the Green and Ampt model or the Corradini et al. (1997) method. Baseflow is simulated with a linear reservoir approach. The erosion model is composed of sheet-type hydraulic and rain drop splash erosion schemes similar to the SHESED model, combined with particle settling and transport capacity simulation. Particle settling velocity is based on the Stokes' law. Transport capacity is described with either the modified Yalins equation or with the Engelund-Hansen method. The equations are solved in the model with either implicit or explicit schemes.

PSEM_2D is an event-based, 2-D distributed, overland flow and erosion model meant for plot-sized areas and small fields (Nord and Esteves 2005). Overland flow is solved with the full Saint Venant equations with an explicit finite difference MacCormack scheme while the friction slopes are approximated with the Darcy-Weisbach equations. Infiltration is calculated with the Green and Ampt model. Soil erosion is simulated with a sediment continuity equation coupled with sheet-type hydraulic erosion and raindrop splash components. The soil surface is divided into original and buffer soil layers. Raindrop impacts detach particles from the original soil layer and deposit them on the buffer layer. The critical shear stress of the particles on the buffer layer is lower than in the original layer and the sediment is thus more easily detached by overland flow. PSEM_2D does not include rill or interrill division with erosion, and supports only one sediment size class. The performance of the model was tested against literature data with good results (Nord and Esteves 2005).

Sharda and Singh (1994) developed a continuous, 1-D overland flow and erosion model. The PDEs are solved with an implicit finite element method (FEM). Overland flow is represented with the kinematic wave approximation and infiltration into soil with a 1-D Richards equation. Onstad's (1984) model is used to compute depression storage. Soil erosion

is simulated with a 1-D sediment continuity equation combined with rill and interrill erosion components. The model simulates only one particle size, because, according to the authors, cohesive particles are usually removed in aggregates and not in primary fractions. Sediment transport capacity is simulated with the Yalins equation. The authors tested four time integration schemes and evaluated their computational efficiency, convergence and stability through L_2 and Chebycheff norms (Prenter 1975). The numerical schemes tested included explicit, Crank-Nicolson, implicit and predictor-corrector schemes. The norms were obtained by comparing hydrographs of analytical kinematic wave (Lighthill and Whitham 1955, Handerson and Wooding 1964) and numerical solutions. Sharda and Singh (1994) found out that the predictor-corrector scheme was the best numerical scheme for time integration for FEM in this application, while the implicit scheme yielded almost comparable results.

2.3.3 Discussion on overland erosion models

The USLE equation was originally designed to simulate annual sediment loads, and not sediment loads from single precipitation events (e.g. Morgan 2005). While CREAMS and WEPP models can simulate individual storm events, they produce only total storm sediment loss because the overland flow conditions are considered to be steady-state (Morgan et al. 1998). The ICECREAM model, developed for Finnish conditions, retains the same hydrology component as the CREAMS model (Tattari et al. 2001). The problem is that the design of erosion control measures requires information on timing and volume of peak runoff events during individual rain storms.

The application of USLE-based models in Europe has been somewhat difficult due to differences in climatic conditions, land use and soil types compared to the USA (Jetten and Favis-Mortlock 2006). When applying the CREAMS model in Finland, Kauppi (1982) estimated excessively high loads compared to the measurements. While the cumulative annual simulation results of Knisel and Turtola (2000) with the GLEAMS model were good, the monthly results showed a serious mismatch when compared to the observed values. Tattari et al. (2001) had to manipulate the regression equations in the ICECREAM model to improve their results in Finnish conditions. Paasonen-Kivekäs et al. (2006) experienced problems with the ICECREAM model in simulating high erosion rates in the autumn at a clayey field in Finland. The authors also recommended recalibration of the model with measurements conducted in Nordic conditions.

Previous studies have not conclusively shown whether single event or continuous simulations are more effective. Morgan et al. (1998) argued that continuous erosion simulations are not needed because 1) they require large

amounts of input data (e.g. weather and land-use), 2) they are sensitive to modelling soil water dynamics and evapotranspiration and 3) they simulate a large number of small events that do not produce significant runoff or soil loss and thus waste computational resources. On the other hand, several authors underline the importance of simulating the hydrological regime properly before attempting to simulate soil erosion. Wicks and Bathurst (1996) used the SHESED model to simulate single events and found that the principle problem was the lack of antecedent soil moisture conditions and infiltration data. Smith et al. (1999) and Schmidt et al. (1999) conjectured that continuous simulations would have improved their results due to more realistic initial conditions. Overland flow in Finland is generated by both Dunne-type and Hortonian mechanisms. Because the Dunne-type mechanism requires information on the antecedent moisture conditions, event based simulations can be problematic (e.g. Morgan et al. 1988, Taskinen and Bruen 2007a). Only four of the reviewed erosion models (Table 2) include a subsurface flow model for simulation of Dunne-type overland flow mechanism (Sharda and Singh 1994, SHESED, WEPP and LISEM).

Table 2. Summary of reviewed erosion models. Abbreviations used: Distr. = Distributed, Conc. = Conceptual, Cont. = Continuous and Mass cons. = Mass conservation.

Model:	Type:	Dimensions:	Overland flow:	Erosion:
CASC2D-SED	Distr./Event	2-D	Diffuse wave	Lumped erosion
CREAMS	Conc./Cont.	1-D	Runoff	Lumped erosion
EROSION 3D	Distr./Event	2-D	Kinematic wave	Sheet and raindrops
EUROSEM	Distr./Event	1-D	See KINEROS2	Rill and interrill, raindrops
GLEAMS	Conc./Cont.	1-D	Runoff	Rill and interrill, raindrops
KINEROS2	Distr./Event	1-D	Kinematic wave	Sheet and raindrops
LISEM	Distr./Event	2-D	Kinematic wave	Rill and interrill, raindrops
ICECREAM	Conc./Cont.	1-D	Runoff	Rill and interrill, raindrops
PSEM_2D	Distr./Event	2-D	Saint Venant	Sheet and raindrops
PSYCHIC	Conc./Cont.	-	Runoff	Sheet and raindrops, transport to drains
Sharda and Singh (1994)	Distr./Cont.	1-D	Kinematic wave	Rill and interrill
SHESED	Distr./Cont.	2-D	Mass cons.	Sheet and raindrops
Taskinen and Bruen (2007a, b)	Distr./Event	2-D	Kinematic wave	Sheet and raindrops
WEPP	Distr./Cont.	1-D	Kinematic wave	Rill and interrill, raindrops

3. Description of the FLUSH model

The FLUSH model was developed to simulate water flow and soil erosion in clayey, subsurface drained agricultural fields. The prototype processes required in the model are presented in Section 3.1 while the realised system is detailed in Section 3.2. The system, comprising of the conceptual and numerical models, is generic and data are still required from an application area to define the initial conditions and parameter values. The reasoning behind the selection of the model components was based on the Literature review (Section 2) and it was presented in Section 1.4. Decisions regarding the model structure and model development are further discussed in Section 5.1. Some of the numerical solutions are tested with theoretical approaches at the end of this section.

3.1 The conceptual model

Refsgaard and Henriksen's (2004) conceptual model approach is adopted here. The conceptual model consists of process descriptions and general mathematical equations. The process descriptions are presented in writing and illustrated with several figures (Figs. 2–6).

In summary, the system functions in the following way. The hydrological cycle is initiated by precipitation. Water on the field surface infiltrates into soil matrix and macropores. When the infiltration capacity of soil is exceeded or the groundwater table rises to the surface, overland flow is initiated. Water is lost from the field via open ditches, evapotranspiration (ET), subsurface drains and groundwater flow. Suspended sediment is produced on the field surface by rain drop splash and hydraulic erosion processes. Suspended sediment is transported to ditches by overland flow and to subsurface drains by preferential flow in macropores. Total subsurface pore volume is partitioned into soil matrix and macropore parts. Soil shrinkage and swelling processes distribute the total pore volume into matrix and macropore fractions according to the moisture state of the matrix.

The structure of the system is presented as a flow chart in Fig. 2. The boxes represent water (Fig. 2a) and suspended sediment reservoirs (Fig. 2b) in the system while the arrows show different processes transferring mass between the reservoirs. The disabled sediment reservoirs and processes are presented with dotted lines. The direction of the arrow describes the direction of the mass flow. Some lines have arrow heads at both ends, indicating that mass can be exchanged both ways. The field is divided into overland and subsurface domains. The two domains are divided by an infinitely thin interface that is called the field surface in the model. Erosive processes extract soil particles from the interface to the overland domain. Suspended sediment in the overland domain may enter the subsurface domain via macropores. Suspended sediment in the subsurface domain is allowed to move only in the macropore system because the sediment particles are considered to be too large to enter the clay soil matrix voids. In addition, the transport of sediment is constrained to macropores between field surface and subsurface drains. In line with the findings of e.g. Yli-Halla et al. (2000) and Vakkilainen and Paasonen-Kivekäs (2004), it is assumed here that the pathways below the drains are too narrow for sediment particles to travel. It is possible that suspended sediment can block macropore pathways but this is not considered in the model. Different processes in the system are discussed next in more detail.

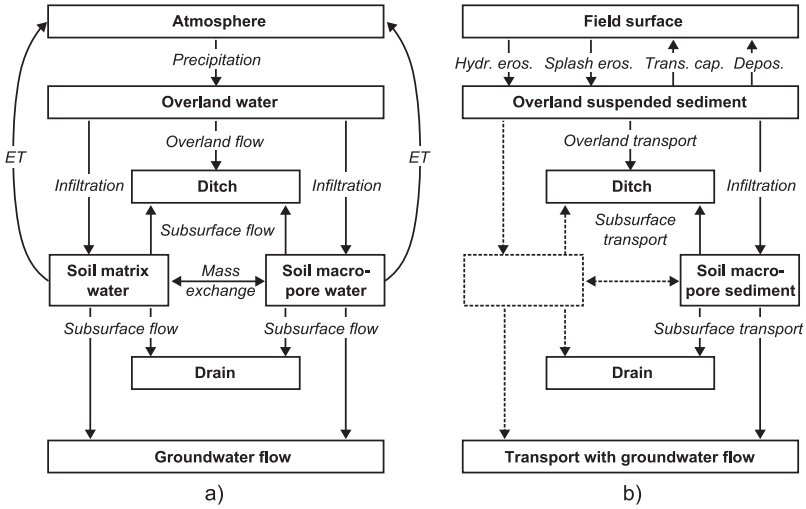

Figure 2. The conceptual model of a) water flow and b) erosion in the field. Dashed lines mark disabled storages and processes for sediment. Abbreviations used: Hydr. eros. = Hydraulic erosion, Transp. cap. = Transport capacity and Depos. = Deposition.

3.1.1 Process descriptions

The processes in the simulated system can be divided into four independent but coupled domains: 1) overland flow, 2) subsurface flow, 3)

overland erosion and 4) subsurface transport of sediment. Detailed descriptions of the processes in each domain are presented below. The written descriptions are linked to the corresponding figures with numbers.

Overland flow

Fig. 3 depicts different processes present in the overland flow domain. Precipitation adds water to the overland flow domain (1 in Fig. 3). Water starts moving on the field surface when a threshold water depth is exceeded. The threshold water depth simulates the storage of water in microdepressions (2). Tillage operations can change the roughness of the field surface and the threshold water depth. Water is also stored in larger depressions in the topography (3). Water moves as 2-D sheet flow according to the topography of the field and pressure differences (4). Overland water discharges via ditches and unobstructed slopes in the field borders (5).

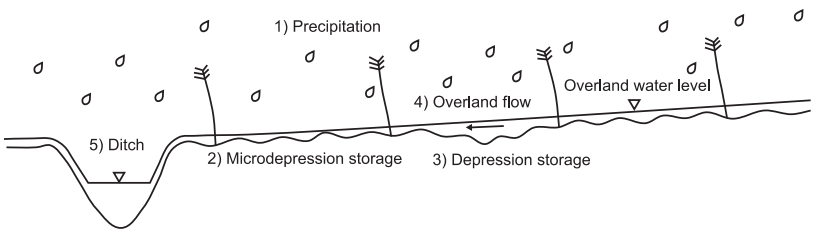

Figure 3. Overview of the processes in the overland flow domain.

Subsurface flow

Fig. 4 depicts different processes present in the subsurface flow domain. Water infiltrates into both soil matrix and macropores from the field surface (1 in Fig. 4). Maximum infiltration capacity into the soil matrix from the overland domain is always calculated with the saturated hydraulic conductivity value. The conductivity of the macropore system is increased to its saturated conductivity value when the overland flow threshold water depth is exceeded to simulate the flow of water into the macropores. Subsurface flow is unsaturated between the field surface and the groundwater table (2) and saturated below the groundwater table (3). Flow is 3-D in both pore systems. Horizontal preferential flow takes place above the compressed tillage pan due to soil hydraulic conductivity differences in the profile (4). Water moving in the soil matrix and macropores can also flow between the pore systems due to pressure differences (5). Water enters the subsurface drains from both matrix and macropore systems (6). Water can also exit the field by seepage into ditches (7) and via groundwater flow (8). Water depth in the ditches is assumed to be constant. Water is lost via

ET from both pore systems (9). PET is distributed in the soil profile according to the root mass distribution, which is the same in both pore systems. ET is decreased from its potential value by too wet and too dry root zone conditions. Soil shrinkage and swelling processes change the size of macropores according to the moisture state of the matrix.

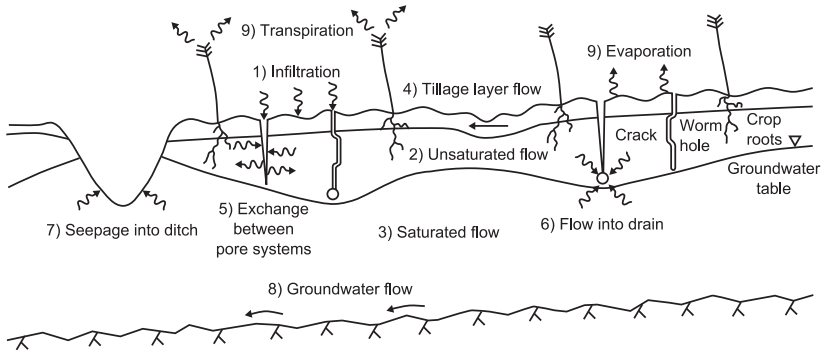

Figure 4. Overview of the processes in the subsurface flow domain.

Overland erosion

Fig. 5 depicts different processes present in the overland erosion domain. Suspended sediment is produced by hydraulic (1 in Fig. 5) and rain drop splash erosion (2). Only sheet-type hydraulic erosion and one sediment particle size are considered in the simulation. Erosion due to leaf drip is not included. Tillage operations can increase the erodibility of the soil. Sediment is moved by water with a 2-D advection transport mechanism (3 in Fig. 5). The amount of sediment moved by water is controlled by the sediment transport capacity of the overland flow (4). If the sediment concentration exceeds the transport capacity of the flow, the additional sediment is deposited back on the surface of the field. After rain, suspended sediment starts to settle due to gravity (5) while during rain, turbulent mixing caused by raindrops cancels deposition. Suspended sediment discharges into open ditches (6).

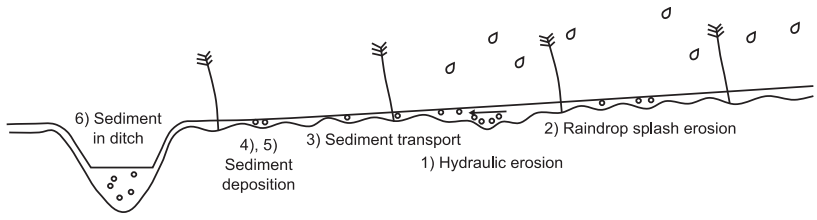

Figure 5. Overview of the processes in the overland erosion domain.

Subsurface transport of sediment

Fig. 6 depicts different processes present in the subsurface transport domain. Suspended sediment infiltrates into macropores from the field surface (1 in Fig. 6). Suspended sediment cannot be transported into the soil matrix with water because the voids in the clay soil matrix are considered to be too small for the particles. Sediment is transported by 3-D advection and dispersion mechanisms in the macropores. Unsaturated transport takes place above the groundwater table (2) and saturated transport below the groundwater table (3). However, macropores below the subsurface drain level are considered to be too small for sediment to enter. Horizontal transport of sediment requires that the macropore network is continuous in the horizontal plane. Suspended sediment is discharged via drains (4) and via seepage to ditches (5). Sediment can be deposited on macropore walls (6) if water is lost through transpiration or exchange into soil matrix. Deposited sediment is flushed onwards again after more water enters the macropores. Some of the infiltrated sediment is transported with groundwater flow when the groundwater table rises above the drain level (7).

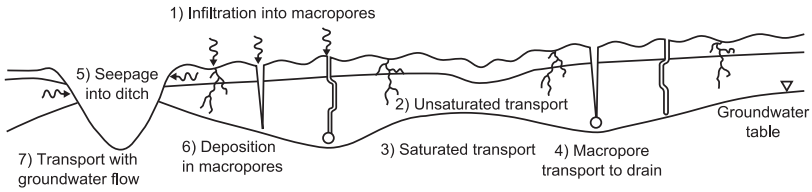

Figure 6. Overview of the processes in the subsurface transport domain.

3.1.2 Mathematical descriptions

The mathematical descriptions of the conceptual model are presented in the same way as the process descriptions by dividing them into the four domains. The numerical model presented later works in an orthogonal grid that is oriented to the Cartesian coordinate system. Spatial coordinates x, y and z are therefore used in all of the PDEs presented here, instead of more general notation. Sources and sinks in each domain are presented in detail alongside the numerical model in Section 3.2.

Overland flow

Overland flow is represented with the diffuse wave simplification of the Saint-Venant equations used, e.g. by Johnson et al. (2000). The effective overland water depth h_W [L] is calculated with the following method:

$$\begin{cases} h_W = h_{W,TOT} - h_{W,THR}, & h_{W,TOT} > h_{W,THR} \\ h_W = 0, & h_{W,TOT} \leq h_{W,THR} \end{cases} \quad (30)$$

where $h_{W,TOT}$ [L] is the total overland water depth and $h_{W,THR}$ [L] is the overland flow threshold water depth. The $h_{W,THR}$ parameter represents the water volume that is stored in the microdepressions. After h_W exceeds the $h_{W,THR}$ value, water starts to flow on the field surface. The continuity equation for overland flow and overland unit flow rate Q [L^2 T^{-1}] are defined as follows (e.g. Taskinen and Bruen 2007a):

$$\frac{\partial h_W}{\partial t} + \frac{\partial Q_X}{\partial x} + \frac{\partial Q_Y}{\partial y} = \pm s_W \quad (31)$$

$$Q_X = U_X h_W \text{ and } Q_Y = U_Y h_W \quad (32)$$

where s_W [L T^{-1}] is the overland water source/sink term and U [L T^{-1}] is the overland flow velocity. U is calculated with the Manning equation:

$$U_X = \frac{1}{n} h_W^{2/3} \sqrt{S_{OX}} \text{ and } U_Y = \frac{1}{n} h_W^{2/3} \sqrt{S_{OY}} \quad (33)$$

where n [-] is the Manning coefficient and S_O [-] is the slope of the overland water surface. Hydraulic radius was replaced with h_W in Eq. 33. The momentum equations for the diffuse wave simplification are the following:

$$S_{OX} = \frac{\partial z_S}{\partial x} - \frac{\partial h_W}{\partial x} \text{ and } S_{OY} = \frac{\partial z_S}{\partial y} - \frac{\partial h_W}{\partial y} \quad (34)$$

where z_S [L] is the soil surface elevation.

Subsurface flow

Ray et al. (1997) and Vogel et al. (2000) presented a general formulation of the theoretical flow model of Gerke and van Genuchten (1993a). The dual-permeability model divides soil bulk properties into matrix and macropore systems in the following way (Vogel et al. 2000):

$$\varepsilon = w\varepsilon_F + (1-w)\varepsilon_M \quad (35)$$

$$\theta = w\theta_F + (1-w)\theta_M \quad (36)$$

$$q = wq_F + (1-w)q_M \quad (37)$$

Flow in both soil matrix and macropore systems is described with the Richards equation. The hydraulic head H [L] is used as a state variable instead of the pressure head h [L] (e.g. Nieber and Feddes 1999):

$$\frac{\partial \theta_F}{\partial t} = \frac{\partial}{\partial x}\left(K_{FX}\frac{\partial H_F}{\partial x}\right) + \frac{\partial}{\partial y}\left(K_{FY}\frac{\partial H_F}{\partial y}\right) + \frac{\partial}{\partial z}\left(K_{FZ}\frac{\partial H_F}{\partial z}\right) - \frac{\Gamma_W}{w} \pm S_{WF} \quad (38)$$

$$\frac{\partial \theta_M}{\partial t} = \frac{\partial}{\partial x}\left(K_{MX}\frac{\partial H_M}{\partial x}\right) + \frac{\partial}{\partial y}\left(K_{MY}\frac{\partial H_M}{\partial y}\right) + \frac{\partial}{\partial z}\left(K_{MZ}\frac{\partial H_M}{\partial z}\right) + \frac{\Gamma_W}{1-w} \pm S_{WM} \quad (39)$$

where S_W [T^{-1}] is the subsurface water source/sink. The K_S values can be different in horizontal and vertical directions. The equations for Γ_W were presented in the literature review (Eqs. 25 and 26 in Section 2.2.4.1). K_A in Γ_W is calculated with the following new approach:

$$\begin{cases} K_A = 0.5(K_F + K_M), & h_F \geq h_M \\ K_A = K_M, & h_F < h_M \end{cases} \quad (40)$$

Water retention properties of soils are simulated with MVG WRC (Mualem 1976, van Genuchten 1980) in both pore systems:

$$\begin{cases} \theta = \theta_R + \dfrac{\theta_S - \theta_R}{(1 + |\alpha_{MVG} h|^{n_{MVG}})^{m_{MVG}}} \\ m_{MVG} = 1 - 1/n_{MVG} \end{cases} \quad (41)$$

where θ_R [L^3 L^{-3}] is the residual water content of the soil. K is a function of S_E:

$$K = K_S S_E^{l_{MVG}} \left[1 - \left(1 - S_E^{1/m_{MVG}}\right)^{m_{MVG}}\right]^2 \quad (42)$$

where l_{MVG} [-] is the pore connectivity parameter. S_E is calculated as follows:

$$S_E = (\theta - \theta_R)/(\theta_S - \theta_R) \quad (43)$$

Overland erosion

The overland erosion model is built around the sediment continuity equation (e.g. Taskinen and Bruen 2007b). Transport is purely advective, combined with sources and sinks:

$$\frac{\partial (h_W C)}{\partial t} + \frac{\partial (Q_X C)}{\partial x} + \frac{\partial (Q_Y C)}{\partial y} = g_R + g_H - w_S U_S C \pm s_S \quad (44)$$

where C [M L^{-3}] is the sediment concentration in the overland water, g_R [M L^{-2} T^{-1}] is the potential raindrop splash erosion rate, g_H [M L^{-2} T^{-1}] is the potential hydraulic erosion rate, w_S [-] is the coefficient for particle settling, U_S [L T^{-1}] is the particle settling velocity and s_S [M L^{-2} T^{-1}] is the overland sediment source/sink. Potential erosion rates in this context signify the maximum amount of sediment produced by the erosion processes when the transport capacity of the flow is not limiting them.

Subsurface transport of sediment

The transport of suspended sediment in the subsurface domain is simulated with a simplified dual-porosity approach. Only the macropore system transports sediment and the exchange of sediment to the matrix system is disabled. While the matrix does not store sediment, it still reserves a large, varying part of the total pore space (Eqs. 35, 36 and 45). Suspended sediment particles are treated as a solute and their dimensions are not considered in the infiltration process into macropores. Neither is sieving of sediment particles in macropores. Soil bulk properties are divided into matrix and macropore systems in the following way (Vogel et al. 2000):

$$\theta c = w\theta_F c_F + (1-w)\theta_M c_M \tag{45}$$

Sediment transport in the macropores is modelled with ADE:

$$\frac{\partial(\theta_F c_F)}{\partial t} = \frac{\partial}{\partial x}\left(\theta_F D_{FXX}\frac{\partial c_F}{\partial x}\right) + \frac{\partial}{\partial y}\left(\theta_F D_{FYY}\frac{\partial c_F}{\partial y}\right) + \frac{\partial}{\partial z}\left(\theta_F D_{FZZ}\frac{\partial c_F}{\partial z}\right) - \frac{\partial}{\partial x}(v_{FX}c_F) - \frac{\partial}{\partial y}(v_{FY}c_F) - \frac{\partial}{\partial z}(v_{FZ}c_F) \pm S_{SF} \tag{46}$$

where S_{SF} [M L^{-3} T^{-1}] is the sediment source/sink. Retardation and degradation processes were not included in the equation because sediment is treated as a non-reactive and conservative solute. Directional components of the dispersion terms for 3-D transport are as follows (Zheng and Bennet 2002):

$$D_{FXX} = \alpha_L\frac{v_{FX}^2}{|v|} + \alpha_T\frac{v_{FY}^2}{|v|} + \alpha_T\frac{v_{FZ}^2}{|v|} + D^* \tag{47}$$

$$D_{FYY} = \alpha_L\frac{v_{FY}^2}{|v|} + \alpha_T\frac{v_{FX}^2}{|v|} + \alpha_T\frac{v_{FZ}^2}{|v|} + D^* \tag{48}$$

$$D_{FZZ} = \alpha_L\frac{v_{FZ}^2}{|v|} + \alpha_T\frac{v_{FX}^2}{|v|} + \alpha_T\frac{v_{FY}^2}{|v|} + D^* \tag{49}$$

where α_L [L] is the longitudinal dispersivity, α_T [L] is the transverse dispersivity and $|v|$ [LT^{-1}] is the magnitude of the velocity vector. The cross terms (D_{FXY}, D_{FYX}, D_{FXZ}...) were assumed to be zero. Flow velocity components are calculated as follows:

$$v_{FX} = \frac{q_{FX}}{w\theta_F}, v_{FY} = \frac{q_{FY}}{w\theta_F} \text{ and } v_{FY} = \frac{q_{FZ}}{w\theta_F} \tag{50}$$

3.2 The numerical model

The numerical model is a realisation of the conceptual model and it includes all the necessary solution algorithms for the general mathematical descriptions (Section 3.1.2) and other processes delineated in the conceptual model. The objective is that the numerical model can be transferred into a computer program form with minimal effort. The design criterion of the computer program is that minimal changes are needed in the code when the model is applied to different field sites. The numerical model is comprised of a model framework and individual submodels. The framework is the backbone of the system and it is responsible for running the submodels and taking care of various other simulation related tasks such as time integration. The domains presented in the conceptual model also apply to the submodels of the numerical model. In addition, soil shrinkage and swelling and crop and tillage effects are stored into separate submodels. The individual submodels and the corresponding solution algorithms are presented next, followed by the description of the model framework.

3.2.1 Submodels

The temporal components in PDEs are solved with the forward finite difference method. The spatial components are solved with the finite volume method (FVM) (e.g. Fletcher 2005, Versteeg and Malalasekera 2007). FVM was adopted because it is relatively simple to implement and it is also suited to distorted and irregular computational grids. The field section is divided with computational grids into 2-D rectangular (overland flow and erosion) and 3-D hexahedric cells (subsurface flow and transport) (see Fig. 7). PDEs are integrated over the area or volume of the cells. The volume integrals containing divergence terms can be changed into surface integrals with the divergence theorem e.g. Kreyszig 1993). It is then possible to solve the state variables from the discretised equations. The cells are connected to each other with water and sediment flux components. The global solutions are achieved by iterating the local solutions in every cell in the grid. In Fig. 7a, a partial view of a 2-D grid is presented with generic fluxes $F_{i+0.5,j}$, $F_{i-0.5,j}$, $F_{i,j+0.5}$ and $F_{i,j-0.5}$ between cells, cell dimensions $L_{i+0.5,j}$, $L_{i-0.5,j}$ $L_{i,j+0.5}$ and $L_{i,j-0.5}$ [L] and the cell area A_{ij} [L^2] used in the numerical formulations. In Fig. 7b, a partial view of a 3-D grid is presented with generic fluxes $F_{i+0.5,j,k}$, $F_{i-0.5,j,k}$, $F_{i,j+0.5,k}$, $F_{i,j-0.5,k}$, $F_{i,j,k+0.5}$ and $F_{i,j,k-0.5}$ between cells. The plane area $A_{i,j,k-0.5}$ and the distance $L_{i+0.5,j,k}$ between adjacent cells are also presented in Fig. 7b.

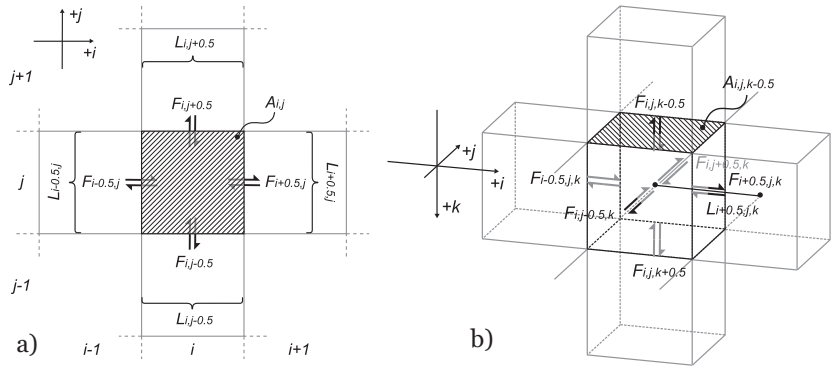

Figure 7. Partial views of the a) 2-D overland and b) 3-D subsurface computational grids and fluxes between cells.

The solution algorithms of PDEs in the submodels are comprised of three phases: 1) the preprocessing phase, where parts of the algorithm that do not change during the iteration phase are calculated, 2) the iteration of the global solution in the grid and 3) the post processing of the results. Each consecutive iteration round refines the global solution until a predefined iteration convergence criterion is fulfilled. Iteration is also stopped if the maximum number of iterations is exceeded. The iteration phase is accelerated with varying methods in each submodel. Boundary conditions and sink and sources used in the submodels are presented at the end of each submodel description. The boundary conditions function as bridges between the domains and define how the derivatives are solved at the grid boundaries. The submodels for soil shrinkage and swelling, and the effects of crop and tillage are modelled explicitly and they do not require an iterative PDE solution.

Overland flow

The implicit, discretised form of overland flow PDE is as follows (e.g. Taskinen 2002):

$$A_{i,j}\frac{h_{W,i,j}^{\eta+1}-h_{W,i,j}^{\eta}}{\Delta t}+L_{i\pm0.5,j}\left[\varsigma_{i\pm0.5,j}U_{i\pm0.5,j}^{\eta+1}h_{W,i,j}^{\eta+1}-\left(1-\varsigma_{i\pm0.5,j}\right)U_{i\pm0.5,j}^{\eta+1}h_{W,i\pm1,j}^{\eta+1}\right]+ \quad (51)$$
$$L_{i,j\pm0.5}\left[\varsigma_{i,j\pm0.5}U_{i,j\pm0.5}^{\eta+1}h_{W,i,j}^{\eta+1}-\left(1-\varsigma_{i,j\pm0.5}\right)U_{i,j\pm0.5}^{\eta+1}h_{W,i,j\pm1}^{\eta+1}\right]=A_{i,j}s_W$$

where η [-] is the simulation time step level. The ς [-] coefficients cancel out the overland flow components going in upstream directions. If water is entering the cell in i, j coordinates, ς is set to zero (Fig. 7a). Otherwise, if water is leaving the cell, ς is set to 1. The value of ς is specified for all four directions. A ± sign convention is used in Eq. 51, and all the following equations, to save space. It signifies that two opposite flux components have been integrated into one (e.g. $F_{i+0.5,j}$ and $F_{i-0.5,j}$ to $F_{i\pm0.5,j}$, see Fig. 7a).

The global solution in the grid is achieved by solving Eq. 51 in each cell in the grid and iterating until convergence criteria are met. Unfortunately, a direct solution of $h_{W,i,j}^{\eta+1}$ from Eq. 51 is not straightforward because $h_{W,i,j}^{\eta+1}$ is also present in the velocity components raised to rational exponents (1/2 and 2/3) in Eq. 33. A numerical root-finding approach called bisection method (e.g. Engeln-Müllges and Uhlig 1996) is applied here to solve $h_{W,i,j}^{\eta+1}$ from Eq. 51 (e.g Taskinen 2002) (see Fig. 8b). The method is initiated by choosing the water depth interval where the root must be residing. Eq. 51 is calculated with trial solutions of $h_{W,i,j}^{\eta+1}$ selected from the endpoints of the interval. Because the trial solutions are not (usually) the exact solutions of Eq. 51 they produce a non-zero error called residual here. Next, the current interval is halved and the residuals are compared to find out in which half of the interval the root is residing. The same process is conducted again for the new interval and repeated until the root has been found within a specified accuracy criterion (epsilon in Fig. 8b).

A flow chart of the overland flow solution algorithm is presented in Fig. 8 and it runs from left to right and from top to bottom.

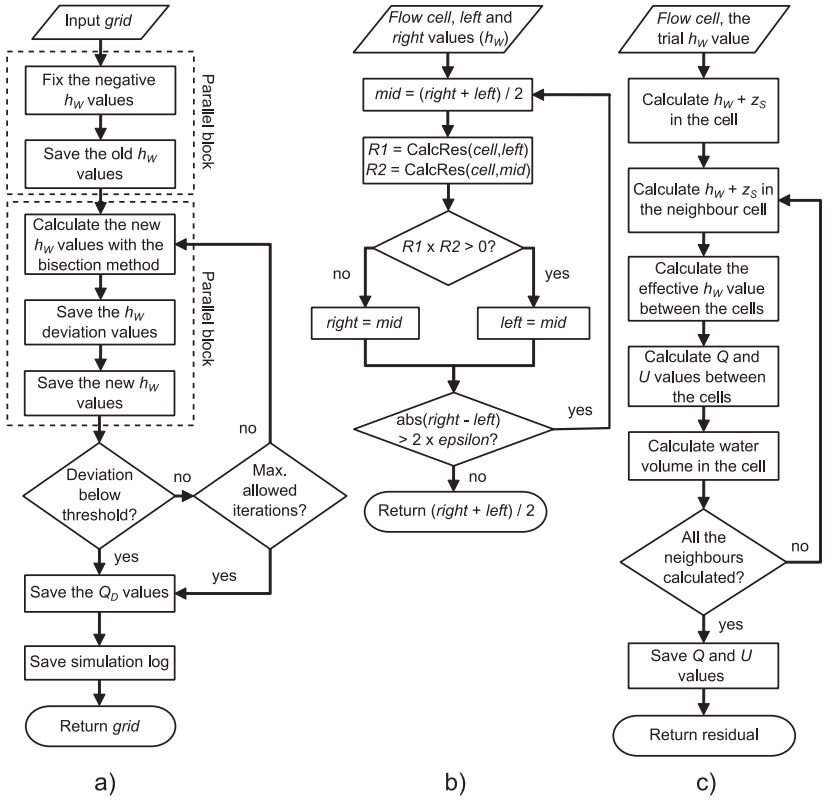

Figure 8. Flow chart of the overland flow solution algorithm divided into a) primary solution, b) bisection method and c) calcRes method parts.

The algorithm can be divided into three parts: a) the primary solution, b) the bisection method and c) the calcRes method. The primary solution part is composed of preprocess, iteration and post-process segments. Parallel blocks marked in Fig. 8 with dashed lines represent code segments that are run in parallel to accelerate the algorithm. The calcRes function (Fig. 8c) solves Eq. 51 with the given trial water depth (input from the bisection method) and returns the residual to the bisection method. The root found by the bisection method, i.e. $h_{W,i,j}^{\eta+1}$ is returned to the primary solution part of the algorithm (Fig. 8a). When iteration in the primary solution part is finished, $h_{W,i,j}^{\eta+1}$ becomes solved in each cell in the overland grid.

Cells that include open ditches function as sinks in the overland domain. Open edges can be simulated by inserting ditches parallel to the edges. The volumetric flux to ditches Q_D [L^3 T^{-1}] is calculated as a sum of fluxes F entering a cell containing a ditch segment:

$$Q_D = \sum F_{i,j} \tag{52}$$

Subsurface flow

Variables θ and h in the Richards equation have a non-linear relationship according to WRC. In order to solve the new H value, a change of variables is implemented in the original form of the Richards equation (Eqs. 38 and 39). By introducing the differential water capacity variable C_W [L^{-1}], θ is eliminated from the equations (e.g. Celia et al. 1990). Karvonen (1988) suggested an approximation of C_W as follows:

$$C_W = \frac{\theta_{i,j,k}^{\eta+1} - \theta_{i,j,k}^{\eta}}{H_{i,j,k}^{\eta+1} - H_{i,j,k}^{\eta}} \tag{53}$$

Discretised, implicit, dual-permeability flow PDEs for macropore and soil matrix systems become as follows:

$$\begin{aligned} &C_{WF,i,j,k}\frac{H_{F,i,j,k}^{\eta+1} - H_{F,i,j,k}^{\eta}}{\Delta t}V_{i,j,k} = A_{i\pm0.5,j,k}K_{FX,i\pm0.5,j,k}^{\eta+1}\left(H_{F,i\pm1,j,k}^{\eta+1} - H_{F,i,j,k}^{\eta+1}\right)/L_{i\pm1,j,k} + \\ &A_{i,j\pm0.5,k}K_{FY,i,j\pm0.5,k}^{\eta+1}\left(H_{F,i,j\pm1,k}^{\eta+1} - H_{F,i,j,k}^{\eta+1}\right)/L_{i,j\pm1,k} + \\ &A_{i,j,k\pm0.5}K_{FZ,i,j,k\pm0.5}^{\eta+1}\left(H_{F,i,j,k\pm1}^{\eta+1} - H_{F,i,j,k}^{\eta+1}\right)/L_{i,j,k\pm1} - \alpha_W\left(H_{F,i,j,k}^{\eta+1} - H_{M,i,j,k}^{\eta+1}\right)/w \end{aligned} \tag{54}$$

$$\begin{aligned} &C_{WM,i,j,k}\frac{H_{M,i,j,k}^{\eta+1} - H_{M,i,j,k}^{\eta}}{\Delta t}V_{i,j,k} = A_{i\pm0.5,j,k}K_{MX,i\pm0.5,j,k}^{\eta+1}\left(H_{M,i\pm1,j,k}^{\eta+1} - H_{M,i,j,k}^{\eta+1}\right)/L_{i\pm1,j,k} + \\ &A_{i,j\pm0.5,k}K_{MY,i,j\pm0.5,k}^{\eta+1}\left(H_{M,i,j\pm1,k}^{\eta+1} - H_{M,i,j,k}^{\eta+1}\right)/L_{i,j\pm1,k} + \\ &A_{i,j,k\pm0.5}K_{MZ,i,j,k\pm0.5}^{\eta+1}\left(H_{M,i,j,k\pm1}^{\eta+1} - H_{M,i,j,k}^{\eta+1}\right)/L_{i,j,k\pm1} + \\ &\alpha_W\left(H_{F,i,j,k}^{\eta+1} - H_{M,i,j,k}^{\eta+1}\right)/(1-w) \end{aligned} \tag{55}$$

where $V_{i,j,k}$ [L³] is the subsurface cell volume. It is possible to solve $H_{i,j,k}{}^{\eta+1}$ in both pore systems directly from Eqs. 54 and 55. The unknown hydraulic heads in Eq. 56 are presented in Fig. 9. The global solution can be derived by iterating through the individual cell solutions in the grid until convergence criteria are met. The iteration process can be accelerated substantially by solving several cells simultaneously instead of solving cells one by one (Fig. 9). The standard way of solving the Richards equation numerically is to apply the tridiagonal matrix algorithm (TDMA) (e.g. Karvonen 1988) to solve a column of cells directly. TDMA functions as a simplified Gaussian elimination algorithm that solves tridiagonal systems of equations (Kreyszig 1993). For the global solution, the columns and pore systems in the grid are iterated until convergence criteria are met.

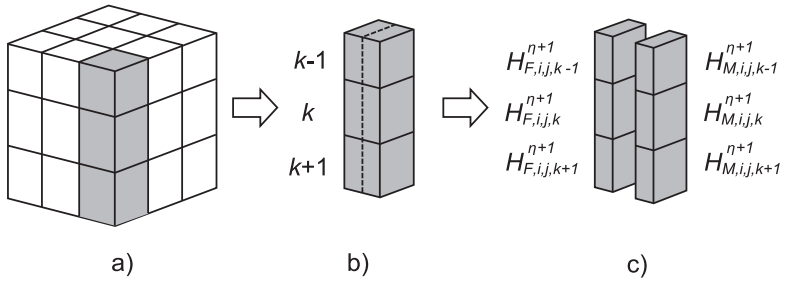

Figure 9. a) The grid, b) the cell column and c) macropore and matrix pore systems.

The iterative TDMA approach can be improved in stability and speed by solving both pore systems in a cell column directly (Fig. 9). A new method that applies the pentadiagonal matrix algorithm (PDMA) (e.g. Fletcher 2005, Engeln-Müllges and Uhlig 1996) is presented here. The function of PDMA is analogous to TDMA, but it solves a pentadiagonal system of equations instead. In order to use the PDMA approach, the variables in Eqs. 54 and 55 are organised in the following way:

$$\boldsymbol{A}_{2k-2}H^{\eta+1}_{M,i,j,k-1} + \boldsymbol{B}_{2k} \times 0 + \boldsymbol{C}_{2k}H^{\eta+1}_{M,i,j,k} + \boldsymbol{D}_{2k}H^{\eta+1}_{F,i,j,k} + \boldsymbol{E}_{2k+2}H^{\eta+1}_{M,i,j,k+1} = \boldsymbol{F}_{2k} \quad (56)$$

$$\boldsymbol{A}_{2k-1}H^{\eta+1}_{F,i,j,k-1} + \boldsymbol{B}_{2k+1}H^{\eta+1}_{M,i,j,k} + \boldsymbol{C}_{2k+1}H^{\eta+1}_{F,i,j,k} + \boldsymbol{D}_{2k+1} \times 0 + \boldsymbol{E}_{2k+3}H^{\eta+1}_{F,i,j,k+1} = \boldsymbol{F}_{2k+1}$$

where $\boldsymbol{A}$, $\boldsymbol{B}$, $\boldsymbol{C}$, $\boldsymbol{D}$, $\boldsymbol{E}$, and $\boldsymbol{F}$ are single band matrices. From this point onwards these matrices are called arrays to avoid the confusion between a mathematical matrix and matrix pore system. They are also presented as 1-D arrays in the computer program implementation. The direct solution is derived for a vertical column of cells (Fig. 9). The variables in the neighbouring columns are considered to be known at this time and the horizontal fluxes are adjusted in iteration. Eqs. 54 and 55 are broken down into terms and the terms are added to the respective arrays. All the terms that include $H_{i,j,k-1}{}^{\eta+1}$ (the cell above the current cell) are added to $\boldsymbol{A}$ while

terms that include $H_{i,j,k+1}^{\eta+1}$ (the cell below the current cell) are included in $\boldsymbol{E}$. The terms with $H_{i,j,k}^{\eta+1}$ (the current cell) are saved into $\boldsymbol{C}$. The exchange coefficient parts of the equations (last components in Eqs. 54 and 55) include the flux term from the other pore system, i.e. $H_{F,i,j,k+1}^{\eta+1}$ in the matrix case and $H_{M,i,j,k+1}^{\eta+1}$ in the macropore system case. These terms are saved into $\boldsymbol{D}$ and $\boldsymbol{B}$ in the matrix and macropore systems, respectively. $\boldsymbol{B}$ is left empty in the matrix system and $\boldsymbol{D}$ in the macropore system. All the known terms (old time step and the neighbouring column flux terms) are added to $\boldsymbol{F}$. In the computer program implementation, both pore systems are saved into the same arrays in an alternating order (e.g. matrix, macropore, matrix etc.). This is the reason why the array indices in the matrix and macropore equations differ by one in Eq. 56 (e.g. $\boldsymbol{A}_{2k\text{-}2}$ in the matrix system and $\boldsymbol{A}_{2k\text{-}1}$ in the macropore system). The variables in $\boldsymbol{A}$, $\boldsymbol{B}$, $\boldsymbol{C}$, $\boldsymbol{D}$, $\boldsymbol{E}$ and $\boldsymbol{F}$ are presented in Appendix A. A system of equations can be formed from the individual cell descriptions (Eq. 56) in a column of cells (Fig. 9c):

$$\boldsymbol{A}_{2k-4}H_{M,i,j,k-2}^{\eta+1} + \boldsymbol{B}_{2k-2} \times 0 + \boldsymbol{C}_{2k-2}H_{M,i,j,k-1}^{\eta+1} + \boldsymbol{D}_{2k-2}H_{F,i,j,k-1}^{\eta+1} + \boldsymbol{E}_{2k}H_{M,i,j,k}^{\eta+1} = \boldsymbol{F}_{2k-2} \quad (57)$$

$$\boldsymbol{A}_{2k-3}H_{F,i,j,k-2}^{\eta+1} + \boldsymbol{B}_{2k-1}H_{M,i,j,k-1}^{\eta+1} + \boldsymbol{C}_{2k-1}H_{F,i,j,k-1}^{\eta+1} + \boldsymbol{D}_{2k-1} \times 0 + \boldsymbol{E}_{2k+1}H_{F,i,j,k}^{\eta+1} = \boldsymbol{F}_{2k-1}$$

$$\boldsymbol{A}_{2k-2}H_{M,i,j,k-1}^{\eta+1} + \boldsymbol{B}_{2k} \times 0 + \boldsymbol{C}_{2k}H_{M,i,j,k}^{\eta+1} + \boldsymbol{D}_{2k}H_{F,i,j,k}^{\eta+1} + \boldsymbol{E}_{2k+2}H_{M,i,j,k+1}^{\eta+1} = \boldsymbol{F}_{2k}$$

$$\boldsymbol{A}_{2k-1}H_{F,i,j,k-1}^{\eta+1} + \boldsymbol{B}_{2k+1}H_{M,i,j,k}^{\eta+1} + \boldsymbol{C}_{2k+1}H_{F,i,j,k}^{\eta+1} + \boldsymbol{D}_{2k+1} \times 0 + \boldsymbol{E}_{2k+3}H_{F,i,j,k+1}^{\eta+1} = \boldsymbol{F}_{2k+1}$$

$$\boldsymbol{A}_{2k}H_{M,i,j,k}^{\eta+1} + \boldsymbol{B}_{2k+2} \times 0 + \boldsymbol{C}_{2k+2}H_{M,i,j,k+1}^{\eta+1} + \boldsymbol{D}_{2k+2}H_{F,i,j,k+1}^{\eta+1} + \boldsymbol{E}_{2k+4}H_{M,i,j,k+2}^{\eta+1} = \boldsymbol{F}_{2k+2}$$

$$\boldsymbol{A}_{2k+1}H_{F,i,j,k}^{\eta+1} + \boldsymbol{B}_{2k+3}H_{M,i,j,k+1}^{\eta+1} + \boldsymbol{C}_{2k+3}H_{F,i,j,k+1}^{\eta+1} + \boldsymbol{D}_{2k+3} \times 0 + \boldsymbol{E}_{2k+5}H_{F,i,j,k+2}^{\eta+1} = \boldsymbol{F}_{2k+3}$$

In the computer program implementation, the system of equations (Eq. 57) is saved into the arrays and passed into PDMA. The algorithm returns a 1-D array which contains the new hydraulic heads for the column of cells in both pore systems in the same alternating order (matrix, macropore, matrix etc.).

A flow chart of the subsurface flow solution algorithm is presented in Fig. 10. The flow chart is divided into three phases (preprocessing, iteration and post-processing). To accelerate the algorithm, parts of the fluxes (flux terms in Fig. 9) that do not change during the iteration phase are precalculated in the preprocessing phase (Fig. 10a). The flux components between cells in Eqs. 54 and 55 have to be divided with w (macropores) or 1-w (matrix) if w is changing between cells in the same pore system. This is not shown in Eqs. 54 and 55 to improve the clarity of the presentation. The computation time in the iteration phase is mostly spent in saving the multipliers of the unknown H values into the 1-D arrays and running PDMA. The successive over-relaxation (SOR) method can be used to accelerate the iteration

(Fletcher 2005). h, θ and C_W are updated after the H values have been solved in the grid during the iteration process. After the iteration phase, volumetric fluxes to sinks are saved for the subsurface transport model.

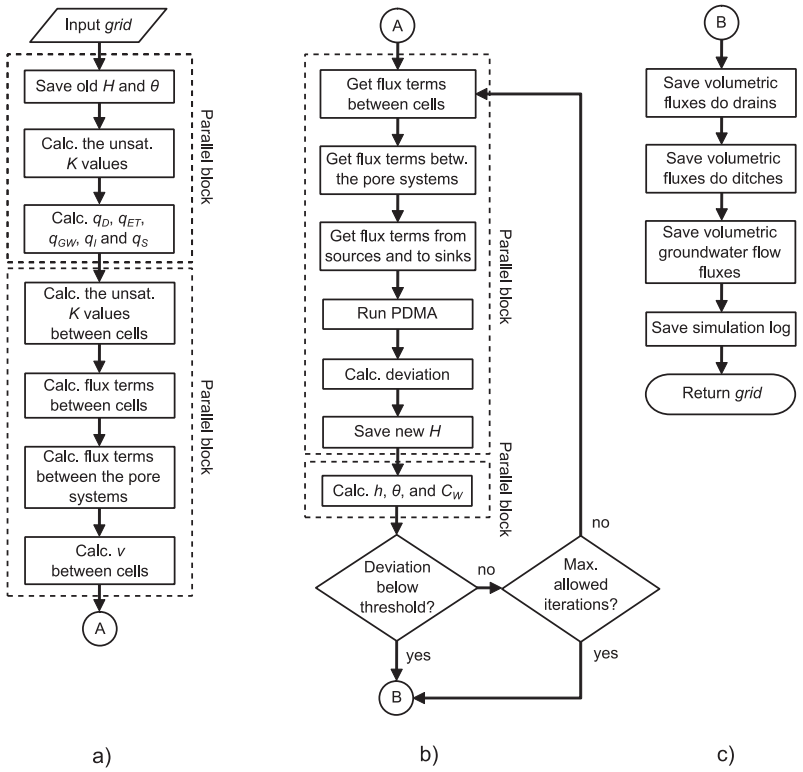

Figure 10. Flow chart of the subsurface flow solution algorithm divided into a) the preprocessing phase, b) the iteration phase and c) the post-processing phase. The algorithm continues from left to right and from top to bottom.

The subsurface flow domain contains several internal sinks (subsurface drains, ditches and ET) and boundary conditions (infiltration and groundwater flow). Sinks remove water from both matrix and macropore systems. The drains are depicted as finite, cylindrically shaped sinks in the soil:

$$q_{S,i,j,k} = K_{i,j,k} A_{S,i,j,k} \frac{H_S - H_{i,j,k}}{\Omega_S}, \; A_S = L_{S,i,j,k} 2\pi R_S \tag{58}$$

where q_S [L^3 T^{-1}] is the volumetric drain flux, A_S [L^2] is the drain surface area, H_S [L] is the hydraulic head in the drain, Ω_S [L] is the drain entrance resistance, L_S [L] is the drain length in the cell and R_S [L] is the drain radius. K is calculated as the arithmetic mean of horizontal and vertical unsaturated hydraulic conductivities. The hydraulic pressure in the drain is assumed to be equal to h_S (atmospheric pressure, h_S = 0.0 m). If H in soil

drops below the H_S [L] threshold, q_S is set to zero. The Ω_S parameter can be given a constant value or calculated with the following empirical equation:

$$\begin{cases} \Omega_S = 21.0 - 20.0h, & h < 1, \\ \Omega_S = 1.0, & h \geq 1, \end{cases} \tag{59}$$

Units in Eq. 59 are in [m]. Seepage to ditches is calculated with an analogous method:

$$q_{D,i,j,k} = K_{i,j,k} A_{D,i,j,k} \frac{H_D - H_{i,j,k}}{\Omega_D},\ A_D = L_{D,i,j,k}\left(z_{i,j,k-0.5} - z_{i,j,k+0.5}\right) \tag{60}$$

where q_D [L^3 T^{-1}] is the volumetric ditch flux, A_D [L^2] is the ditch surface area against the horizontal flux, H_D [L] is the hydraulic head in the ditch, Ω_D [L] is the ditch entrance resistance, L_D [L] is the ditch length and z [L] is the vertical position. The Ω_D parameter is set by default to one quarter of the horizontal length of a cell. The cell height in Eq. 60 is calculated from the vertical positions (z) of the top and bottom planes of the cell. K is deduced in the same way as in Eq. 58. The ditch functions as a sink only when H in the surrounding soils is higher than in the ditch. Otherwise q_D is set to zero. The groundwater flow flux q_{GW} [L^3 T^{-1}] is presented as follows for the four horizontal directions:

$$q_{GWX,i\pm0.5,j,k} = K_{i,j,k} A_{i\pm0.5,j,k} \frac{z_{i,j,k} - z_{i\mp0.5,j,k}}{L_{i\mp0.5,j,k}} \tag{61}$$

$$q_{GWY,i,j\pm0.5,k} = K_{i,j,k} A_{i,j\pm0.5,k} \frac{z_{i,j,k} - z_{i,j\mp0.5,k}}{L_{i,j\mp0.5,k}}$$

The gradient is calculated between the two outermost cells at the grid boundary and only elevation heads are used to estimate the hydraulic gradient. K in Eq. 61 is set to the horizontal conductivity value of the soil. Additional water is not allowed to enter the grid, i.e. if water is entering the grid, q_{GW} is set to zero. Volumetric actual ET flux is solved as follows:

$$q_{ET,i,j,k-0.5} = A_{i,j,k-0.5} \alpha_{F,i,j,k} R_{i,j,k} PET \tag{62}$$

The α_F is calculated with the method of Feddes et al. (1978) presented in the literature review (Fig. 1). Infiltration from the overland domain is calculated as a flux between the overland and subsurface cells:

$$q_{I,i,j,0.5} = K_{i,j,1} A_{i,j,0.5} \frac{h_{W,TOT,i,j} - h_{i,j,1}}{\left(z_{i,j,0.5} - z_{i,j,1}\right)} \tag{63}$$

where K is set to the vertical hydraulic conductivity value of the pore system. In the matrix system, K is always set to the saturated value. In the macropore system, K is set to the saturated value if the overland water depth is above $h_{W,THR}$ (Eq. 30). q_I is explicitly solved in the preprocessing

phase and adjusted before the iteration phase in the following way. If the infiltration volume during a time step is higher than the volume of water in the overland cell, the flux is reduced to accommodate this. Conversely, if the empty pore space in the soil is less than the infiltration volume the flux is reduced accordingly. These precautions are taken to reduce mass balance errors and to prevent over-saturation of the subsurface flow cells.

Groundwater levels during a simulation are specified by inspecting cell columns in the grid from bottom to top, until an unsaturated cell is found. The groundwater level inside the unsaturated cell is specified with linear interpolation. The levels are defined separately for the soil matrix and macropore systems.

Overland erosion

The implicit, discretised form of overland erosion PDE is as follows (e.g. Taskinen 2002):

$$A_{i,j}\frac{\frac{C_{i,j}^{\eta+1}+C_{i,j}^{\eta}}{2}\frac{h_{W,i,j}^{\eta+1}-h_{W,i,j}^{\eta}}{\Delta t}+A_{i,j}\frac{\frac{h_{W,i,j}^{\eta+1}+h_{W,i,j}^{\eta}}{2}\frac{C_{i,j}^{\eta+1}-C_{i,j}^{\eta}}{\Delta t}+}{} \tag{64}$$

$$L_{i\pm0.5,j}\frac{\frac{C_{i,j}^{\eta+1}+C_{i\pm1,j}^{\eta+1}}{2}\left[\varsigma_{i\pm0.5,j}U_{X,i\pm0.5,j}^{\eta+1}h_{W,i,j}^{\eta+1}-\left(1-\varsigma_{i\pm0.5,j}\right)U_{X,i\pm0.5,j}^{\eta+1}h_{W,i\pm1,j}^{\eta+1}\right]+}{}$$

$$L_{i\pm0.5,j}\frac{\frac{\varsigma_{i\pm0.5,j}U_{X,i\pm0.5,j}^{\eta+1}h_{W,i,j}^{\eta+1}-\left(1-\varsigma_{i\pm0.5,j}\right)U_{X,i\pm0.5,j}^{\eta+1}h_{W,i\pm1,j}^{\eta+1}}{2}\left(C_{i,j}^{\eta+1}-C_{i\pm1,j}^{\eta+1}\right)+}{}$$

$$L_{i,j\pm0.5}\frac{\frac{C_{i,j}^{\eta+1}+C_{i,j\pm1}^{\eta+1}}{2}\left[\varsigma_{i,j\pm0.5}U_{Y,i,j\pm0.5}^{\eta+1}h_{W,i,j}^{\eta+1}-\left(1-\varsigma_{i,j\pm0.5}\right)U_{Y,i,j\pm0.5}^{\eta+1}h_{W,i,j\pm1}^{\eta+1}\right]+}{}$$

$$L_{i,j\pm0.5}\frac{\frac{\varsigma_{i,j\pm0.5}U_{Y,i,j\pm0.5}^{\eta+1}h_{W,i,j}^{\eta+1}-\left(1-\varsigma_{i,j\pm0.5}\right)U_{Y,i,j\pm0.5}^{\eta+1}h_{W,i,j\pm1}^{\eta+1}}{2}\left(C_{i,j}^{\eta+1}-C_{i,j\pm1}^{\eta+1}\right)=}{}$$

$$A_{i,j}g_{R,i,j}^{\eta+1}+A_{i,j}g_{H,i,j}^{\eta+1}-A_{i,j}w_S U_{S,i,j}^{\eta+1}C_{i,j}^{\eta+1}-s_S A_{i,j}C_{i,j}^{\eta+1}$$

$C_{i,j}^{\eta+1}$ can be solved directly from Eq. 64:

$$C_{i,j}^{\eta+1}=\left[L_{i\pm0.5,j}C_{i\pm1,j}^{\eta+1}\left(1-\varsigma_{i\pm0.5,j}\right)U_{X,i\pm0.5,j}^{\eta+1}h_{W,i\pm1,j}^{\eta+1}+L_{i,j\pm0.5}C_{i,j\pm1}^{\eta+1}\left(1-\right.\right. \tag{65}$$

$$\left.\left.\varsigma_{i,j\pm0.5}\right)U_{Y,i,j\pm0.5}^{\eta+1}h_{W,i,j\pm1}^{\eta+1}+A_{i,j}\frac{C_{i,j}^{\eta}h_{W,i,j}^{\eta}}{\Delta t}+A_{i,j}g_{R,i,j}^{\eta+1}+A_{i,j}g_{H,i,j}^{\eta+1}\right]/$$

$$\left(\varsigma_{i\pm0.5,j}U_{X,i\pm0.5,j}^{\eta+1}h_{W,i,j}^{\eta+1}+\varsigma_{i,j\pm0.5}U_{Y,i,j\pm0.5}^{\eta+1}h_{W,i,j}^{\eta+1}+A_{i,j}\frac{h_{W,i,j}^{\eta+1}}{\Delta t}+A_{i,j}w_S U_{S,i,j}^{\eta+1}+s_S A_{i,j}\right)$$

A flow chart of the overland erosion solution algorithm is presented in Fig. 11. Sediment mass in the overland domain is converted into a solute concentration at the preprocessing phase and back to mass at the post-processing phase to maintain mass balance outside the algorithm. Transport capacity of the overland flow and potential hydraulic and rain drop splash erosion rates are calculated in the preprocessing phase with the overland flow velocity and water depth results. To identify whether net erosion occurred in a cell and which process introduced the sediment into the cell, a following approach is adopted. In the iteration phase (Fig. 11b),

Eq. 65 is initially solved in two parts: 1) the numerator and 2) the denominator. It is then possible to add equation coefficients into one or the other (numerator or denominator) and recalculate $C_{i,j}^{\eta+1}$ without noticeable increase in the computational load. $C_{i,j}^{\eta+1}$ is calculated three times in each cell: 1) after fluxes between neighboring cells and to ditches, 2) after hydraulic erosion and 3) after rain drop splash erosion results have been added (Fig. 11b). After each time, the resulting concentration is compared to the transport capacity of the flow to determine if more sediment can be introduced into the cell.

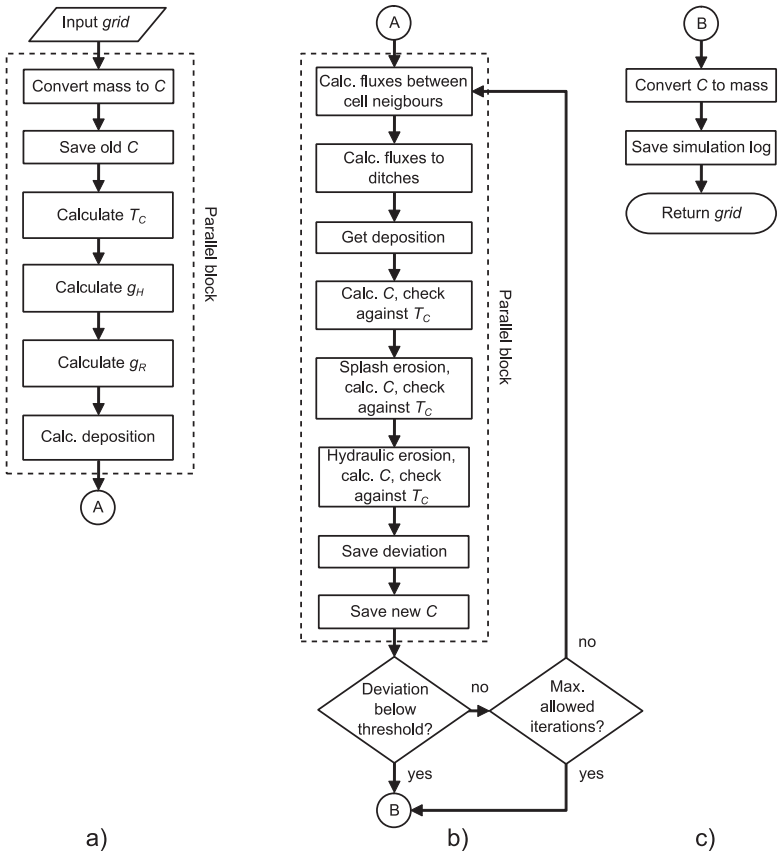

Figure 11. Flow chart of the overland erosion solution algorithm divided into a) the preprocessing phase, b) the iteration phase and c) the post-processing phase. The algorithm continues from left to right and from top to bottom.

The overland erosion submodel includes several sink and source processes. The sediment flux into a ditch is calculated by multiplying the volumetric water flux to the ditch (Eq. 52) with the sediment concentration in the cell. The rain drop splash erosion description is derived from the SHESED model, without the leaf drip component (Wicks and Bathurst 1996):

$$g_{R,i,j} = k_{R,i,j} F_{W,i,j} \left(1 - C_{G,i,j}\right)\left(1 - C_{C,i,j}\right) M_R \quad (66)$$

where k_R [M^{-1} L^{-2} T^2] is the raindrop splash soil erodibility coefficient, F_W [-] is the overland water depth correction factor, C_G [-] is the proportion of soil covered by ground cover, C_C [-] is the proportion of soil covered by canopy cover and M_R [M^2 T^{-3}] is the momentum squared for rain. F_W is calculated with the following method:

$$\begin{cases} F_{W,i,j} = \exp(1 - h_W / D_R), & h_W > D_R \\ F_{W,i,j} = 1, & h_W \leq D_R \end{cases} \quad (67)$$

where D_R [L] is the median raindrop diameter. D_R in turn is determined from the Laws and Parsons (1943) equation:

$$D_R = 0.00124\, I^{0.182} \quad (68)$$

where I is the rainfall intensity. The unit of I is in [mm h^{-1}] and D_R in [m]. M_R is calculated as follows:

$$M_R = \alpha_R I^{\beta_R} \quad (69)$$

where α_R and β_R [-] are empirical coefficients. They are defined according to the value of I (Table 3).

Table 3. Parameters for the relationship between momentum squared and rainfall intensity (Wicks and Bathurst 1996).

Rainfall intensity, I [mm h^{-1}]:	α_R [-]:	β_R [-]:
I < 10	2.69 × 10^{-8}	1.6896
10 ≤ I < 50	3.75 × 10^{-8}	1.5545
50 ≤ I < 100	6.12 × 10^{-8}	1.4242
100 ≤ I < 250	11.75 × 10^{-8}	1.2821

g_H is calculated as follows (Taskinen 2002):

$$\begin{cases} g_{H,i,j} = k_{H,i,j} \left(\dfrac{\tau_{i,j}}{\tau_C} - 1\right)^{\kappa}, & \tau_{i,j} > \tau_C \\ g_{H,i,j} = 0, & \tau_{i,j} \leq \tau_C \end{cases} \quad (70)$$

where k_H [M L^{-2} T^{-1}] is the overland flow erodibility coefficient, τ [M T^{-2} L^{-1}] is the shear stress of the overland flow, τ_C [M T^{-2} L^{-1}] is the critical shear stress defined by the Shields diagram and κ is a fitting exponent. The Shields diagram was originally designed for channel erosion but it is also applied in overland erosion studies (e.g. Taskinen 2007b). τ is calculated as follows (Taskinen 2002):

$$\tau_{i,j} = \rho_W g h_{W,i,j} S_{OA,i,j} \quad (71)$$

where S_{OA} [-] is the average slope of the overland water surface. S_{OA} is calculated as follows:

$$S_{OA,i,j} = \sqrt{S_{OX,i,j}^2 + S_{OY,i,j}^2} \tag{72}$$

τ_C is defined with the modified Shields method for small particles proposed by Mantz (1977) and further improved by Yalin (1977). The ordinate of the Shields diagram Y_{CR} [-] is as follows:

$$\begin{cases} Y_{CR} = \left(\frac{\psi}{\sqrt{\Xi}}\right)^{2/3}, & \sqrt{\Xi} < 10 \\ Y_{CR} = 0, & \sqrt{\Xi} \geq 10 \end{cases} \tag{73}$$

where ψ [-] is a constant and its value is 0.142. The value of Ξ [-] is determined as follows:

$$\Xi = \frac{\gamma_S D_S^3}{\rho_W \upsilon^2} \tag{74}$$

where γ_S [M L^{-2} T^{-2}] is the specific weight of sediment in fluid, D_S [L] is the mean particle diameter and υ [L^2 T^{-1}] is the kinematic viscosity of water. Parameters γ_S and τ_C are defined as follows (e.g. Taskinen 2002):

$$\gamma_S = g(\rho_s - \rho_W) \tag{75}$$

$$\tau_C = Y_{CR}\gamma_S D_S \tag{76}$$

where ρ_S [M L^{-3}] is the sediment particle density. The second to last term on the right hand side of the sediment continuity equation (Eq. 44) represents suspended particles falling back to the field surface due to gravity. U_S can be calculated with the Stokes law:

$$U_S = \frac{D_S^2 g(S_G - 1)}{18\upsilon} \tag{77}$$

where S_G [-] is the sediment specific gravity in water, i.e. sediment particle density divided by water density. During precipitation turbulent mixing caused by raindrops cancels deposition and U_S is set to zero (Taskinen 2002). Taskinen (2002) noted that Eq. 77 is strictly valid only up to Reynolds number Re [-] of 0.5. Re is calculated as follows:

$$Re = U_S D_S/\upsilon \tag{78}$$

The transport capacity of the flow T_C [ppm] limits potential rain drop splash and hydraulic erosion and it is based here on the Yalins equation (Yalin 1963):

$$T_{C,i,j} = \frac{6.35 \times 10^5 \delta S_G D_S U_{SH,i,j}}{U_{R,i,j} h_{W,i,j}} \left[1 - \frac{1}{a_Y \delta_{i,j}} \ln\left(1 + a_Y \delta_{i,j}\right)\right] \tag{79}$$

where U_{SH} [L T^{-1}] is the overland shear velocity, U_R [L T^{-1}] is the overland resultant flow velocity and a_Y [-] and δ [-] are parameters. U_{SH} and U_R are calculated as follows:

$$U_{SH,i,j} = \sqrt{g h_{W,i,j} S_{OA,i,j}} \tag{80}$$

$$U_{R,i,j} = \sqrt{U_{X,i,j}^2 + U_{Y,i,j}^2} \tag{81}$$

Parameters δ and a_Y are defined as follows:

$$\begin{cases} \delta_{i,j} = \dfrac{Y_{i,j}}{Y_{CR}} - 1, & Y_{i,j} > Y_{CR} \\ \delta_{i,j} = 0, & Y_{i,j} \leq Y_{CR} \end{cases} \tag{82}$$

$$a_Y = 2.45 Y_{CR}^{0.5} S_G^{-0.4} \tag{83}$$

Parameter Y [-] is determined from the following equation:

$$Y_{i,j} = \frac{U_{SH,i,j}^2}{(S_G - 1) g D_S} \tag{84}$$

A possibility was also included in the model to set a minimum value for T_C in standing water.

Subsurface transport in macropores

The implicit, discretised form of subsurface transport PDE is as follows:

$$\begin{aligned} & V_{i,j,k} \frac{\theta_{F,i,j,k}^{\eta+1} c_{F,i,j,k}^{\eta+1} - \theta_{F,i,j,k}^{\eta} c_{F,i,j,k}^{\eta}}{\Delta t} = \\ & A_{i\pm0.5,j,k} \theta_{F,i\pm0.5,j,k}^{\eta+1} D_{FXX,i\pm0.5,j,k}^{\eta+1} \left(c_{F,i\pm1,j,k}^{\eta+1} - c_{F,i,j,k}^{\eta+1}\right) / L_{i\pm1,j,k} + \\ & A_{i,j\pm0.5,k} \theta_{F,i,j\pm0.5,k}^{\eta+1} D_{FYY,i,j\pm0.5,k}^{\eta+1} \left(c_{F,i,j\pm1,k}^{\eta+1} - c_{F,i,j,k}^{\eta+1}\right) / L_{i,j\pm1,k} + \\ & A_{i,j,k\pm0.5} \theta_{F,i,j,k\pm0.5}^{\eta+1} D_{FZZ,i,j,k\pm0.5}^{\eta+1} \left(c_{F,i,j,k\pm1}^{\eta+1} - c_{F,i,j,k}^{\eta+1}\right) / L_{i,j,k\pm1} - \\ & A_{i\pm0.5,j,k} \left[\zeta_{F,i\pm0.5,j,k} v_{FX,i\pm0.5,j,k}^{\eta+1} c_{F,i,j,k}^{\eta+1} - \left(1 - \zeta_{F,i\pm0.5,j,k}\right) v_{FX,i\pm0.5,j,k}^{\eta+1} c_{F,i\pm1,j,k}^{\eta+1}\right] - \\ & A_{i,j\pm0.5,k} \left[\zeta_{F,i,j\pm0.5,k} v_{FY,i,j\pm0.5,k}^{\eta+1} c_{F,i,j,k}^{\eta+1} - \left(1 - \zeta_{F,i,j\pm0.5,k}\right) v_{FY,i,j\pm0.5,k}^{\eta+1} c_{F,i,j\pm1,k}^{\eta+1}\right] - \\ & A_{i,j,k\pm0.5} \left[\zeta_{F,i,j,k\pm0.5} v_{FZ,i,j,k\pm0.5}^{\eta+1} c_{F,i,j,k}^{\eta+1} - \left(1 - \zeta_{F,i,j,k\pm0.5}\right) v_{FZ,i,j,k\pm0.5}^{\eta+1} c_{F,i,j,k\pm1}^{\eta+1}\right] \end{aligned} \tag{85}$$

The ζ [-] variables cancel out the advective components going against the water pressure gradient between the cells. When water is flowing into the cell in i, j and k coordinates (Fig. 7b), ζ is set to zero while in the opposite case it is set to 1. The ζ variables are specified for all six directions. In this approach, absolute values of v are used. Iteration in the solution algorithm is accelerated with TDMA. Similarly to PDMA applied in the subsurface flow submodel, the variables in Eq. 85 have to be organised in a specific

way. Multipliers of $c_{F,i,j,k-1}{}^{\eta+1}$, $c_{F,i,j,k}{}^{\eta+1}$ and $c_{F,i,j,k+1}{}^{\eta+1}$ in Eq. 85 are saved into 1-D arrays $\boldsymbol{A}$, $\boldsymbol{B}$ and $\boldsymbol{C}$ and the known terms are saved into $\boldsymbol{D}$.

$$\boldsymbol{A}c_{F,i,j,k-1}^{\eta+1} + \boldsymbol{B}c_{F,i,j,k}^{\eta+1} + \boldsymbol{C}c_{F,i,j,k+1}^{\eta+1} = \boldsymbol{D} \tag{86}$$

The terms in $\boldsymbol{A}$, $\boldsymbol{B}$, $\boldsymbol{C}$ and $\boldsymbol{D}$ are presented in Appendix B. A system of equations can be assembled from the descriptions of the individual cells (Eq. 86) in a cell column (Fig. 9) and presented compactly in an array form:

$$\begin{bmatrix} \boldsymbol{B}_{k-1} & \boldsymbol{C}_{k-1} & 0 \\ \boldsymbol{A}_k & \boldsymbol{B}_k & \boldsymbol{C}_k \\ 0 & \boldsymbol{A}_{k+1} & \boldsymbol{B}_{k+1} \end{bmatrix} \begin{bmatrix} c_{F,i,j,k-1}^{\eta+1} \\ c_{F,i,j,k}^{\eta+1} \\ c_{F,i,j,k+1}^{\eta+1} \end{bmatrix} = \begin{bmatrix} \boldsymbol{D}_{i,j,k-1} \\ \boldsymbol{D}_{i,j,k} \\ \boldsymbol{D}_{i,j,k+1} \end{bmatrix} \tag{87}$$

The arrays are then passed into TDMA, which returns an array with the new concentration values for the column of cells.

A flow chart of the subsurface transport solution algorithm is presented in Fig. 12. Similarly to the overland erosion submodel, sediment is treated as mass outside the algorithm, converted into solute concentration in the preprocessing phase (Fig. 12a) and back to mass in the post-processing phase (Fig. 12c).

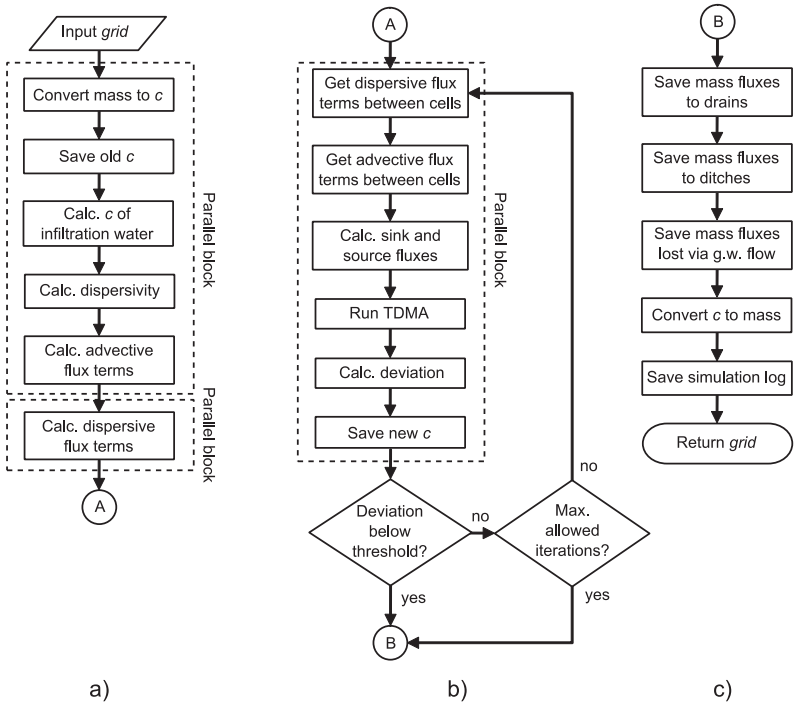

Figure 12. Flow chart of the subsurface transport solution algorithm divided into a) the preprocessing phase, b) the iteration phase and c) the post-processing phase. The algorithm continues from left to right and from top to bottom.

The approach minimises the sediment mass balance error caused by dynamic macroporosity changes due to tillage and soil shrinkage and swelling processes. Otherwise the algorithm functions similarly to the subsurface flow solution algorithm (Section 3.2.1.2).

The advective and dispersive flux terms are precalculated in the preprocessing phase to accelerate the algorithm in the iteration phase (Fig. 12a). However, new concentration values are included in the fluxes in the iteration phase. The advection components are also solved implicitly to ensure the stability of the algorithm. This can lead to severe numerical dispersion when long time steps are used during fast preferential transport events. However, suspended sediment is produced in the overland domain by erosive processes in a diffuse manner and not in sharp fronts, making the problem less critical. Transport of sediment is restricted to the volume between the field surface and subsurface drains. This is achieved in the model by calculating the solution only in the cells located above the drains and forcing the influxes and outfluxes at the domain border to zero. Iteration is accelerated with TDMA presented above. After the iteration phase, sediment mass fluxes to sinks are saved for inspection.

Sediment sinks, sources and boundary conditions in the subsurface transport domain are bound to the corresponding processes in the subsurface flow domain. The sediment mass introduced into a transport cell via infiltration is calculated by multiplying q_I (Eq. 63) with the sediment concentration in the overland erosion cell. The sediment fluxes to ditches, subsurface drains and groundwater flow are calculated by multiplying the corresponding volumetric water fluxes (Eqs. 60, 58 and 61) with the sediment concentrations in the subsurface transport cells.

Soil shrinkage and swelling

Soil shrinkage and swelling processes are simulated by changing macroporosity of the subsurface cells according to the moisture state of the matrix cells. Drying of the matrix pore system increases the volumetric fraction of the macropore system (w), while wetting does the reverse. While there is no hysteresis effect in the shrinkage and swelling processes, anisotropic water exchange creates hysteresis in the moisture flow between the pore systems (Eq. 40). The soil shrinkage and swelling model by Kroes et al. (2008) (Eqs. 88–92) and SSCC by Kim et al. (1992) (Eq. 3) are adopted here. The dynamic crack volume V_{DY} [L^3 L^{-3}] is calculated from overall and vertical shrinkage as follows:

$$V_{DY} = V_{SH} - V_{SU} \tag{88}$$

where V_{SH} [L^3 L^{-3}] is the volume fraction of overall matrix shrinkage and V_{SU} [L^3 L^{-3}] is the volume fraction of subsidence shrinkage. The correction to V_{DY} when ignoring vertical changes to soil matrix profile is as follows:

$$V_{DY} = \frac{V_{SH} - V_{SU}}{1 - V_{SU}} \tag{89}$$

When static macropores V_{ST} [L^3 L^{-3}] are present, the horizontal area fraction of the matrix equals $1 - V_{ST}$. The V_{DY} parameter is then calculated as follows:

$$V_{DY} = (1 - V_{ST})\frac{V_{SH} - V_{SU}}{1 - V_{SU}} \tag{90}$$

The vertical shrinkage component is determined from the overall matrix shrinkage:

$$V_{SU} = 1 - (1 - V_{SH})^{1/r_S} \tag{91}$$

V_{SH} is equal to the fraction of volume loss in the soil matrix which in turn equals the fraction loss of pore volume:

$$V_{SH} = -\Delta V_M = -\Delta V_P = -\Delta e V_{SOL} = -(e - e_S)V_{SOL} \tag{92}$$

where V_M [L^3 L^{-3}] is the soil matrix volume fraction and V_P [L^3 L^{-3}] is the pore volume fraction. Eq. 90 is adopted to calculate V_{DY} because vertical changes of the soil profile are ignored in the model and there are static macropores present (e.g. earth worm holes and crop root tunnels). The r_S parameter is set to a constant value of 3.0 to reflect 3-D isotropic shrinkage (Kroes et al. 2008).

A flow chart of the soil shrinkage and swelling solution algorithm is presented in Fig. 13. Geometry of the macropores (e.g. shape, diameter, tortuosity and connectivity) can have a big impact on the hydraulic properties of the macropore network. Unfortunately, there are little data on the effects of different macropore structures on hydraulic conductivity. In the model, saturated hydraulic conductivity of the macropore system is directly proportional to the macroporosity of soil:

$$K_{FS} = wK_{FS,MUL} \tag{93}$$

where $K_{FS,MUL}$ [L T^{-1}] is the macropore saturated hydraulic conductivity multiplier. This is a reasonable assumption because the dynamic macropore volume is presumed to consist of cracks and they transform primarily along one axis during shrinkage or swelling. A similar approach was used previously by Messing and Jarvis (1990) and in the MACRO model (e.g. Larsbo and Jarvis 2003).

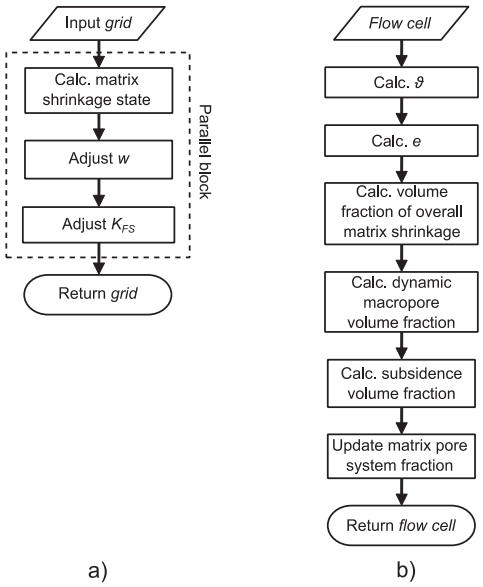

Figure 13. Flow chart of the soil shrinkage and swelling submodel divided into a) the primary solution and b) the matrix shrinkage state method.

Cropping and tillage effects

The cropping and tillage effects submodel changes the properties of different subareas of the field over time to simulate crop growth and effects of tillage operations. Several parameters can be modified at predefined points in time in the overland domain including the Manning's coefficient (Eq. 33), the overland flow threshold water depth (Eq. 30) and the overland flow and raindrop splash erodibility coefficients (Eqs. 70 and 66).

In the subsurface domain, root growth of crops can be represented by listing root depths at predefined points in time. The model will linearly interpolate the depths between these points. The distribution of root mass between field surface and maximum root depth is calculated with a linearly decreasing function (linear with depth from surface). The root distribution is the same in both pore systems. The static macroporosity values can be changed to a predefined tillage depth at different points in time to simulate the change of macroporosity due to tillage.

3.2.2 The model framework

The model framework is responsible for creating the computational grid, running the submodels and taking care of time integration and various bookkeeping tasks. The framework can be divided into three parts: 1) the preprocessing phase, 2) the simulation phase and 3) the post-processing phase. A flow chart of the framework is presented in Fig. 14. In the preprocessing phase, data files are loaded and the computational grid is

generated. The total simulation time is divided into global time steps that are further divided into local submodel time steps. Each submodel algorithm presented earlier simulates one local time step at a time. Precipitation is applied to the grid in a separate process (Fig. 14b), rather than in the overland flow submodel, to make it possible to run submodels separately. After each global time step, groundwater table levels and mass balances are updated in the grid. After all the global time steps have been calculated, the simulation is over and the results are saved to disk.

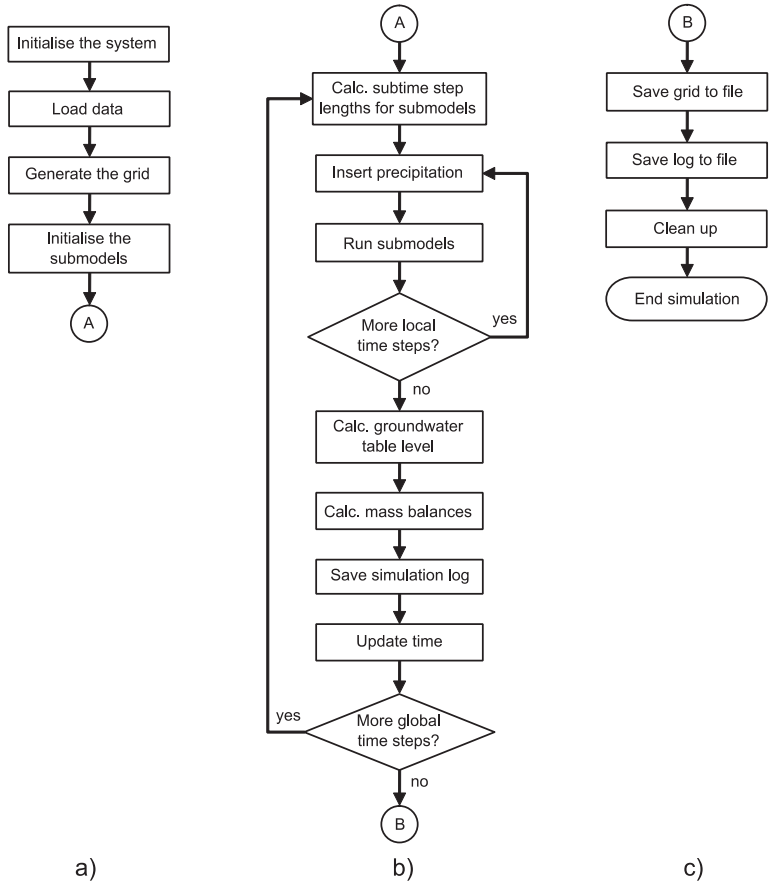

Figure 14. Flow chart of the model framework divided into a) the preprocessing phase, b) the simulation phase and c) the post-processing phase. The algorithm continues from left to right and from top to bottom.

The time stepping system

A custom time stepping system was derived to divide global time steps into local time steps for each submodel. A global time step is partitioned into local time steps with the following exponential formula:

$$\Delta t = \frac{\Delta t_{MAX}}{2^{\chi}} \tag{94}$$

where Δt [T] is the local time step, Δt_{MAX} [T] is the global time step and χ [-] is the time step level. The maximum number of Δt:s is 1024 (χ = 10) and the minimum is one (χ = 0). With a one hour Δt_{MAX} the χ values of 10 and 0 translate into 3.5 s and 1 hour, respectively. With this approach, the submodels using different values of Δt:s will automatically synchronise at the multiples of Δt_{MAX}. Each Δt_{MAX} is stepped through with the minimum time step (χ = 10) in the framework. The number of local time steps in a Δt_{MAX} as a function of χ is presented in Fig 15a. An example simulation with different local time steps within a Δt_{MAX} is shown in Fig. 15b.

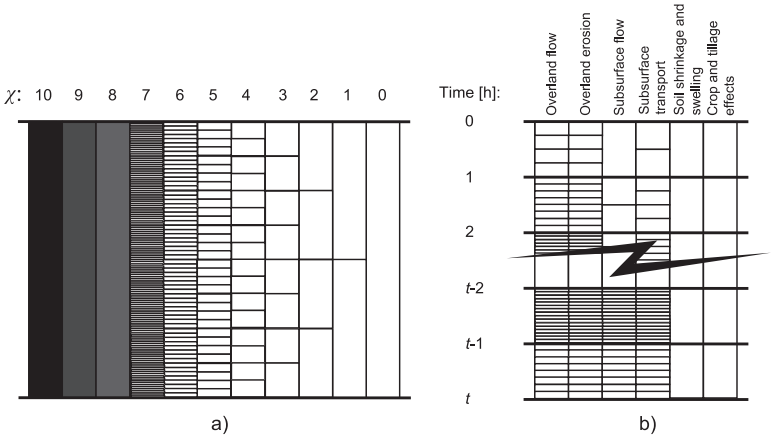

Figure 15. a) Division of local time steps in a global time step as a function of χ and b) submodels with different local time steps within global time steps. Between global time steps *t*-2 and *t*-1 a rainstorm passes the study area in the model and the local times steps in the submodels are set to the minimum value.

When the cumulative time within Δt_{MAX} coincides with Δt of a submodel, the model is run. Even though they are still run sequentially, the system maximises the parallel operation of the submodels. Precipitation is inserted into the grid always with the minimum Δt or with the maximum χ value of 10. Because all the dynamic solution algorithms are implicit, the usual Δt constraints concerning explicit solution approaches do not apply (e.g. Courant–Friedrichs–Lewy condition)(e.g. Fletcher 2005). In order to produce realistic results, small values of Δt are still needed during rapid flow events.

The χ values are changed at the beginning of each Δt_{MAX} with a set of rules that were derived experimentally with the numerical model. Similar systems are used, e.g. in the SWAP model (e.g. Kroes et al. 2008) and in the HYDRUS model (e.g. Šimůnek et al. 2006). The submodels for soil shrinkage and swelling and crop and tillage effects are always run with χ

values of zero, i.e. with the value of Δt_{MAX}. The value of χ in the submodels is adjusted according to the following rules:

Increase χ by 2 if:

- It is raining.
- The maximum number of iterations was reached by the submodel during the last Δt_{MAX}.
- The value of h_W is above zero (water level is above $h_{W,THR}$) in any cell in the overland grid (this rule concerns only the overland flow and erosion submodels).

Decrease χ by 2 if:

- None of the rules above apply.

The value of χ has lower and upper limits of 0 and 10, respectively. In addition to the criteria shown above, two special rules are included. 1) Overland erosion and subsurface transport models always operate with the same or higher value of χ than the corresponding flow model. 2) In case of a rainstorm event, the χ is set to the maximum value of 10 for overland flow and erosion and subsurface flow and transport submodels (Fig 15b). The threshold precipitation intensity corresponding to a rainstorm event is prescribed by the modeller.

The automatic grid generation system

An automatic grid generation system (AGGS) was developed to generate grids with different resolutions for the numerical model. The primary purpose of AGGS is to assist in finding the minimum resolution at which the results from the numerical model are resolution independent. After this point is found, it is not necessary to use higher resolution grids in the simulation, which saves computational resources. AGGS produces structured 3-D grids according to the specified settings and provided data. The grid cells are square shaped in the horizontal plane but their thicknesses can vary arbitrarily. However, the discretisation of the vertical profile has to be the same everywhere in the grid. Field sections with complex shapes can be represented with structured grids by applying area masks to identify and group active and inactive cells. The computational load is not increased by the inactive cells although they consume additional memory. A set of spatial input data is presented in Fig. 16a as an example. Several grids with different resolutions generated from the data are presented in Fig. 16b. Theoretical tests are conducted with the grids later in this section.

Areas (active field area, cropping and tillage areas and soil profile areas) and drainage lines (ditches and subsurface drains) are inputted into the system as vector data. Separate sets of ditch data are used for the overland and subsurface domains because it is possible that there are embankments built along ditches to direct overland flow to certain discharge points in the field. On the other hand, subsurface seepage into ditches is not hindered by the embankments. Digital elevation models (DEM) are represented as raster data and soil data, soil layer properties and general settings are saved as tabular data.

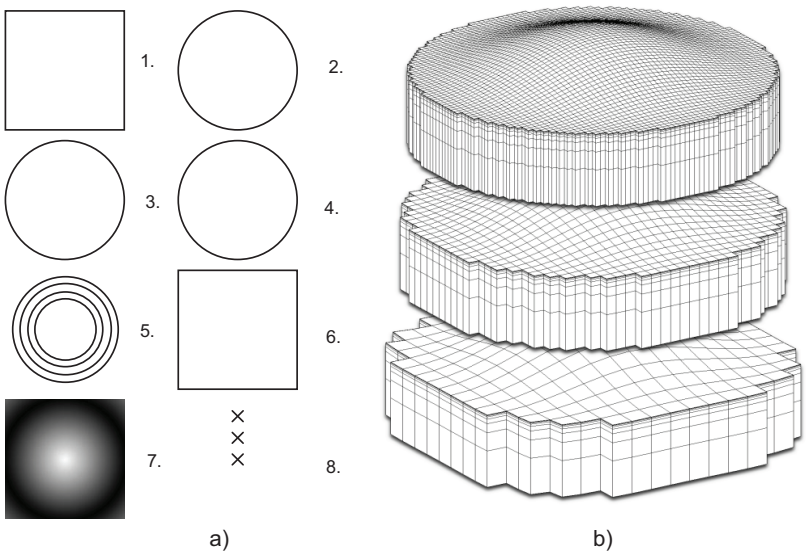

Figure 16. a) Geometry data used by AGGS (1. tillage areas, 2. active field areas, 3. ditches (not embanked), 4. ditches, 5. subsurface drains (concentric circles), 6. soil profile areas, 7. DEM and 8. groundwater table level measurement tube positions) and b) three different resolution grids generated by the system.

A flow chart of AGGS is presented in Fig. 17. First, a structured 3-D grid is created to the specified coordinates. Three types of algorithms are applied to transfer spatial data to the grid: 1) a vector tracing algorithm used for ditches and drains, 2) a point-in-polygon based algorithm used with the area data (active field area, soil profiles and cropping tillage areas) and 3) a down-scaling system used for the raster data (DEM). The length of drainage line (subsurface drains and open ditches) in each cell is determined with the vector tracing algorithm. The resulting length is either saved into the cell in the specified depth in the case of subsurface drains or into each cell between the surface and the specified depth in the case of open ditches. The grid topography and profile is offset according to DEM and profile geometry. If the grid resolution is less than the DEM resolution, an

arithmetic mean is calculated from the DEM pixel elevations in the cell area. In the end, initial conditions are saved into the grid. The hydraulic heads, pressure heads and water contents in both pore systems are calculated from the specified initial groundwater table depth.

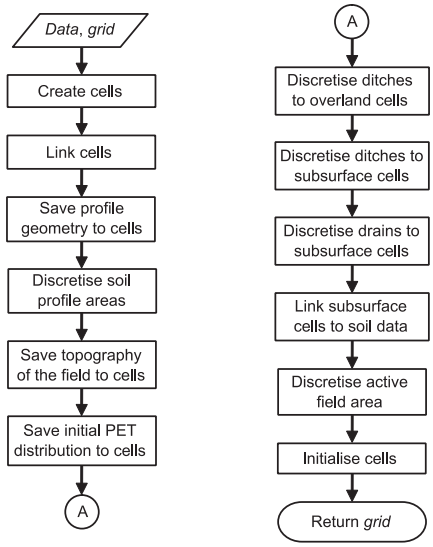

Figure 17. Flow chart of AGGS. The algorithm continues from left to right and from top to bottom.

Software implementation

The FLUSH model was implemented with the C++ programming language and developed with the Microsoft Visual Studio 2008. The model is targeted at desktop workstations with Microsoft Windows Vista or 7 operating systems. In addition to the numerical model, a visualisation program was developed with the OpenGL application programming interface (API) to visualise the computational grids (Figs. 16b, 33, 82-83 and 84-87). All the components including the submodels, the grid and the cells were coded with an object oriented paradigm. The cells residing in the grid object are divided into two container objects for the overland and subsurface cells. The cells store the values of all spatially changing parameters and variables. They are linked to each other with pointers in the grid creation process (Fig. 17). The cells can then access their neighbours with their internal methods to calculate inter-cell properties such as hydraulic conductivity and dispersion. Inheritance is used to add functionality to the cell classes in layers without making a single, bloated class that includes all the cell properties.

The operation of the submodels is parallelised with OpenMP API. Environmental modelling studies using OpenMP were presented previously, e.g. by Innocenti et al. (2009) and Neal et al. (2009). OpenMP

supports shared memory multiprocessing programming (http://www.openmp.org/, 1.1.2010) and it is fairly easy to implement into existing simulation models. The start and end of parallel sections in code are marked with a set of clauses provided in API. The approach facilitates parallelisation of loops and creation of parallel sections in code. The API also includes tools for synchronisation of threads and methods to handle shared variables between threads. Currently OpenMP support is available only for C/C++ and FORTRAN programming languages.

Parallelised blocks of code in the submodels are presented with dashed lines in Figs. 8 and 10–13. The grid is divided dynamically into column strips that are solved with separate execution threads. Because the cells are connected to each other with pointers, it is still possible for the cells to access their neighbours in different strips. Due to the iterative nature of the dynamic solution algorithms, it does not matter if the state variables are changed in the strips at different times. However, it is very important to minimise the access to shared variables during the execution of several threads. This can lead to slowing down of the simulation as the threads queue to make changes to the variables. In the model, only the deviation of the state variables in the iteration phases is treated as a shared variable. Everything else is stored locally in the cells.

3.3 Validation of the numerical model

Performance of the numerical model is evaluated with various approaches. The solution of the Richards equation is tested against results calculated with an analytical model because the equation is notoriously difficult to solve numerically. The operation of the model framework and the system of submodels is analysed with a theoretical test case. The new PDMA method is compared to the traditional TDMA approach, and the acceleration effect due to parallelisation with OpenMP is investigated with a different number of processor cores.

3.3.1 The numerical solution of the Richards equation

Analytical solutions of the Richards equation are difficult to derive due to the highly nonlinear aspect of PDE (Tracy 2007). The relative hydraulic conductivity K_R [L T^{-1}] and the volumetric water content θ are both functions of the pressure head h in unsaturated soils, which causes the strong nonlinearity. 2-D and 3-D analytical solutions were derived by Tracy (1995) without a gravity term. Later Tracy (2006, 2007) developed analytical 3-D models which included the gravity term and several different

boundary conditions. The analytical models by Tracy (2007) were applied here to test the 3-D numerical solution of the Richards equation. The goal was that the presented numerical solution produced similar results compared to the analytical model. The analytical model simulates moisture flow in a box-shaped soil sample with a rectangular source area in the middle of the top face. Steady and transient variants are presented in the Tracy's study with two boundary conditions: 1) with open sides and 2) with closed sides. Only the transient versions were applied here. The solution in the analytical model is based on iterative Fourier series-based approaches. The resulting equations are rather lengthy and thus are not presented here.

The modelled box-shaped soil sample is presented in Fig. 18. The pressure heads computed by the analytical and numerical models were compared at 12 points inside the sample (P1–P12 in Fig. 18). Resolution of the computational grid used in the numerical model was 64×64×20 cells in *x*-, *y*- and *z*-directions.

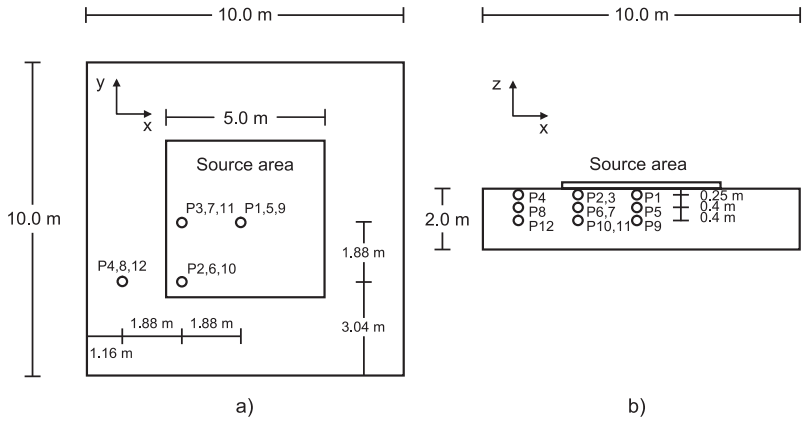

Figure 18. a) Top view and b) front view of the simulation geometry. The 12 points (P1–P12), where the results from the analytical and numerical models are compared, are drawn as open circles.

In the analytical model, the hydraulic conductivity varies with the pressure head according to Gardner's exponential model (Gardner 1958). The following modifications to the description of K_R and θ are required in the numerical model:

$$K_R = \exp(\alpha_G h) \tag{95}$$

$$\theta = \theta_R + (\theta_S - \theta_R) K_R \tag{96}$$

where α_G [L^{-1}] is a parameter of Gardner's WRC. The pressure head in the source area (Fig. 18) is set to 0.0 m at the beginning of the simulation. In the numerical model, the pressure heads in the whole top cell layer were derived from the analytical model. The approach decreased the sharp

discontinuity between the source area and the surrounding area, and made the numerical solution more accurate. Initial pressure head in the soil sample was set to a value of -10.0 m. In the open-sided case, the side pressure heads were set to a constant value of -10.0 m. In both open- and closed-sided cases, the bottom side remained at a constant -10.0 m pressure head. The boundary conditions in the numerical model were assigned to the outermost cell layer in the grid. The simulation parameter values are presented in Table 4.

Table 4. The simulation parameter values in the analytical and numerical models.

Parameter:	Value:	Unit:
Width of the soil sample	10.0	[m]
Length of the soil sample	10.0	[m]
Depth of the soil sample	2.0	[m]
Initial h in the soil sample	-10.0	[m]
α_G	0.25	[m^{-1}]
θ_R	0.1	[m^3 m^{-3}]
θ_S	0.4	[m^3 m^{-3}]
K_S	0.5	[m h^{-1}]
Simulation time	0.6	[h]
Δt (numerical model)	0.001	[h]

Due to the larger width of the soil sample compared to the height of the sample (10.0 vs. 2.0 m), the difference between the open-sided and closed-sided models was not notable. Instead of presenting the same points from the two tests, different points in the grid are shown from the two tests. The comparison between the open-sided models is presented in Fig. 19. The mean absolute error (Appendix D) between the analytical and numerical model results in Fig. 19 was less than 0.28 m. The average mean absolute error in the points was 0.17 m.

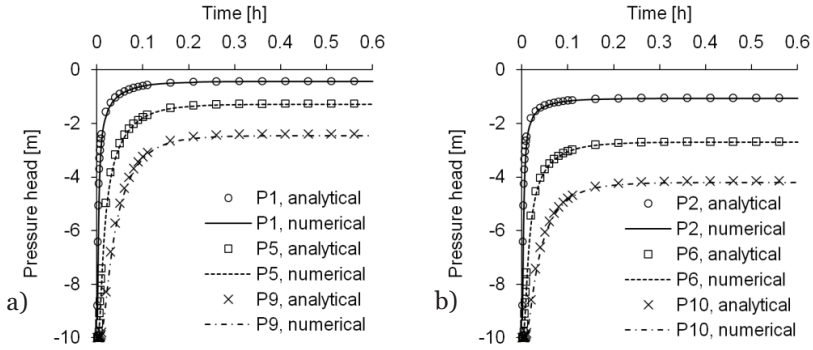

Figure 19. Pressure heads calculated with the open-sided analytical and numerical models at the points P1, P2, P5, P6, P9 and P10.

It only took approximately 0.6 h to reach steady-state conditions in the simulations due to the relatively well permeable soil. The steady-state pressure heads reached with the open-sided models are presented in Table 5. The largest and smallest differences between the analytical and

numerical model results were found at the locations of P9 and P2, respectively.

Table 5. Steady-state pressure heads [m] calculated with the open-sided analytical and numerical models at the points P1, P2, P5, P6, P9 and P10.

Model:	P1:	P2:	P5:	P6:	P9:	P10:
Analytical	-0.421	-1.044	-1.258	-2.681	-2.386	-4.144
Numerical	-0.432	-1.053	-1.292	-2.695	-2.466	-4.197

The pressure heads calculated with the closed-sided models (Fig. 20) were slightly higher than the results calculated with the open-sided versions because water could not drain through the sides of the soil sample. The points P4, P8 and P 12 (Fig. 20b) were selected from the vicinity of the grid side which is the reason for the lower pressure head results. The scale of the *y*-axis (pressure head) in Fig 20b was adjusted to accommodate this.

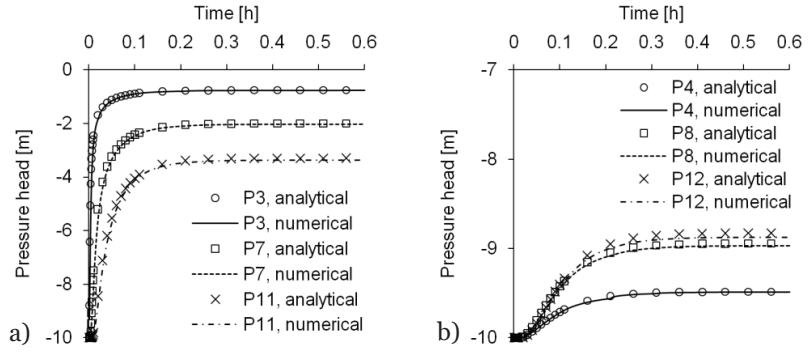

Figure 20. Pressure heads calculated with the closed-sided analytical and numerical models at the points P3, P4, P7, P8, P11 and P12.

The pressure heads produced by the numerical model in Fig. 20 were lower (up to 1.6 m at the point P3 at 0.002 h) than the values simulated by the analytical model. The average mean absolute error was 0.07 m. The steady-state results from the closed-sided models are presented in Table 6. The largest difference between the model results was discovered at the point P11, while the smallest difference was found at the point P3.

Table 6. Steady-state pressure pressure heads [m] calculated with the closed-sided analytical and numerical models at the points P3, P4, P7, P8, P11 and P12.

Model:	P3:	P4:	P7:	P8:	P11:	P12:
Analytical	-0.756	-9.484	-1.999	-8.945	-3.296	-8.828
Numerical	-0.762	-9.490	-2.020	-8.969	-3.362	-8.873

The conclusion of the test was that the results calculated with the numerical solution of the Richards equation were comparable to the results calculated with the analytical model. According to the results, the steady-state error in the numerical solution increased as a function of distance from the source area.

3.3.2 Numerical tests with a theoretical test case

The performance of the whole system, consisting of the framework and submodels, was investigated with a theoretical test case that can be repeated elsewhere if required. The objective of the test was to ensure that the crucial parts of the system were functioning as intended. The test case is presented below.

The geometry consisted of a circular plot area (radius 32.0 m, area 0.3217 ha) with a single hill in the middle (Fig. 16). The vertical axis in Fig. 16 has been increased eightfold. The topography of the hill can be described with a sine function with peak-to-peak amplitude of 1.28 m and wavelength of 64.0 m. The average slope was 0.04. The plot was completely surrounded by an unobstructed ditch. The width and depth of the ditch was 1.0 m and it is full of water. Four concentric circular subsurface drain lines (radii 16.0, 20.0, 24.0 and 28.0 m) surrounded the hill. The drains were installed at a depth of 1.0 m. The diameter of the drainpipe was 0.05 m and the pipes were at atmospheric pressure. Vegetation covered the hill with a root depth of 0.1 m (e.g. grass). A similar profile with three different soil layers (0.0 – 0.31, 0.31–1.27 and 1.27–2.55 m) was assumed to exist everywhere in the plot.

The soil parameters for the three soil layers are presented in Table 7. The values of the saturated and residual water contents (θ_S and θ_R) were set to 0.5 and 0.1 $m^3\ m^{-3}$, respectively, in each soil layer. The $K_{FS,MUL}$ parameter (Eq. 93) was assigned a value of 80.0 $m\ h^{-1}$. Water exchange rate coefficient parameters (d, β and γ_W in Eq. 26) between pore systems were lumped together (e.g. Ray et al. 1997) and a value of 0.01 m^{-2} was applied for the three soil layers. The erodibility parameters k_H and k_R were set to values of 1.0×10^{-6} kg m^{-2} s and 1.0 J^{-1}, respectively while the dispersivities α_L and α_T were set to values of 0.1 and 0.01 m. Three different grid resolutions (16×16×8, 32×32×8 and 64×64×8) were generated with AGGS (Fig. 16). The thicknesses of the vertical layers were 0.01, 0.02, 0.04, 0.08, 0.16, 0.32, 0.64 and 1.28 m.

Table 7. Soil parameters used in the three soil layers. w describes static macroporosity of the soil.

Layer: [-]	$\alpha_{MVG,M}$: [m^{-1}]	$n_{MVG,M}$: [-]	K_{SM}: [$m\ h^{-1}$]	$\alpha_{MVG,F}$: [m^{-1}]	$n_{MVG,F}$: [-]	w: [$m^3\ m^{-3}$]	α_K: [-]	β_K: [-]	γ_K: [-]
1	10.0	1.1	1.0×10^{-2}	7.0	2.0	2.0×10^{-2}	0.7	1.3	0.8
2	3.4	1.1	1.0×10^{-4}	7.0	2.0	2.0×10^{-3}	0.6	1.2	0.9
3	3.4	1.1	1.0×10^{-6}	7.0	2.0	2.0×10^{-4}	0.6	1.2	0.9

The duration of the simulation was 11 days. Three 24 hour precipitation events occurred after the 2nd, 5th and 8th days. The precipitation sum in each event was 92 mm and the maximum hourly precipitation was 8.0 mm. The

precipitation sum was divided into the 24 hour period with a sine function. A constant PET value of 0.1 mm h^{-1} was assumed in the scenario. Initially, groundwater table level was set to the drainage depth (1.0 m) and overland water depths were set to zero. The simulations were run on a workstation with Intel Core i7 920 processor (4 physical cores + 4 Hyper-Threading cores) overclocked to 3.0 GHz and with 6 GBs of RAM.

The adaptive time stepping system (Section 3.2.2.1) was tested by running the presented scenario with and without the system. The mass balance results from the simulations are presented in Table 8. The mass balance errors are caused by rounding errors due to iteration in the algorithms.

Table 8. Mass balance results with the adaptive and constant time stepping systems. Abbreviations used: Sed. = Sediment.

Time stepping system:	Adaptive	Constant	Adaptive	Constant
Storage or runoff value:	Water [mm]:	Water [mm]:	Sed. [kg ha^{-1}]:	Sed. [kg ha^{-1}]:
Surface (initial state)	0	0	0	0
Matrix (initial state)	1224	1224	0	0
Macropore (initial state)	5	5	0	0
Surface (end state)	0	0	0	0
Matrix (end state)	1265	1265	0	0
Macropores (end state)	2	2	0	0
Precipitation (corrected)	276	276	-	-
ET	26	26	-	-
Surface net erosion	-	-	1722	1696
Surface runoff	117	116	914	913
Infiltration into soil	160	162	814	788
Subsurface drainflow	77	78	609	577
Seepage to ditches	17	18	197	203
Groundwater flow	1	1	8	7
Mass balance error	0	+3	+6	+5

In the constant time step case, the local time step was kept at 0.000977 h (3.5 s) throughout the simulation. A one hour global time step was used in both simulations and the simulations were conducted with the 64×64×8 (in *x*-, *y*- and *z*-directions) cell grid resolution. The rain storm threshold value was set to 4.0 mm h^{-1} in the adaptive time stepping case. The simulation run with the adaptive time stepping system took 78 min, while the simulation run with constant time steps lasted for 223 min, i.e. approximately 2.9 times longer. The highest relative differences were apparent in sediment infiltration into soil (814 vs. 788 kg ha^{-1}) and sediment loads via drainflow (609 vs. 577 kg ha^{-1}).

The effect of grid resolution on simulation results was investigated with three resolutions (16×16×8, 32×32×8 and 64×64×8 cells in *x*-, *y*- and *z*-directions) (Fig. 16). Cumulative surface runoff and drainflow results are presented in Fig. 21. Cumulative surface runoff decreased 5.5% and drainflow increased 8.4% with the 64×64×8 grid compared to the results calculated with the 16×16×8 grid.

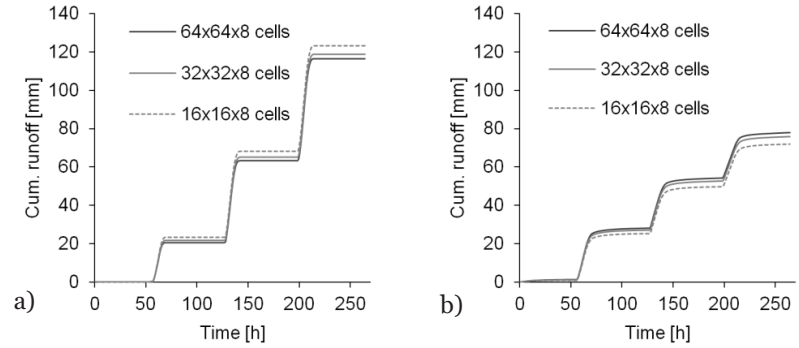

Figure 21. a) Cumulative surface runoff and b) drainflow results with different horizontal grid resolutions (number of cells in *x*-, *y*- and *z*-directions).

Changes in cumulative sediment loads (Fig. 22) were reversed and smaller compared to the changes in surface runoff and drainflow results. Sediment load via surface runoff increased 1.1 % while the sediment load via drainflow decreased 1.0% when the grid resolution was increased from 16×16×8 to 64×64×8.

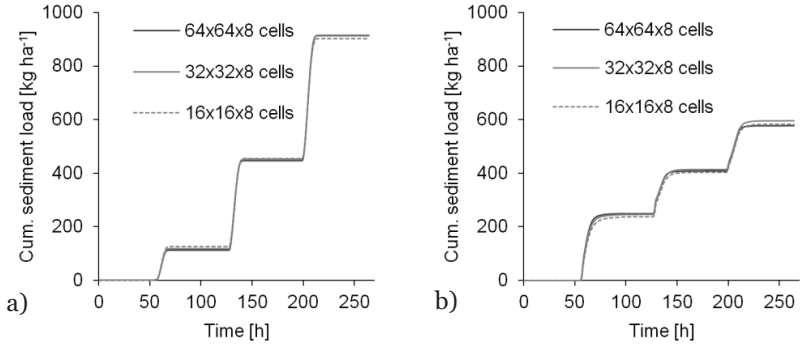

Figure 22. Cumulative sediment loads via a) surface runoff and b) drainflow with different horizontal grid resolutions (number of cells in *x*-, *y*- and *z*-directions).

Spatially distributed processes in the plot were studied by visualising data from the simulations. Overland water depths and flow velocities during a rainstorm event at 205 h are presented in Fig. 82a in Appendix C. The precipitation sum right before the event was 54 mm. The highest overland flow velocity value at the time was 0.022 m s^{-1} and the deepest flow depth value was 0.0028 m. Net soil erosion patterns after the simulation are presented in Fig. 82b in Appendix C. The maximum net erosion value was 0.21 kg m^{-2}. The erosion patterns in Fig. 82b are artifacts caused by the rectangular grid cells set to represent a circular hill and they are not caused by the model parameterisation. Pressure heads in the soil matrix and macropores after the simulation are presented in Fig. 83 in Appendix C. Pressure head in the soil matrix varies more gradually as a function of elevation compared to the macropore system. The symmetric form of

overland water depths, flow velocities (Fig. 82a), net erosion patterns (Fig. 82b) and pressure head distributions in soil (Fig. 83) indicate that all the directional flux components are working as intended.

3.3.3 Comparison of TDMA and PDMA

Performance of PDMA introduced in the subsurface flow submodel (Section 3.2.1.2) was compared to the standard TDMA approach (Section 3.2.1.4) with the simulation setup presented in Section 3.3.2. TDMA and PDMA consist of 19 × n_I - 14 and 76 × n_I - 52 operations (addition, subtraction, multiplication, division, comparison and assignment), respectively. The variable n_I [-] denotes the number of cells in a vertical column. The ratio of number of operations in PDMA and TDMA seems to approach two as the number of cells in a vertical column approaches infinity. However, TDMA has to be run once for each pore system in the submodel. Thus, the number of operations is nearly equal in the two algorithms. The numerical simulations were conducted with both TDMA and PDMA and three different grid resolutions (16×16×8, 32×32×8 and 64×64×8 cells in *x*-, *y*- and *z*-directions). In addition, the values for the maximum number of iterations in the submodels were varied to investigate how the parameter affects simulation times. The results of the comparison are presented in Table 9. The simulation times with a different maximum number of iterations indicated that the performances of the algorithms were almost the same. On average, TDMA was 5.7% faster than the new PDMA approach.

Table 9. Comparison of TDMA and PDMA with different grid resolutions. The maximum number of iterations in the submodels was varied between 25 and 100. Abbreviations used: Max. iter. = Maximum number of iterations and Sim. = Simulation.

	Max. iter.:	25	50	75	100
Resolution:	Algorithm:	Sim. *t* [min]:	Sim. *t* [min]:	Sim. *t* [min]:	Sim. *t* [min]:
16×16×8	TDMA	2.4	2.4	2.4	2.5
16×16×8	PDMA	2.4	2.5	2.9	2.6
32×32×8	TDMA	11.7	13.8	14.2	15.0
32×32×8	PDMA	12.8	12.9	13.5	19.0
64×64×8	TDMA	76.8	89.6	91.9	111.5
64×64×8	PDMA	78.0	92.0	99.6	114.1

The hourly surface runoff and drainflow simulated with TDMA (max. iterations 100) and PDMA (max. iterations 25) are presented in Figs. 23 and 24. The results produced by the two algorithms with a different maximum number of iterations produced a mean absolute error (Appendix D) of 0.0013 mm h^{-1} in surface runoff peak values and 0.003 mm h^{-1} in drainflow peak values. The values are small and it is difficult to separate the effect of the algorithm from the fluctuation generated by the parallel computing method.

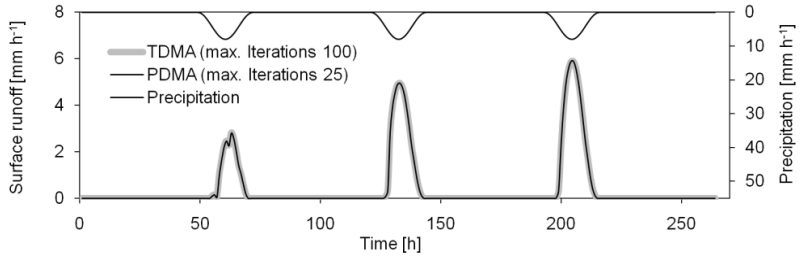

Figure 23. Hourly surface runoff simulated with TDMA (max. iterations 100) and PDMA (max. iterations 25).

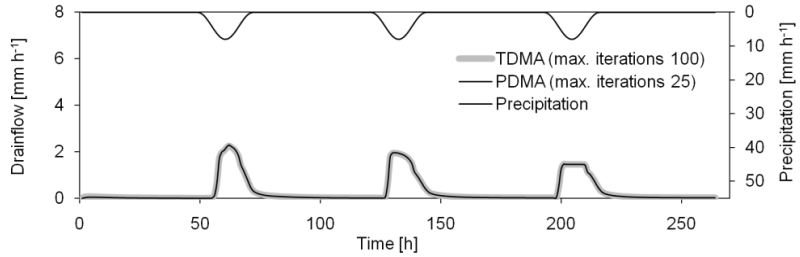

Figure 24. Hourly drainflow simulated with TDMA (max. iterations 100) and PDMA (max. iterations 25).

3.3.4 Tests with OpenMP parallelisation

The performance gains from the OpenMP parallelisation (Section 3.2.2.3) were tested with the same simulation setup presented in Section 3.3.2. Numerical simulations were conducted with three different grid resolutions (16×16×8, 32×32×8 and 64×64×8 cells) and with 1 to 4 physical processor cores. The Hyper-Threading technology in the Intel Core i7 processor allows a single physical core to be divided into two logical cores by duplicating certain sections of the processor but not the main execution resources (www.intel.com, 06.01.2011). The speed-up multipliers due to OpenMP parallelisation are presented in Table 10. The speed-up multipliers were calculated by dividing the simulation times calculated with a single core by the simulation times calculated with 1 to 8 cores (4 physical + 4 Hyper-Threading cores). The single core simulations took 7.0, 44.9 and 263.5 min with the 16×16×8, 32×32×8 and 64×64×8 cell grids, respectively. With higher resolution grids, each additional core provided a clear performance increase.

Table 10. Speed-up multipliers [-] with different number of processor cores.

Resolution \ cores:	1:	2:	3:	4:	5:	6:	7:	8:
16×16×8	1.0	1.9	2.4	2.9	2.7	2.9	2.7	2.9
32×32×8	1.0	1.9	2.2	2.9	3.0	3.0	3.2	3.5
64×64×8	1.0	1.8	2.2	2.8	3.0	3.1	3.3	3.4

4. Model application

The numerical model is applied to two clayey, subsurface drained agricultural fields in Finland. The resulting systems, implemented for the case study sites, are called here computational models. The hypotheses and research questions presented in Section 1 are tested with the computational models. Results from the simulations are presented at the end of this section.

4.1 Descriptions of the data sets

Data from two experimental fields in southern Finland was used in the model applications (Figs. 25 and 29). The Sjökulla experimental field is located in Kirkkonummi, while the Hovi experimental field is located in Vihti, approximately 30 km apart. Climate in southern Finland is temperate with mean annual precipitation of 700 mm (uncorrected value) and mean annual air temperature of +5 ºC. The data sets were provided by several organisations including Aalto University, University of Helsinki, Finnish Environment Institute (FEI), MTT Agrifood Research Finland (MTT) and Finnish Meteorological Institute. It should be noted that the soil data set from the Hovi field is scantier than the data available from the Sjökulla field. The missing data on soil properties in the Hovi field were completed with data from the Sjökulla field. Model calibration and validation was conducted with data from two separate years in both case studies (1998 and 1996 in the Sjökulla case and 1988 and 1984 in the Hovi case). Temporal data including runoff and rainfall measurements from the field sites are shown in Section 4.3 in conjunction with the simulation results.

4.1.1 Sjökulla experimental field

The Sjökulla experimental field site was maintained by the Water Resources Laboratory of the Helsinki University of Technology (Aalto University) in the 1990s to monitor field-scale runoff, erosion and nutrient

transport (e.g. Vakkilainen and Paasonen-Kivekäs 2004). After the monitoring period, extensive measurements on soil properties of the field were carried out by MTT in 2001–2003 (Alakukku et al. 2003, 2010a). Several studies have been published using the data from the field including, e.g.: Koivusalo (1993, 1997), Kankaanranta (1996), Al-Soufi (1999), Koivusalo et al. (1999), Paasonen-Kivekäs et al. (1999, 2000, 2006, 2008), Uusitalo et al. (2001, 2003), Taskinen (2002), Hintikka (2003), Jauhiainen (2004), Paasonen-Kivekäs and Koivusalo (2006), Peltovuori (2006), Karvonen and Paasonen-Kivekäs (2007), Warsta (2007), Hintikka et al. (2008), Warsta et al. (2008a, 2008b, 2009) and Räsänen (2009).

Description of the field

The Sjökulla farm is located between Lake Hepari and Sjökullantie road in Kirkkonummi (60° 14' 28" N 24° 23' 5" E, Fig. 21). The experimental site for runoff and groundwater measurements embodies a field section of about 3.3 ha within a larger area of arable land. The location and map of the field are presented in Fig. 25. In the model application, the studied field area is extended to 3.6 ha to include a field section outside the subsurface drainage system in order to facilitate a more appropriate implementation of side boundary conditions. The topography of the field section is variable and it is bounded by a ditch, an adjacent field and wetland**.** The steepest hill slope is almost 5%, but the lowest area along the ditch has a slope less than 2%. A paved road runs along the southern side of the field and a gravel road along the western side. The roads are separated from the field by shallow ditches. A main ditch (partly piped) runs along the northern side of the field. The ditch is buffered from the field by about 1.0 m wide vegetation strip. The eastern half of the north side (above the pipe line) is connected to an adjacent field seamlessly. The eastern side is partly delimited to alluvial land (wetland) and partly to arable land.

The subsurface drainage system, comprised of clay tiles, was installed in 1951. The distance between the drains is 10–15 m and the drain depth varies between 0.7–1.5 m (Fig. 25). The inner and outer diameters of the tile drain are 0.04 and 0.06 m, respectively. The design capacity of the drains is 1.0 l s^{-1} ha^{-1}. The water from the drains discharges into two collector pipes with drainage areas of 3.14 ha (S1 in Fig. 25) and 0.18 ha (S2). Drainage waters from the pipe line discharge into a wetland next to Lake Hepari. Subsurface drainflow from the larger drainage area was monitored during intermittent periods in the 1990s. Surface runoff was measured in the two sub-catchments of 0.63 (P1 in Fig. 25) and 2.04 ha (P2) within the experimental field. Embankments were built on the north and north-east sides of the field to direct overland flow to the measurement weirs (Fig. 25). The depth of the

groundwater table was monitored with several measurement tubes along a single slope (Fig. 25).

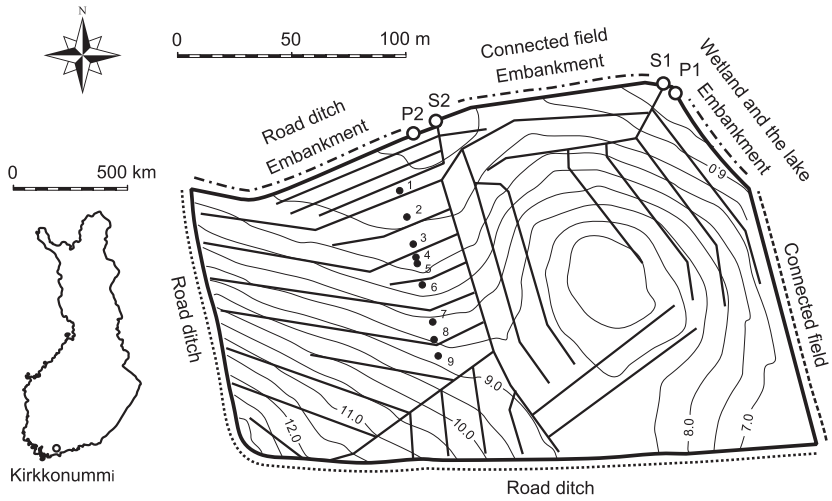

Figure 25. Location of Kirkkonummi in Finland and map of the Sjökulla experimental field. Thin lines inside the field borders are the elevation contours (elevations are presented in [m]), the thicker lines are the subsurface drains and the white circles (P and S) are the surface runoff and subsurface drainflow measurement points. The black circles (1–9) mark the locations of the groundwater table level measurement tubes.

The field section was under conventional crop cultivation during the years when the hydrological measurements and the intensive field campaign on soil properties were carried out. The land use information of the field section is presented in Table 11.

Table 11. The Sjökulla field land use information.

Date:	Land use:
1 Aug. 1995	Sowing of autumn rye
26 Aug. 1996–1 Sep. 1996	Harvesting
10 Oct. 1996	Ploughing
1 May 1998	Sowing of spring wheat
24 Sep. 1998–25 Sep. 1998	Harvesting
2 Oct. 1998–7 Oct. 1998	Stubble cultivation, ploughing

Soil properties

Soil of the Sjökulla field is post-glacial clay classified as very fine Aeric Cryaquept by Peltovuori et al. (2002) following the classification of Soil Survey Staff (1998). The main clay mineral is illitic mica. The soil has a strong tendency to crack during dry periods. For example in summer 2001, cracking was observed at least down to a depth of 0.6 m (Alakukku et al. 2010a). The topsoil layer (0.0–0.25 m) has a clay content of 38–59% while the deeper layers have a clay content of 46–90%. Soil texture and organic matter content of the soil from different depths are presented in Table 12. The measurements were carried out at a midpoint between the drain lines.

Table 12. Mean clay, silt and organic carbon content [g g^{-1}]. Range is in parentheses (minimum / maximum values) (Alakukku et al. 2003).

Depth [m]:	Clay (≤ 0.002 mm):	Silt (0.002 – 0.02 mm):	Organic carbon:
0.0–0.25	0.47 (0.38 / 0.59)	0.28 (0.22 / 0.33)	0.026 (0.017 / 0.044)
0.25–0.45	0.60 (0.46 / 0.83)	0.24 (0.09 / 0.33)	0.009 (0.004 / 0.019)
0.45–0.65	0.73 (0.52 / 0.90)	0.18 (0.07 / 0.33)	0.003 (0.002 / 0.009)
0.65–0.80	0.78 (0.46 / 0.89)	0.16 (0.06 / 0.39)	0.004 (0.002 / 0.009)

Macroporosity and saturated hydraulic conductivity of the soil were studied at three distances from the drain: right above the drain, 2.0 m from the drain and at a midpoint between the drain lines (Alakukku et al. 2003, 2010a). Locations of the studied drain lines are presented in Fig. 26 with rectangles. The dividing diameter between macropores and micropores was assumed to be 300 µm. Measured macroporosity and saturated hydraulic conductivity values are presented in Table 13. The measurements from the three distances from the drainlines were lumped together because no definite differences were found in macroporosities between the samples except in the amount of earthworm holes (Alakukku et al. 2010a). While the differences in saturated hydraulic conductivities and macroporosities across the slope (east-west) were small, there were differences along the slope (south-north) (Table 13).

Table 13. Measured mean, median, minimum and maximum values of K_S [mm h^{-1}] and w [m^3 m^{-3}] of the soil samples taken along the five drain lines (Alakukku et al. 2003, Alakukku et al. 2010a).

	Depth [m]:	0.0–0.23 K_S:	0.23–0.38 K_S:	0.38–0.50 K_S:	0.0–0.23 w:	0.23–0.38 w:	0.38–0.50 w:
L1	Mean:	151	11	0.05	0.035	0.006	0.002
	Median:	119	0.07	0.04	0.034	0.004	0.002
	Min:	9	0	0.006	0.017	0.0003	0.001
	Max:	454	143	0.25	0.058	0.017	0.004
L2	Mean:	165	125	0.06	0.03	0.005	0.003
	Median:	67	28	0.04	0.031	0.005	0.002
	Min:	2	0.02	0.005	0.018	0.001	0.001
	Max:	1005	462	0.24	0.041	0.009	0.005
L3	Mean:	212	97	21	0.027	0.006	0.004
	Median:	155	43	0.07	0.025	0.005	0.002
	Min:	26	0.004	0.01	0.013	0.002	0.001
	Max:	607	306	246	0.043	0.022	0.025
L 4	Mean:	111	115	31	0.026	0.007	0.003
	Median:	38	10	0.06	0.024	0.005	0.003
	Min:	1	0.04	0.02	0.018	0.001	0.001
	Max:	498	491	206	0.038	0.02	0.006
L5	Mean:	21	1	7.19	0.023	0.004	0.004
	Median:	14	0.3	0.09	0.023	0.004	0.004
	Min:	4	0.04	0	0.005	0.002	0.002
	Max:	52	52	29	0.054	0.006	0.007

Three soil profile areas were defined for the computational model according to the field contour curves and soil sampling locations (Fig 26). The parameters of the soil profile area 2 in Fig 26 were calculated as an arithmetic mean of sample properties from the lines 2, 3 and 4 (Table 13). The parameters of the soil profile areas 1 and 3 were taken from the lines 1 and 5, respectively.

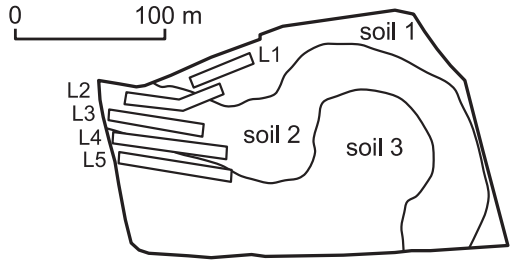

Figure 26. Soil sample locations (rectangles) and different soil profile areas (soil 1, 2 and 3) defined in the Sjökulla field computational model.

Measured WRCs were available from the tillage layer (0.05–0.1 m) and bottom soil (0.65–0.70 m) from three different points. Kankaanranta (1996) extrapolated the measured curves to wilting point suction with empirical curves devised by Karvonen (1988). Parametric MVG WRCs were fitted to the measured curves (Kankaanranta 1996). The dual-permeability flow model requires a parameterisation for the macropore system as well. The total porosity of the soil is divided into soil matrix (1-w) and macropore parts (w). Due to the inherent difficulties associated with the direct measurement of macropore WRC, a modified curve of gravel was used instead (e.g. Ray et al. 1997). WRCs are presented in Fig. 27.

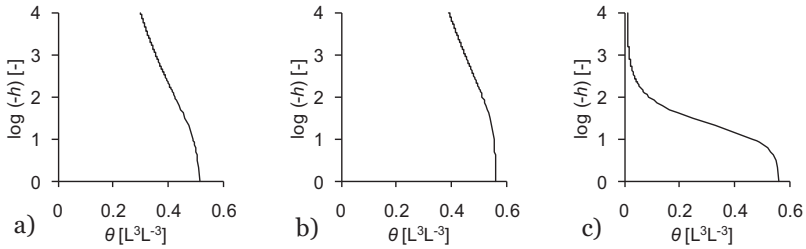

Figure 27. MVG WRCs of a) tillage layer, b) bottom soil and c) macropores in the Sjökulla field computational model (Kankaanranta 1996).

The MVG WRC parameters are presented in Table 14. These WRCs were applied to all the soil profiles in the computational model. The saturated volumetric water content (θ_S) in the macropore system is the same as in the corresponding matrix system (Table 14).

Table 14. Parameters of MVG WRCs of tillage layer, bottom soil and macropores in the Sjökulla field computational model (Kankaanranta 1996).

Parameter:	Tillage layer:	Bottom soil:	Macropores:
α_{MVG} [m^{-1}]	9.51	3.40	7.0
n_{MVG} [-]	1.1077	1.0793	2.0
θ_S [m^3 m^{-3}]	0.5175	0.5643	0.5175 / 0.5643
θ_R [m^3 m^{-3}]	0.1	0.1	0.01

Kankaanranta (1996) studied shrinkage and swelling properties of the soil from three points and two depths (0.1–0.15 and 0.4–0.45 m) and fitted parametric SSCC by Kim et al. (1992) to the data. SSCCs are presented in Fig. 28.

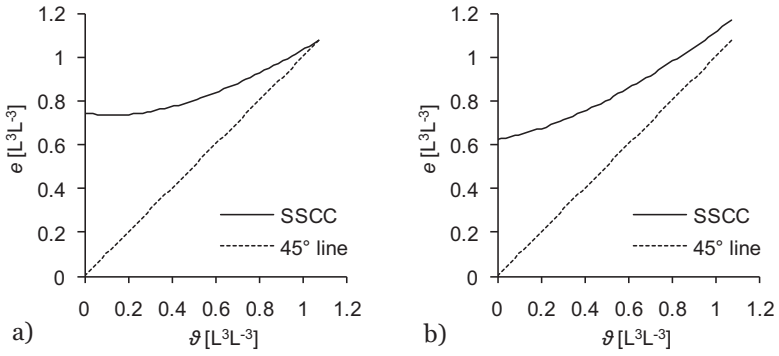

Figure 28. SSCCs of a) tillage layer and b) bottom soil in the Sjökulla field computational model (Kankaanranta 1996).

Parameters of SSCC are presented in Table 15. As with WRCs, the same curves are used everywhere in the field in the computational model.

Table 15. Parameters of SSCCs of tillage layer and bottom soil in the Sjökulla field computational model (Kankaanranta 1996).

Parameter [-]:	Tillage layer:	Bottom soil:
α_K	0.7430	0.6236
β_K	1.3057	1.2369
γ_K	0.8292	0.9318

Runoff and meteorological data

The hourly surface runoff and subsurface drainflow data cover the two periods: May–November in 1996 and May–October in 1998 (e.g. Paasonen-Kivekäs et al. 2008). Outflow from the subsurface drainage system was measured at a well with a v-notched weir intercepting the collector pipe (Fig. 25, measuring point S1). Surface runoff was measured at the lowest points of the field section with a v-notched weir (Fig. 25, measurement points P1 and P2). Water levels at the weirs were measured every 15–30 minutes with a pressure transducer or an ultrasonic sensor. Hourly runoff values [mm h^{-1}] were calculated from the measurements using the basic stage-discharge relationships of the weirs. The water quality data are comprised of total suspended solids (TSS) concentrations in surface runoff and drainflow samples. Grab samples of subsurface drainflow were collected manually at irregular intervals throughout May–November 1996. An autosampler with a 4-hour sampling interval was applied in May–October 1998. Samples of surface runoff during the study periods were

collected manually. The hourly estimates of TSS loads were calculated by multiplying hourly runoff volumes with measured concentrations (Paasonen-Kivekäs et al. 2008).

Meteorological variables were measured with a micrometeorological station, which recorded precipitation, air temperature, solar radiation, relative humidity and wind speed at a height of about 2 m above ground. Precipitation measurements were conducted with a collector bucket installed on a scale. The measurement frequency was 15–30 minutes and hourly values were calculated from the data (Paasonen-Kivekäs et al. 2008). The measured precipitation was corrected with a constant factor of 1.05 (Førland et al. 1996) in the simulations. The PET values were adopted from Hintikka (2003), who produced PET with the Penman-Monteith equation implemented in the MACRO model (e.g. Larsbo and Jarvis 2003).

4.1.2 Hovi experimental field

The Hovi experimental field is one of the small catchments where nutrient loads are monitored in Southern Finland by FEI. Currently, Uusimaa Centre for Economic Development, Transport and the Environment is taking care of the actual measurements. Data from the Hovi field has been used in several previous studies including, e.g.: Seuna and Kauppi (1981), Kauppi (1982), Bengtsson et al. (1992), Posch and Rekolainen (1993), Taskinen (2002), Puustinen et al. (2007, 2010), Taskinen and Bruen (2007a, b) and Vakkilainen et al. (2010).

Description of the field

The Hovi experimental field is located between Kirkkosillantie road to the north and Nurmijärventie road to the south, in Vihti (60° 25' 20" N 24° 22' 7" E, Fig. 29). The 12 ha field section is roughly L-shaped and embedded within a larger area of arable land. The topography is undulating with a general flow direction spiraling clockwise from south-east to north-east. The average slope is 2.8% (Seuna and Kauppi 1981). A new DEM of the field was provided by MTT with a pixel resolution of 2.0×2.0 m (Kaivosoja 2009). DEM was measured with a real time kinematic global positioning system mounted on a tractor. There is also an older 20.0×20.0 m DEM available created by Taskinen (2002). The new DEM features a large oval-shaped depression (~100×50 m) in the middle of the field (Fig. 29), not present in the old DEM. The field section is not a natural catchment but defined according to the subsurface drainage system. Embankments were ploughed along the north-east side to direct surface runoff to the open ditch

(Fig. 29). A road ditch borders the north-west side of the field. At the south-west side, the field is delimited by a natural water divide and a farm yard.

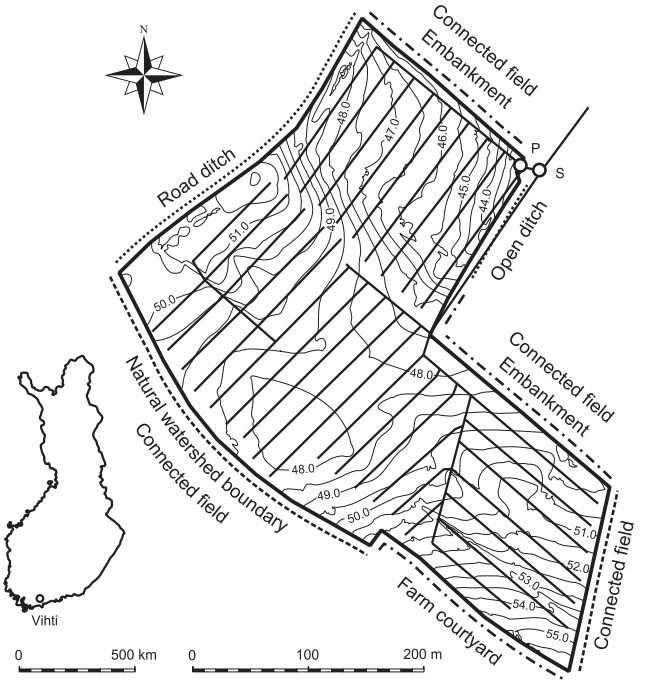

Figure 29. Location of Vihti and map of the Hovi experimental field. Thin lines inside the field borders are the elevation contours (elevations are presented in [m]), the thicker lines are the subsurface drains and the white circles (P and S) are the surface runoff and subsurface drainflow measurement points.

During the simulation years the field was divided into two land use areas (Fig. 30).

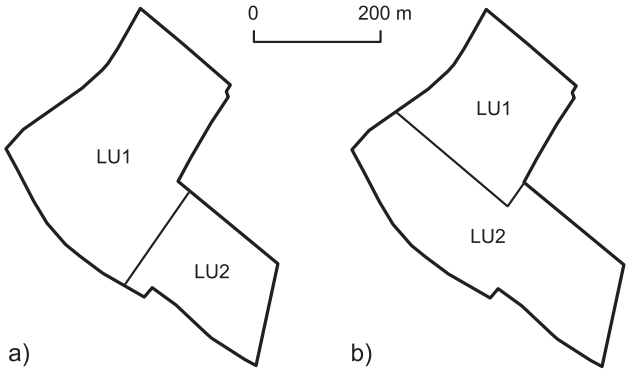

Figure 30. The Hovi field land use areas (LU1 and LU2) in a) 1984 and b) 1988.

The land use information corresponding to the areas LU1 and LU2 in Fig. 30 is presented in Table 16.

Table 16. The hovi field land use information.

Date:	LU1:	LU2:
3 Oct. 1983–8 Oct. 1983	Ploughing	Ploughing
1 May 1984	Seeding of spring wheat	Fallow
17 Aug. 1984	Harvesting	Rye seeding
13 Sep. 1984	-	Rye springing up
23 Oct. 1984	Ploughing	-
29 Sep. 1987	Ploughing	Ploughing
10 May 1988	Fallow	Harrowing
11 May 1988	-	Seeding of spring wheat
17 Aug. 1988	-	Harvesting
9 Sep. 1988	Ploughing, harrowing, seeding of autumn wheat	-
29 Sep. 1988	Autumn wheat springing up	ploughing

The subsurface drainage system was installed in 1971 with a drainage density of 443 m ha^{-1} (Seuna and Kauppi 1981) and a drain spacing of 22.0 m. The drainage area is the whole field section. Plastic tubes with a diameter of 0.055 m were installed for the lateral drains and steel and plastic tubes with a diameter of 0.1 m for the collector drains. Vertical gravel drains were installed with the subsurface drains with a spacing of 10.0 m (Bengtsson et al. 1992). Subsurface drainflow and total runoff in the main ditch were measured in the north-east corner of the field (Fig. 29).

Soil properties

The soil properties of the Hovi field have been investigated separately at least two times in the past. Taskinen (2002) presented particle size distributions of three different soil areas in the field (Fig. 31a). Ristolainen and Pesonen (2010) measured particle size distributions, organic carbon contents and hydraulic properties of the soil from several locations above and between the drain lines in the northeast part of the field in the Täsmä-NP project (Fig. 31b).

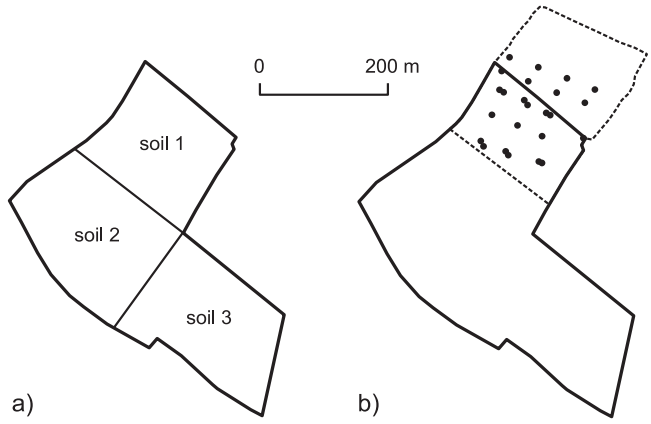

Figure 31. a) Soil areas presented by Taskinen (2002) and b) soil sample locations by Ristolainen and Pesonen (2010). The Täsmä-NP project field section (3.2 ha) is drawn with a dashed line.

In the data presented by Taskinen (2002), the clay content was 51–59 % while the silt content was 26–33%. The data describes only the top 0.6 m of the profile. Conversely, in the data measured by Ristolainen and Pesonen (2010) the clay content varied between 0.54 and 0.77 and silt content between 0.27 and 0.17. The samples were taken from three different depths (0.0–0.2, 0.2–0.35 and 0.35–0.6 m) (Table 17). Clay, silt and organic carbon contents are presented in Table 17.

Table 17. Mean clay, silt and organic carbon contents [g g^{-1}]. Range is in parentheses (minimum / maximum values) (Ristolainen and Pesonen 2010).

Depth [m]:	Clay (≤ 0.002 mm):	Silt (0.002–0.02 mm):	Organic carbon:
0.0–0.2	0.54(0.32 / 0.75)	0.27(0.15 / 0.36)	0.02(0.02 / 0.03)
0.2–0.35	0.71(0.40 / 0.86)	0.20(0.09 / 0.38)	0.01(0.003 / 0.02)
0.35–0.6	0.77(0.64 / 0.89)	0.17(0.06 / 0.28)	0.003(0.002 / 0.004)

The measured hydraulic properties (Ristolainen and Pesonen 2010) included saturated hydraulic conductivities, macroporosities and WRCs. Data were available from both between and above the drain lines but only data between the drain lines were used. It was thought that it better described the general soil properties of the field. The measurements were conducted with samples collected from the same depths as the soil texture data (Table 17). The dividing diameter between macropores and micropores was assumed to be 300 µm. Macroporosity of the soil was higher in the samples taken above the drain lines compared to the samples taken between the drain lines, except in the tillage layer. Because data on hydraulic properties of the soil was only available from the northeast part of the field, arithmetic mean values of the data were applied to the whole field area. Macroporosity values and saturated hydraulic conductivities of the Hovi field (Table 18) were smaller compared to the Sjökulla values (Table 13).

Table 18. Measured mean, median and minimum/maximum values of K_S [mm h^{-1}] and w [m^3 m^{-3}] of the soil samples (Ristolainen and Pesonen 2010).

Depth [m]:	0.0–0.20 *Ks*:	0.20–0.35 *Ks*:	0.35–0.55 *Ks*:	0.0–0.20 *w*:	0.20–0.35 *w*:	0.35–0.55 *w*:
Mean:	163	85	0.6	0.019	0.003	0.001
Median:	85	23	0.1	0.019	0.002	0.001
Min:	0.1	0.01	0.01	0.0	0.0	0.0
Max:	752	545	7	0.043	0.013	0.003

WRCs were measured from two different depths (0.05–0.1 and 0.35–0.4 m) in the field (Ristolainen and Pesonen 2010). Arithmetic mean values of the measured water contents at prescribed suction values were calculated from the data set and MVG WRCs were fitted to the resulting curves. The curves were further adjusted in the model calibration phase. Macropore WRC was parameterised with the same approach used in the Sjökulla case

(Table 14, Fig. 27c). WRCs (adjusted), applied to the whole field area in the model application, are presented in Fig. 32.

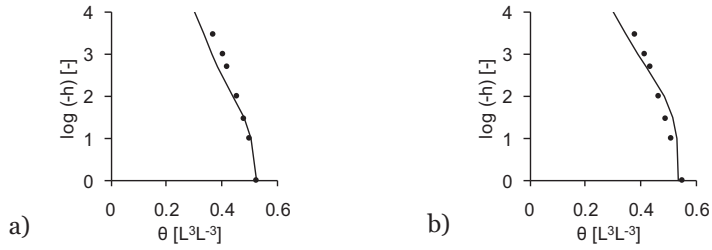

Figure 32. MVG WRCs of a) tillage layer and b) bottom soil in the Hovi field.

The corresponding MVG WRC parameters are presented in Table 19.

Table 19. Parameters of MVG WRCs for tillage layer and bottom soil in the Hovi field.

Parameter:	Tillage layer:	Bottom soil:
α_{MVG} [m^{-1}]	7.2011	1.3807
n_{MVG} [-]	1.0884	1.1197
θ_S [m^3 m^{-3}]	0.5294	0.5352
θ_R [m^3 m^{-3}]	0.01	0.01

Runoff and meteorological data

The subsurface drainflow and total runoff (drainflow + surface runoff) data cover the whole year in 1984 and 1988. Water levels at the runoff weirs were originally recorded with a limnograph on paper (Fig. 29, measurement points P and S) and later digitised and converted into hourly data [l s^{-1} km^2]. The intensities can be derived by dividing the addition of the amount by the time increment. Suspended sediment concentration measurements were available at irregular intervals throughout April–October in 1988. Only a few measurements from the ditch and subsurface drainflow were available from 1984.

Precipitation was recorder with Pluviographs with Wild-type collectors on pieces of paper which were later digitised into breakpoint data (Taskinen 2002). Posch and Rekolainen (1993) have described the rainfall measurement system in the Hovi catchment. The data were discretised into hourly series [mm h^{-1}] used in the model. Precipitation data cover a period between May and October in 1984 and 1988. The measured precipitation was corrected with a constant 1.05 factor (Førland et al. 1996) in the simulations. PET was calculated from daily Class A evaporation pan results from Maasoja weather station (60° 25' 7" N 24° 23' 54" E) located 2.5 km from the field. The pan results were multiplied with the monthly correction coefficients of Vakkilainen (1982) to derive the daily PET values.

4.2 Computational models

A computational model is comprised of the generic numerical model and the data from the field. Data are required to create the computational grids, assign boundary conditions, set simulation parameters and provide dynamic data such as precipitation and PET values for the numerical model.

The models were calibrated and validated with the available runoff and sediment data and measured groundwater levels. The years 1998 and 1988 were used for calibration and 1996 and 1984 for validation in the Sjökulla and Hovi models, respectively. The performances of the computational models were assessed with visual inspection and statistical approaches. The calibration-validation process was conducted manually due to the heavy computational load associated with the numerical model. The parameterisations of the Sjökulla and Hovi computational models are presented side by side in the following section to facilitate easy comparison between the fields.

4.2.1 Computational grids

Several computational grid resolutions were employed in the simulations to accelerate the calibration process and to test the effect of grid resolution on the results. The grids were created automatically with AGGS (Section 3.2.2.2). Horizontal resolutions of the Sjökulla field grids were 18×13, 36×26, 72×52 and 144×104, whereas resolutions of the Hovi field grids were 13×18, 26×36, 52×72 and 104×144 cells in x- and y-directions. The computational grids are presented in Fig. 33.

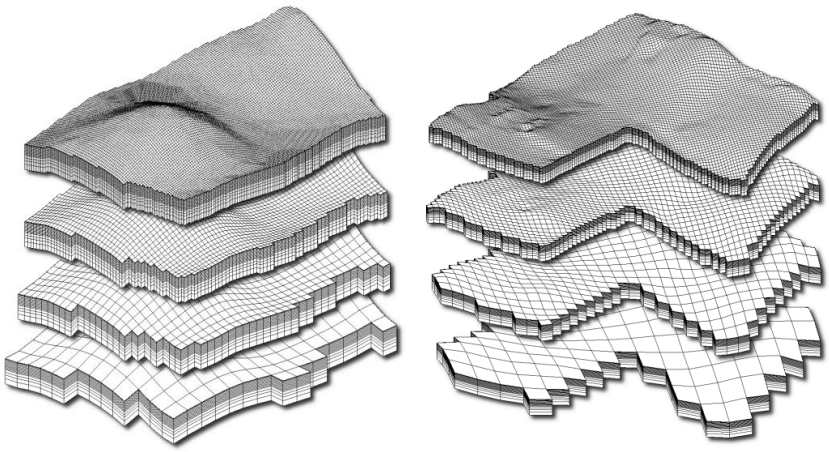

Figure 33. The computational grids of a) the Sjökulla and b) Hovi experimental fields. The vertical resolution is exaggerated tenfold to accentuate the topography. The fields are not shown to scale.

The corresponding horizontal lengths of cell sides were 16.0, 8.0, 4.0 and 2.0 m (Sjökulla) and 32.0, 16.0, 8.0 and 4.0 m (Hovi). As the horizontal resolution increases, the active part of the grid conforms more precisely to the shape of the field section. The total grid areas (active + inactive parts) were 59904 (Sjökulla) and 239616 m² (Hovi). The horizontal resolutions, active field areas and number of active cell columns in the grid (absolute number and percentage of the total number of columns) are presented in Table 20. The horizontal resolution steps were also given identifiers that describe the relative grid resolution in this thesis (Low, Medium, High and Very high).

Table 20. Horizontal grid resolutions, active field areas and number of active cell columns in the grids (absolute number and percentage of the total number of columns). Abbreviations used: res. = resolution and Act. col. = Active columns.

Grid:	*x*-res. [-]:	*y*-res. [-]:	Act. area [m^2]:	Act. col. [-]:	Act. col. [%]:
Sjökulla (Low)	18	13	45824	179	76
Sjökulla (Medium)	36	26	43136	674	72
Sjökulla (High)	72	52	41664	2604	70
Sjökulla (Very high)	144	104	41044	10261	69
Hovi (Low)	13	18	120832	118	50
Hovi (Medium)	26	36	115200	450	48
Hovi (High)	52	72	112576	1759	47
Hovi (Very high)	104	144	111440	6965	47

The number of active cells in the grid can be calculated by multiplying the number of active columns in Table 20 by the number of cells in a column. Two different vertical resolutions (16 and 30 cells) were investigated to test the effect of vertical resolution on results. The vertical profiles are presented in Fig. 34.

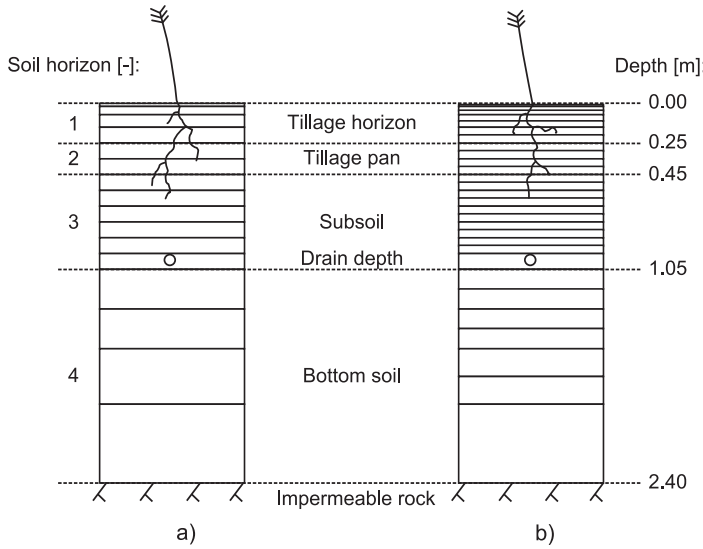

Figure 34. Vertical grid profiles with a) 16 and b) 30 cells.

The depth of the soil profile was 2.4 m. Most of the vertical resolution was concentrated into the volume between the field surface and subsurface drains. The layer depths of the 16 cell profile (Fig. 34) were: 0.02, 0.05, 0.08, 0.1×9, 0.25×2, 0.35 and 0.5 m. The 30 cell profile can be derived from the 16 cell profile by dividing all the cell depths into two, except the top cell and the subsurface drain cell depths, which are kept the same.

4.2.2 Initial and boundary conditions

The simulation periods start in the beginning of May, when snow cover has already melted in southern Finland but there is still no vegetation with notable transpiration capacity growing in the fields. The equilibrium moisture conditions in both pore systems were calculated from the assigned initial groundwater table depths. Arithmetic means of groundwater table depth measurements were adopted as initial values in the Sjökulla case due to a limited amount of measurements available from the field. The values were adjusted by comparing simulation results to the early summer runoff measurements. In the Hovi simulations, it was assumed that the groundwater table level was at the drain depth (1.0 m from the surface) because no measurements were available from the field. The levels were adjusted according to the runoff results. In particular, the Hovi 1988 groundwater table depth had to be increased drastically from the initial value. The initial groundwater table depths are presented in Table 21.

Overland water depths and sediment concentrations, as well as subsurface sediment concentrations were set to zero at the beginning of the simulations.

Table 21. Measured groundwater table depths in the observation tubes (arithmetic mean) and calibrated initial values.

Simulation:	Measured value [m]:	Simulation value [m]:
Sjökulla 1998	0.97	1.0
Sjökulla 1996	0.50	0.9
Hovi 1988	-	0.1
Hovi 1984	-	1.2

Boundary conditions in the computational models were set either explicitly (ditches and drains) or automatically (groundwater flow) (Fig. 35). The widths and depths of the ditches were set to 2.0 and 1.0 m, respectively. The cross section of the ditch was considered to be triangular. Constant water depth of 0.3 m was maintained in the ditch network because water levels in the ditches were not simulated by the model. Part of the ditch running on the north and northeast side of the Sjökulla field was embanked. Overland flow can enter the ditch only at the non-embanked parts while subsurface waters can seep into the ditch also along the

embanked parts. Open ditch sections associated with the overland domain are presented in Fig. 35a (upper row) while the sections used in the subsurface domain are presented in Fig. 35b. Overland waters flowing over the eastern side of the Sjökulla field to the adjacent field section were removed with a ditch section in the simulations (Fig. 35a top row). No embankments were built along the open ditch at the Hovi field (Fig. 35a, b lower row).

The subsurface drainage networks were presented in Figs. 25 and 29. The drains were set to a depth of 1.0 m from the surface and the radius of the drainage pipe (R_S) was set to 0.025 m. The groundwater flow sides were assigned by AGGS according to the topography of the field (Section 3.2.1.2). The sides of the fields, which lose water as groundwater flow, are presented in Fig 35c. The grid bottom was assumed to be impermeable at all locations.

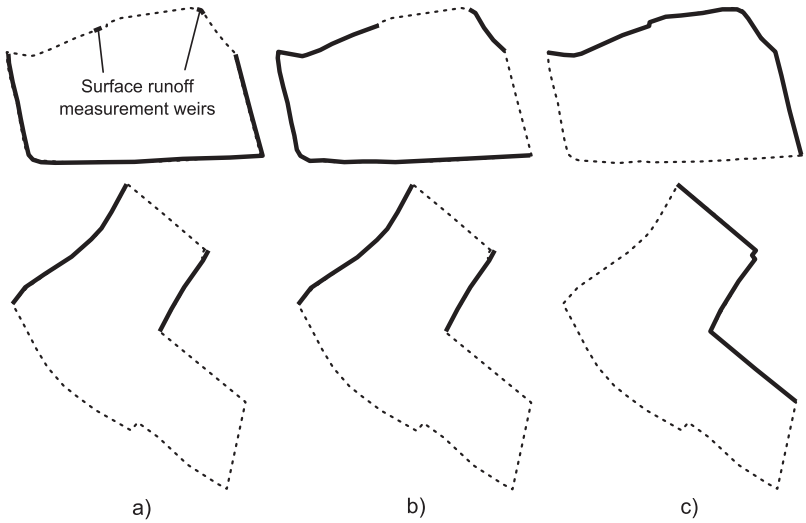

Figure 35. Location of a) ditches in the overland domain, b) ditches in the subsurface domain and c) groundwater flow boundaries in the Sjökulla (upper row) and Hovi (lower row) fields drawn with thick, continuous lines. Dashed lines represent the field boundaries.

4.2.3 Parameterisations of the computational domains

Submodel parameterisations are divided into four computational domains: 1) overland flow, 2) subsurface flow, 3) overland erosion and 4) subsurface transport. Parameter values from literature and the calibrated values in the Sjökulla and Hovi computational models are presented side by side for ease of comparison. The cropping and tillage effects and the soil shrinkage and swelling submodel parameters are integrated into the four computational domains presented above.

Overland flow

Overland flow is adjusted in the simulations by two spatially varying parameters, Manning's n and overland flow threshold depth $h_{W,THR}$. It is probable that n and $h_{W,THR}$ are connected in some manner even though they are handled separately in the model. Both parameters can vary with different land use types and with time due to crop growth and tillage operations conducted in the field.

Sharda et al. (1994) recommended n values between 0.05–0.12 for cropped conditions, depending on the crop growth stage. Singh (1996) presented n values from several studies. For a fallow field, the range was from 0.01 (smooth rain packed) to 0.7 (rough turn-ploughed) while for a cropped field, the range was from 0.05 (grass) to 0.4 (small grain crops). Wicks and Bathurst (1996) set the n values to 0.050 during growing season (soybeans and corn) and to 0.029 after tillage. Li and Zhang (2001) developed an analytical model which can calculate n values for different conditions including bare land after autumn ploughing and land with spring wheat. The corresponding average n values were 0.0303 and 0.0390. Taskinen and Bruen (2007a) reported values exceeding 1.0 for some surface conditions. Higher values were associated with rough conditions after tillage and with the presence of fully developed crops in the field.

Hoogmoed and Bouma (1980), Kankaanranta (1996) and Köhne et al. (2006) set the $h_{W,THR}$ parameter to 0.002 m while Novák et al. (2000) calibrated the value into 0.001 m. $h_{W,THR}$ can also be determined with the analytical method of Onstad (1984).

Both n and $h_{W,THR}$ were calibrated in this study. The parameter values are presented in Table 22. n was calibrated directly against measured surface runoff while $h_{W,THR}$ had to be calibrated indirectly by inspecting precipitation and infiltration rates and the ensuing surface runoff rates. While it was possible to change both n and $h_{W,THR}$ in spatial and temporal dimensions in the model, in practice, it was difficult to calibrate the distributed parameter values with the available measurements. In the Sjökulla field computational model, n was fixed to a constant value because tillage operations in the autumn did not have a notable effect on the surface roughness. The calibrated n values in the Hovi computational model were high compared to the Sjökulla values. The high calibrated values could have been caused by a number of factors, including the method of measuring surface runoff by subtracting drainflow from the total runoff, tillage layer flow or dampening of surface runoff by the long ditch strip (~100 m). In addition, no data were available about the presence of vegetation in the fallow areas during the simulation years. In the end, a single n value was applied throughout the Hovi field. However, it became evident in the

calibration phase that the value increased notably after tillage in the autumn. The same $h_{W,THR}$ value was used in both simulations (Table 22).

Table 22. Overland flow domain parameters. The two *n* values in the Hovi column represent surface roughness before and after tillage in the autumn.

Parameter:	Sjökulla:	Hovi:	Unit:
n	0.1	1.0 / 3.0	[-]
$h_{W,THR}$	0.001	0.001	[m]

Subsurface flow

The subsurface flow computational domain includes a number of parameters to adjust PET and to define hydraulic properties of the soil layers. Geometry-related parameters (ditches, drains, groundwater flow) were presented earlier in Sections 3.2.1.2 and 4.2.2.

The precalculated PET value is distributed into the soil profile according to the root mass distribution in the model. Crop root depths change between the prescribed minimum and maximum root depths in the simulations. Linnér et al. (2006) reported maximum crop root depths of 0.75–1.0 m for autumn rye and spring wheat in Sweden. The crop root growth can be around 0.02–0.03 m d^{-1} during the growing season (e.g. Båth 1993). The precalculated PET values are decreased with the stress factor α_F (Feddes et al. 1978, Fig. 1) in dry or wet conditions. Gärdenäs et al. (2006) used pressure heads of 160.0, 15.0 and 0.1 m for h_4, h_3 and h_2 (absolute values) in a study conducted in Sweden. In Finland, h_3 is usually set to 5.0 m and h_4 to wilting point suction (150.0 m) (Vakkilainen 1982).

The parameters associated with root depths z_R and ET are presented in Table 23. The maximum z_R value was decreased compared to the presented measurements in the calibration. The minimum z_R value was applied in the beginning of the simulations in May, after harvesting in the autumn and in the fallow areas (Fig. 30 and Table 16). The threshold pressure heads in α_F (h_1, h_2, h_3 and h_4) were taken from past studies.

Table 23. Crop root depth and stress factor α_F (Fig. 1, Feddes et al. 1978) parameter values.

Parameter:	Value [m]:
z_R (min)	0.05
z_R (max)	0.6
h_1 (in α_F)	0.0
h_2 (in α_F)	-0.1
h_3 (in α_F)	-5.0
h_4 (in α_F)	-150.0

The soil profile was divided into four soil horizons in both computational models (Fig. 34). In the Sjökulla model, the field was divided into three different soil profile areas with different macroporosity values (Fig. 26). In the Hovi model, the same profile was applied to the whole field because data were available only from the northeast part of the field. Tillage layer

WRCs (Tables 14 and 19, Figs. 27 and 32) were used in the tillage layer matrix pore system (Fig. 34, soil horizon 1). The bottom soil WRCs were assigned to the soil matrix pore system in the rest of the profile. The macropore WRC (Table 14, Fig. 27c) was employed in all the soil horizons in both computational models. SSCCs (Table 15 and Fig. 28) were applied to the profile in the same way as WRCs. SSCCs from the Sjökulla field were also used in the Hovi field simulations.

Generally, saturated hydraulic conductivity of soil rises with the increase of macroporosity (e.g. Germann and Beven 1981b, Messing and Jarvis 1990). Macroporosity of clayey soil changes according to the moisture state of the soil matrix due to shrinkage and swelling phenomena. The saturated hydraulic conductivity measurements (Tables 13 and 18) represent the whole cross-sectional area of the soil sample while water moves mostly in the limited macropore fraction (e.g. Bouma and Wösten 1979). When the conductivity of the soil matrix was assumed to approach zero, an approximation of the saturated hydraulic conductivity of the macropores was derived by dividing the measured conductivity value with the measured macroporosity fraction. An approximation of the macropore saturated hydraulic conductivity multiplier $K_{FS,MUL}$ (130.25 m h^{-1}) was obtained by fitting Eq. 93 to the data (mean values in Table 13). Four data points out of 15 were removed from the data set because they exhibited high saturated conductivity values (25.0–10.3 m h^{-1}) against small macroporosity values (0.007-0.003 m^3 m^{-3}). $K_{FS,MUL}$ was further adjusted with calibration against drainflow data to 80.0 m h^{-1}. The resulting value was used in both computational models.

Initial static macroporosity (w) values of the soil were derived from Tables 13 and 18. The tillage layer (horizon 1 in Fig. 34) static w values were decreased by 60% from the measured values in the calibration of the Sjökulla computational model. In the Hovi case the initial static w values had to be increased in the lower parts of the profile (horizons 3 and 4 in Fig. 34). The static w values in the tillage layer had to be decreased by the cropping and tillage effects submodel in both computational models in the autumn after tillage operations to increase surface runoff. The static w values were decreased to 25% and 67% of the original values in 1998 and 1996, respectively, in the Sjökulla field. In the Hovi simulations, static w values were decreased to 40% of the original values during both years after tillage.

Groundwater flow was assumed to be responsible for the water loss in the fields evident in the measurements. Relatively high static w values were set in the bottom soil layer (Fig. 34, soil horizon 4) to achieve this. Horizontal and vertical saturated hydraulic conductivities were kept the same in each

horizon, i.e. no anisotropy was detected within the horizons. Saturated hydraulic conductivity of the soil matrix K_{SM} was derived with calibration. K_{SM} values and static w values in the soil profiles are presented in Table 24. The three static w values (1/2/3) in the Sjökulla column in Table 24 correspond to the three soil profile areas in the Sjökulla field (soil 1/2/3) presented in Fig. 26.

Table 24. Calibrated K_{SM} and static w values in the soil profiles. The three static w values in the Sjökulla column correspond to the soil profile areas in the Sjökulla field (soil 1/2/3) presented in Fig. 26.

Soil horizon:	K_{MS} [m h^{-1}]:	Sjökulla, static w [m^3 m^{-3}]:	Hovi, static w [m^3 m^{-3}]:
1	1.0×10^{-2}	2.1×10^{-2} / 1.7×10^{-2} / 1.4×10^{-2}	1.9×10^{-2}
2	1.0×10^{-4}	6.0×10^{-3} / 6.0×10^{-3} / 4.0×10^{-3}	3.4×10^{-3}
3	1.0×10^{-4}	2.0×10^{-3} / 3.3×10^{-3} / 4.0×10^{-3}	2.0×10^{-3}
4	1.0×10^{-4}	1.5×10^{-3}	1.5×10^{-3}

Water exchange rate between the pore systems is governed by the first order water exchange coefficient α_W (Eq. 26). α_W in turn, contains parameters β (macropore geometry coefficient), γ_W (scaling coefficient) and d (radius of the matrix structure). Skopp et al. (1981) reported β values of 1 for planar cracks and 3 for spherical macropores. Van Genuchten and Dalton (1986) presented values of 3 and 15 for planar cracks and spherical macropores, respectively. The parameter γ_W varies with the initial water content and hydraulic parameters, but not strongly according to Larsbo and Jarvis (2003). Gerke and van Genuchten (1993b) derived a value of 0.4 for γ_W that seemed to work well with different macropore geometries. Vogel et al. (2000) and Gerke and Köhne (2002) reported a value of 0.01 m for the parameter d while Christiansen et al. (2004) set the value of d to 0.055 m. Gärdenäs et al. (2006) used d values of 0.11–0.17 m in their 2-D simulation of a tile-drained field site in Sweden. Villholt and Jensen (1998) calibrated the parameter d to enhance the simulation fit to measurements in glacial till soil. The authors had to use very large values of d (20.0 m) on some occasions. Jarvis et al. (2007) derived a set of pedotransfer functions to approximate d in the MACRO model.

The parameter values in the water exchange function (Eq. 26) in the model are presented in Table 25. The calibration of the parameter d in this study was conducted by comparing hourly simulated and measured drainflow results and simulated ET and calculated PET results. Similar to Villholt and Jensen (1998), d was calibrated to a high value.

Table 25. First order water exchange coefficient parameter values.

Parameter:	Value:	Unit:
β	3.0	[-]
γ_W	0.4	[-]
d	11.0	[m]

Overland erosion

Overland erosion processes are based on simulated flow velocities, water depths and measured precipitation amounts. Constant parameters in the model include gravitational acceleration g, kinematic viscosity υ, density of water ρ_W, sediment particle diameter D_S and sediment particle density ρ_S (Table 26).

According to e.g. Meyer et al. (1980) and Smith et al. (1999), cohesive soils are removed partly in aggregates and not solely as primary particles. Sharda et al. (1994) set the particle diameter D_S in the simulations to the median diameter of the sediment particles (4.8×10^{-4} m). Taskinen and Bruen (2007) simulated three different particle sizes (clay, silt and sand). The diameter of the suspended soil particles was set here to approximately tenfold of a single clay soil particle to represent the presence of aggregates.

Table 26. Constant parameters in the overland erosion domain.

Parameter:	Value:	Unit:
υ	1.0×10^{-6}	[m^2 s^{-1}]
ρ_S	2650.0	[kg m^{-3}]
ρ_W	1000.0	[kg m^{-3}]
D_S	1.5×10^{-5}	[m]
g	9.81	[m s^{-2}]

Susceptibility of the soil to hydraulic and rain drop splash erosion is defined with the erodibility coefficients k_H and k_R. Ariathurai and Arulanandan (1978) derived a range from 5.0×10^{-4} to 5.0×10^{-3} kg m^{-2} s^{-1} for k_H. Wicks and Bathurst (1996) reported k_H values of 4.1×10^{-7}, 1.4×10^{-7} and 3.3×10^{-7} kg m^{-2} s^{-1}. Taskinen (2002) calibrated k_H to a range from 3.5×10^{-8} to 18.0×10^{-8} kg m^{-2} s^{-1} before ploughing and 0.32×10^{-6} to 10.0×10^{-6} kg m^{-2} s^{-1} after ploughing in simulations of the Sjökulla field. Meyer and Harmon (1984) presented k_R values of 19 J^{-1} for clay soil. Bradford et al. (1987a, b) reported value of 73.5 J^{-1} while Wicks and Bathurst (1996) presented values of 28, 66 and 82 for clayey soils.

The erodibility coefficients in the computational models were calibrated directly against the measured sediment data (loads or concentrations). The values of the coefficients increased after tillage in both fields. The calibrated erodibility coefficients before and after tillage operations are presented in Table 27. A complication was that the Hovi field was partly under fallow during 1988 (6 ha) and 1984 (4 ha). Unfortunately, no information was available whether the fallow was bare or grass was grown on the areas. In the Hovi simulations, the hydraulic erosion process did not produce coherent results compared to the measurements, while sediment loads produced by rain drop splash erosion were much closer to the data.

Previously, Taskinen reported problems in producing hydraulic erosion in Hovi field simulations (Taskinen 2002).

Table 27. Calibrated erodibility parameters before and after tillage in the fields.

Field:	Before tillage k_R [J^{-1}]:	After tillage k_R [J^{-1}]:	Before tillage k_H [kg $m^{-2}s^{-1}$]:	After tillage k_H [kg $m^{-2}s^{-2}$]:
Sjökulla 1998	1.2	1.2	1.0×10^{-7}	2.2×10^{-6}
Sjökulla 1996	1.2	1.2	1.0×10^{-7}	2.2×10^{-6}
Hovi 1988 LU1	4.0 (fallow)	20.0 (fallow)	0.0 (fallow)	0.0 (fallow)
Hovi 1988 LU2	4.0	20.0	0.0	0.0
Hovi 1984 LU1	4.0	20.0	0.0	0.0
Hovi 1984 LU2	4.0 (fallow)	20.0 (fallow)	0.0 (fallow)	0.0 (fallow)

Other parameters in the erosion process descriptions that had to be defined included ground shielding factors C_C and C_G. There was no information available on the crop growing stages during the simulation periods. Consequently, C_C and C_G were set to zero to decrease the number of calibrated variables. This action could decrease the value of k_R because the soil was not shielded by crops.

In addition, it was found in the Sjökulla field computational model calibration that a minimum value had to be defined for the transport capacity coefficient T_C (Eq. 79). A high value of 5.0 g l^{-1} was used in the Sjökulla field simulations while in the Hovi simulations a minimum value was not required.

Subsurface transport

Two transport mechanisms, dispersion and advection, are responsible for the transport of suspended sediment in the macropores. The advection transport mechanism is based purely on the results of the subsurface flow simulation, i.e. no additional parameters are required. For the dispersion transport mechanism, dispersivities (α_L and α_T) and molecular diffusion D^* coefficients have to be specified. In contrast to laboratory scale measurements where dispersivities are often limited to a range of 0.0001–0.01 m, field situations require values several magnitudes higher to produce realistic results (Zheng and Bennet 2002). The disparity arises because macroscopic heterogeneities are responsible for the dispersion at field-scale, rather than pore-scale heterogeneity. Dispersion, and consequently dispersivity, in the longitudinal direction of the flow is higher than in the transverse direction, i.e. $\alpha_L > \alpha_T$ (Boast 1973). The value of the α_L coefficient can be approximated by multiplying the main transport direction distance by 10% (Spitz and Moreno 1996) while the value of α_T can be assumed to be 10% of the α_L coefficient (e.g. Spitz and Moreno 1996 and Gärdenäs et al. 2006). Although some studies have shown that α_L and α_T are dependent on flow velocity (e.g. Skopp and Gardner 1992, Forrer et al. 1999 and Vanderborght et al. 2000), it is assumed here that they are constants. Beven

et al. (1993) presented a review on dispersion parameters in undisturbed partially saturated soils.

In dual-permeability model studies, the dispersivity values are usually considered to be the same in both pore systems. Ray et al. (1997) reported values of 0.01 m for α_L and 3.6 × 10^{-6} m^2 h^{-1} for D^* in a 2-D transport simulation. The soil sample dimensions were 0.38×0.48 m in *x*– and *z*-directions. Vogel et al. (2000) used a value of 0.05 m for α_L in a 2-D soil profile (2.0×1.5 m in *x*- and *z*-directions) while Haws et al. (2005) presented values of 0.15 and 0.015 m for α_L and α_T, respectively (grid size 15.0×2.0 m in *x*- and *z*-directions). Gärdenäs et al. (2006) set values of 0.1 and 0.01 and 0.2 and 0.02 m for α_L and α_T, respectively, in a simulated 2-D profile section (length 50.0 m and depth ~3 m). Köhne et al. (2006) ended up with α_L value of 0.5 m in 2-D simulations (soil section width 5–9 m and depth ~2 m). Gerke and Köhne (2004) applied a value of 0.04 m in the soil matrix and 0.1 m in the macropore system for the α_L in a 1-D simulation. They argued that the α_L value was higher in the macropore system because it was composed of different heterogeneous components such as interaggregate pore spaces, root channels and worm burrows. Gwo et al. (1995) fitted the 1-D multi-pore region model MURT to transport data measured in an undisturbed soil core (height 0.24 m and radius 0.0425 m) under different pressure heads. In contrast to Gerke and Köhne (2004), dispersivity coefficients for macro-, meso- and micropore systems were 0.08, 0.12 and 0.26 m in saturated soil, i.e. the value of α_L was lower in the macropore system than in soil matrix. The dispersivity values decreased as the pressure head in the soil decreased below saturation point.

The dispersivity coefficients in this study could not be calibrated properly with the available data because the effect of dispersion was masked out by mixing in the subsurface drains, advection in the soil and non-uniform soil erosion on the field surface. The method of Spitz and Moreno (1996) was applied here to derive the values of α_L and α_T, i.e. the transport distance from the surface to the drains is divided by 10.0 to calculate α_L. Parameter values used in the simulations are presented in Table 28.

Table 28. Dispersion coefficients in the subsurface transport domain.

Parameter:	Value:	Unit:
α_L	0.1	[m]
α_T	0.01	[m]
D^*	3.6×10^{-6}	[m^2 h^{-1}]

4.2.4 Simulation settings

The computational models were run with a 1.0 h global time step according to the meteorological measurements. The rainstorm threshold

intensity was set to 4.0 mm h^{-1}. The simulation periods and duration times are presented in Table 29.

Table 29. Simulation periods and durations.

Simulation:	Start date:	End date:	Duration [h]:
Sjökulla 1998	1 May	31 Oct.	4416.0
Sjökulla 1996	1 May	30 Nov.	5136.0
Hovi 1988	1 May	24 Oct	4237.0
Hovi 1984	1 May	8 Nov.	4617.0

Convergence of iteration in the subsurface flow submodel took a large number of iterations and consequently increased the computational load substantially with the High and Very high resolution grids (Table 20). It was noticed initially with the theoretical test case (Section 3.3.3) that after around 25 iterations, the results did not change substantially around the grid anymore. The same result was also evident in the computational models of the fields. Simulations conducted with lower resolution grids that converged better were used to cross-check the results. Conversely, if the iteration convergence threshold value was increased, mass balance errors were introduced into the results. To decrease the time to run the simulations with larger computational grids, a more pragmatic approach was adopted. The mass balances were continuously checked and they were not allowed to oscillate or increase above a 5.0% threshold of the introduced mass (precipitation, eroded sediment), while the maximum number of iterations was limited to 25 in each submodel. The simulations were run on a workstation with Intel Core i7 920 processor (4 physical cores + 4 Hyper-Threading cores) overclocked to 3.0 GHz and with 6 GBs of RAM. The iteration parameters used in the submodels are presented in Table 30.

Table 30. Submodel iteration parameters.

Parameter:	Value:	Unit:
Number of iterations	25	[-]
Iteration threshold, overland flow	1.0×10^{-5}	[m]
Bisection method, iteration threshold	1.0×10^{-8}	[m^3]
Bisection method, right side value	5.0	[m]
Iteration threshold, overland erosion	1.0×10^{-10}	[kg m^{-3}]
Iteration threshold, subsurface flow	1.0×10^{-5}	[m]
Iteration threshold, subsurface transport	1.0×10^{-7}	[kg m^{-3}]

4.3 Results

The simulation results are presented concisely in this section. Results from the Sjökulla and Hovi simulations are divided into separate sections (Sections 4.3.1 and 4.3.2). Sensitivity analysis was conducted to address uncertainty in the results (Section 4.3.3).

4.3.1 Sjökulla field simulation results

The Sjökulla field simulation results were calculated with the Very high grid resolution (144×104×16 cells in *x*-, *y*- and *z*-directions) (Section 4.2.1). Horizontal cell dimensions were 2.0×2.0 m. Simulated and measured water and sediment mass balances in the system are presented in Table 31.

Table 31. Simulated/measured water and sediment mass balances in 1998 and 1996. Abbreviations used: n.d. = not defined and Sed. = Sediment.

Year:	1998	1998	1996	1996
Storage or runoff value:	Water [mm]:	Sed. [kg ha^{-1}]:	Water [mm]:	Sed. [kg ha^{-1}]:
Surface (initial state)	0 / n.d.	0 / n.d.	0 / n.d.	0 / n.d.
Matrix (initial state)	1287 / n.d.	0 / n.d.	1293 / n.d.	0 / n.d.
Macropore (initial state)	6 / n.d.	0 / n.d.	5 / n.d.	0 / n.d.
Surface (end state)	0 / n.d.	13 / n.d.	0 / n.d.	18 / n.d.
Matrix (end state)	1341 / n.d.	0 / n.d.	1340 / n.d.	0 / n.d.
Macropores (end state)	1 / n.d.	3 / n.d.	1 / n.d.	10 / n.d.
Corrected precipitation	603	- / -	584	- / -
ET / PET	276 / 277	- / -	288 / 335	- / -
Surface net erosion	- / -	4353 / n.d.	- / -	6489 / n.d.
Surface runoff	61 / 68	1905 / 2367	67 / 58	2196 / 2669
Infiltration into soil	543 / n.d.	2434 / n.d.	517 / n.d.	4272 / n.d.
Drainflow	88 / 91	1290 / 1282	78 / 104	2245 / 2937
Seepage to ditches	46 / n.d.	757 / n.d.	45 / n.d.	1308 / n.d.
Groundwater flow	84 / n.d.	384 / n.d.	65 / n.d.	709 / n.d.
Mass balance error	1 / n.d.	-2 / n.d.	1 / n.d.	-4 / n.d.

The water and sediment mass balance errors in the simulations were +0.17% and -0.04% of the precipitation and net erosion amounts in 1998 and +0.17% and -0.06% in 1996, respectively. The mass balance errors were caused by rounding errors due to iteration in the algorithms.

Cumulative corrected precipitation, PET and simulated ET in 1998 and 1996 are presented in Fig. 36. In 1998, the simulated cumulative ET was equal to the cumulative calculated PET, whereas in August and September 1996 the simulated cumulative ET was less than the calculated PET value due to minimal precipitation and dry root zone moisture conditions (Fig. 1). The calculated PET values were not adjusted during the calibration.

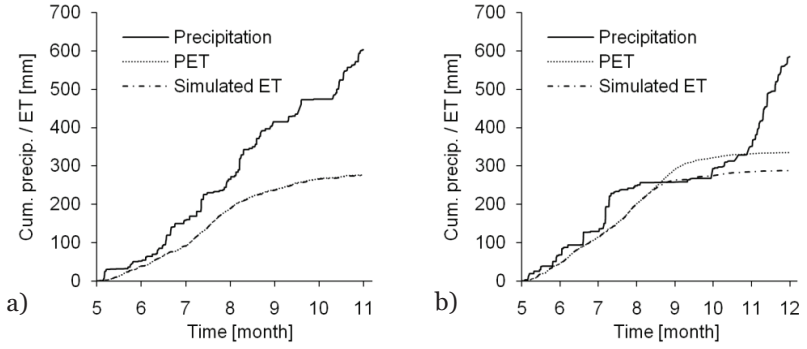

Figure 36. Cumulative corrected precipitation, PET and simulated ET in a) 1998 and b) 1996 in the Sjökulla field.

Relative magnitudes of the simulated water fluxes in the field during the growing season and autumn of 1998 (Table 31) are visualised with arrows in Fig. 37. The mass balance indicates that the water loss via groundwater flow is notable (13.9 % of precipitation) and in the same order of magnitude as subsurface drainflow (14.6% of precipitation). Surface runoff is 10.1% of precipitation.

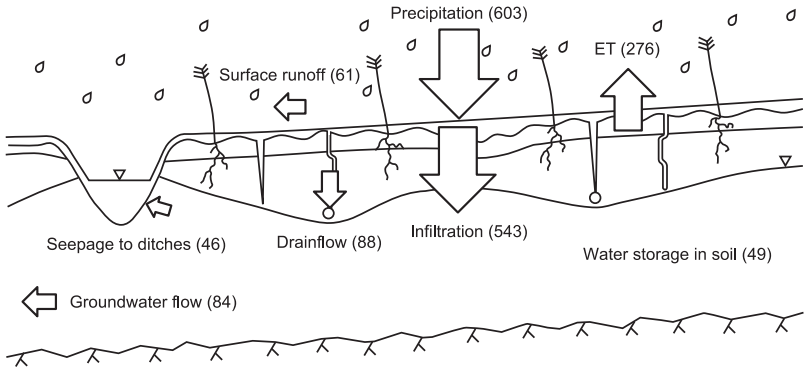

Figure 37. Water fluxes [mm] in the overland and subsurface domains in 1998 in the Sjökulla field.

Fig. 38 illustrates the relative magnitudes of the simulated sediment fluxes in the field in 1998 (Table 31). Approximately 29.6 % of the entrained sediment in the overland domain ends up in the subsurface drains while 43.8 % of the sediment is transported via surface runoff. Groundwater flow transports 8.8% of entrained sediment out of the field through subsurface pathways, and seepage flow transports 17.4% to open ditches.

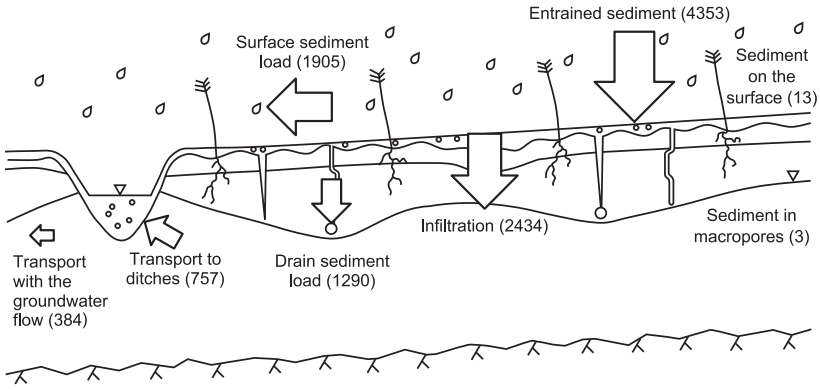

Figure 38. Sediment fluxes [kg ha^{-1}] in the overland and subsurface domains in 1998 in the Sjökulla field.

Cumulative runoff and sediment load results in 1998 and 1996 in the Sjökulla field

Model calibration was conducted with data from 1998, while data from 1996 were used for validation. Cumulative measured and simulated surface runoff and drainflow results are presented for both years in Fig. 39. A common feature visible in the 1998 and 1996 runoff results is that the simulated events are not as peaky as the measured events. Also, approximately 99.5% of the drainflow originated from the macropore system during both years. In 1996, modelled drainflow started later in the autumn than the measured drainflow and was therefore lower than the total measured cumulative result.

The Nash-Sutcliffe model efficiency coefficients (Appendix D) for surface runoff and drainflow were 0.809 and 0.645, respectively, in 1998 and 0.841 and 0.613 in 1996. The calibration and validation results in Sjökulla were similar in terms of the efficiency coefficients. This confirms the high quality of the field data and indicates that the model functions properly. The corresponding bias values (Appendix D) for surface runoff and drainflow were -0.0015 and -0.0006 mm h^{-1}, respectively, in 1998 and +0.0017 and -0.0050 mm h^{-1} in 1996. The bias values can be compared to the average measured surface runoff and drainflow values during the study periods (0.015 and 0.021 mm h^{-1} in 1998 and 0.011 and 0.020 mm h^{-1} in 1996). The efficiency coefficients and and bias values were calculated from the hourly runoff results, which are presented in more detail in the next sections.

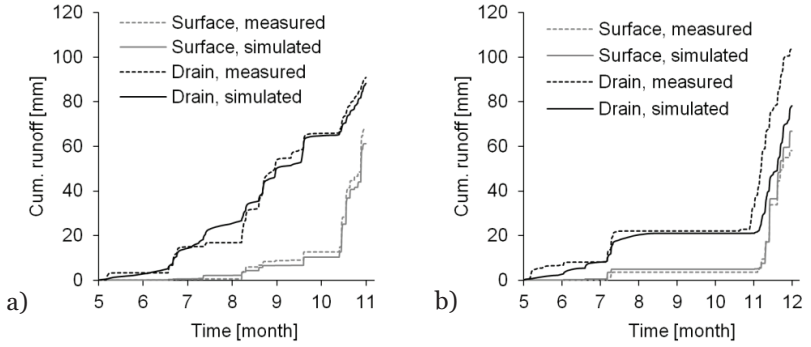

Figure 39. Measured and simulated cumulative surface runoff and subsurface drainflow results in a) 1998 (calib.) and b) 1996 (valid.) in the Sjökulla field.

Cumulative seepage to ditches and groundwater flow are presented in Fig. 40. Because 1998 was wetter than 1996 (see Fig. 36), groundwater flow was continuous during the simulation. In 1996, groundwater flow ceased almost totally between the middle of August and the end of October due to lack of precipitation.

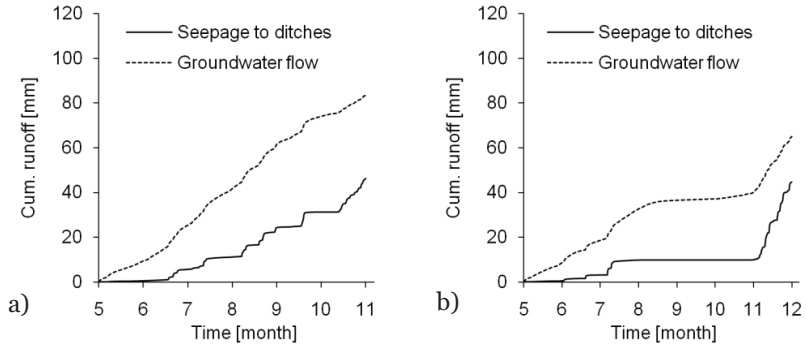

Figure 40. Simulated cumulative seepage to ditches and groundwater flow in a) 1998 (calib.) and b) 1996 (valid.) in the Sjökulla field.

Cumulative measured and simulated sediment loads via surface runoff and drainflow are presented in Fig. 41. According to the calibrated model, which quantifies the erosion components (Eqs. 66 and 70), rain drop splash erosion was responsible for the sediment load before the autumn tillage operations (May to September in 1988 and May to October in 1996). The sharp increases in the sediment loads after tillage operations in October 1998 and in November 1996 were produced by hydraulic erosion. The Nash-Sutcliffe coefficients (Appendix D) for sediment loads via surface runoff and drainflow were 0.107 and 0.750, respectively, in 1998 and 0.693 and 0.953 in 1996. The bias values (Appendix D) for sediment loads via surface runoff and drainflow were -0.10 and +0.0019 kg ha^{-1} h^{-1}, respectively, in 1998 and -0.27 and -0.13 kg ha^{-1} h^{-1} in 1996. The average sediment loads via surface runoff and drainflow during the study periods were 0.54 and 0.29 kg ha^{-1} h^{-1} in 1998 and 0.52 and 0.57 kg ha^{-1} h^{-1} in 1996. The Nash-Sutcliffe coefficients and bias values were calculated from the hourly load results, which are presented in the next section.

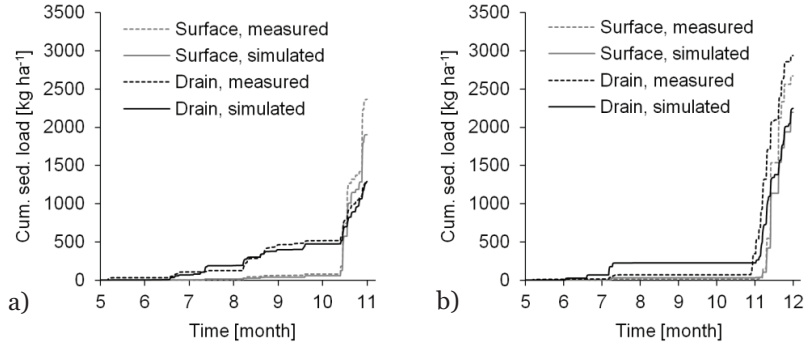

Figure 41. Measured and simulated sediment loads via surface runoff and drainflow in a) 1998 (calib.) and b) 1996 (valid.) in the Sjökulla field.

Hourly runoff and sediment load results in 1998 in the Sjökulla field

Hourly measured and simulated surface runoff results in the calibration year 1998 are presented in Fig. 42. Precipitation is presented in the second *y*-axis. Only October is drawn in Fig. 42 because surface runoff was minimal in the summer and early autumn. Timing of the surface runoff events closely matched the timing of the measurements, which indicates consistency between the weather and runoff data. However, the simulated runoff peaks are clearly lower and wider than the measured peaks. The mean absolute error (Appendix D) between the measured and modelled peak values was 0.042 mm h^{-1} for the eight events shown in Fig. 42.

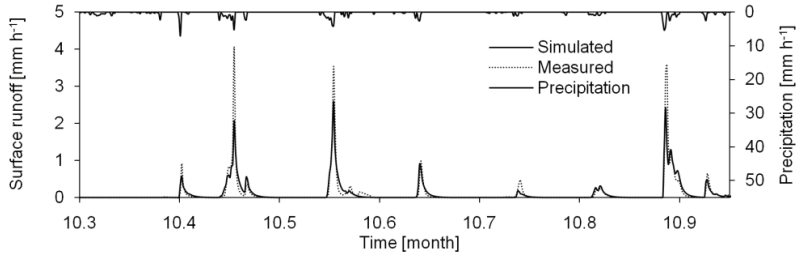

Figure 42. Hourly measured and simulated surface runoff results in 1998 in the Sjökulla field.

The simulated drainflow results compared well (with an efficiency coefficient of 0.645) to the measurements before the autumn tillage event (Fig. 43). After the tillage events in October, the first three runoff peaks were initially too low (mean absolute error 0.022 mm h^{-1}), but the rest of the modelled peaks were reproduced with a mean absolute error of 0.014 mm h^{-1}. An exceptional precipitation event (constant 0.4 mm precipitation value for 61 hours) in the middle of September produced an abnormal drainflow event compared to measurements.

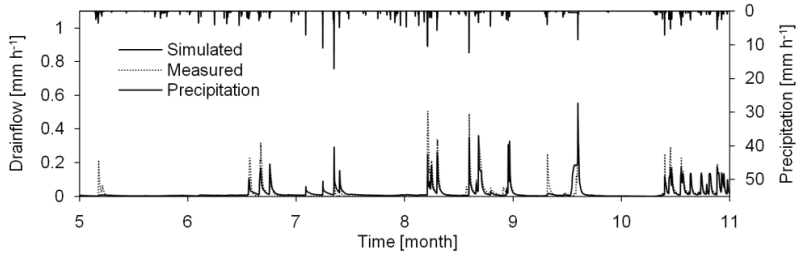

Figure 43. Hourly measured and simulated drainflow results in 1998 in the Sjökulla field.

The dynamics of the simulated overland sediment load (Fig. 44) were similar to the simulated surface runoff results (Fig. 42). The Nash-Sutcliffe coefficient was lower for the modelled sediment load via surface runoff

(0.107) than the coefficient for the surface runoff (0.809), which is due to the more pronounced under-prediction of peaks in Fig. 43 compared to Fig. 42.

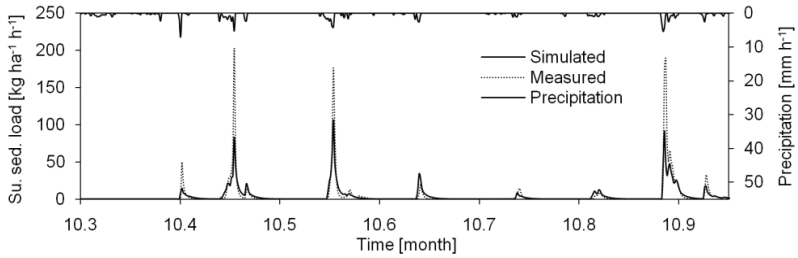

Figure 44. Hourly measured and simulated sediment loads via surface runoff in 1998 in the Sjökulla field.

Similarly to the overland flow, the drain sediment load dynamics closely resembled (Fig. 45) drainflow patterns (Fig. 43). In terms of Nash-Sutcliffe efficiency, the sediment load via drains (0.750) was modelled more accurately than the sediment load via surface runoff (0.107).

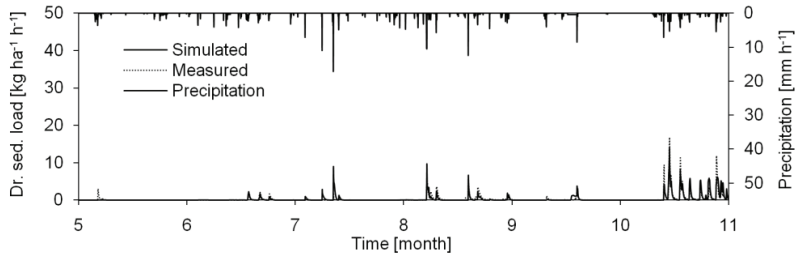

Figure 45. Hourly measured and simulated sediment loads via drainflow in 1998 in the Sjökulla field.

Hourly runoff and sediment load results in 1996 in the Sjökulla field

Only November is presented in the surface runoff graph from the validation year 1996 because surface runoff was minimal during the summer and early autumn (Fig. 46).

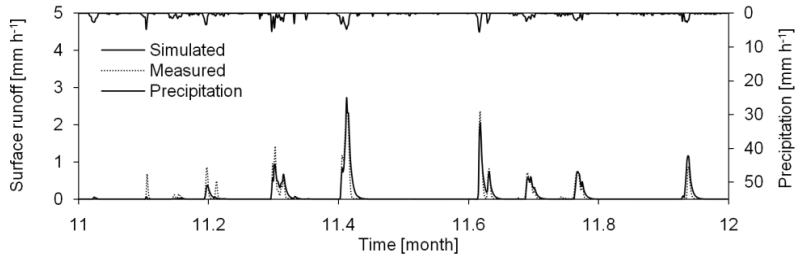

Figure 46. Hourly measured and simulated surface runoff results in 1996 in the Sjökulla field.

The simulated surface runoff peaks were followed by a longer falling limb compared to the measurements (Fig. 46). The early measured peaks in November were not reproduced in the simulated results. This is an indication of either excessively dry antecedent soil moisture conditions resulting from evapotranspiration, or uncertainty related to the precipitation measurements.

The drainflow reproduction in 1996 by the model (Fig. 47) was successful in terms of the Nash-Sutcliffe coefficient value (0.613). The simulated drainflow peaks were lower than the measured peaks during the summer and especially at the time of the first autumn peaks. As in the case of the simulated surface runoff results, too dry antecedent moisture conditions or missing precipitation observations may be the cause of the under-prediction of the simulated drainflow results in late October and early November. A large rainstorm event by Finnish standards (21 mm in one hour) occurred in the beginning of July and led to the highest measured drainflow peak (0.61 mm h^{-1}) in the simulation period.

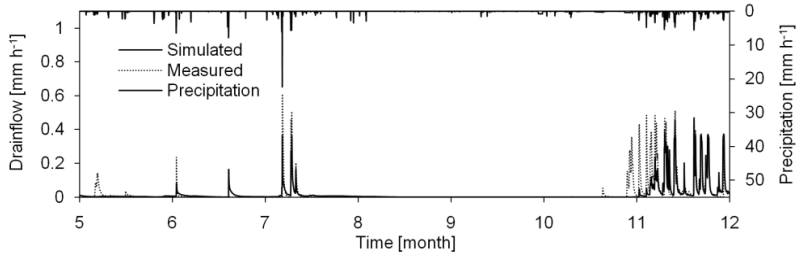

Figure 47. Hourly measured and simulated drainflow results in 1996 in the Sjökulla field.

The dynamics of sediment load via surface runoff in 1996 (Fig. 48) was qualitatively similar to the surface runoff results in 1996 (Fig. 46). The simulated sediment load peaks via surface runoff were lower with longer falling limbs than the measured load. In contrast to the results of 1998, the sediment load via surface runoff was modelled almost as well as surface runoff in terms of Nash-Sutcliffe coefficient (0.693 vs. 0.841).

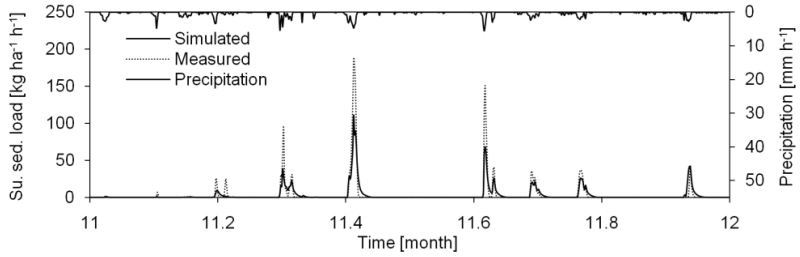

Figure 48. Hourly measured and simulated sediment loads via surface runoff in 1996 in the Sjökulla field.

The large rainstorm event in the beginning of July produced a sediment peak via drainflow (Fig. 49) but only minimal sediment load via surface runoff. Again, there is a strong similarity between drainflow (Fig. 47) and its sediment load dynamics. The Nash-Sutcliffe coefficient value for sediment load via drainflow was the highest efficiency value (0.953) reached in the simulations.

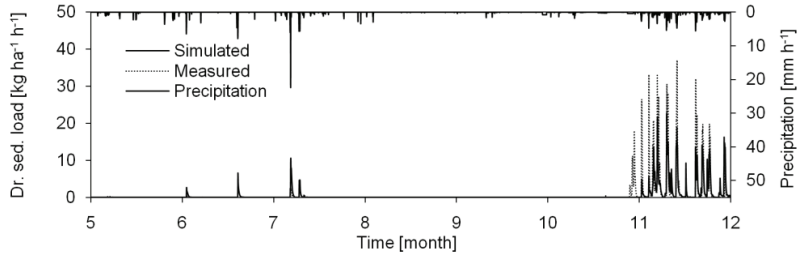

Figure 49. Hourly measured and simulated sediment loads via drainflow in 1996 from the Sjökulla field.

Groundwater table level results

Measured and simulated groundwater tables levels in tubes 1, 2, 3, 5, 7 and 9 in 1998 are presented in Figs. 50–52. Simulated levels in both soil matrix and macropore systems are drawn. The locations of the tubes are presented in Fig. 25. The sudden drops in the simulated water levels in the soil matrix were caused by groundwater flow emptying cells in deeper parts of the profile and steepness of WRCs. The large drop in the groundwater table level in the matrix pore system in October (Fig. 50–52) was caused by the long dry period extending from the end of September to the beginning of October. A general trend visible in both measured and simulated levels is that the water level is lower in tubes at higher elevations in the field. The modelled water table in Figs. 50-52 shows a quicker response to rainfall events than the measured water table.

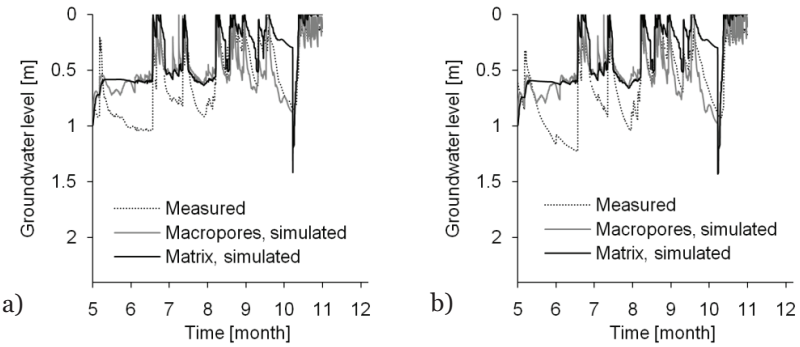

Figure 50. Measured and simulated groundwater table levels in tubes a) 1 and b) 2 in 1998 in the Sjökulla field.

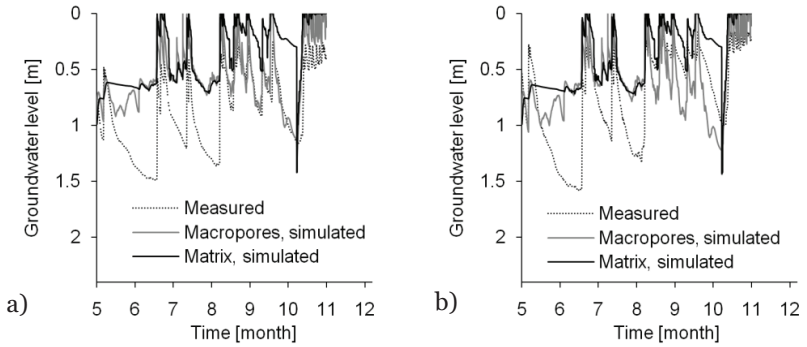

Figure 51. Measured and simulated groundwater table levels in tubes a) 3 and b) 5 in 1998 in the Sjökulla field.

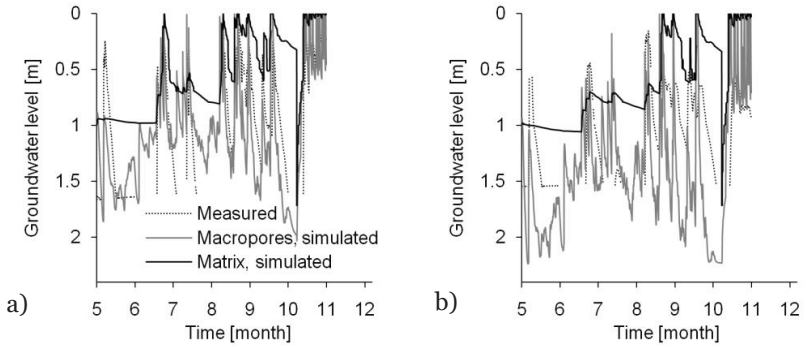

Figure 52. Measured and simulated groundwater table levels in tubes a) 7 and b) 9 in 1998 in the Sjökulla field. Fig. 52b legend is the same as in Fig. 52a.

Groundwater table level was measured at different locations in 1996 (tubes 4, 6 and 8) than in 1998 (Figs. 53–54). A drop, down to a depth of less than 1.0 m in the simulated matrix water level, is apparent in Figs. 53 and 54 in October 1996. A similar drop was experienced in October 1998 (Figs. 50-52). Again, the drop was preceded by a long dry period (e.g. Fig. 47).

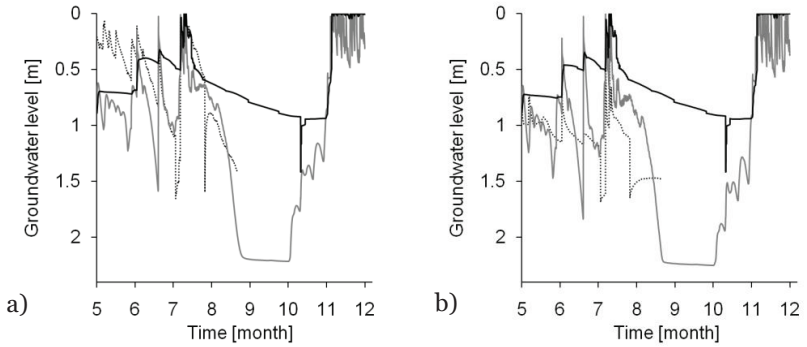

Figure 53. Measured and simulated groundwater table levels in tubes a) 4 and b) 6 in 1996 in the Sjökulla field. See legends in Figs. 50–52.

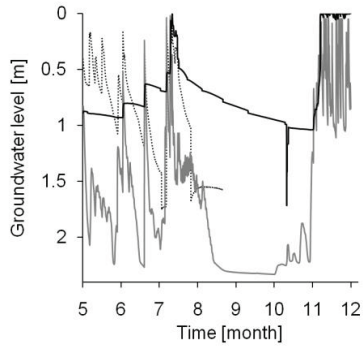

Figure 54. Measured and simulated groundwater table levels in tube 8 in 1996 in the Sjökulla field. See legends in Figs. 50–52.

Flow and erosion patterns on the field surface in the Sjökulla field

Overland flow routes in the Sjökulla field were inspected by visualising overland water depths and flow velocities immediately after rain storm events (28 Oct. in 1998 and 13 Nov. in 1996). Precipitation sums during the studied four-hour periods were 12.1 and 13.7 mm in 1998 and 1996, respectively. The conditions immediately after the events are presented in Fig. 84 in Appendix E. Overland flow velocities are presented with vectors indicating the velocity and direction of the flow. Maximum overland water depths and flow velocities were 0.195 m and 0.095 m s^{-1}, respectively, in 1998 and 0.212 m and 0.102 m s^{-1} in 1996. Overland net erosion results in the field at the end of the simulation periods are presented in Fig. 85 in Appendix E. Negative net erosion values denote sediment deposition in the cell. The maximum and minimum simulated net erosion results were +9.3 and -182.2, respectively, in 1998 and +5.4 and -102.5 kg m^{-2} in 1996. It is obvious from Figs. 84 and 85 that concentrated overland water movement and soil erosion are located in the same areas in the field.

4.3.2 Hovi field simulation results

The Hovi field simulation results were calculated with the Very high grid resolution (104×144×16 cells in *x*-, *y*- and *z*-directions) (Section 4.2.1). The horizontal dimensions of a cell were 4.0×4.0 m. Simulated and measured water and sediment mass balances in the system are presented in Table 32. The water and sediment mass balance errors were +0.52 % and 0.0% of the precipitation and net erosion amounts, respectively, in 1988 and +0.42% and 0.0% in 1984 (Table 32). As in the Sjökulla case, the mass balance errors were caused by rounding errors due to iteration in the solution algorithms.

Table 32. Simulated/measured water and sediment mass balances in 1988 and 1984. Abbreviations used: n.d. = not defined and Sed. = Sediment.

Year:	1988	1988	1984	1984
Storage or runoff value:	Water [mm]:	Sed. [kg ha^{-1}]:	Water [mm]:	Sed. [kg ha^{-1}]:
Surface (initial state)	0 / n.d.	0 / n.d.	0 / n.d.	0 / n.d.
Matrix (initial state)	1277 / n.d.	0 / n.d.	1239 / n.d.	0 / n.d.
Macropore (initial state)	4 / n.d.	0 / n.d.	4 / n.d.	0 / n.d.
Surface (end state)	6 / n.d.	21 / n.d.	15 / n.d.	32 / n.d.
Matrix (end state)	1278 / n.d.	0 / n.d.	1281 / n.d.	0 / n.d.
Macropores (end state)	1 / n.d.	0 / n.d.	2 / n.d.	1 / n.d.
Corrected precipitation	384	- / -	476	- / -
ET / PET	225 / 328	- / -	243 / 289	- / -
Surface net erosion	- / -	244 / n.d.	- / -	222 / n.d.
Surface layer runoff	25 / 25	81 / n.d.	25 / 41	47 / n.d.
Infiltration into soil	369 / n.d.	161 / n.d.	449 / n.d.	157 / n.d.
Drainflow	78 / 69	115 / n.d.	86 / 83	117 / n.d.
Groundwater flow	55 / n.d.	28 / n.d.	69 / n.d.	26 / n.d.
Error	+2 / n.d.	0 / n.d.	+2 / n.d.	0 / n.d.

Cumulative corrected precipitation, PET and simulated ET in 1988 and 1984 are presented in Fig. 55. Cumulative precipitation in the Hovi field is smaller than in the Sjökulla simulations (Fig. 36) while cumulative PET is in the same order of magnitude. Simulated cumulative ET is already lower than PET during the period from May to June in both 1988 and 1984, which results from the simulated low root zone moisture content and its impact on evapotranspiration efficiency.

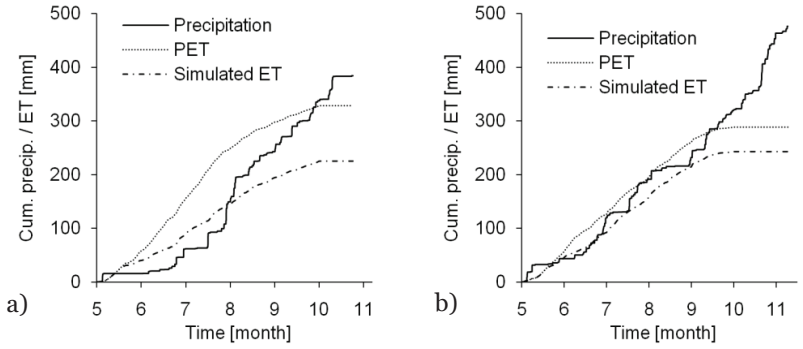

Figure 55. Cumulative corrected precipitation, PET and simulated ET in a) 1988 (calib.) and b) 1984 (valid.) in the Hovi field.

The relative magnitudes of the simulated water fluxes in the field in 1988 (Table 32) are visualised with arrows in Fig. 56. Compared to the Sjökulla results (Fig. 37), surface runoff is less important (2.9% of the precipitation). ET is the primary water loss component and it comprises 58.6% of the precipitation. Surface layer runoff in Table 32 is the sum of seepage to ditches and surface runoff components (Fig. 56). Groundwater flow in Hovi has as important role as in Sjökulla (14.3% of precipitation).

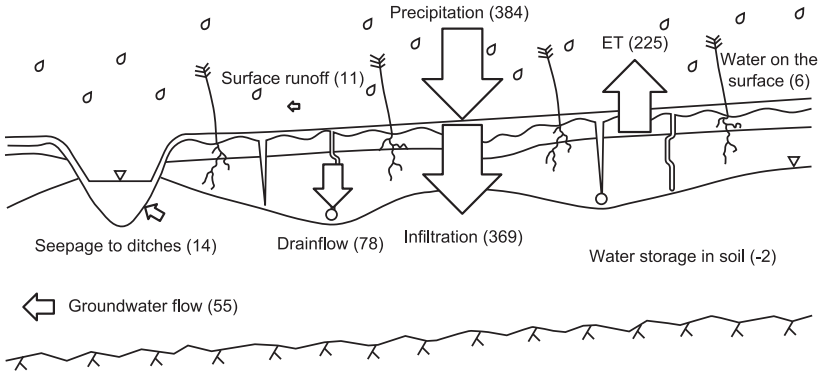

Figure 56. Water fluxes [mm] in the overland and subsurface domains in 1988 in the Hovi field.

Relative magnitudes of the simulated sediment fluxes in the field in 1988 (Table 32) are drawn with arrows in Fig. 57. The entrained sediment amounts are smaller in the Hovi field than in Sjökulla field (Fig. 57). Most of the suspended sediment is detached by rain drop impacts due to lack of surface runoff (Fig. 56) and transported to drains via macropores. In the Sjökulla field hydraulic erosion was responsible for the bulk of the sediment load.

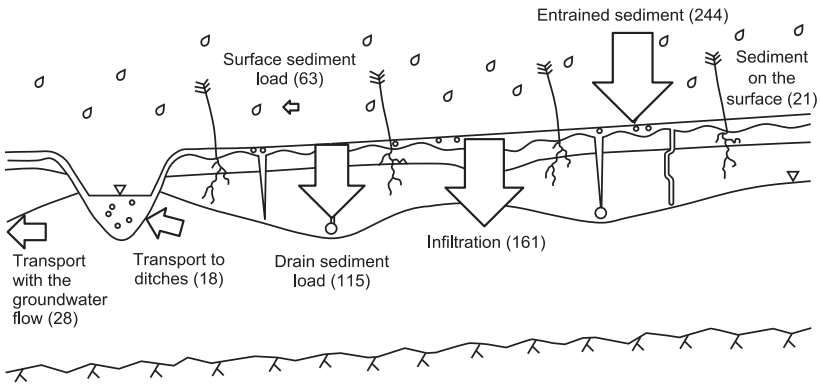

Figure 57. Sediment fluxes [kg ha^{-1}] in the overland and subsurface domains in 1988 in the Hovi field.

Cumulative runoff and sediment load results in 1988 and 1984 in the Hovi field

The model was calibrated with data from 1988 and validated with data from 1984. Cumulative measured and simulated surface layer runoff and drainflow results are presented in Fig. 58. Simulated surface layer runoff is comprised of (actual) surface runoff and seepage to ditches components. In 1988 98.5% of the drainflow came from the macropore system. In 1984 the share grew to 99.6%. Cumulative drainflow was over-predicted in

September and October 1988, while in 1984 simulated drainflow was lower in July compared to the measured values. Cumulative surface layer runoff was smaller than the measured runoff in October 1984.

The Nash-Sutcliffe model efficiency coefficients (Appendix D) for surface layer runoff and drainflow were 0.496 and 0.514, respectively, in 1988 and 0.669 and 0.717 in 1984. The coefficients were better in the validation year because runoff events were concentrated into a shorter interval at the end of the simulation period (Fig. 58b). The bias values (Appendix D) for surface layer runoff and drainflow were -0.0001 and +0.002 mm h^{-1}, respectively, in 1988 and -0.0035 and +0.00067 mm h^{-1} in 1984. The average surface layer runoff and drainflow rates were 0.0058 and 0.016 mm h^{-1} in 1988 and 0.0090 and 0.018 mm h^{-1} in 1984. The results in terms of the performance criteria were similar between the calibration and validation periods. The Nash-Sutcliffe coefficients and bias values were calculated from the hourly runoff results (see next section for details of the hourly simulation results).

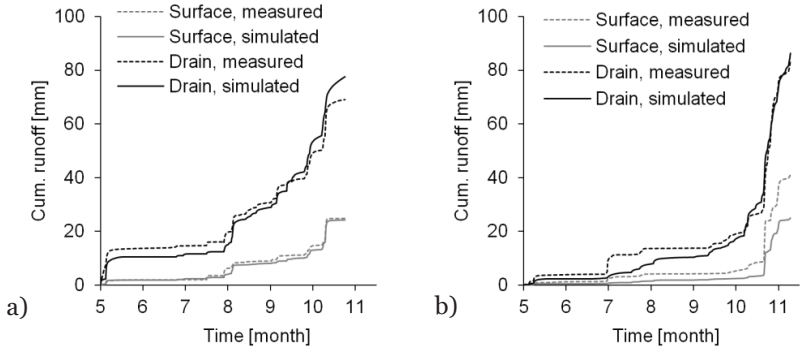

Figure 58. Measured and simulated surface layer runoff and drainflow in a) 1988 (calib.) and b) 1984 (valid.) in the Hovi field. Surface layer runoff is composed of surface runoff and seepage to ditches components (see Fig. 59).

The components of the cumulative surface layer runoff, i.e. surface runoff and seepage to ditches and groundwater flow are presented in Fig. 59.

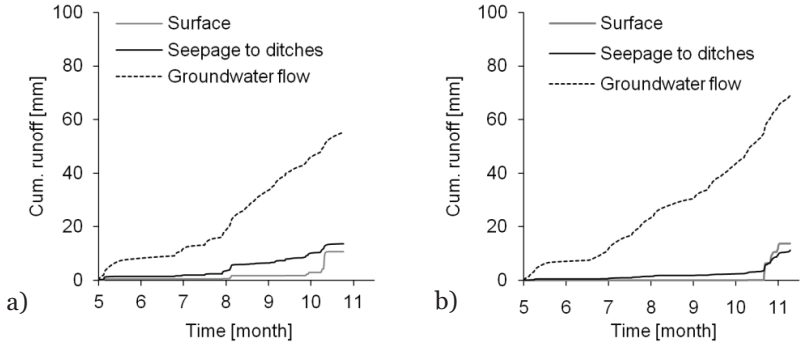

Figure 59. Simulated cumulative surface runoff, seepage to ditches and groundwater flow in a) 1988 (calib.) and b) 1984 (valid.) in the Hovi field.

Actual surface runoff is generated only in October in 1988 and at the end of October and beginning of November in 1984 (Fig. 59). The rest of the surface layer runoff is produced by the seepage to ditches component.

No Nash-Sutcliffe coefficients or bias values were calculated for the sediment load results (Fig. 60) because only a few sediment concentration measurements were available. In 1988, the sediment load is mainly generated by precipitation events in the end of July and in the beginning of October. In 1984, most of the sediment load is generated in October.

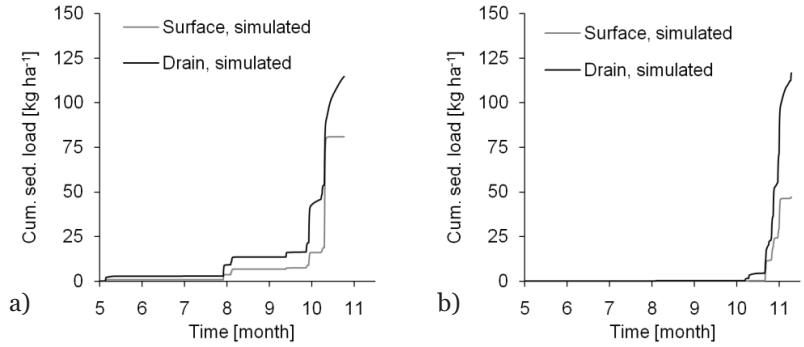

Figure 60. Simulated cumulative sediment loads via surface layer runoff and drainflow in a) 1988 (calib.) and b) 1984 (valid.) in the Hovi field.

Hourly runoff and sediment concentration results in 1988 in the Hovi field

Hourly measured and simulated surface layer runoff values in the calibration year 1988 are presented in Fig. 61. Only the end of September and the beginning of October are presented in the graph because surface layer runoff was minimal during the summer and early autumn. The simulated results compared well to the measurements in terms of the fitness criteria presented in the previous section. However, a high Manning's *n* value (3.0) had to be used to reproduce the measured pattern.

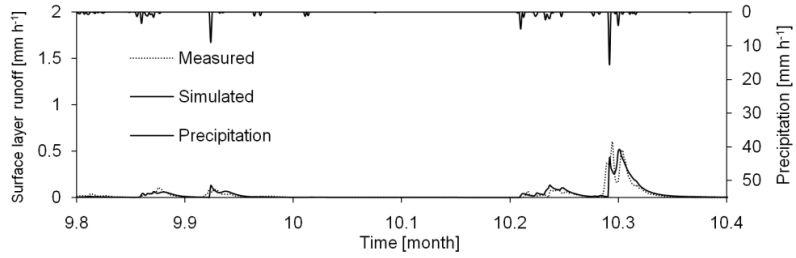

Figure 61. Hourly measured and simulated surface layer runoff results in 1988 in the Hovi field.

The Nash-Sutcliffe coefficient between the measured and simulated drainflow (0.514) was not as high in Hovi as in Sjökulla (0.645 and 0.613 in

1998 and 1996, respectively). The coefficient was affected by occasional mismatches between the measured and simulated peaks in early May, August and late October (Fig. 62). The simulated drainflow results were similar to measurements, except that the early May period and the final flow peak in October were not reproduced well (Fig. 62). In the model, decrease of macroporosity due to soil swelling and tillage operations can cause drainflow peaks to get lower and wider. In the field, some of the macropores probably close altogether, while some pathways stay open. This leads to downscaling of the peaks while the shape of the runoff curves remains the same.

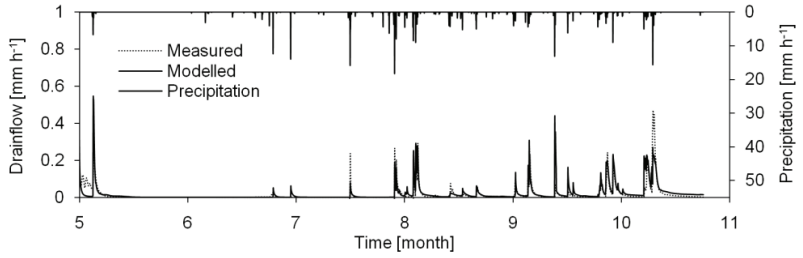

Figure 62. Hourly measured and simulated drainflow results in 1988 in the Hovi field.

Simulation results of sediment transport were compared to sediment concentration measurements instead of sediment loads in the Hovi field. Only a handful of concentration measurements were available from the field and an accurate estimation of loads would have been difficult. Because no sediment concentration measurements were available from drainflow in 1988, the simulated drainflow concentrations were plotted against concentrations measured in the ditch for comparison (Fig. 63).

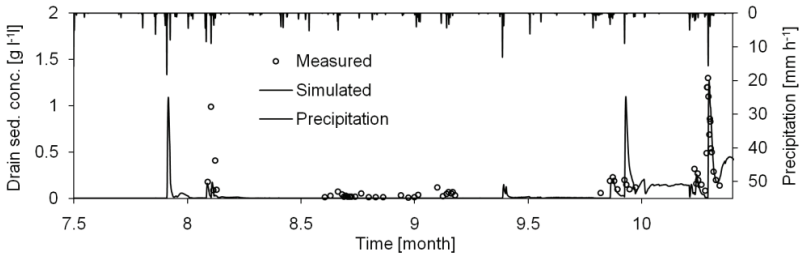

Figure 63. Hourly simulated sediment concentrations in drainflow in 1988 in the Hovi field. Concentrations in the ditch are plotted for comparison because drainflow concentration measurements were not available.

The beginning of the simulation period is not shown because concentrations were minimal in both measurements and simulations. As presented earlier, suspended sediment in the Hovi field simulations was produced solely by rain drop splash erosion (Table 27). Although Fig. 63

only presents an overview of the events in 1988 it can be seen that the timing of erosion events is similar to the measurements. The mean absolute error and bias (Appendix D) between the measured and simulated concentration values for the period shown in Fig. 63 were 0.17 g l^{-1} and -0.084 g l^{-1} (average measured concentration 0.25 g l^{-1}), respectively. Some simulated peaks such as the one in the end of July were not measured.

Measured and simulated sediment concentrations in the ditch are presented in Fig. 64 together with the simulated concentrations calculated from both drainflow and surface layer runoff entering the ditch. Only the end of September and beginning of October are shown, because the dynamics of the simulated ditch concentrations are similar to the sediment concentrations in drainflow (Fig. 63). The timing of the simulated peaks were similar to the measurements. The simulated peak at the end of September is not visible in the measurements. The mean absolute error between the measured and simulated concentration values was 0.28 g l^{-1} and the bias was -0.091 g l^{-1} (average measured concentration 0.42 g l^{-1}).

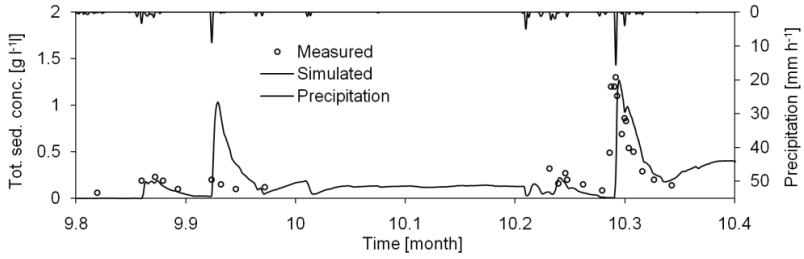

Figure 64. Hourly measured and simulated sediment concentrations in the ditch in 1988 in the Hovi field.

Hourly runoff and sediment concentration results in 1984 in the Hovi field

Hourly measured and simulated surface layer runoff results in the validation year 1984 are presented in Fig. 65. Only October and the beginning of November are presented in the graph (Fig. 65) because runoff was minimal during the summer and early autumn.

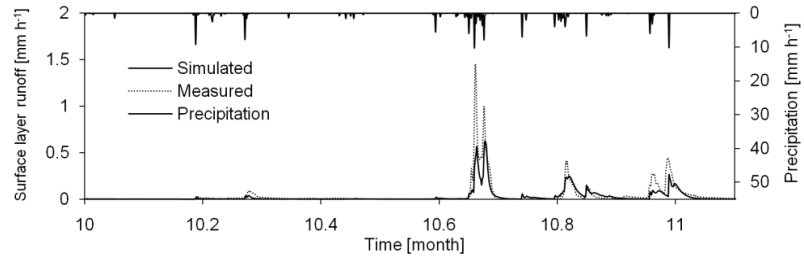

Figure 65. Hourly measured and simulated surface layer runoff results in 1984 in the Hovi field.

Simulated surface layer runoff peaks were lower than the measurements but the timing was similar (Fig. 65). The lower simulated peaks could have been caused by too high infiltration rates and high values of Manning's coefficient.

The large drainflow event in the end of June was not reproduced in the simulated drainflow results (Fig. 66) and the peaks in the end of October were smaller than the measured peaks. In the end of June, soil was presumably too dry to produce drainflow due to ET in the model. The drop in drainflow intensities in the end of October is caused by the soil swelling process in the model. In terms of the Nash-Sutcliffe coefficient values, the surface layer runoff and drainflow results from the validation year 1984 were better than the results from the calibration year 1988.

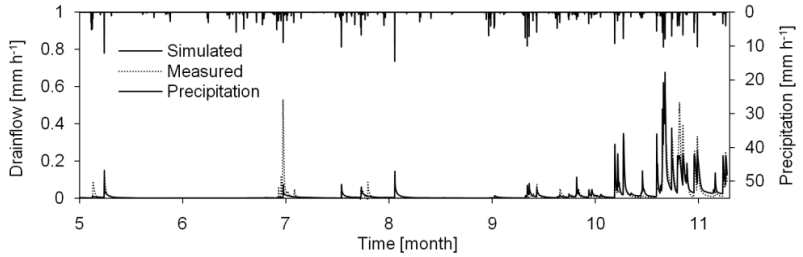

Figure 66. Hourly measured and simulated drainflow results in 1984 in the Hovi field.

Only four concentration measurements were available from drainflow in 1984 (Fig. 67). The simulated sediment concentrations in the drainflow started to rise steeply only after the middle of October, while according to the measurements, concentrations actually started to rise already in the beginning of October.

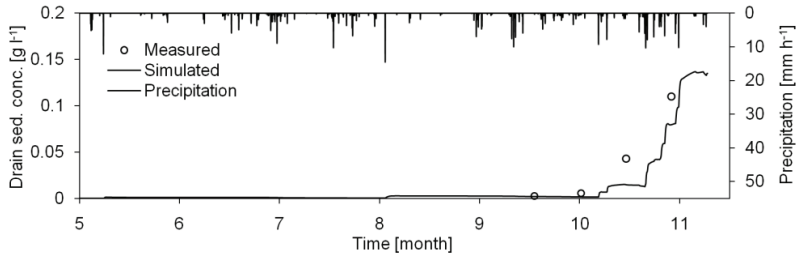

Figure 67. Hourly measured and simulated drainflow sediment concentrations in 1984 in the Hovi field.

The simulated concentration results in the ditch (Fig. 68) were calculated from the surface layer runoff and drainflow results. The measured ditch concentrations (Fig. 68) were slightly higher than the sediment concentrations in the drainflow (Fig. 67). The sparse data available from the ditch does not validate the simulated concentration results (Fig. 68). Also,

the concentration measurements do not coincide with the precipitation events. Concentration scales (y-axis) in Figs. 67 and 68 are different due to differences between drainflow and ditch concentrations.

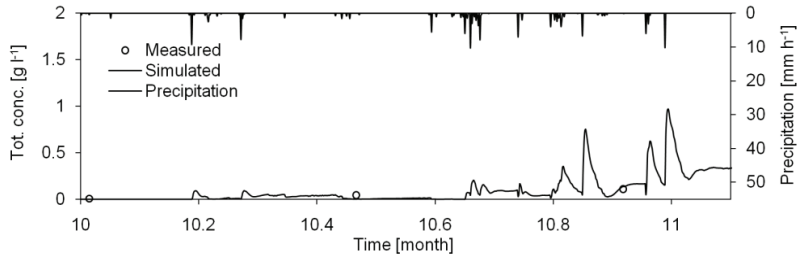

Figure 68. Hourly measured and simulated sediment concentrations in the ditch in 1984 in the Hovi field.

Flow and erosion patterns on the field surface in the Hovi field

Overland flow patterns in the Hovi field were inspected by visualising overland water depths and flow velocities immediately after rain storm events (10 Oct. in 1988 and 21 Oct. in 1984). Precipitation sums during the single hour periods were 14.9 and 10.3 mm in 1988 and 1984, respectively. The conditions immediately after the events are presented in Fig. 86 in Appendix E. Overland flow velocities are presented with vectors indicating the velocity and direction of the flow. Maximum overland water depths and flow velocities were 0.383 m and 0.007 m s^{-1}, respectively, in 1988 and 0.227 m and 0.022 m s^{-1} in 1984. The flow velocities were low compared to the Sjökulla results (Section 4.3.1.5). Overland net erosion results in the field at the end of the simulation periods are presented in Fig. 87 in Appendix E. Negative erosion values denote sediment deposition in the cell. The maximum and minimum simulated net erosion results were +0.14 and -3.30 kg m^{-2}, respectively, in 1988 and +0.13 and -2.61 kg m^{-2} in 1984.

4.3.3 Model sensitivity analysis

Several methods or frameworks have been published that address uncertainty in hydrological modelling (e.g. Beven and Binley 1992 and Refsgaard and Henriksen 2004). The principal problems are the uniqueness of the solution and the role of uncertainty in simulation results. Model sensitivity to parameter values, grid resolution and the effect of spatial variation of macroporosity is analysed to address uncertainties in the results. In addition, the roles of tillage and soil shrinkage and swelling processes in the simulations are investigated. The effect of grid dimension (1-D, 2-D or 3-D grid) on simulation results is tested in the end of the

section. The model sensitivity analyses were conducted with the calibrated computational models.

Parameter sensitivity analysis

Parameter sensitivity analysis was employed to detect the parameters that had the greatest influence on simulation results. Sensitive parameters were calibrated with greater care compared to the less sensitive ones. Effects of the parameters on results were assessed by offsetting them from their initial values by +10 and -10%. The resulting simulated surface runoff, drainflow and sediment loads via surface runoff and drainflow were compared to the original simulation results. The relative changes to runoff and load results due to the parameter modifications are presented in Table 33. The rankings were calculated by subtracting the +10% change from the -10% change (Table 33), squaring the result and summing up the runoff and sediment load components.

Table 33. Parameter sensitivity analysis results [%]. Abbreviations used: SR = surface runoff, DF = drainflow, SL = sediment load via surface runoff, DL = sediment load via drainflow, G.w. depth = initial groundwater depth and Dit. w. depth = ditch water depth. H1–4 refer to the soil horizons in the profile (Fig. 34). Root depth parameter refers to the maximum root depth value (Table 23).

Rank:	Offset: Parameter:	+10% SR [%]:	-10% SR [%]:	+10% DF [%]:	-10% DF [%]:	+10% SL [%]:	-10% SL [%]:	+10% DL [%]:	-10% DL [%]:
1	$n_{MVG,M}$, H2–4	80.3	118.4	87.2	109.8	79.2	112.9	94.5	99.5
2	Drain depth	94.5	112.9	113.1	75.8	95.8	107.7	110.2	80
3	$n_{MVG,M}$, H1	96.4	99.2	89.5	107.2	99.6	95.6	89.6	113.3
4	θ_S, H2–4	91.4	108	99	100.9	91.2	107.1	101.9	98.1
5	θ_S, H1	92.8	107.5	98.4	100.5	94.4	104.8	98.7	99.9
6	$h_{W,THR}$	99.2	101.6	100.4	99	101.5	99.4	106.1	92.4
7	$K_{FS,MUL}$	96.1	106.1	99.9	99	97.2	105.7	102.3	97
8	w, H3	96.9	103.3	102.9	96.5	97.8	102.7	103.1	96.2
9	γ_K, H2–4	96.6	102.8	100.3	100	96.5	102	101.9	99.5
10	γ_K, H1	97.2	103.9	99.9	99.7	97.8	103.1	100.1	100
11	G.w. depth	97.9	101.9	96.8	103.4	98.3	101.3	100.4	100.1
12	k_H	100.3	99.9	99.8	99.9	103.1	97.3	101.6	97.4
13	Ditch depth	97.8	102	96.9	101.7	98.8	101.7	99.5	100.6
14	Root depth	98.6	101.6	99.6	100.5	97.6	102.3	102.8	98.6
15	k_R	100.1	99.7	99.9	100.4	100.6	99.7	103.4	97.5
16	w, H1	97.9	102.2	100.5	99.2	98	102	100	99.9
17	w, H4	99.3	101.7	97.3	102.1	99.5	101.7	99.8	99.3
18	$\alpha_{MVG,M}$, H2–4	97.9	101.7	99.6	100.8	97.9	102	100.6	99.5
19	$n_{MVG,F}$	99.4	102.7	99.4	101.2	99.6	101.8	99.2	100.5
20	K_{SM}, H1	99.3	101.3	100.5	99.1	98.9	101.9	98.8	100.7
21	$\alpha_{MVG,F}$	100	100.5	100.8	98.4	100.6	100.2	101.6	98.7
22	n	99.9	100.3	99.9	99.8	101.6	98.7	100.6	99.1
23	α_K, H1	101.5	99.1	99.5	99.9	101	99.5	100.8	100.4
24	$\alpha_{MVG,M}$, H1	98.9	101.1	100	100.2	99.1	100.9	99.9	99.8
25	Dit. w. depth	100.4	99.6	100.5	99.6	100.6	99.6	100.6	99.6
26	α_K, H2–4	100.1	98.7	100.2	100.4	99.6	98.4	100.5	101
27	θ_R, H1	100.3	99.2	100.6	99.8	100.1	99.2	100.3	100.4
28	α_T	100	100	100	100	100.3	100	99.2	100.6
29	w, H2	100.4	100.2	99.5	100.1	100.6	100.2	99.1	100.1
30	K_{SM}, H2–4	99.8	99.7	99.9	100.2	99.7	99.3	99.5	100.5
31	d	99.6	100.3	100.3	99.7	99.9	100.3	100	100.4
32	β_K, H1	99.9	100.2	99.9	100.1	99.8	99.8	100.2	100.9
33	α_L	99.6	100.2	100.3	99.9	99.9	100.2	100.1	100
34	β_K, H2–4	99.3	99.7	100.2	100.3	99.3	99.5	100.9	101
35	D_S	99.6	99.9	100.3	100.2	99.8	99.5	100.5	100.4

The results were calculated only with the Sjökulla 1998 parameterisation and with the Low grid resolution (18×13×16 cells in *x*-, *y*- and *z*-directions). Due to the parallel computing approach (Section 3.2.2.3), some fluctuation was evident in the results. Small deviations around the original results could have been caused by this phenomenon. The $n_{MVG,M}$ parameters were decreased only by 5% because the value of the parameter had to be higher than 1.0. According to the test, the results were sensitive to the adjustment of the soil matrix MVG WRC parameters n_{MVG} and θ_S (Table 33). Other parameters that were found out to strongly influence the results included subsurface drain depth, $h_{W,THR}$ and $K_{FS,MUL}$. Surprisingly, manipulation of the characteristic radius d in the first order water exchange coefficient had only minor effects on the results.

Effect of grid resolution on results

The effect of computational grid resolution on runoff and sediment load simulation results was analysed by increasing grid resolution in the horizontal and vertical directions (Section 4.2.1). Simulation times with different grid resolutions are presented in Table 34. The Hovi simulation times were shorter than the corresponding Sjökulla times because there were fewer active cell columns in the grids (Section 4.2.1). Every time the horizontal resolution was quadrupled, the simulation time was increased approximately sevenfold. When the vertical resolution was doubled, i.e. the total number of cells was doubled, the simulation time was also approximately doubled. However, the effect of vertical resolution was investigated with only two different resolution steps, making it difficult to draw any definite conclusions from the result.

Table 34. Simulation times [min] with different grid resolutions.

Resolution / Simulation:	Sjökulla 1998:	Sjökulla 1996:	Hovi 1988:	Hovi 1984:
Low	11	11	9	9
Medium (*z* = 16 cells)	94	79	50	47
Medium (*z* = 30 cells)	323	162	110	148
High	713	503	440	469
Very High	4763 (3d, 7h)	3414 (2d, 8h)	3391 (2d, 9h)	3282 (2d, 7h)

Convergence of the results was assessed only visually from the simulation results with different grid resolutions. The term “convergence” in this context means that at a certain resolution step the results do not change any more. The Sjökulla surface runoff results in 1998 and 1996 converged at the High resolution step (72×52×16 cells in *x*-, *y*- and *z*-directions) but the drainflow results did not converge with the calculated resolutions (Fig. 69), However, the difference between the resolution steps was not notable (Fig. 69).

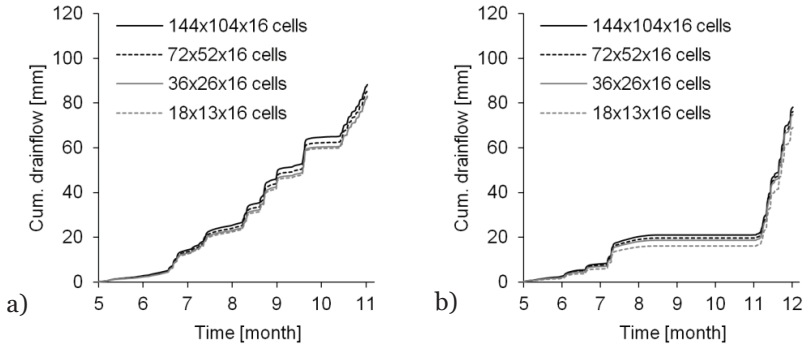

Figure 69. Simulated cumulative subsurface drainflow in a) 1998 b) 1996 with the Sjökulla field computational model with different horizontal grid resolutions (number of cells in *x*-, *y*- and *z*-directions).

Cumulative sediment loads via surface runoff in the Sjökulla field did not converge within the simulated resolution steps and additionally the results fluctuated between the steps (Fig. 70). Cumulative sediment load results via drainflow converged at the Medium resolution step (36×26×16), even though drainflow changed between the resolution steps (Fig. 69). The two tested vertical resolutions (36×26×16 and 36×26×30) produced almost identical results in the Sjökulla field. The absolute changes in cumulative runoff and sediment load results were below 5% between the vertical resolution steps during both years.

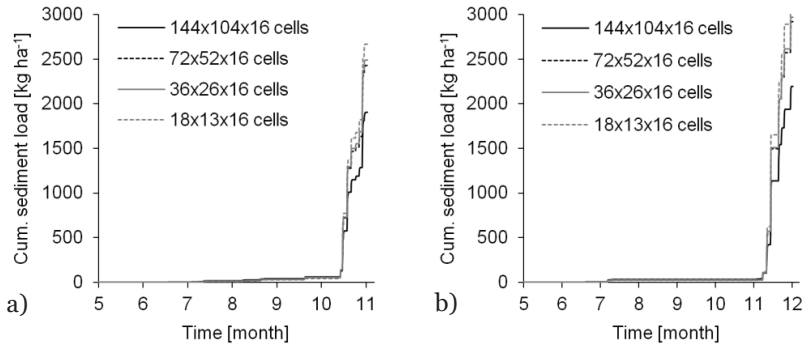

Figure 70. Simulated cumulative sediment loads via surface runoff in a) 1998 b) 1996 with the Sjökulla field computational model with different horizontal grid resolutions (number of cells in *x*-, *y*- and *z*-directions).

The Hovi simulation results converged already at the Medium resolution step (26×36×16). With the higher vertical resolution (26×36×30) there was some decrease apparent in the 1988 drainflow result (71.2 vs. 75.9 mm) but not in the 1984 result (Fig. 71). The main reason for the better convergence in the Hovi computational model seemed to be the more gentle slopes in the field compared to the Sjökulla field. Groundwater in the Sjökulla field flowed with an increased flow rate towards the lower areas in the grid compared to the Hovi field, due to steeper slopes. This in turn, increased

drainflow as the groundwater table rose closer to the field surface in the lower parts of the field.

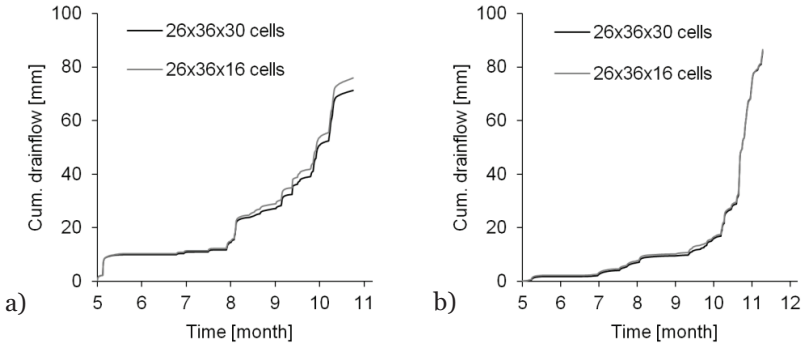

Figure 71. Cumulative subsurface drainflow results in a) 1988 b) 1984 with the Hovi field computational model with different vertical grid resolutions (number of cells in *x*-, *y*- and *z*-directions).

Effect of spatial variability of macroporosity on results

The effect of spatial variation of macroporosity in the field area on the simulation results was investigated with the Sjökulla field computational model (Fig. 25). The Hovi field was not studied in this section because no data on spatial variation of soil hydraulic properties were available. The structure of the profile was presented in Fig. 34 and the macropore parameters (static macroporosity) in Table 24. The High grid resolution step (72×52×16) was used in the test (Section 4.2.1). Four scenarios were developed to test the effect of spatial variation of macroporosity on runoff and sediment load results. In Scenarios 1, 2 and 3, soil profile areas 1, 2 and 3 (Fig. 26, Table 24) were applied separately to the whole field area. In the Scenario 4, an arithmetic mean was calculated between the parameters of the three soil profile areas and the mean values were applied to the whole field area. The results are presented in Fig. 72.

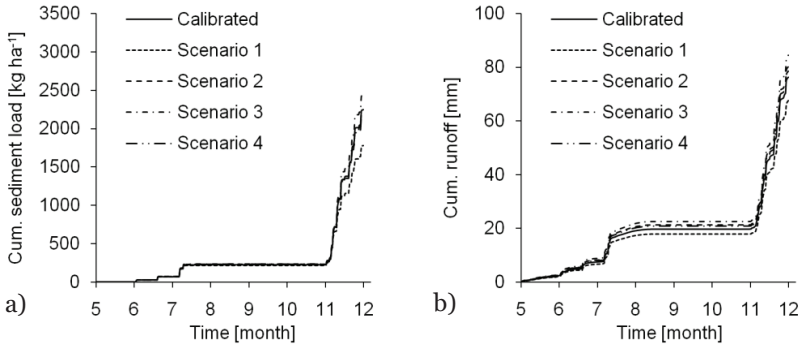

Figure 72. The effect of different macroporosity scenarios on a) sediment load via drainflow and b) drainflow with the Sjökulla field computational model in 1996.

In the 1998 case, the absolute changes to surface runoff, drainflow and sediment load results via surface runoff and drainflow were all below 6%. In the 1996 case, sediment load via drainflow decreased -21% in the Scenario 1 (Fig. 72a). Other notable changes in 1996 included the decrease of drainflow (-11%) in the Scenario 1 and increase of drainflow (+11%) in the Scenario 3. All other changes in 1996 were under 10% (absolute). The decrease in drainflow and sediment load via drainflow in the Scenario 1 in 1996 was probably caused by the decrease of static macroporosity in the lower parts of the profile near subsurface drains.

Effects of soil shrinkage and swelling processes and tillage operations on results

The effects of soil shrinkage and swelling processes and tillage operations on runoff and sediment load results were tested by turning the processes off in the model one at a time. The high resolution grids were used in the comparison (Section 4.2.1). Surface runoff in the Sjökulla field increased +64% and +47% in 1998 and 1996, respectively, when the shrinkage and swelling processes were inactivated (Fig. 73). Drainflow and groundwater flow were in turn decreased. In the Hovi field, drainflow increased +13% and +25% in 1988 and 1984, respectively, when the soil shrinkage and swelling processes were not active. Surface layer runoff increased +19% and +21% in 1988 and 1984, respectively. The increase in drainflow in the Hovi field site was attributed to the decrease of groundwater flow.

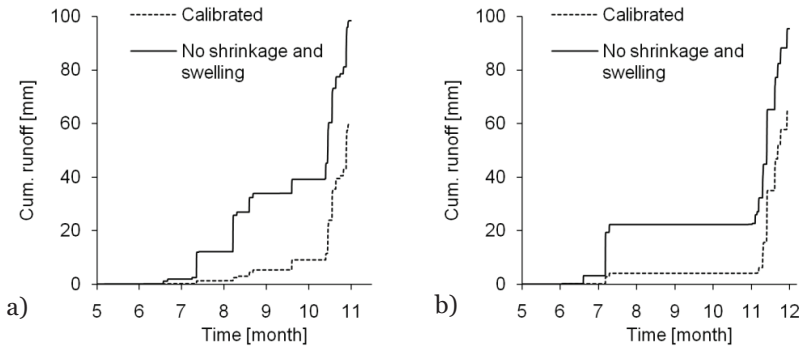

Figure 73. Simulated cumulative surface runoff results with and without soil shrinkage and swelling processes in a) 1998 b) 1996 with the Sjökulla field computational model.

The corresponding cumulative sediment loads via surface runoff in the Sjökulla field increased +25% and +24% in 1998 and 1996, respectively (Fig. 74). In the Hovi field, the cumulative sediment load via surface runoff increased +12 and +7% in 1988 and 1984, respectively. The cumulative sediment load via drainflow increased +26 and +40% during the same simulation periods.

The increase in surface runoff, when the soil shrinkage and swelling processes were inactive, was caused by the decreased infiltration capacity of the profile and loss of water storage volume due to smaller macropore system. Although surface runoff was increased in the summer months, the corresponding sediment load did not increase as much (Fig. 74) because erodibility of the soil was increased only after tillage operations in the autumn.

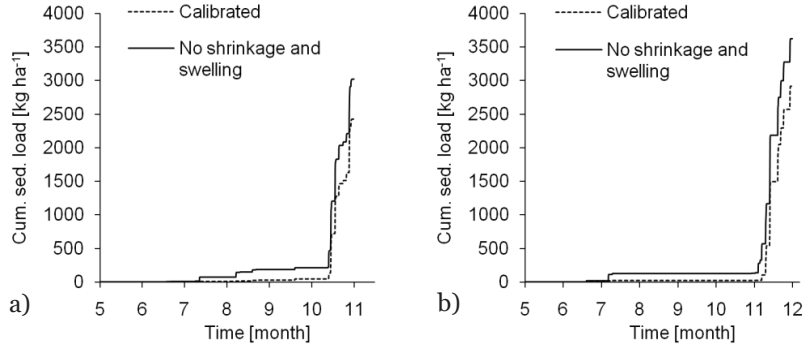

Figure 74. Simulated cumulative sediment loads via surface runoff with and without soil shrinkage and swelling processes in a) 1998 b) 1996 with the Sjökulla field computational model.

The tillage operations in the autumn had a big impact on runoff and sediment load results in the computational models. When the tillage effects were turned off, i.e. macroporosity in the tillage layer was not decreased and the soil erodibility was not increased, cumulative surface runoff in the Sjökulla field decreased -56% and -30% in 1998 and 1996, respectively (Fig. 75). Cumulative drainflow increased +21% and +13% during the same years. In the Hovi field, cumulative surface runoff decreased -21% in 1988 and -25% in 1984. Cumulative drainflow increased +6 and +20% in 1988 and 1984, respectively.

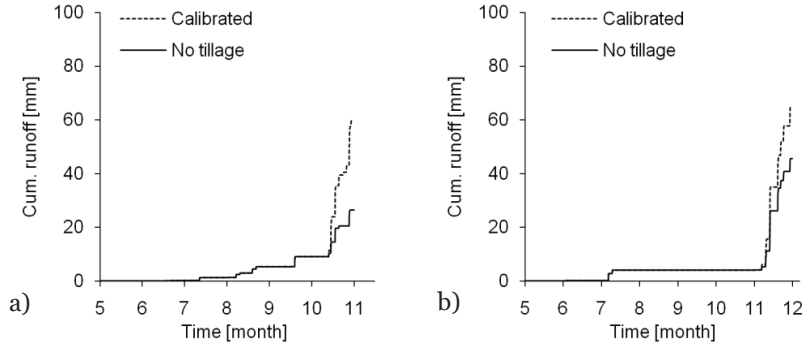

Figure 75. Simulated cumulative surface runoff results with and without tillage changes to macroporosity of the tillage layer in a) 1998 b) 1996 with the Sjökulla field computational model.

The largest differences were apparent in the sediment load results via surface runoff. In 1998, the cumulative load decreased -67% while in 1996 the decrease was -33% (Fig. 76). The changes in cumulative sediment loads via drainflow were not so drastic, increasing +14% in 1998 and decreasing -1% in 1996. The cumulative loads in the Hovi field decreased to approximately one third of the original load results during both years (Table 32 and Fig. 60).

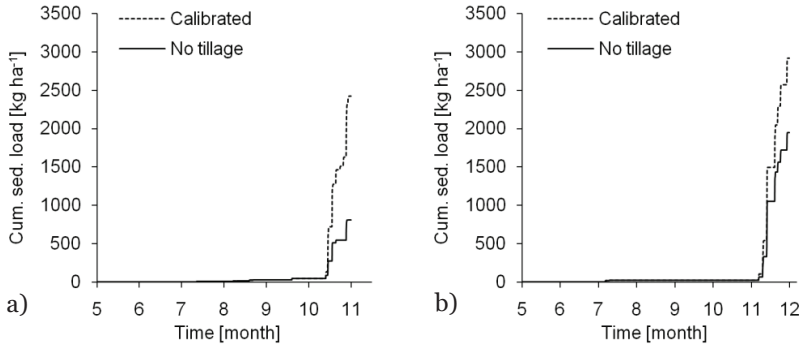

Figure 76. Simulated cumulative sediment loads via surface runoff with and without tillage changes to macroporosity of the tillage layer in a) 1998 b) 1996 with the Sjökulla field computational model.

Effect of grid dimension on results

Most of the previous preferential flow studies were conducted with 1-D or 2-D models (Section 2.2). To see how the parameterisations derived in this study functioned with lower dimension grids, the Sjökulla simulations were rerun with 1-D and 2-D grids generated with AGGS. The locations and section views of the 1-D and 2-D grids are presented in Fig. 77. The resolution of the 1-D grid had to be set to 3×3×16 cells in *x*-, *y*- and *z*-directions because the model required the extra cells to decipher the slope of the field. The average slope and area of the grid were 0.027 and 36 m^2, respectively. The 2-D grid is composed of a string of 102 active cell columns and it was positioned in a location where water will naturally collect and flow towards the discharge point (Figs. 77 and 84). The average slope and area of the grid were 0.016 and 204 m^2, respectively. The incoming and outgoing groundwater fluxes perpendicular to the running direction of the 2-D grid were set to zero. The same vertical profiles (Fig. 34) and horizontal cell diameters (2.0×2.0 m) were used in the 1-D, 2-D and 3-D grids. The soil parameters were set according to the locations of the grids (Fig. 26) (soil 2 used in the 1-D grid). Because the 1-D profile was located on a slope in the field, water was flowing horizontally into and out of the profile. The horizontal multipliers of the saturated hydraulic conductivity parameters were modified from 1.0 to 0.01 to adjust the net water loss due to groundwater flow.

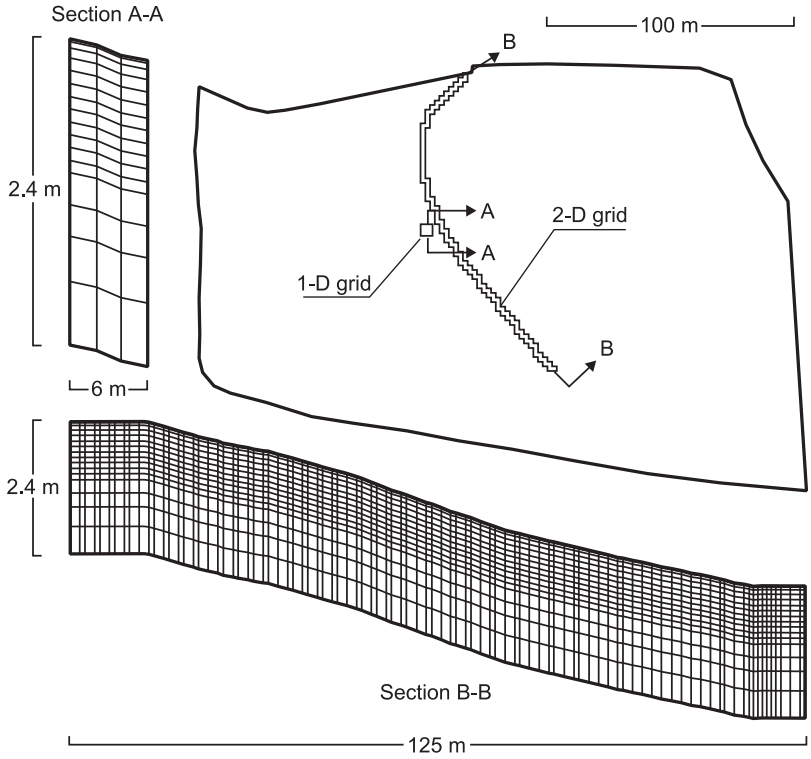

Figure 77. The locations of the 1-D and 2-D grids in the Sjökulla field and section views of the grids (the vertical axis has been magnified tenfold in the section views to accentuate topography).

Surface runoff and drainflow and the respective sediment load results simulated with the 1-D, 2-D and 3-D grids are presented in Figs. 78–81. The 3-D grid results were calculated with the Very high grid resolution (Section 4.2.1).

While the simulations with the 2-D grid resulted in similar surface runoff values compared to the 3-D grid (55.2 and 61.1 mm in 1998 and 51.6 and 66.9 mm in 1996), the 1-D grid exaggerated surface runoff considerably (92.8 mm in 1998 and 1996) (Fig. 78).

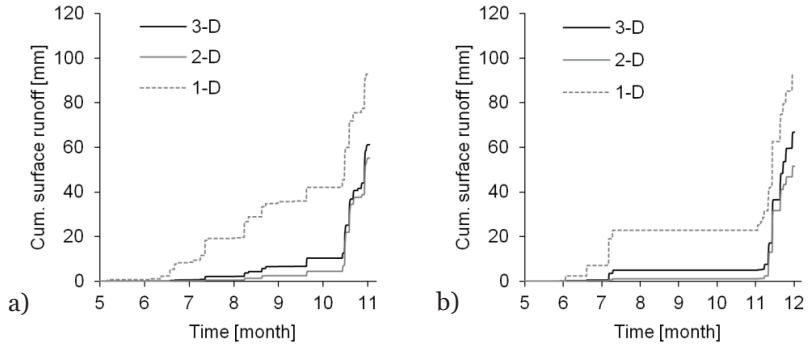

Figure 78. Simulated cumulative surface runoff in the Sjökulla field with the 1-D, 2-D and 3-D grids in a) 1998 and b) 1996.

On the other hand, the 1-D grid produced similar drainflow results to the 3-D grid (87.3 and 88.2 mm in 1998 and 76.7 and 78.1 mm in 1996) but simulations with the 2-D grid resulted in too much drainflow during both simulation years (191.1 and 164.6 mm in 1998 and 1996, respectively) (Fig. 79).

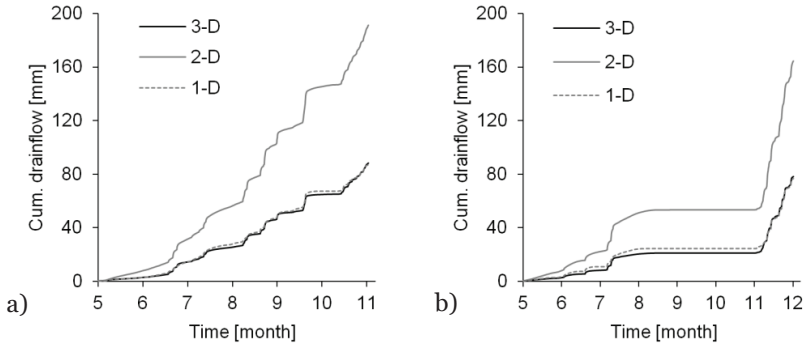

Figure 79. Simulated cumulative drainflow with the 1-D, 2-D and 3-D grids in the Sjökulla field in a) 1998 and b) 1996.

The cumulative sediment load via surface runoff simulated with the 1-D grid (Fig. 80) was approximately half of the results simulated with the 2-D and 3-D grids. The foot of the hill, where most of the net erosion took place in the 2-D and 3-D grids due to higher flow depths (Fig. 85), was missing from the 1-D grid. Sediment loads calculated with the 2-D and 3-D grids were similar (2182 and 1905 kg ha^{-1} in 1998 and 2042 and 2196 kg ha^{-1} in 1996) (Fig. 80).

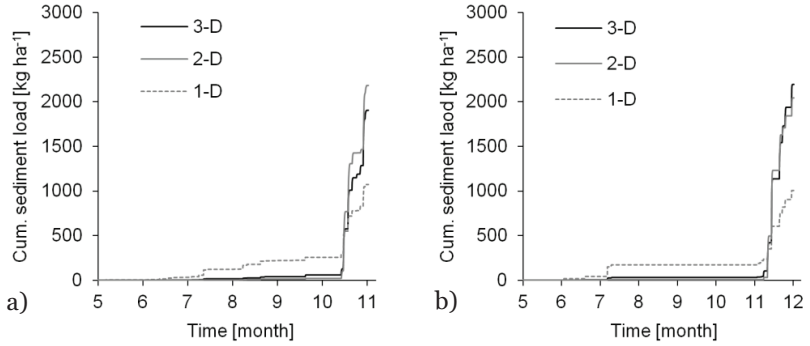

Figure 80. Simulated cumulative sediment loads via surface runoff in the Sjökulla field with the 1-D, 2-D and 3-D grids in a) 1998 and b) 1996.

The sediment load results via drainflow simulated with the 1-D, 2-D and 3-D grids (Fig. 81) did not exhibit the same behavior as the sediment load results via surface runoff. In 1998, the sediment loads simulated with the 1-D and 3-D grids were similar except in October where the 3-D grid produced higher loads (881 and 1290 kg ha^{-1}) (Fig. 81a). In 1996, the

sediment load via drainflow simulated with the 3-D grid was notably higher compared to the 1-D grid result (2245 and 1186 kg ha^{-1}) (Fig. 81b). The sediment load simulated with the 2-D grid (1976 and 2680 kg ha^{-1} in 1998 and 1996, respectively) was higher than the results calculated with the 1-D and 3-D grids during both years. This was probably caused by the increased drainflow in the 2-D grid (Fig. 79).

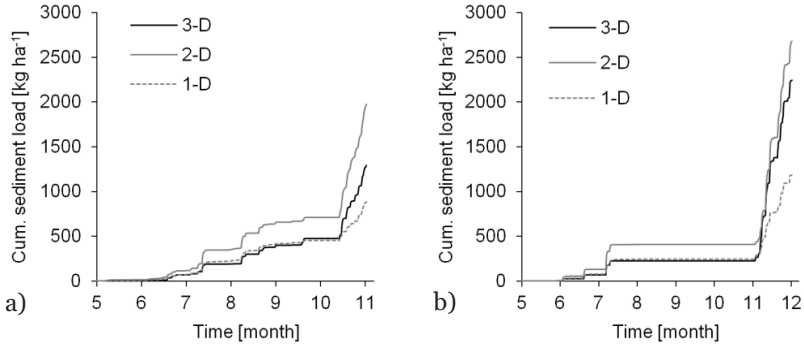

Figure 81. Simulated cumulative sediment loads via drainflow in the Sjökulla field with the 1-D, 2-D and 3-D grids in a) 1998 and b) 1996.

The grid dimension test showed that the results simulated with the 1-D and 2-D grids depended on the position of the computational grid in the field. Neither the 1-D, nor 2-D grid could reproduce both surface runoff and drainflow results simulated with the 3-D grid. However, it is likely that other 1-D and 2-D grid-specific parameterisations exist which would produce comparative results. It is also possible that 1-D and 2-D parameterisations have to be changed with the position of the grid. Another drawback with the 1-D and 2-D grids was that they could not reproduce the spatial distribution of water and sediment related processes in the field with the same fidelity as the 3-D grid (Figs. 84–85). Although surface runoff was increased notably in the simulation with the 1-D grid, the flow depths remained low due to a relatively steep slope. The lack of concentrated overland flow was probably the reason why sediment loads in the 1-D grid remained lower than in the simulations with the 2-D and 3-D grids (Figs. 80-81).

5. Discussion

The objectives of the thesis were to produce new computational approaches and knowledge on flow and erosion processes in clayey, subsurface drained agricultural fields. A new numerical model (FLUSH) was developed, which included preferential flow and transport and soil shrinkage and swelling processes and simulation of rudimentary cropping and tillage effects. The discussion section is divided into two parts. In the first part, programming details of the FLUSH model are discussed. In addition, some of the decisions regarding the structure of the numerical model are explained. In the second part, the results are analysed via answers to the hypotheses and research questions posed in Section 1.3, and comparisons are made against previously published studies.

5.1 Model features and computational aspects

The FLUSH model was developed primarily for research purposes and it is geared towards dynamic, continuous, 3-D, field-scale problems. However, it is possible to apply the model to steady-state, event-based and 1-D and 2-D problems (Section 4.3.3.5). Currently, the automatic grid generation system (AGGS) (Section 3.2.2.2) can only produce grids with uniform layer depths everywhere in the grid, although it is possible to use different soil types in different parts of the field in the profile. The system is based on an object oriented paradigm and is composed of a set of C++ classes which can be combined together and extended as required. There is no dedicated user interface to run the system, although a primitive program was developed to visualise the input data and the 3-D computational grids with colors, text and (velocity) vectors. An earlier version of the model was applied to field conditions by Jalonen (2008) and to a laboratory scale experiment by Kesäniemi (2009). The new version of the model was applied to a clayey field in southern Finland which contained several connected field sections by Turunen (2011).

The major assumptions made in the conceptual model are the lack of winter time processes and the simplified description of evapotranspiration. However, these features were ruled out of scope in Section 1.3 and they are therefore not discussed further. Regarding the subsurface sediment transport description, the key assumptions were that soil is not eroded in the macropore system and that suspended sediment is not transported into the soil matrix. These decisions are further discussed in Section 5.2.3.

The main new feature of the numerical model is the integration of 2-D overland flow and erosion and 3-D subsurface flow and transport domains. The subsurface domain also supports preferential flow and suspended sediment transport in macropores. Soil shrinkage and swelling processes govern macroporosity and hydraulic conductivity of the soil profile as a function of moisture state of the soil matrix (Section 3.2.1.5). No previous 3-D models were found that included soil shrinkage and swelling simulation. The effects of cropping and tillage operations can be simulated by changing overland and subsurface soil parameters at specified points in time. Several new approaches were developed to speed up simulations in a desktop workstation environment. The model includes a new time-stepping system that can be used to run several submodels in a parallel fashion with different time steps (Section 3.2.2.1). PDMA algorithm can make iteration in dual-permeability systems more stable and decrease the number of iterations needed for convergence in implicit solution algorithms (Sections 3.2.1.2 and 3.3.3). The solution algorithms are parallelised with OpenMP API to utilise the latest processor technology to its full extent (Sections 3.2.2.3 and 3.3.4).

The numerical model was developed specifically for this study but the system also retains parts of previously published algorithms, as such or in modified forms. The overland flow model by Taskinen (2002) was adapted to the system. The finite difference method-based numerical solution was converted to FVM and the kinematic wave approach was changed to the diffuse wave approach. The theoretical dual-permeability flow model followed the methods of Gerke and van Genuchten (1993a). The Richards equation (Richards 1931) was used to simulate flow in both pore systems. The method presented by Karvonen (1988) was applied to approximate differential water capacity in the solution. The models by Van Genuchten (1980) were employed to represent WRCs and to simulate unsaturated hydraulic conductivity in both pore systems. TDMA, usually found in subsurface flow solution algorithms, was replaced with the new PDMA approach to solve both pore systems simultaneously. The soil shrinkage and swelling system in the SWAP model (e.g. Kroes et al. 2008) was adopted

here. The stress factor by Feddes et al. (1978) (Fig. 1) was applied to decrease evapotranspiration in very moist and dry conditions.

The erosion model originated from various sources including Taskinen (2002) (principal solution algorithm and hydraulic erosion), Wicks and Bathurst (1996) (rain drop splash erosion) and Yalin (1963), Mantz (1977) and Yalin (1977) (transport capacity for small particles). The solution algorithm of the sediment continuity equation was also converted to FVM. A minimum transport capacity value had to be defined for the suspended clay particles in standing water to improve the results. A simplified theoretical dual-porosity model was adopted to simulate sediment transport in soil. Suspended sediment was allowed to move only in the macropore system, due to the relatively large size of clay aggregates compared to the voids in the clay soil matrix.

Numerical solution of PDEs was carried out with FVM, rather than with FEM, even though FEM is known for its flexibility with the element shape and accuracy due to interpolation inside the elements (e.g. Zienkiewicz 1971, Pinder and Gray 1977, Fletcher 2005). The FVM based model development was initiated by Warsta (2005) and further developed by Warsta (2007), Warsta et al. (2008a, b) and Warsta et al. (2009). The flexibility with the element shape is not an issue with FVM because the method supports also irregular and distorted geometry. At any rate, Karvonen (1988) showed with a FEM approach that increasing grid resolution around subsurface drains did not improve the simulation results substantially due to the uncertainties in the measurement data. Fipps and Skaggs (1986) came to a similar conclusion. Recoding of the system with FEM paradigm was not seen necessary at this point.

According to Sun (1994), two problems have to be solved when building a groundwater model: 1) the forward problem (simulation) and 2) its inverse (calibration). The two ways to approach calibration are trial and error and parameter identification (e.g. Strecker and Chu 1986). Theory and a case study on the issue of automatic parameter identification were presented by, e.g. Neuman and Yakowitz (1980) and Neuman et al. (1980). The inverse problem in this study was solved solely with trial and error calibration because the numerical model was computationally too demanding for automatic calibration approaches with the current desktop hardware. Automatic parameter identification was used in several recent erosion and preferential flow and transport studies including, e.g. Schwartz et al. (2000), Abbaspour et al. (2001), Taskinen (2002) and Jarvis et al. (2007). Kokkonen (1997) showed that automatic parameter identification methods also suffer from the uniqueness problem, i.e. there are a large number of parameter combinations that produce the same simulation results.

5.2 Answers to the hypotheses and research questions

The results presented in this thesis are analysed by answering the hypotheses and research questions posed in Section 1.3. Since it is difficult to generalise results from only two study fields, evidence is presented either for or against the presented hypotheses.

5.2.1 Hypothesis 1

Preferential flow via macropores has a major impact on runoff dynamics and water balance in clayey, subsurface drained agricultural fields.

By using rough estimates for macroporosity (3.3×10^{-3} m^3 m^{-3}) and saturated hydraulic conductivities for soil matrix and macropores (1.0×10^{-4} and 0.248 m h^{-1}) in the drain depth, the volumetric drainflux via macropores was approximately eightfold compared to the soil matrix. However, according to the simulation results on average 99% of the drainflow originated from the macropore system. This indicated that preferential flow was generated in non-equilibrium conditions in the model and dominated water flow into subsurface drains. Furthermore, the parameter *d* (Eq. 26) which describes the diffusion length between the soil matrix and macropores had to be calibrated into a high value (11 m) indicating that water exchange rate between the pore systems was very limited. The non-equilibrium preferential flow manifested itself as peaky drainflow events (Figs. 43, 47, 62, 66) as the water moving in the macropores was unable to drain into the soil matrix.

Evidence of the effect of macropore flow on drainflow was available from the simulation results from both fields. In both measurements and simulations, drainflow started quickly after precipitation events. For example a precipitation event (16 mm h^{-1}) on 10 July 1998 in the Sjökulla field started producing drainflow within the same hour and reached its maximum in the next hour (Fig. 43). The same trend was evident in a precipitation event (9 mm h^{-1}) on 5 October 1984 in the Hovi field (Fig. 66). Without preferential flow in macropores, water could not have reached the drains in such a short time frame. Obviously, many factors affected the timing and volume of drainflow events, including the presence of cracks, antecedent moisture conditions in the soil and duration and intensity of the precipitation events. Other authors have presented similar modelling results. Koivusalo et al. (1999) reported that the total water balance of the simulated hillslope in the Sjökulla field was dominated by evapotranspiration and subsurface drainflow through macropores. In the

study by Gärdenäs et al. (2006) with the HYDRUS model, drainflow waters originated almost entirely from macropores while surface runoff was minimal. Larsson et al. (2007) found that 40% of the simulated drainflow originated from macropores in a study conducted with a modified ICECREAM model. Groundwater flow and surface runoff were assumed to be negligible. Hintikka et al. (2008) reported that 96–99% of modelled drainflow was a result of preferential flow in macropores in the Sjökulla field.

Further evidence was available from the sensitivity analysis. When the macroporosity value in the profile was decreased, the drainflow volumes decreased (Fig. 72b, Scenario 1). A more radical effect was achieved when the soil shrinkage and swelling processes were disabled in the model. According to modelling results, surface runoff increased in the Sjökulla field +64% and +47% in 1998 and 1996, respectively. In the Hovi field, the effect was not visible because surface layer runoff was minimal during the simulation periods. A previous modelling study conducted with the MACRO model and Sjökulla data indicated that cracks had only a minor effect on runoff results (Hintikka et al. 2008). Unfortunately, data available on cracks in the fields were limited, e.g. Alakukku et al. (2010a) reported that cracks reached at least a depth of 0.6 m in the Sjökulla field. A clear change in runoff distribution between surface runoff and drainflow was detected after the tillage operations in the autumn in the computational models (Figs. 75). The relative volume of drainflow decreased while surface runoff increased. The change was presumably caused by tillage operations and liquefaction of clay soil, disrupting direct macropore connections between field surface and drains.

The measured water balance (precipitation, surface runoff and drainflow) did not match in the two fields. In addition to grossly underestimated PET values, the only other source for the error that seemed conceivable was groundwater flow. Because there was little information available on the soil types below the subsurface drains in the Sjökulla and Hovi fields, it was assumed here that the heavy clay soil continued down to bedrock below. Preferential flow could take place in permanent fractures, silt lenses and soil–bedrock interface. The Sjökulla field simulation results indicated that 84 and 65 mm water were lost via groundwater flow in 1998 and 1996, respectively. In the Hovi field simulations, 55 and 69 mm were lost in 1988 and 1984, respectively. Groundwater flow also had a notable effect on water balance in other studies. Gustafson (1987) reported an annual water loss of 20–70 mm via groundwater flow. Gärdenäs et al. (2006) experienced over-estimation of drainflow and the authors hypothesised that the reason was the lack of a groundwater flow process in the model. On the other hand,

Vakkilainen et al. (2010) reported that runoff even exceeded precipitation due to additional water entering the experimental field section from the surrounding land area.

According to the presented results, it would have been very difficult to describe the runoff dynamics and water balance in the computational models without a preferential flow description. The results from the four different growing periods and two separate fields calculated with the 3-D dual-permeability model provided further evidence that preferential flow had an important effect on runoff dynamics and water balance in clayey, subsurface drained agricultural fields. It is asserted here that Hypothesis 1 is valid.

5.2.2 Hypothesis 2

Mechanisms of preferential flow can be represented, and the related mass fluxes can be quantified using computational methods presented in the literature.

According to the results presented in Hypothesis 1, it is evident that preferential flow is important to runoff dynamics and water balance in the studied fields. In the Hypothesis 2, the methods applied to simulate preferential flow in the model are investigated in more detail. Preferential flow was implemented in the model by dividing the total porosity into separate but interacting macropore and soil matrix pore systems (e.g. Gerke and van Genuchten 1993a). Flow in both macropore systems was represented with the Richards equation and the saturated hydraulic conductivity value in the macropore system was approximated with a linear model as a function of macroporosity of the soil (Eq. 93). In a model presented by Messing and Jarvis (1990), the value of K_{SF} was calculated with an exponential function. In Hypothesis 1, it was found that the drainflow waters originated largely from the macropore system. The success of the presented method for simulating macropore flow could be quantified by inspecting hourly drainflow results from the fields (Figs. 43, 47, 62, 66). Even though there are several discrepancies in the results, the system works relatively well in describing the intensities and lengths of the measured drainflow events. The short delay in drainflow initiation after a precipitation event indicated that the macropore network formed a short and direct connection between the field surface and subsurface drains. The calculated Nash-Sutcliffe coefficients for drainflow provided more evidence that the model was able to describe the phenomenon relatively well (Sections 4.3.1.1 and 4.3.2.1.). The coefficients were calculated from 4416–5136 measurement-simulation pairs.

The effect of macroporosity on drainflow in different soil horizons was investigated with several methods. Parameter sensitivity analysis showed that the system was very sensitive to the macroporosity value *w* in horizon 3 (Fig. 34, Table 24). This was due to the location of drains and thickness of the horizon in the profile. The system was not particularly sensitive to the macroporosity values in horizons 1, 2 and 4. The effect of spatial variance of macroporosity on runoff and sediment load results in the Sjökulla field was also investigated in the sensitivity analysis (Section 4.3.3.3). In Scenario 1, macroporosity of the tillage horizon was increased, but the macroporosity of horizon 3 (Fig. 34, Table 24) was decreased. The result was that drainflow (Fig. 72b) and the corresponding sediment load decreased (Fig. 72a). According to the simulation results, the macroporous soil profile functioned as a funnel, i.e. even though the macroporosity value of the upper part was increased, the lower part still acted as a bottleneck governing drainflow. Furthermore, simulation tests without static macropores at the drainage depth produced only minimal drainflow throughout the simulation periods compared to the measurements (results not shown).

The change in runoff distribution after autumn tillage operations, already mentioned in Hypothesis 1, was achieved by decreasing the static macroporosity of the soil in the tillage horizon with the cropping and tillage effects submodel (Fig. 75b). Without the explicit change to the static macroporosity, it was difficult to achieve the change in the runoff distribution. This indicated that the effect was not solely caused by soil swelling process. A greater decrease in static macroporosity was required in 1998 in the Sjökulla field compared to 1996. It is possible that the greater decrease in 1998 was due to the wetter soil compared to 1996. According to Alakukku (1996a), moist mineral soils are prone to damage by compaction and loss of structure. On the other hand, in the Hovi field the decrease of static macroporosity was the same during both years. The effects of tillage operations on macroporosity are rarely taken into account in simulation studies (e.g. Ray et al. 1997).

Simulated groundwater table movement in macropores and soil matrix were compared to the groundwater level data measured at the Sjökulla field (Figs. 25, 50–54). Neither the simulated matrix nor macropore levels corresponded well to the levels in the measurement tubes. Simulated matrix levels changed relatively slowly and were generally higher than the measured levels. Simulated macropore levels, on the other hand, fluctuated too rapidly but otherwise resembled the measured levels more closely. It was found in the simulations that the matrix groundwater table level was governed by the water exchange rate between the pore systems and

transpiration extracted by crop roots. The low saturated hydraulic conductivity K_{SM} and steepness of WRC of the soil matrix caused sudden drops in the simulated matrix groundwater table levels. Increase of K_{SM} brought the matrix groundwater table levels closer to the measured levels. However, the increase of K_{SM} also resulted in more diffuse drainflow results as the importance of preferential flow was diminished. In previous studies, Jauhiainen 2004 and Hintikka et al. (2008) presented groundwater table level simulation results that corresponded relatively well to the measurements from the Sjökulla field.

The calibration results indicated that water exchange between the pore systems was much slower when water was flowing from the soil matrix to the macropore system than in the opposite direction. When an arithmetic mean of hydraulic conductivities in the pore systems was employed in the first order water exchange coefficient α_W (Eq. 26), the matrix system drained too quickly, resulting in diffuse drainflow events (not shown). On the other hand, if solely matrix conductivity was used, infiltration from the matrix to the macropore system was too slow and drainflow increased steeply (not shown). The hysteresis effect in the water exchange between pore systems was represented with Eq. 40. In a previous study, Othmer et al. (1991) set the value of hydraulic conductivity in the matrix-macropore interface K_A to the hydraulic conductivity value of the soil matrix. Gerke and van Genuchten (1993b) studied the magnitude of K_A by simulating a 2-D, single pore system sample with a macropore region parameterised into the centre of the grid surrounded by soil matrix cells. The authors compared the results from the 2-D simulation to results derived with a 1-D dual-permeability model, applying different formulations for K_A. They found out that the arithmetic mean of hydraulic conductivities of macropore and soil matrix pore systems described the mass exchange most accurately in the context of the simulated 2-D system.

The characteristic length d in α_W (Eq. 26) had to be calibrated to a very large value (11 m). This indicated that water exchange between the pore systems was very slow. The sensitivity of the parameter d was found to be low in the parameter sensitivity analysis (Table 33). Previously, Villholt and Jensen (1998) also had to use large values of d in their simulations. Additionally, Gerke and Köhne (2004) had to reduce K_A by a factor of 1000 compared to the hydraulic conductivity value of the soil matrix due to coatings on clay aggregates. Unfortunately no data were available to assess whether the assumption made by Gerke and Köhne (2004) was also applicable to the soils in this study.

A lot of uncertainties remain in the representation of preferential flow in the model. The current configuration does not allow simulation of local

pathways that stay open even after the soil has swollen shut. Examples of such pathways are large earth worm tunnels and vertical gravel drains. Instead, the total macroporosity value is averaged out to the whole volume of the cell. In the simulations, drainflow events got lower and wider instead of just shrinking while retaining their shape when macroporosity was decreased. This was visible in the hourly Hovi drainflow results in 1988 (Fig. 62), where the last drainflow event became lower and wider compared to the measured peak. Small scale features could be simulated with spatially changing conductivity fields studied, e.g. by Vogel et al. (2000) and Taskinen (2002). However, this approach would require denser simulation grids and more computing resources. The method used to approximate the saturated hydraulic conductivity of the macropore system (Eq. 93) is problematic because hydraulic conductivity may not solely be a function of the macropore porosity of soil, but a combination of macropore porosity, geometry and connectivity of the macropore network. As anticipated, approximately one third of the high saturated hydraulic conductivity values in the Sjökulla measurements were associated with low macroporosity values (Table 13). This illustrates the fact that, e.g. a few wormholes can be responsible for the preferential flow through the soil layers. In some models like SWAP (e.g. Kroes et al. 2008) and RZWQM (e.g. Cameira et al. 2000), the macropore system is divided into a disconnected dead end pore system and an actual connected pore system that reaches down to the subsurface drain depth. Finally, one can argue that the value of MVG WRC parameter α (Fig. 27 and Table 14) used in the study is too small (7 m^{-1}) to represent the macropore system. The corresponding air entry value is approximately 0.14 m which is unrealistic for gravel material simulated with WRC. The result is that the modelled macropore system can conduct water relatively well even in high tensions. The problem was discusses earlier by Jarvis (2007). However, a more realistic value of 30 m^{-1} produced instability problems in simulation tests (not shown). This issue should be addressed in future studies.

It was found possible to quantify preferential flow in macropores by comparing simulated hourly drainflow results to the drainflow measurements. However, the dual-permeability concept was not fully verified as neither of the simulated pore systems corresponded very well to the measured groundwater table levels, and parameterisations applied in α_W (namely K_A) in previous studies did not work in the computational models. More data are required, at least from three different areas, including macroporosity-saturated hydraulic conductivity of soil relation, the effects of soil shrinkage and swelling processes on preferential flow, and more detailed information on water exchange between the pore systems.

Due to difficulties and uncertainties related to the representation of preferential flow in the studied fields, it is not possible to fully confirm Hypothesis 2.

5.2.3 Hypothesis 3

The sediment load via subsurface drains in the studied clayey fields can be simulated when the sediment load is assumed to originate from the tillage layer of the fields.

In the model, suspended sediment is introduced into the field in the overland domain by hydraulic and rain drop splash erosion processes. The sediment is then distributed between sediment loads via surface runoff and drainflow according to the flow simulation results. Hypothesis 3 has been integrated into the structure of the conceptual and numerical models presented earlier. Thus the proposed numerical model is a quantitative mechanism for testing the hypothesis, i.e. if it is possible to validate the model with the high resolution data, the hypothesis is asserted to be true.

In the Sjökulla field computational model, the sediment load before autumn rains was generated almost exclusively by rain drop splash erosion (Fig. 41). Larger scale erosion in October 1998 and November 1996 was attributed to hydraulic erosion instead (Fig. 41). The sediment load was distributed between surface runoff and drainflow well during both years (Tables 31 and 32). However, the Nash-Sutcliffe coefficient (0.107) indicated that there were problems with the sediment load results via surface runoff in 1998 (Fig. 41a). Visual inspection revealed nothing else than slightly lower cumulative load results compared to the measurements (Figs. 41a and 44). It is possible that the low Nash-Sutcliffe value was caused by delayed simulation peaks compared to the measured peaks.

In the Hovi field, the sediment load was produced almost totally by rain drop splash erosion in the simulations. Taskinen (2002) came to the same conclusion previously. The simulated concentrations were in agreement with the concentration measurements from the ditch in 1988, and with the concentration measurements from both drainflow and the ditch in 1984. The lack of hydraulic erosion was a consequence of limited overland flow in the field. In addition, simulated overland flow was very slow compared to the Sjökulla results, indicating that the water might have moved in the tillage horizon above the compressed tillage pan instead. Lack of overland flow and hydraulic erosion kept the sediment loads in the Hovi field approximately 20 times lower compared to the sediment loads simulated in the Sjökulla field. The Sjökulla field was also steeper, had optimal conditions for concentrated overland flow on the slopes, and a flat area

close to the outlet where water and suspended sediment could accumulate (Figs. 25, 84 and 85). The sediment load results in both fields were comparable to the measurements without a sediment sieving process description in the model. Thus, it seemed that sediment sieving in the macropore system was not an important process in the studied fields. The lack of sieving was probably caused by the small size of clay aggregates and direct preferential flow routes to the subsurface drains disclosed in Hypotheses 1 and 2.

Only two previous modelling studies were found that simulated both soil erosion on the field surface and transport of suspended sediment into the subsurface drains. Knisel and Turtola (1999) simulated soil erosion with the GLEAMS model combined with a separate model that described sediment transport via preferential flow paths into subsurface drains. The authors postulated that erosion occurred on the field surface and suspended sediment travelled to drains via shrinkage cracks over subsurface drain lines. The simulated cumulative sediment load via drains (3255 kg ha^{-1}) was approximately half of the sediment load via surface runoff (7911 kg ha^{-1}) during the seven year study period conducted at a clayey field in Finland. Larsson et al. (2007) applied a modified ICECREAM model to a silty clay field site in Sweden. The suspended sediment was also generated on the field surface. According to the authors, the cumulative sediment loads via drains were similar to the measurements (simulated 231 kg ha^{-1} vs. measured 261 kg ha^{-1}) but simulated individual events did not match measurements very well. The authors resorted to a sediment sieving process in the macropore system to decrease the sediment load via drains.

Compromises were required in the conceptual and numerical erosion models to simplify the system. Interrill and rill erosion were lumped into a single sheet-like erosion process and only a single particle size was simulated. Interrill and rill erosion were not simulated separately because no data were available to calibrate the processes. Several other authors ended up lumping interrill and rill erosion (e.g. Wicks and Bathurst 1996, Taskinen 2002) and simulating only a single sediment size class (e.g. Sharda and Singh 1994, Nord and Esteves 2005). On the other hand, simulation of several sediment particle size classes was recommended by, e.g. Heilig et al. (2001) and Beuselinck et al. (2002). However, both study fields were clayey and the sediment loads were composed mostly of suspended, fine clay aggregates (Tables 12 and 17). It is possible that simulation of several particle size classes would have unnecessarily complicated the overland erosion and subsurface transport models. Additionally, according to the sensitivity analysis in Table 33, particle size was the most insensitive tested parameter in the system. One of the major

assumptions made in the conceptual model was that suspended sediment was transported only in the macropore system. The voids in the clay soil matrix are exceptionally small which was reflected on the low saturated hydraulic conductivity value of the matrix system in the model (10^{-4} m h^{-1}). Also, the exchange rate of water between the macropore and matrix systems was limited (see Hypotheses 1 and 2). Therefore, if the sediment transport was enabled also in the soil matrix, both infiltration into soil matrix and movement in the matrix would be very slow. Presumably, the suspended sediment would block the available flow routes in the matrix relatively quickly. Also, valuable computational resources were saved by not simulating sediment transport in the matrix system.

Some problems were found in the hydraulic erosion (Eqs. 70–72) and transport capacity descriptions in the overland erosion model (Eqs. 73–84). Because hydraulic erosion was estimated as a function of shear stress τ of overland flow and not flow velocity (Eq. 70), soil erosion actually increases when surface roughness n is increased. When n is increased, flow velocity decreases, but flow depth increases. The value of τ was calculated as a function of flow depth. The effect was visible, albeit faintly, in the parameter sensitivity analysis (Table 33), i.e. when n was increased, sediment loads via surface runoff and drainflow were increased. The same effect was reported previously by Sharda et al. (1994).

Several authors (e.g. Julien and Simons (1985), Taskinen and Bruen 2007b) recommended the Yalins transport capacity (T_C) equation for overland erosion simulation. The adopted Yalins equation (Yalin 1962, Mantz 1977, Yalin 1977) worked well in the Hovi field simulations, but failed to perform adequately in the Sjökulla case. Clay soil in the low lying areas in the Sjökulla field can get very wet and liquefy, creating a thick clay particle-water mixture. The theoretical assumptions made in the transport capacity formulation probably do not apply to this kind of case. Previously, Wicks and Bathurst (1996) encountered similar problems in their simulations. The method by Engelund and Hansen (1967) was also tried but the simulation results were not improved (not shown). It is conjectured here that the Yalins method, even with the modifications for small particles (Eqs. 73–84), does not work well with very fine particles. Both Yalins and Engelund–Hansen methods include flow velocity terms in the formulations, and when the flow velocity drops to zero, the transport capacity also equals zero. In the Sjökulla field, water can move very slowly or even stand still in the low lying areas on the northern side (Figs. 25, 84 and 85). The assumption that particles drop immediately from suspension might be valid for larger particles but not necessarily for clay particles (Stokes law, eq. 77). The problem was bypassed by introducing a minimum T_C value for standing

water. The sediment settling process was included in the overland erosion submodel to decrease sediment concentration gradually in standing water.

Even though a lot of uncertainty is included in the results, and some problems were encountered with the process descriptions, the model was still able to simulate sediment loads in the studied fields relatively well. Strictly according to the definition of the Hypothesis 3 presented in the beginning of the section, the hypothesis is asserted to be true. Another option, that is only discussed here, is that the sediment load from subsurface drains originated partly from internal erosion in macropores. According to the empirical evidence (Laubel et al. 1999, Uusitalo et al. 2001), the sediment load in clayey fields was detached from the soil surface layer. Also, sediment concentration in the drainflow was similar to the concentration in surface runoff waters (Turtola and Paajanen 1995, Uusitalo et al. 2001, Paasonen-Kivekäs et al. 2008). The model results point indirectly into the same direction as these studies. However, one can still argue that the sediment load from subsurface drains originates partly from internal erosion in macropores. With the current parameterisation, the average maximum flow velocities in cracks was a magnitude lower compared to the maximum simulated overland flow velocities. In addition, the erosive force of rain drop impacts is absent in cracks. According to this information, the same mathematical model that was used in the overland domain would not have detached particles from the macropore walls. Unfortunately, without further empirical measurements on actual flow velocities in cracks, this problem cannot be fully resolved.

5.2.4 Hypothesis 4

A distributed problem domain, including separate 2-D overland and 3-D subsurface domains with different process descriptions, is required for a holistic simulation of water flow and soil erosion in undulating, clayey, subsurface drained agricultural fields.

Hypothesis 4 was developed from a notion that both flow and erosion processes in undulating, clayey, subsurface drained agricultural fields were temporally and spatially varying, and that this variation had a notable effect on runoff and sediment load results. With the “holistic simulation” term, it is meant that simulation of an arbitrary part of a field is difficult due to complex boundary conditions caused by interactions between the selected part and the surrounding areas. The main reason for dividing the computational domain into separate overland and subsurface domains was the possibility to apply existing methods for simulating the governing processes. In Section 4.3.3.5, a sensitivity analysis was conducted to

investigate the effect of grid dimension (1-D, 2-D and 3-D) on the simulation results. In the following paragraphs, the term 3-D grid represents a grid that is divided into 2-D overland and 3-D subsurface domains (Fig. 33), while a 2-D grid is divided into 1-D overland and 2-D subsurface domains (Fig. 77). A 1-D grid is composed of point-like overland and 1-D subsurface parts (Fig. 77).

In the sensitivity analysis, the 1-D grid was positioned in the middle of a slope in the Sjökulla field (Fig. 77). Simulations with the 1-D grid resulted in excess surface runoff during both calibration and validation years, indicating that the effective slope of the grid should have been less than the slope of the hillside (Fig. 78). Also, the flow routes taken by the overland flow are totally omitted in 1-D simulations. While this might be justified for overland runoff, erosion phenomenon is comprised of interacting particle detachment and deposition processes that vary in spatial and temporal dimensions. When overland flow routes are not simulated, either erosion is overemphasised, because particle deposition processes are not simulated, or detachment is underestimated to compensate for the lack of deposition in the field. Previously, Hintikka et al. (2008) suggested that 1-D models could be used to quantify average water balance and total runoff on a clayey hillslope, but the authors recommended 2-D and 3-D models when the distribution of runoff between surface runoff, drainflow and groundwater flow was investigated. Köhne et al. (2006) found out that a 2-D flow and transport model with preferential flow and transport support described solute transport better in a tile-drained agricultural field than the equivalent 1-D model.

With the 2-D grid, investigated in the sensitivity analysis, it was possible to simulate a single flow path in the field and erosion processes along the path (Fig. 77). Simulations with the 2-D grid produced comparable surface runoff (Fig. 78) and erosion results (Figs. 80 and 81) to the 3-D grid results. However, simulated drainflow increased because groundwater flow was removed only from the foot of the slope (Fig. 79). Removal of groundwater flow can be problematic in 2-D grids because the flow direction orthogonal to the running direction of the 2-D grid is not simulated. Obviously, it is possible to place sinks into the grid that simulate transverse groundwater flow from the grid. The problem is that the magnitudes of these fluxes are not known at the different parts of the slope. The position of the 2-D grid in the Sjökulla field (Fig. 77) was chosen so that it was located in a depression (Fig. 25), where outgoing groundwater fluxes orthogonal to the running direction of the grid were at a minimum. The 2-D grid could represent the field better than the 1-D grid because the spatial variability of the soil properties could be taken into account with a careful positioning of the grid.

In an earlier study, Mohanty et al. (1998) applied a 2-D model (Mohanty et al. 1997) to a subsurface drained, silty clay loam field. The authors deduced from the results that subsurface drains do not necessarily provide a good integrated field-scale flow and transport behaviour. The authors suggested that a 3-D model would have better suited the problem than the 2-D approach used in the modelling. Koivusalo et al. (1999) found out in a 2-D simulation of a hillslope in the Sjökulla field that the water table could not fall below the subsurface drain level because groundwater flow below the root zone was not simulated. Haws et al. (2005) simulated water flow and solute transport in a subsurface drained, silty clay loam field with 2-D single porosity and dual-porosity models (HYDRUS 2-D). The authors attributed the problems encountered in the solute transport simulations to the non-uniqueness of the parameters and the problem of representing a 3-D heterogeneous system with a 2-D homogenous system.

Although the 2-D grid (Fig. 77) could describe a single overland flow path and erosion dynamics along the path, it could not reproduce the complex flow (Figs. 84 and 86) and erosion patterns (Figs. 85 and 87) on the field surface which are evident in the 3-D grid results. The sensitivity analysis indicated that spatial variability of macroporosity had a notable effect on the runoff and sediment load results in the Sjökulla computational model (Fig. 72). On the other hand, even without spatial variation of soil parameters in the Hovi field, complex overland flow and erosion patterns emerged in the simulations due to topography and soil moisture variations alone. Lower areas in the fields, especially in the Sjökulla field, were wetter, increasing probability of Dunne-type overland flow and hydraulic erosion. This was visible in the Sjökulla field rainstorm simulation results (Fig. 84) where overland waters were accumulating in the middle of the north side (the red areas). The same areas were also prone to soil erosion in the model (Fig. 85) (the red areas). The results of Bronstert and Plate (1997), simulated with the 3-D HILLFLOW model, indicated that in addition to the vertical, subsurface flow fluxes, horizontal fluxes are also required for realistic simulation results. Christiansen et al. (2004) showed with the MIKE-SHE model that preferential flow and transport can vary strongly at a catchment scale with topography and depth of groundwater.

Other models that can simulate 2-D overland flow and 3-D subsurface flow in a single pore system include, e.g. MIKE-SHE (Abbot et al. 1986a, b), MOHID (Trancoso et al. 2010) and HYDRUS 3-D (e.g. Šimůnek et al. 2006) with a separate overland flow module. HYDRUS 3-D can also simulate preferential flow with the dual-porosity approach. A separate module is available for MIKE-SHE that adds preferential flow and transport options to the model (e.g. Christiansen et al. 2004).

According to the evidence from the simulations and results from previous studies, Hypothesis 4 seems to be true. Previously, Jetten et al. (1999) noted that modellers are usually more concerned with how much water and sediment is leaving the study area than with investigating what are the main processes controlling water movement and erosion within the area. While an attempt was made in this study to address the issue, it was difficult to verify the spatially distributed flow and erosion results in the field (Figs. 84-87) due to lack of data. The waterlogged conditions in the Sjökulla field were confirmed in the field site by Paasonen-Kivekäs et al. (2008) but no data were available to show if the simulated soil loss patterns coincided with erosion in the studied fields. Thus, more distributed data are required from fields to further verify the hypothesis, including soil moisture measurements, macroporosity data, overland flow depth and velocity information and spatial soil erosion results. An interesting application of the model would be to study runoff generation mechanisms in fields that are partly compacted due to, e.g. wheeltracks, tramlines, and headlands (Alakukku 1996a). Hortonian runoff mechanism would be a dominant mechanism in the compacted areas while Dunne type mechanism would be predominant elsewhere. From the point of view of applying the developed model, this would require a dense measurement data set and a smaller study area in order to keep the computational load manageable.

5.2.5 Answers to the computational modelling questions

Answers to the computational modelling questions are presented briefly because they have already been answered implicitly in the text.

1) How can processes operating in different temporal scales be combined?

In theory, the problem of the thesis could be approached by solving all the governing PDEs in a single solution process. Due to the mathematical complexity of the approach, the system was built from several separate submodels instead. An added benefit is that submodels can be easily removed or modified. The primary problems concerning the presented system were how to connect the separate domains, and how to choose the execution order and time step lengths of the submodels?

Separate overland and subsurface domains in the numerical model required definitions for mass exchange mechanisms between the domains. Both implicit and explicit methods were tested during the development of phase. An implicit, flux-like boundary condition often drained the overland water depths to negative values, causing problems in the overland flow and

erosion models. An explicit infiltration scheme was adopted in the end, even though it had its own set of problems. For example, infiltration volumes could be smaller, compared to the implicit approach, with longer time step lengths. Previously, Vassilev and Yotov (2010) were able to solve Stokes-Darcy flow PDEs simultaneously. A drawback of this approach is that the resulting models are mathematically complicated and computationally demanding. In addition, solutions are currently available only for saturated, single pore system, subsurface flow and transport cases. Weill et al. (2009) presented a coupled overland-subsurface system modelled with the Richards equation. The advantage of this approach is that no mass exchange mechanisms are required between the domains. Unfortunately, the model supports only single pore system subsurface flow.

In the current configuration, the submodels are always run in the same order, but depending on the submodel time step the model might not be run during every subtime step loop (Fig. 15). Theoretical tests were conducted with persistent small time steps across all submodels to confirm that this approach worked (Section 3.3.2). Still, more work is needed to find the optimum time steps for each submodel in different circumstances.

2) What is the effect of computational grid resolution on results and is it possible to achieve resolution-independent results?

AGGS was developed partly to accelerate the calibration process and partly to conduct sensitivity analysis on the effect of grid resolution on the results (Section 4.3.3.2). The lowest resolution 3-D grids used to represent Hovi and Sjökulla fields in the study took 9 and 11 minutes to simulate (Table 34), respectively. The simulation time was increased approximately sevenfold every time the resolution was quadrupled. While it is possible to simulate larger areas than field sections, the computational load quickly becomes overwhelming for personal workstations as the number of cells in the grids increase. Convergence of runoff and load results with the increase of grid resolution was more pronounced in the Hovi simulations. In the Sjökulla simulations convergence was not attained with drainflow (Fig. 69) and sediment load results via surface runoff (Fig. 70). Wicks and Bathurst (1996) conjectured that the values of the erodibility coefficients could vary with the resolution of the grid due to the areal averaging of soil erosion and overland flow parameters. In this study, tests with the numerical model indicated that increased groundwater flow losses created the non-convergent behavior (not shown). The rate of groundwater flow was related to the topography and steepness of slopes in the field. Additionally, the maximum horizontal resolutions applied in the study were still not high

enough to accurately describe pressure fields created by subsurface drains. Other pertinent studies that investigated the effects of grid resolution on simulation results include Tiihonen (2007) and Zinke et al. (2010).

3) Is it possible to accelerate the performance of the numerical model with special algorithms and hardware?

According to the numerical tests conducted during the development of the model, the most computationally intensive part of the system was the subsurface flow model. This was due to the weak iteration convergence in the solution algorithm especially in simulations with high resolution grids. The convergence problem was probably due to the non-linear nature of the Richards equation (Tracy 2007), coupled with WRCs of clay soil. WRCs of clay soils can be very steep with low suction values increasing non-linearity in the solution (Section 4.1.1.2 and 4.1.2.2). The numerical solution of the Richards equation was also analysed with an analytical model developed by Tracy (2007)(Section 3.3.1). The conclusion of the examination was that optimisation efforts had to be concentrated on the subsurface flow solution algorithm. The approaches could be applied to accelerate the analogous subsurface transport solution algorithm too.

A PDMA-based method was developed to solve the pentadiagonal linear system which arose from the numerical solution of the dual-permeability flow equations (Section 3.2.1.2). According to the theoretical tests (Section 3.3.3), the new method was approximately as fast as the standard TDMA method. However, the tests were made with relatively low vertical resolutions. Higher vertical resolutions might prove to be advantageous for PDMA. Also, soils with high exchange rates between the pore systems might benefit from the method, making the simulations more stable. Previously, Gerke and van Genuchten (1993a) found out that a direct solution method of the linear system of equations, derived from the discretised dual-permeability flow and transport equations, was more stable than an iterative one.

The OpenMP API was used to parallelise the solution algorithms in all submodels (Section 3.3.4). It was possible to decrease the simulation times to one third by distributing the computational load over several processor cores. It is possible that additional physical cores would further accelerate the simulations. Because the model also has serially processed parts and some resources have to be invested in task distribution itself, the speed increase was under the hypothetical limit. More robust approaches are required in the future. GPU computing (graphics processing units) and supercomputer options are both viable alternatives.

6. Conclusions

A new numerical model was developed in the study which can simulate water flow and soil erosion in clayey subsurface drained agricultural fields. The model was applied successfully to two field sites in southern Finland and to four different growing seasons. Even though the model cannot yet be used to simulate actual nutrient loads, the groundwork is completed for the simulation of both phosphorus and nitrogen (and other compounds) in the future. Currently the model can simulate growing season processes but does not include descriptions for winter time processes. Soil freezing and thawing, as well as snow cover simulation are not included in the current model version. The conclusions derived from the simulation results are divided into four sections according to the main hypotheses presented in Section 1. Answers to the hypotheses were presented in Section 5.

According to the simulation results, preferential flow had a major impact both on runoff dynamics and water balance in the studied fields, verifying Hypothesis 1. Drainflow waters originated almost entirely from the macropore system. The modelling results indicated that shrinkage cracks decreased surface runoff during the summer. Tillage operations, soil swelling, clay soil liquefaction or a combination of these three factors changed the runoff distribution in the autumn. Additionally, groundwater flow, presumably occurring in permanent fractures, silt lenses and at the soil-bedrock interface, had a substantial impact on the water balance in the studied fields.

With respect to Hypothesis 2, the dual-permeability approach used to simulate preferential flow in the model did not perfectly describe the flow processes in the fields. However, the system was able to simulate the intensity and duration of drainflow events in the two fields. The saturated hydraulic conductivity of the macropore system was described with a linear model as a function of macroporosity. The measured dynamics of the groundwater table level was not reproduced well and the water exchange description between the pore systems had to be exchanged into a custom function. Water exchange exhibited a hysteresis effect, which was described

and quantified using the hourly drainflow measurements. Laboratory measurements in soil columns and dye experiments in the field would be helpful in further improving the computational description of preferential flow.

The model could describe soil erosion in the studied fields, and provide realistic estimates of sediment load transported in subsurface drains (Hypothesis 3). The successful simulations provide further evidence that sediment load via drainflow in the two fields originate in their entirety from the tillage horizon. According to the results from the Sjökulla field, hydraulic erosion was the main source of suspended sediment and the sediment load was notably increased by tillage operations in the autumn. In the Hovi field, autumn tillage did not increase the erosion risk because overland flow was minimal during the simulation periods. The results show that it is important to minimise overland flow in order to decrease the effects of hydraulic erosion. The sediment load produced by rain drop splash erosion was relatively small, particularly in the Sjökulla field. The simulations also indicated that sieving in the macropore system was minimal and that simulation of a single particle size was sufficient in the studied fields. Also, according to the results, transport capacity methods should be further refined for very fine particles.

In Hypothesis 4, the effects of grid dimension and spatial variation of macroporosity were investigated. Simulations with the 3-D grids predominantly used in the study yielded results that compared well with the measurements, while the 1-D and 2-D grid simulations had trouble in reproducing the runoff measurements. On sloping fields, it can be difficult to choose a position for a 1-D or a 2-D grid that effectively captures the spatially varying soil properties and topography. Furthermore, defining boundary conditions in a 1-D or a 2-D grid can be complicated when the grid is located on a slope. Spatial variation of macroporosity had a notable effect on the runoff and sediment load results in the simulations. An interesting finding was that even without spatial variation of soil properties, 3-D grids could provide useful results on the spatial distribution of overland flow and soil erosion in the field. The spatial variability is then due to differences in topography and soil moisture conditions alone. Conversely, in a large and flat field application of a 3-D model may not be necessary because subsurface drains are likely to govern the water balance and hence the results are symmetrical around each drainline. The drawback with 3-D grids is that high resolution grids can be computationally demanding. In addition, more spatially distributed data are required from fields. For example data on macroporosity, soil moisture, overland water depths and

flow velocities and erosion would be necessary to further verify the simulation results.

Computation speed of the numerical model was successfully accelerated with a new time stepping system and parallelisation of the submodels with the OpenMP API. The proposed PDMA approach to solve flow in a dual-permeability system was equally fast with the standard TDMA approach. It is possible that the new algorithm performs better when the water exchange rate between the soil matrix and macropores is increased. Faster algorithms and hardware are still required to increase the horizontal resolution in the 3-D grids, in order to capture the pressure fields around subsurface drains in more detail.

According to the presented study, the key new features of the model are: 1) implementation of a 3-D model with both overland and subsurface flow simulation, 2) combined simulation of soil shrinkage and swelling and preferential flow in macropores, 3) overland erosion combined with sediment load simulation via surface runoff and subsurface drainflow and 4) new distributed numerical solution algorithms that take full advantage of the processing power in modern workstations.

7. Summary

Problems caused by soil erosion vary geographically, and range from loss of available top soil in agriculture to sedimentation and eutrophication of waterways. In Finland, the soil loss itself is not of great concern but the loss of adsorbed nutrients into surface waters can cause water quality problems. In Finnish fields, soil erosion is induced mainly by overland flow and rain drop impacts on the field surface. Suspended sediment is lost via two main routes: 1) surface runoff and 2) subsurface drainflow. In low permeable soils, suspended particles are assumed to move with preferential flow via macropores and drain trench backfill material down to the subsurface drains. Considerable resources have been invested in curbing nutrient losses from agricultural fields. Recent studies indicate that more research is still needed to identify more effective conservation methods. The objective of the study was to develop a new numerical model which can be applied to investigate mechanisms of water flow and soil erosion in clayey, subsurface drained agricultural fields. The model can be used as a basis for future nutrient leaching models.

A literature review was conducted to assess the current state of overland erosion and subsurface flow and transport models. The conceptual models applied in erosion prediction in Finland have several deficiencies, including empirical erosion components based on foreign soil data and lack of subsurface drain simulation. Process-based erosion models can be used alongside conceptual models to improve simulation results. Most of the reviewed process-based erosion models are built around the sediment continuity equation combined with different erosion process descriptions. However, preferential transport of suspended sediment in macropores to drains is not considered in the models. The published literature on preferential flow and transport is extensive, suggesting dozens of different ways to simulate the processes. According to the review, a dual-permeability approach where the total pore space is divided into two separate pore systems would be best suited for the current study. While no existing models that could directly be applied to the problem were found, a

new model could be constructed by combining different available models and algorithms together.

The modelling approach followed in the thesis can be divided into conceptual, numerical and computational parts. The conceptual model consisted of process descriptions and general mathematical equations. The model was divided into four parts: 1) overland flow, 2) overland erosion, 3) subsurface flow and 4) subsurface transport. Overland flow was simulated with the diffuse wave simplification of the Saint Venant equations. Overland erosion was built around the sediment continuity equation including hydraulic erosion, rain drop splash erosion, simulation of transport capacity and sediment deposition processes. Subsurface flow was represented with the dual-permeability model wherein both pore systems were simulated with the Richards equation. Subsurface transport of suspended sediment particles were simulated with a simplified dual-porosity model and the advection-dispersion equation. The numerical model in turn was comprised of the model framework and six submodels, including submodels corresponding to the parts of the conceptual model listed above. Additional submodels were used to simulate soil shrinkage and swelling processes and the cropping and tillage effects. The partial differential equations in the submodels were solved numerically with an implicit finite volume method. A new method, based on pentadiagonal matrix algorithm, was developed to solve subsurface flow in the two pore systems simultaneously. The result is that one iteration round is removed from the algorithm as iteration does not have to be conducted between the pore systems. A novel time stepping system enabled the individual submodels to be run in a concurrent fashion. The solution algorithms in the submodels were parallelised with the OpenMP application interface to further optimise the computing. An automatic grid generation system created grids with different resolutions for the numerical model.

In order to study the mechanisms of water flow and soil erosion, the model was applied to two clayey, subsurface drained agricultural fields in southern Finland. The 3.3 ha Sjökulla experimental field is located in Kirkkonummi while the 12.0 ha Hovi experimental field is located in Vihti. Data from two years were used to calibrate and validate the computational models. The calibration and validation processes were carried out manually due to the heavy computational load associated with the model. The simulations started in May and ended in October or November, before temperatures fell below freezing. The simulation results included mass balance tables and cumulative and hourly runoff and sediment load results. In addition, distributions of overland flow after rainstorm events and net erosion in the fields in the end of the simulation periods were produced.

Performances of the computational models were assessed with visual inspection and statistical measures. A sensitivity analysis was conducted to approximate uncertainty in parameter values and processes in the models.

The results were analysed by presenting answers to the hypotheses formulated at the beginning of the study. According to the results, preferential flow had a major impact on water balance, runoff dynamics and erosion in the fields. Most of the drainflow originated from the macropore system. Macroporosity, soil shrinkage and swelling processes and tillage operations had notable effects on preferential flow, and as a consequence on the water balance. It was possible to quantify preferential flow with the presented method and to verify the results with hourly drainflow measurements. However, more laboratory and field data are required to further adjust the description of the preferential flow mechanism. In particular, while water exchange between the pore systems has a major impact on the model results, its magnitude is hard to estimate with existing measurements.

Hydraulic erosion in the autumn was responsible for the bulk of the sediment load in the Sjökulla field, while rain drop splash erosion alone created the sediment load in the Hovi field. Tests with different grid dimensions (1-D, 2-D and 3-D) and sensitivity analysis with spatially varying macroporosity data indicated that the 3-D grids were best suited for simulation of sloping clayey fields. According to the results, lower dimension grids (1-D and 2-D) are more suited to flat fields where water balance is dominated by subsurface drains. Drawbacks of using 3-D grids include that 1) more spatially distributed data are needed to verify the results, and 2) more computing power is required to run the simulations. In the near future, 3-D modelling will become even more attractive due to the increased availability of GIS data and computational resources.

References

Aakkula, J., Manninen, T. and Nurro, M. (ed.)(2010), Maatalouden ympäristötuen vaikuttavuuden seurantatutkimus (MYTVAS 3) – Väliraportti, Maa- ja metsätalousministeriön julkaisuja, 145 p.

Aarrevaara, H. (1993), Suomen salaojituksen historia, Salaojituksen Tukisäätiö, Jyväskylä, 276 p.

Abbaspour, K., Kohler, A., Simunek, J., Fritsch, M. and Schulin, R. (2001), Application of a two-dimensional model to simulate flow and transport in a macroporous agricultural soil with tile drains, *Eur. J. Soil Sci.*, 52, 433–447.

Abbott, M.B., Bathurst, J.C., Cunge, J.A., O'Connell, P.E. and Rasmussen, J. (1986a), An introduction to the European Hydrological System - Système Hydrologique Européen, 'SHE', 1: History and philosophy of a physically-based, distributed modelling system, *J. Hydrol*, 87, 45–59.

Abbott, M.B., Bathurst, J.C., Cunge, J.A., O'Connell, P.E. and Rasmussen, J. (1986b), An introduction to the European Hydrological System - Système Hydrologique Européen, 'SHE', 2: Structure of a physically-based, distributed modelling system, *J. Hydrol*, 87, 61–77.

Abrahamsen, P. and Hansen, S., (2000), Daisy: an open soil-crop-atmosphere system model, *Env. Mod. & Software*, 15, 313–330.

Aksoy, H. and Kavvas, M. (2005), Review of hillslope and watershed scale erosion and sediment transport models, *Catena*, 64, 247–271.

Alakukku, L. (1996a), Persistence of soil compaction due to high axle load traffic. I Short-term effects on the properties of clay and organic soils, *Soil Till. Res.*, 37, 211–222.

Alakukku, L. (1996b), Persistence of soil compaction due to high axle load traffic. II Long-term effects on the properties of fine-textured and organic soils, *Soil Till. Res.*, 37, 223–238.

Alakukku, L., Nuutinen, V., Ketoja, E., Koivusalo, H. and Paasonen-Kivekäs, M. (2010a), Soil macroporosity in relation to subsurface drain location on a sloping clay field in humid conditions, *Soil Till. Res.*, 106, 275–284.

Alakukku, L., Nuutinen, V., Koivusalo, H. and Paasonen-Kivekäs, M. (2003), Macroporosity of three arable clays in relation to subdrain location. Proceedings of the 16th Triennial Congress (July 2003), of the International Soil Tillage Research Organisation (ISTRO), Brisbane, Australia, 6 p.

Al-Soufi, R.W. (1999), Analysis of macropore flow in Sjökulla research field, Laboratory of Water Resources, Helsinki University of Technology, Otaniemi, 26 p.

Allen, R.G., Smith, M., Perrier, A. and Pereira, L.S. (1994), An update for the definition of Reference Evapotranspiration, *ICID Bulletin*, 43, 1–92.

Andersson, S. (1969), Markfysikaliska undersökningar i odlad jord: XIX. Teoretiska modellstudier av kapillära systems k-värden som funktioner av porstoleksfördelning bindningstryck och vattenhalt, *Grunförbättring*, 22, 143–154.

Anthony, S. (2003), The MCDM model: a monthly calculation of water balance for use in decision support systems, Unpublished, ADAS internal document.

Ariathurai, R. and Arulanandan, K. (1978), Erosion rates of cohesive soils. *Proc. Am. Soc. Civ. Eng., J. Hydraul. Div.*, 104, 279–283.

Armstrong, A.C., Matthews, A.M., Portwood, A.M., Leeds-Harrison, P.B. and Jarvis, N.J. (2000), CRACK-NP: a pesticide leaching model for cracking clay soils, *Agric. Wat. Man.*, 44, 183–199.

Aura, E. (1995), Finite element modeling of subsurface drainage in Finnish heavy clay soils, *Agric. Wat. Man.*, 28, 35–47.

Aura, E., Saarela, K. and Räty, M (2006), Savimaiden eroosio, *Proceedings of Agrifood Research Finland MTT*, 118, Agrifood Research Finland MTT, 32 p.

Averjanov, S.F. (1950), About permeability of subsurface soils in case of incomplete saturation, *Eng. Collect.*, 7.

Banton, O., Larocque, M., Lafrance, P., Montminy, M. and Gosselin, M.A. (1997), De´veloppement d'un outil d'e´valuation des pertes environnementales de pesticides: inte´gration d'un module PestiFlux au logiciel AgriFlux, Scientific Report INRS-Eau. Ste-Foy, Que´bec, Canada, 144 p.

Bear, J. (1979), Hydraulics of Groundwater, McGraw-Hill, 569 p.

Bengtsson, L., Seuna, P., Lepistö, A. and Saxena, R.K. (1992), Particle movement of melt water in a subdrained agricultural basin, *J. Hydrol*, 135, 383–398.

Berndt, H. and Coughlan, K.J. (1976), The nature of changes in bulk density with water content in a cracking clay, *Aus. J. Soil Res.*, 15, 27–37.

Beuselinck, L., Hairsine, P.-B., Govers, G., Poesen, J. (2002), Evaluating a single-class net deposition equation in overland flow conditions, *Water Resour. Res.*, 38, 1110, doi:10.1029/2001WR000248.

Beven, K.J. and Binley, A.M. (1992), The future of distributed models: model calibration and uncertainty prediction, *Hydrol. Proc.*, 6, 279–298.

Beven, K. and Germann, P. (1981), Water flow in soil macropores II. A combined flow model, *J. Soil Sci.*, 32, 15–29.

Beven, K. and Germann, P. (1982), Macropores and Water Flow in Soils, *Water Resour. Res.*, 18, 1311–1325.

Beven, K.J., Henderson, D.E. and Reeves, A.D. (1993), Dispersion parameters for undisturbed partially saturated soil, *J. Hydrol*, 143, 19–43.

Bibby, R. (1981), Mass transport of solutes in dual-porosity media, *Water Resour. Res.*, 17, 1075–1081.

Boast, C.W. (1973), Modeling the movement of chemicals in soils by water, *Soil Sci.*, 115, 224–230.

Booltink, H.W.G. and Bouma, J. (1991), Physical and morphological characterization of bypass flow in a well-structured clay soil, *Soil Sci. Soc. Am. J.*, 55, 1249-1254.

Borah, D.K., Krug, E.C. and Yoder, D., Watershed sediment yield, in Garcia, M.H. (ed.)(2008), Sedimentation Engineering, Processes, Measurements, Modeling and Practice, American Society of Civil Engineers, 827–858.

Bouma, J. and Dekker, L.W. (1978), A case study on infiltration into dry clay soil I. Morphological observations, *Geoderma*, 20, 27-40.

Bouma, J. and Dekker, L.W. and Wösten, J.H.M. (1978), A case study on infiltration into dry clay soil, II Physical measurements, *Geoderma*, 20, 41–51.

Bouma, J., Jongerius, A., Boersma, O. Jager, A. and Schoonderbeek, D. (1977), The function of different types of macropores during saturated flow through four swelling soil horizons, *Soil Sci. Soc. Am. J.*, 41, 945-950.

Bouma, J. and Wösten, J.H.M. (1979), Flow patterns during extended saturated flow in two, undisturbed swelling clay soils with different macrostructures, *Soil Sci. Soc. Am. J.*, 43, 16-22.

Boreli, M. and Vachaud, G. (1966), Note sur la determination de la teneur en eau résiduelle et sur la variation de la pérmeabilité relative dans les sols non saturés, *C. R. Acad. Sci.*, 263, 698–701.

Bradford, J.M., Ferris, J.E. and Remley, P.A. (1987a), Interrill soil erosion processes: I. Effects of surface sealing on infiltration, runoff, and soil splash detachment, *Soil Sci. Soc. Am. J.*, 51, 1566–1571.

Bradford, J.M., Ferris, J.E. and Remley, P.A. (1987b), Interrill soil erosion processes: II. Relationship of splash detachment to soil properties, *Soil Sci. Soc. Am. J.*, 51, 1571–1575.

Bronstert, A. and Plate, E.J. (1997), Modelling of runoff and soil moisture dynamics for hillslopes and micro-catchments, *J. Hydrol*, 198, 177–195.

Bronswijk, J.J.B. (1988), Modeling of water balance, cracking and subsidence of clay soils, *J. Hydrol*, 97, 199–212.

Bronswijk, J.J.B. (1990), Geometry of shrinkage of a heavy clay soil at various loads, *Soil Sci. Soc. Am. J.*, 54, 1500–1502.

Bronswijk, J.J.B. (1991), Drying, cracking, and subsidence of a clay soil in a lysimeter, *Soil Sci.*, 152, 92–99.

Bronswijk, J.J.B., Hamminga, W. and Oostindie, K. (1995), Field-scale solute transport in a heavy clay soil, *Water Resour. Res.*, 31, 517-526.

Brooks, R.H. and Corey, A.T. (1964), Hydraulic properties of porous media, *Hydrol. Pap. 3*, Colo. State Univ. Fort Collins.

Brusseau, M.L. and Rao, P.S.C. (1990), Modeling solute transport in structured soils: A review, *Geoderma*, 46, 169–192.

Brutsaert, W. (1967), Some methods of calculating unsaturated permeability, *Trans. ASAE*, 10, 400–404.

Buckingham, E. (1907), Studies on the movement of soil moisture, Bulletin 38, USDA Bureau of Soils, Washington DC.

Burdine, N.T. (1953), Relative permeability calculation from size distribution data, *Trans. AIME*, 198, 71–78.

Båth, A. (1993), Studier av rotutveckling och markvattenhalt i försök med marktäckningen, Sveriges Lantbruksuniversitet, Avdelningsmeddelande 93:7, Uppsala.

Bärlund, I., Tattari, S., Puustinen, M., Koskiaho, J., Yli-Halla, M. and Posch, M. (2009), Soil parameter variability affecting simulated fieldscale water balance, erosion and phosphorus losses, *Agric. and Food Sci.*, 18, 402–416.

Bärlund, I., Lehtonen, H. and Tattari, S. (2005), Assessment of environmental impacts following alternative agricultural policy scenarios, *Wat. Sci. & Tech.*, 51, 117–125.

Cameira, M., Ahuja, L., Fernando, R. and Pereira, L. (2000), Evaluating field measured soil hydraulic properties in water transport simulations using RZWQM, *J. Hydrol*, 236, 78–90.

Celia, M.A., Bououtas, E.T. and Zarba, R.L. (1990), A general mass-conservative numerical solution for the unsaturated flow equation, *Water Resour. Res.*, 26, 1483–1496.

Chertkov, V. (2000), Modeling the pore structure and shrinkage curve of soil clay matrix, *Geoderma*, 95, 215–246.

Chertkov, V.Y. (2003), Modelling the shrinkage curve of soil clay pastes, *Geoderma*, 112, 71–95.

Chertkov, V.Y. and Ravina, I. (1998), Modeling the crack network of swelling clay soils, *Soil Sci. Soc. Am. J.*, 62, 1162–1171.

Chertkov, V.Y. and Ravina, I. (2002), Combined effect of interblock and interaggregate capillary cracks on the hydraulic conductivity of swelling clay soils, *Water Resour. Res.*, 38, 1157–1157.

Childs, E.C. (1969), An introduction to the physical basis of soil water phenomena, J. Wiley & Sons, London.

Childs, E.C. and Collis-George, N. (1950), The permeability of porous materials, *Proc. Roy. Soc., Ser. A*, 201, 392–405.

Christiansen, J.S., Thorsen, M., Clausen, T., Hansen, S. and Refsgaard, J.C. (2004), Modelling of macroporous flow and transport processes at a catchement scale, *J. Hydrol*, 299, 136–158.

Clothier, B.E., Green, S.R. and Deurer, M. (2008), Preferential flow and transport in soil: progress and prognosis, *Eur. J. Soil Sci.*, 59, 2–13.

Coats, K.H. and Smith, B.D. (1964), Dead-end pore volume and dispersion in porous media, *SPEJ*, 4, 73–84.

Cornelis, W.M., Corluy, J., Medina, H., Díaz, J., Hartmann, R., Van Meirvenne, M. and Ruiz, M.E. (2006), Measuring and modelling the soil shrinkage characteristic curve, *Geoderma*, 137, 179–191.

Corradini, C., Melone, F. and Smith, R.E. (1997), A unified model for infiltration and redistribution during complex rainfall patterns, *J. Hydrol*, 192, 104–124.

Darcy, H. (1856), Les fontaines publique de la ville de Dijon, Dalmont, Paris.

Davison, P.S., Withers, P.J.A., Lord, E.I., Betson, M.J. and Strömqvist, J. (2008), PSYCHIC – A process based model of phosphorus and sediment mobilisation and delivery within agricultural catchments. Part 1: Model description and parameterisation, *J. Hydrol*, 350, 290–302.

De Roo, A.P.J., Wesseling, C.G., Jetten, V.G. and Ritsema, C.J. (1996a), LISEM: a single-event physically based hydrological and soil erosion model for drainage basins. I: Theory, input and output, *Hydrol. Proc.*, 10, 1107–1117.

De Roo, A.P.J., Wesseling, C.G., Jetten, V.G. and Ritsema, C.J. (1996b), LISEM: a physically-based hydrological and soil erosion model incorporated in a GIS, HydroGIS 96: Application of Geographic Information Systems in Hydrology and Water Resources Management, Proceedings of the Vienna Conference, April 1996, IAHS Publ. no. 235, 395–403.

Djodjic F., Ulén B. and Bergström L. (1999), Temporal and spatial variations of phosphorus losses and drainage in a structured clay soil, *Wat. Res.*, 34, 1987–1695.

Dooge, J.C.I. (1959), A general theory of the unit hydrograph, *J. Geophys. Res.*, 64, 241–256.

Duguid, J.O. and Lee, P.C.Y. (1977), Flow in fractured porous media. *Water Resour. Res.*, 13, 558–566.

Dunne, T., Field studies of hillslope flow processes, in Kirkby, M.J. (ed.)(1978), Hillslope hydrology, Wiley, New York, 227–293.

Dykhuizen, R.C. (1990), A new coupling term for double porosity models, *Water Resour. Res.*, 26, 351–356.

Edwards, W.M., van der Ploeg, R.R. and Ehlers, W. (1979), A numerical study of the effects of noncapillary-sized pores upon infiltration, *Soil Sci. Soc. Am. J.*, 43, 851–856.

Engeln-Müllges, G. and Uhlig, F. (1996), Numerical algorithms with C, Springer, 568 p.

Engelund, F. and Hansen, E. (1967), A monograph on sediment transport in alluvial streams, Teknisk Forlag: Copenhagen.

Ernst, L.F. (1975), Formulae for groundwater flow in areas with subirrigation by means of open conduits with a raised watet level, Misc. Reprints 178, Institute for Land and Water Management Research, Wageningen, The Netherlands, 32 p.

Ernst, L.F. (1962), Grondwaterstromningen in de verzadigde zone en hun berekening bij de aanwezigheid van horizontale evenwijdige open leidingen, Versl. Landbouwk. Onderz., 67.15. PUDOC, Wageningen, 189 p.

Farrel, D.A. and Larson, W.E. (1972), Modeling the pore structure of porous media, *Water Resour. Res.*, 8, 669–706.

Feddes, R.A. (1988), Effects of drainage on crops and farm management, *Agric. Wat. Man.*, 14, 3–18.

Feddes, R. A., Bresler, E. and Neuman, S. P. (1974), Field test of a modified numerical model for water uptake by root systems, *Water Resour. Res.*, 10, 1199–1206.

Feddes, R.A., Kowalik, P.J. and Zaradny, H. (1978), Simulation of field water use and crop yield, Wageningen, 189 p.

Feyen, J., Jacques, D., Timmerman, A. and Vanderborght, J. (1998), Modelling water and solute transport in heterogenous soils: A review of recent approaches, *J. agric. Engng Res.*, 70, 231–256.

Finland's environmental administration (2007), Vesiensuojelun suuntaviivat vuoteen 2015 Valtioneuvoston periaatepäätös, Suomen ympäristö 55/2006, 90 p.

Finnish Field Drainage Association (2011), Salaojitetut peltohehtaarit Suomessa, Finnish Field Drainage Association, 8 p. http://www.salaojayhdistys.fi/tilastot/salaojatilastot.pdf.

Fipps, G. and Skaggs, R.W. (1989), Influence of slope on subsurface drainage of hillsides, *Water Resour. Res.*, 25, 1717–1726.

Fipps, G., Skaggs, R.W. and Nieber, J.L. (1986), Drains as a boundary condition in finite elements, *Water Resour. Res.*, 22, 1613–1621.

Fletcher, C. (2005), Computational techniques for fluid dynamics, Volume 1 Fundamental and general techniques, Springer, 401 p.

Førland, E.J., Allerup, P., Dahlström, B., Elomaa, E., Jónsson, T., Madsen, H., Perälä, J., Rissanen, P., Vedin, H. and Vejen, F. (1996), Manual for Operational Correction of Nordic Precipitation Data, Norwegian Meteorol. Inst., Report 24, KLIMA, 66 p.

Forrer, I., Kasteel, R., Flury, M. and Flühler, H. (1999), Longitudinal and lateral dispersion in unsaturated field soil, *Water Resour. Res.*, 35, 3049–3060.

Foster, G.R. and Meyer, L.D., A closed-form soil erosion equation for upland areas, in Shen, H.W. (Ed.)(1972), Sedimentation Symposium in Honor Prof. H.A. Einstein, Colorado State University, Fort Collins, CO, 12.1–12.19.

Foster, G.R., Modeling the Erosion Processes, in Haan, C. T., Johnson, H. P. and Brakensiek, D. L. (editors)(1982), Hydrologic Modeling of Small Watersheds, ASAE, St. Joseph, Michigan, pp. 297-380.

Gallo, C., Paniconi, C. and Gambolati, G. (1996), Comparison of solution approaches for the two-domain model of nonequilibrium transport in porous media, *Adv. Wat. Res.*, 19, 241–253.

Gardner, W.R. (1958), Some steady-state solutions of the unsaturated moisture flow equation with application to evaporation from a water table, *Soil Sci.*, 85, 228–232.

Gerke, H.H. (2006), Review article: Preferential flow descriptions for structured soils, *Journal of Plant Nutrition and Soil Science*, 169, 382–400.

Gerke, H.H. and Köhne, J.M. (2002), Estimating hydraulic properties of soil aggregate skins from sorptivity and water retention, *Soil Sci. Soc. Am. J.*, 66, 26–36.

Gerke, H.H. and Köhne, J.M. (2004), Dual-permeability modelling of preferential bromide leaching from a tile-drained glacial till agricultural field, *J. Hydrol*, 289, 239–257.

Gerke, H.H. and van Genuchten, M.T. (1993a), A dual-porosity model for simulating the preferential movement of water and solutes in structured porous media, *Water Resour. Res.*, 29, 305–319.

Gerke, H.H. and van Genuchten, M.T. (1993b), Evaluation of a first order water transfer term for variably saturated dual-porosity flow models, *Water Resour. Res.*, 29, 1225–1238.

Gerke, H.H. and van Genuchten, M.Th. (1996), Macroscopic representation of structural geometry for simulating water and solute movement in dual-porosity media, *Adv. Wat. Res.*, 19, 343–357.

Germann, P. and Beven, K. (1981a), Water flow in soil macropores I. An experimental approach, *J. Soil Sci.*, 32, 1-13.

Germann, P. and Beven, K. (1981b), Water flow in soil macropores III. A statistical approach, *J. Soil Sci.*, 32, 31-39.

Germann, P. and Beven, K. (1985), Kinematic wave approximation to infiltration into soils with sorbing macropores, *Water Resour. Res.*, 21, 990–996.

Gerwitz, A. and Page, E.R. (1974), An empirical mathematical model to describe plant roots systems, *J. Appl. Ecol.*, 11, 773–781.

Green, W.H. and Ampt, G.A. (1911), Studies on soil physics: I. The flow of air and water through soils, *J. Agric. Sci.*, 4, 1–24.

Gustafson, A. (1987), Simulation of water discharge rates from a clay-till soil over a ten year period, *J. Hydrol*, 92, 263–274.

Gwo, J.P., Jardine P.M., Wilson, G.V. and Yeh G.T. (1995), A multiple-pore-region concept to modeling mass transfer in subsurface media, *J. Hydrol*, 164, 217–237.

Gwo, J., Jardine, P. Wilson, G. and Yeh, G. (1996), Using a multiregion model to study the effects of advective and diffusive mass transfer on local physical nonequilibrium and solute mobility in a structured soil, *Water Resour. Res.*, 32(3), 561–570.

Gärdenäs, A., Simunek, J. Jarvis, N. and van Genuchten, M. (2006), Two-dimensional modelling of preferential water flow and pesticide transport from a tile-drained field, *J. Hydrol*, 329, 647–660.

Handerson, F.M. and Wooding, R.A. (1964), Overland flow and groundwater flow from steady rainfall of finite duration, *J. Geophys. Res.*, 69, 1531–1540.

Haude, W. (1958), Über die Verwendung verschiedener Klimafaktoren zur Berechnung der potentiellen Evaporation und Evapotranspiration, *Meteorologische Rundschau*, 11, 96–99.

Haws, N.W., Rao, P.S., Simunek, J. and Poyer, I.C. (2005), Single-porosity and dual-porosity modelling of water flow and solute transport in subsurface-drained fields using effective field-scale parameters, *J. Hydrol*, 313, 257–273.

Heilig, A., DeBruyn, D., Walter, M., Rose, C., Parlange, J., Steenhuis, T., Sander, G., Hairsine, P., Hogarth, W. and Walker, L. (2001), Testing a mechanistic soil erosion model with a simple experiment, *J. Hydrol*, 224, 9–16.

Hendriks, R.F.A., An analytical equation for describing the shrinkage characteristics of peat soils, in Päivänen, J. (ed.)(2004), Wise Use of Peatlands, Proceedings of the 12th International Peat Congress, Tampere, Finland.

Hendriks, R., Oostindie, K. and Hamminga, P. (1999), Simulation of bromide tracer and nitrogen transport in a cracked clay soil with the FLOCR/ANIMO model combination, *J. Hydrol*, 215, 94–115.

Hillel, D. (1998), Environmental soil physics, Academic Press, 771 p.

Hintikka, S., Koivusalo, H., Paasonen-Kivekäs, M., Nuutinen, V. and Alakukku, L. (2008), Role of macroporosity in runoff generation on a sloping subsurface drained clay field - a case study with MACRO model, *Hydr. Res.*, 39, 143–155.

Hintikka, S.-M. (2003), Makrohuokoston vaikutus salaoja- ja pintavaluntaan savimailla, Master's thesis, Helsinki University of Technology, 87 p.

Hooghoudt, S.B. (1940), Algemene beschouwing van het probleem van de detailontwatering en de infiltratie door middel van parallel loopende drains, greppels, slooten en kanalen. No. 7 in de serie: Bijdragen tot de

kennis van eenige natuurkundige grootheden van den grond, Bodemkundig Instituut te Groningen, Rijksuitgeverij Dienst van de Nderlandse Staatscourant, 's-Gravenhage, Algemeene Landsdrukkerij.

Hoogmoed, W.B. and Bouma, J. (1980), A simulation model for predicting infiltration into cracked clay soi, *Soil Sci. Soc. Am. J.*, 44, 458–461.

Horton, R.E. (1933), The role of infiltration in the hydrologic cycle, *Trans. Am. Geophys. Union*, 14, 446–460.

Innocenti, E., Silvani, X., Muzy, A., Hill, D.R.C. (2009), A software framework for fine grain parallelization of cellular models with OpenMP: Application to fire spread, *Env. Mod. & Software*, 24, 819–831.

Irmay, S. (1954), On the hydraulic conductivity of unsaturated soils, *Eos Trans. AGU*, 35, 463–467.

Jaakkola, E. (2009), ICECREAM-malli peltolohkojen fosforikuormituksen vähentämisen arvioinnissa. Esimerkkinä eteläsuomalainen osavaluma-alue, Master's thesis, Department of Geography, University of Helsinki, 66 p.

Jacobsen, O., Moldrup, P., Larsen, C., Konnerup, L. and Petersen, L. (1997), Particle transport in macropores of undisturbed soil columns, *J. Hydrol*, 196, 185–203.

Jalonen, J. (2008), The effectiveness of controlled drainage as a way to manage groundwater table levels and drainage runoff in acid sulfate soils, Master's thesis, Helsinki University of Technology, 89 p.

Jarvis, N. (2007), A review of non-equilibrium water flow and solute transport in soil macropores: principles, cotrolling factors and consequences for water quality, *Eur. J. Soil Sci.*, 58, 523–546.

Jarvis, N. (1994), The MACRO model (version 3.1), Technical description and sample simulations, Department of soil Science, Swedish University of Agricultural Sciences, Uppsala, Sweden, Reports and Dissertation 19.

Jarvis, N.J. (1989a), A simple empirical model of root water uptake, *J. Hydrol*, 107, 57–72.

Jarvis, N.J. (1989b), CRACK – model of water and solute movement in cracking clay soils: Technical description and user notes, Rep. 159, Div. Agric. Hydrotech, Soil Manage., Dep. Soil Sci., Swedish University of Agricultural Sciences, Uppsala, 38 p.

Jarvis, N., Etana, A. and Stagnitti, F. (2008), Water repellency, near-saturated infiltration and preferential solute transport in macroporous clay and soil, *Geoderma*, 143, 223–230.

Jarvis, N., Larsbo, M., Roulier, S., Lindahl, A. and Persson, L. (2007), The role of soil properties in regulating non-equilibrium macropore flow and solute transport in agricultural topsoils, *Eur. J. Soil Sci.*, 58, 282–292.

Jarvis, N.J. and Larsson, M.H. (1998), The MACRO model (version 4.1), Technical description, http://130.238.110.134/bgf/Macrohtm/macro.htm.

Jarvis, N.J. and Leeds-Harrison, P.B. (1990), Field test of a water balance model of cracking clay soils, *J. Hydrol*, 112, 203–218.

Jarvis, N.J. and Leeds-Harrison, P.B. (1987), Modelling water movement in drained clay soil. I. Description of the model, sample output and sensitivity analysis, *J. Soil Sci.*, 38, 487–498.

Jauhiainen, M. (2004), Relationships of particle size distribution curve, soil water retention curve and unsaturated hydraulic conductivity and their implications on water balance of forested and agricultural hillslopes, Doctoral dissertation, Helsinki University of Technology, 165 p.

Jetten, V. and Favis-Mortlock, D., Modelling soil erosion in Europe, in Boardman, J. and Poesen, J. (ed.)(2006), Soil erosion in Europe, John Wiley & Sons, 695–716.

Jetten, V., Roo, A. and Davis-Mortlock, D. (1999), Evaluation of field-scale and catchment-scale soil erosion models, *Catena*, 37, 521–541.

Johnson, B.E., Julien, P.Y., Molnar, D.K. and Watson, C.C. (2000), The two-dimensional upland erosion model CASC2D-SED, *J. Am. Wat. Res. Ass.*, 36, 31–42.

Julien, P.Y., Saghafian, B. and Ogden, F.L. (1995), Raster-Based Hydrologic Modeling of Spatially-Varied Surface Runoff, *Wat. Res. Bull.*, 31, 523–536.

Julien, P.Y. and Simons, D.B. (1985), Sediment transport capacity of overland flow, *Trans. ASEA*, 28, 755-762.

Jussila, P. (2007), Thermomechanics of swelling unsaturated porous media, Compacted bentonite clay in spent fuel disposal, Doctoral Dissertation, Helsinki University of Technology, Radiation and Nuclear Safety Authority, STUK-A223, 199 p.

Kaivosoja, J. (2009), Digital Elevation map of the Hovi catchment, unpublished data, MTT Agrifood Research Finland.

Kallio, K., Rekolainen, S., Ekholm, P., Granlund, K., Laine, Y., Johnsson, H. and Hoffman, M. (1997), Impacts of climatic change on agricultural nutrient losses in Finland, *Bor. Env. Res.*, 2, 33–52.

Kankaanranta, J. (1996), Veden virtaus ja ravinteiden huuhtoutuminen savimaassa, Master's thesis, Helsinki University of Technology, 79 p.

Karvonen, T. (1988), A model for predicting the effect of drainage on soil moisture, soil temperature and crop yield, Doctoral dissertation, Helsinki University of Technology, 215 p.

Karvonen, T. and Paasonen-Kivekäs, M. (2007), Makrohuokosten vaikutus infiltraatioon, sekä pinta- ja salaojavaluntaan: 2D-CROPWATN mallin kuvaus, Research report, Helsinki University of Technology, 30 p, http://www.water.tkk.fi/wr/kurssit/3d_world/ppt/Makro_Mallin_kuvaus.pdf, 26.01.2011.

Karvonen, T. and Kleemola, J., CROPWATN: prediction of water and nitrogen limited potato production, in Kabat, P., Marshall, B., van den Broek, B.J., Vos, J. and van Keulen, H. (1995), Modelling and

Parameterization of the Soil-Plant-Atmosphere System, Wageningen, 335–369.

Kauppi, L. (1982), Testing the applicability of the CREAMS model to estimation of agricultural nutrient losses in Finland, *Publications of the Water Research Institute*, National Board of Waters, Finland, No. 49, 30–39.

Kesäniemi, O. (2009), Hydraulic properties of peat soils, Licentiate thesis, Helsinki University of Technology, 144 p.

Kim, D.J., Vereecken, H., Feyen, J., Boels, D. and Bronswijk, J.J.B. (1992), On the characterization of properties of an unripe marine clay soil I. Shrinkage processes of an unripe marine clay soil in relation to physical ripening, *Soil Sci.*, 153, 471–481.

Kirkby, M., Impacts of environmental changes on soil erosion across Europe, in Boardman, J. and Poesen, J. (ed.)(2006), Soil erosion in Europe, John Wiley & Sons, 729–742.

Kladivko, E.J. (2001), Tillage systems and soil ecology, *Soil Till. Res.*, 61, 61–76.

Klepsch, S., Gerzabek, M.H., Loiskandl, W. and Bossew, P. (2005), Water and solute movement in soils – concepts and models for migration phenomena apart from classical convection-dispersion equation, *OICMS*, 249–261.

Knisel, W.G. and Turtola, E. (2000), Gleams model application on a heavy clay soil in Finland, *Agric. Wat. Man.*, 43, 285–309.

Knisel, W.G., (ed.)(1980), CREAMS - A field scale model for chemicals, runoff, and erosion from agricultural management systems, USDA, Conservation Report NO. 26, US Department of Agriculture, Washington DC.

Koivusalo, H. (1997), Hillslope hydrological processes - surface runoff and snowmelt on an agricultural field, Licentiate thesis, Helsinki University of Technology 60 + 142 p.

Koivusalo, H. (1993), Peltoalueen pintavalunta ja eroosio, Master's thesis, Helsinki University of Technology, 84 p.

Koivusalo, H. and Karvonen, T. (1995), Modeling surface runoff – A case study of a cultivated field in Southern Finland, *Nordic Hydrology*, 26, 205–222.

Koivusalo, H., Karvonen, T. and Paasonen-Kivekäs, M. (1999), Application of a two-dimensional model to calculate water balance of an agricultural hillslope, *Phys. Chem. Earth (B)*, 24, 313–318.

Kokkonen, T. (1997), Parameter identification in groundwater models PART I: Bayesian approach to the inverse groundwater problem PART II: Groundwater model application in Pakri peninsula, Licentiate thesis, Helsinki University of Technology, 106 p.

Koskiaho, J., Kivisaari, S., Vermeulen, S., Kauppila, R., Kallio, K. and Puustinen, M. (2002), Reduced tillage: Influence on erosion and nutrient losses in a clayey field in southern Finland, *Agric. and Food Sci.*, 11, 37–50.

Kosugi, K. (1994), Three-parameter lognormal distribution model for soil water retention, *Water Resour. Res.*, 30, 891–901.

Kosugi, K. (1999), General model for unsaturated hydraulic conductivity for soils with lognormal pore-size distribution. *Soil. Sci. Soc. Am. J.*, 63, 270–277.

Kreyszig, E. (1993), Advanced engineering mathematics, 7th edition, John Wiley & Sons Inc., 1271 p.

Kroes, Van Dam, Groenendijk, P., Hendriks, R.F.A. and Jacobs, C.M.J. (2008), SWAP version 3.2 Theory description and user manual, Alterra-report, Wageningen, 262 p.

Kändler, M. (2006), Vergleichende Analyse der Modellansätze von ICECREAM und EROSION 2D bezüglich der hydrologischen Komponenten, Master's thesis, Internationales Hochschulinstitut Zittau, 68 p.

Köhne, S., Lennatz, B., Köhne, M. and Simunek, J. (2006), Bromide transport at a tile-drained field site: experiment, and one- and two-dimensional equilibrium and non-equilibrium numerical modelling, *J. Hydrol*, 321, 390–408.

Laine-Kaulio, H. (2008), Subsurface flow in a forested till slope - Soil analysis, tracer experiments and physics-based modeling, Licentiate thesis, Helsinki University of Technology, 100 p.

Lapidus, L. and Amundson, N.R. (1952), A descriptive theory of leaching. Mathematics of adsorptive beds. *J. Phys. Chem.*, 56, 984–988.

Larsbo, M and Jarvis, N. (2003), MACRO 5.0. A model of water flow and solute transport in macroporous soil. Technical description, Swedish University of Agricultural Sciences, 40 p.

Larsson, M.H., Persson, K., Ulén, B., Lindsjö, A. and Jarvis, N.J. (2007), A dual porosity model to quantify phosphorus losses from macroporous soils, *Ecol. Mod.*, 205, 123–134.

Laubel, A., Jacobsen, O.H., Kronvang, B. Grant, R. and Andersen, H.E. (1999), Subsurface drainage loss of particles and phosphorous from field plot experiments and a tile-drained catchment, *J. Environ. Qual.*, 28, 576–584.

Lauritzen, C.W and Stewart, A.J. (1941), Soil-volume changes and accompanying moisture and pore-space relationships, *Soil Sci. Soc. Am. Proc.*, 6, 113–116.

Laws, J.O. and Parsons, D.A. (1943), The relation of raindrop-size to intensity, *Trans. Am. Geo. Un.*, 24, 452–460.

Leeds-Harrison, P.B., Shipway, C.J.P., Jarvis, N.J. and Youngs, E.G. (1986), The influence of soil macroporosity on water retention, transmission and drainage in a clay soil, *Soil Use Manag*., 2, 47–50.

Léonard, J., Perrier, E. and De Marsily, G. (2001), A model for simulating the influence of a spatial distribution of large circular macropores on surface runoff, *Water Resour. Res*., 37, 3217–3225.

Leonard, R.A., Knisel, W.G. and Still, D.A. (1987), GLEAMS: Groundwater loading effects of agricultural management systems, *Trans. Am. Soc. Agric. Eng*., 30, 1403–1418.

Li, Z. and Zhang, J. (2001), Calculation of field Manning's roughness coefficient, *Agric. Wat. Man*., 49, 153–161.

Lighthill, M.J. and Whitham G.B. (1955), On kinematic waves: Flood movement in long rivers, *Proc. R. Soc. London A*, 229, 281–316.

Linnér et al. (2006), Bearbetning av kapitlet bevattning i Växtodling 1. Marken, Bevattning, www-pot.lt.slu.se/dokument/Bevattning.pdf.

Maasilta, A., Pekkarinen, M., Tuononen, E. and Vakkilainen, P. (1980), Ainehuuhtoutumista pelto- ja metsävaltaisella valuma-alueella Siuntionjoen vesistössä, Vesitekniikan laitos, Teknillinen korkeakoulu, Julkaisu 18, 36 p.

Makkink, G.F. (1957), Testing the Penman formula by means of lysimeters, *J. Inst. Wat. Engrs*., 11, 277–288.

Mantz, P.A. (1977), Incipient transport of fine grains and flakes by fluids-extended Shields diagram. *Proc. Am. Soc. Civ. Eng., J. Hydraul. Div*., 103, 601–615.

McKay, L.D., Gillham, R.W. and Cherry, J.A. (1993), Field experiments in a fractured clay till 2. Solute and Colloid transport, *Water Resour. Res*., 29, 3879–3890.

Messing, I., Jarvis, N.J. (1990), Seasonal variation in field-saturated hydraulic conductivity in two swelling clay soils in Sweden, *J. Soil Sci*., 41, 229-237.

Meyer, L.D. and Harmon, W.C. (1984), Susceptibility of agricultural soils to interrill erosion. *Soil Sci. Soc. Am. J*., 48, 1152–1157.

Meyer, L.D., Harmon, W.C. and McDowell, L.L., (1980), Sediment sizes eroded from crop row sideslopes, *Trans. ASAE*, 23, 891–898.

Mikkelsen, H.E. and Olesen, J.E. (1991), Sammenligning af metoder til bestemmelse af potentiel vandfordampning, *Tidsskrift for Planteavl*, Beretning S2157.

Mohanty B.P., Castiglione, P. Shouse, P.J. and van Genuchten, M.Th. (1997), New piecewise-continuous hydraulic functions for modelling preferential flow in an intermittent-flood-irrigated field, *Water Resour. Res*., 33, 2049–2063.

Mohanty, B.P., Bowman, R.S., Hendrickx, M.H., Simunek, J. and van Genuchten, M.T. (1998), Preferential transport of nitrate to a tile drain in an intermittent-flood-irrigated field: Model development and experimental evaluation, *Water Resour. Res.*, 34, 1061–1076.

Monteith, J.L. (1981), Evaporation and surface temperature, *Q. J. R. Meteorol. Soc.*, 107, 1–27.

Monteith, J.L. (1965), Evaporation and environment, *Symp. Soc. Exp. Biol.*, 19, 205–224.

Morgan, R.P.C. (2005), Soil Erosion and Conservation, 3rd edition, Wiley-Blackwell, 320 p.

Morgan, R.P.C, Quinton, J.N., Smith, R.E., Govers, G., Poesen, J.W.A., Auerswald, K., Chisci, G., Torri, D. and Styczen, M.E. (1998), The European soil erosion model (EUROSEM): A dynamic approach for predicting sediment transport from fields and small catchments, *Earth Surf. Proc. Landf.*, 23, 527–544.

Morgan, R.P.C. (2001), A simple approach to soil loss prediction: a revised Morgan–Morgan–Finney model, *Catena*, 44, 305–322.

Mualem, Y. (1976), A new model for predicting the hydraulic conductivity of unsaturated porous media, *Water Resour. Res.*, 14, 513–522.

Nash, J.E. and Sutcliffe, J.V. (1970), River flow forecasting through conceptual models part I — A discussion of principles, *J. Hydrol*, 10, 282–290.

Neal, J., Fewtrell, T. and Trigg M. (2009), Parallelisation of storage cell flood models using OpenMP, *Env. Mod. & Software*, 24, 872–877.

Neuman, S.P. and Yakowitz, S. (1980), A statistical approach to the inverse problem of aquifer hydrology, 1, theory, *Water Resour. Res.*, 15, 845–860.

Neuman, S.P., Fogg, G.E. and Jacobson, E.A, A statistical approach to the inverse problem of aquifer hydrology, 2, case study, *Water Resour. Res.*, 16, 33–58.

Nieber, J. (2001), The relation of preferential flow to water quality and its theoretical and experimental quantification, Preferential Flow Water: Movement and Chemical Transport in the Environment, Proc. of 2nd Intl. Symp. 3.–5. January 2001, Honolulu, Hawaii, USA, 1–10.

Nieber, J. and Feddes, R. (1999), Solutions for combined saturated and unsaturated flow, Agricultural drainage, Agronomy Monograph no. 38, American Society of Agronomy, Crop Science Society of America, Soil Science Society of America, 145–212.

Nimmo, J.R. and Landa, E.R. (2005), The soil physics contributions of Edgar Buckingham, *Soil Sci. Soc. Am. J.*, 69, 328–342.

Nord, G. and Esteves, M. (2005), PSEM_2D: A physically based model of erosion processes at the plot scale, *Water Resour. Res.*, 41, 1–14.

Novak, S. M., Banton, O. and Schiavon, M. (2003), Modelling metolachlor exports in subsurface drainage water from two structured soils under maize (eastern France), *J. Hydrol*, 270, 295–308.

Novák, V., Šimůnek, J. and van Genuchten, M. (2000), Infiltration of water into soil with cracks, *J. Irrigat. Drain. Eng.*, 126, 41–47.

Nuutinen, V., Butt, K.R. (2003), Interaction of Lumbricus terrestris L. burrows with subdrains, *Pedobiologia*, 47, 578–581.

Nyholm, A-M, Mallitarkastelu suojakaistan vaikutuksesta valuntaan ja eroosioon, in Virkajärvi, P. and Uusi-Kämppä, J. (ed.)(2006), Laitumien ja rajavyöhykkeiden ravinnekierto ja ympäristökuormitus, MTT Agrifood Research Finland, 76, 149–166.

Nyroos, H., Partanen-Hertell, M., Silvo, K. and Kleemola, P. (ed.)(2006), Vesiensuojelun suuntaviivat vuoteen 2015 – Taustaselvityksen lähtökohdat ja yhteenveto tuloksista, Suomen ympäristö 55/2006, 68 p.

O'Callaghan, J.F. and Mark, D.M. (1984), The extraction of drainage networks from digital elevation data, *Comput. Vis. Graph. Image Process.*, 28, 323–344.

Onstad, C.A. (1984), Depressional storage on tilled soil surfaces, *Trans. ASAE*, 27, 729–732.

Oostindie, K. and Bronswijk, J.J.B. (1992), FLOCR – A simulation model for the calculation of water balance, cracking and surface subsidence of clay soils, The Winand Staring Center for Integrated Land, Soil and Water Research, Report 47.

Othmer, H., Diekkrüger, B. and Kutilek, M. (1991), Bimodal porosity and unsaturated hydraulic conductivity, *Soil Sci.*, 152, 139–150.

Øygarden, L., Kværner, J. and Jenssen, P.D. (1997), Soil erosion via preferential flow to drainage systems in clay soils, *Geoderma*, 76, 65–86.

Paasonen-Kivekäs, M. and Koivusalo, H. (2006), Losses of sediment and phosphorus through subsurface drains in a clay field in southern Finland, Proceedings of NJF Seminar No. 373 Transport and retention of pollutants from different production systems – with respect to implementation of the Water Framework Directive, 11.–14. June 2006, Tartu, Estonia, 95–100.

Paasonen-Kivekäs, M., Karvonen, T. and Vakkilainen, P., Vesitalouden säädön vaikutus ravinteiden huuhtoutumiseen, in Vakkilainen (ed.)(2000), Peltoviljelyn ravinnehuuhtouman vähentäminen pellon vesitaloutta säätämällä, Salaojituksen tutkimusyhdistys Ry, 25, 103 p.

Paasonen-Kivekäs, M., Koivusalo, H., Bärlund, I., Tattari, S. and Alakukku, L. (2006), Modelling runoff and erosion in agricultural soil: application of ICECREAM model to a field site in southern Finland, Proceedings of NJF Seminar No. 373 Transport and retention of pollutants from different production systems – with respect to implementation of the Water Framework Directive, 11.–14. June 2006, Tartu, Estonia.

Paasonen-Kivekäs, M., Koivusalo, H., Karvonen, T., Vakkilainen, P. and Virtanen, J. (1999), Nitrogen transport via surface and subsurface flow in

an agricultural field, Proceedings of IUGG 99 Symposium HS3, Birmingham, July 1999, *IAHS Publ.*, 257, 163–169.

Paasonen-Kivekäs, M., Vakkilainen, P. and Karvonen, T. (2008), Nutrient transport through tile drains on a clayey field, 10th International Drainage Workshop of ICID Working Group on Drainage, Helsinki-Tallinn, Finland-Estonia, 6-11 July 2008, Conference proceedings, 142–152.

Peltovuori, T., Uusitalo, R. and Kauppila, T. (2002), Phosphorus reserves and apparent phosphorus saturation in four weakly developed cultivated pedons, *Geoderma*, 110, 35–47.

Peltovuori, T. (2006), Phosphorus in agricultural soils of Finland - characterization of reserves and retention in mineral soil profiles, Doctoral dissertation, University of Helsinki, 69 p + original articles.

Peng, X. and Horn, R. (2005), Modeling soil shrinkage curve across a wide range of soil types, *Soil Sci. Soc. Am. J.*, 69, 584–592.

Penman, H.L. (1948), Natural evaporation from open water, bare soil and grass, *Proc. Royal Met. Soc. (A)*, 193, 120–146.

Peters, R.R. and Klavetter, E.A. (1988), A continuum model for water movement in an unsaturated fractured rock mass, *Water Resour. Res.*, 24, 416–430.

Philip, J.R. (1957), The theory of infiltration: 1. The infiltration equation and its solution, *Soil Sci.*, 83, 345–357.

Pinder, G.F. and Gray, W.G. (1977), Finite element simulation in surface and subsurface hydrology, Academic Press, 295 p.

Posch, M. and Rekolainen, S. (1993), Erosivity factor in the universal soil loss equation estimated from Finnish rainfall data, *Agricultural Science in Finland*, 2, 271–279.

Prenter, P.M. (1975), Splines and variational methods, John Wiley, New York.

Priestley, C.H.B. and Taylor, R.J. (1972), On the assessment of surface heat flux and evaporation using large-scale parameters, *Monthly Weather Rev.*, 100, 81-92.

Pruess K., Oldenburg, C. and Moridis G. (1999), TOUGH2 User's guide, Version 2.0, Earth Sciences Division, Lawrence Berkeley National Laboratory, University of California, 210 p.

Puustinen, M., Koskiaho, J. and Peltonen, K. (2005), Influence of cultivation methods on suspended solids and phosphorus concentrations in surface runoff on clayey sloped fields in boreal climate, *Agr. Ecosyst. Environ.*, 105, 565–579.

Puustinen, M., Tattari, S., Koskiaho, J. and Linjama, J. (2007), Influence of seasonal and annual hydrological variations on erosion and phosphorus transport from arable areas in Finland, *Soil Till. Res.*, 93, 44-55.

Puustinen, M., Turtola, E., Kukkonen, M., Koskiaho, J., Linjama, M., Niinioja, R. and Tattari, S. (2010), VIHMA - A tool for allocation of measures to control erosion and nutrient loading from Finnish agricultural catchments, *Agr. Ecosyst. Environ.*, 138, 306–317.

Rankinen, K., Tattari, S. and Rekolainen, S. (2001), Modelling of vegetative filter strips in catchment scale erosion control, *Agric. and Food Sci.*, 10, 99–112.

Rasa, K., Horn, R., Räty, M., Yli-Halla, M., Pietola, L. (2009), Shrinkage properties of differently managed clay soils in Finland, *Soil Use Manag.*, 25, 175–182.

Ray, C., Ellsworth, T.R., Valocchi, A.J. and Boast, C.W. (1997), An improved dual porosity model for chemical transport in macroporous soils, *J. Hydrol*, 193, 270–292.

Refsgaard, J.C. and Henriksen, H.J. (2004), Modelling guidelines – terminology and guiding principles, *Adv. Wat. Res.*, 27, 71–82.

Rekolainen, S., Ekholm, P., Heathwaite, L., Lehtoranta, J. and Uusitalo, R., Off-site impacts of erosion: Eutrophication as an example, in Boardman, J. and Poesen, J. (ed.)(2006), Soil erosion in Europe, John Wiley & Sons, 775–789.

Rekolainen, S., Grönroos, J., Bärlund, I., Nikander A. and Laine, Y., (1999), Modelling the impacts of management practices on agricultural phosphorus losses to surface waters of Finland, *Wat. Sci. Technol.*, 39, 265–272.

Rekolainen, S. and Posch, M. (1993), Adapting the CREAMS model for Finnish conditions, *Nordic Hydrology*, 24, 309–322.

Richards, L.A. (1931), Capillary conduction of liquids through porous mediums, *Physics*, 1, 318–333.

Rijtema, P.E. and Kroes, J.G. (1991), Some results of nitrogen simulations with the model ANIMO, *Fert. Res.*, 27, 189–198.

Ristolainen, A. and Pesonen, L. (2010), soil data from the Hovi experimental field in Finland, unpublished data, Täsmä-NP project, MTT Agrifood Research Finland.

Ross, P.J. and Smettem, K.R. (2000), A simple treatment of physical non-equilibrium water flow in soils, *Soil Sci. Soc. Am. J.*, 64, 1926–1930.

Ruan, H. and Illangesekare, T.H. (1998), A model to couple overland flow and infiltration into macroporous vadose zone, *J. Hydrol*, 210, 116–127.

RZWQM Team (1998), RZWQM: Simulating the effects of management on water quality and crop production, *Agric. Syst.*, 57, 161–195.

Räsänen, T. (2009), Veden ja typen käyttäytymisen mallintaminen hieta- ja savimaassa HYDRUS-mallilla, Master's thesis, Helsinki University of Technology, 133 p.

Savabi, M.R. (1993), Runoff with WEPP, *J. Irrigat. Drain. Eng.*, 119, 801–813.

Schmidt, J., Werner, M.V., Michael, A. (1999), Application of the EROSION 3D model to the CATSOP watershed, The Netherlands, *Catena*, 37, 449–456.

Schmieder, F. (2008), Application of the ICECREAM model under different climatic conditions and variable field properties, Master's thesis, Internationales Hochschulinstitut Zittau, 74 p.

Schwartz, F.W. (1977), Macroscopic dispersion in porous media: The controlling factors, *Water Resour. Res.*, 13, 743–752.

Schwartz, R., Juo, A. and McInnes, K. (2000), Estimating parameters for a dual-porosity model to describe non-equlibrium, reactive transport in a fine-textured soil, *J. Hydrol*, 229, 149–167.

Seuna, P. and Kauppi, L. (1981), Influence of sub-drainage on water quantity and quality in a cultivated area in Finland, Publications of the Water Research Institute, National Board of Waters, Finland, No. 43, 32–47.

Sharda, V.N. and Singh, S.R. (1994), A finite element model for simulating runoff and soil erosion from mechanically treated agricultural lands 1. Governing equations and solutions, *Water Resour. Res.*, 30, 2287–2298.

Sharda, V.N., Singh, S.R., Sastry, G. and Dhruvanarayana, V.V. (1994), A finite element model for simulating runoff and soil erosion from mechanically treated agricultural lands 2. Field validation and applications, *Water Resour. Res.*, 30, 2299–2310.

Shipitalo, M.J., Nuutinen, V. and Butt, K.R. (2004), Interaction of earthworm burrows and cracks in a clayey, subsurface-drained, soil, *Appl. Soil Ecol.*, 26, 209–217.

Šimůnek, J., Huang, K., Šejna, M., van Genuchten, M.Th., Majerčák, J., Novák, V. and Šutor, J. (1997), The HYDRUS-ET software package for simulating the one-dimensional movement of water, heat and multiple solutes in variably saturated media, Version 1.1., Institute of Hydrology, Slovak Academy of Sciences, Bratislava, Slovakia.

Šimůnek, J., Jarvis, N.J., van Genuchten, M.Th. and Gärdenäs, A. (2003), Review and comparison of models for describing non-equilibrium and preferential flow and transport in the vadosa zone, *J. Hydrol*, 272, 14–35.

Šimůnek, J. and van Genuchten, M. (2008), Modeling nonequilibrium flow and transport processes using HYDRUS, *Vadose Zone J.*, 7, 782–797.

Šimůnek, J., van Genuchten, M. and Šejna, M. (2006), The HYDRUS software package for simulating the two- and three-dimensional movement of water, heat and multiple solutes in variably-saturated media, Technical manual, 241 p.

Simunek, J., Vogel, T. and van Genuchten, M.Th. (1994), The SWMS-2D Code for simulating water flow and solute transport in two-dimensional variably saturated media, Version 1.21, Research Report No. 132, USDA-ARS U.S. Salinity Laboratory, Riverside, California.

Šimůnek, J., Wendroth, O., Wypler, N., van Genuchten, M.Th. (2001), Nonequilibrium water flow characterized from an upward infiltration experiment, *Eur. J. Soil Sci.*, 52, 13–24.

Singh, V. (1996), Kinematic wave modeling in water resources: surface-water hydrology, Wiley-Interscience, 1424 p.

Sippola, J. (1974), Mineral composition and its relation to texture and to some chemical properties in Finnish subsoils, *Annales Agriculturae Fenniae*, 13, 169–234.

Skaggs, R. (1980), A water management model for shallow water table soils, Report No. 134, Water Resour. Res. Institute of the University of North Carolina, Raleigh, NC.

Skopp, J. and Gardner, W.R. (1992), Miscible displacement: an interacting flow region model, *Soil. Sci. Soc. Am. j.*, 56, 1680–1686.

Skopp, J. and Warrick, A.W. (1974), A two-phase model for the miscible displacement of reactive solutes in soils, *Soil. Sci. Soc. Am. Proc.*, 38, 545–550.

Skopp, J., Gardner, W.R. and Tyler, E.J. (1981), Solute movement in structured soils: Two-region model with small interaction, *Soil. Sci. Soc. Am. J.*, 45, 837–842.

Smettem, K.R.J. and Kirkby, C. (1990), Measuring the hydraulic properties of a stable aggregated soil. *J. Hydrol.*, 117, 1–13.

Smith, R.E., Goodrich, D.C. and Unkrich, C.L. (1999), Simulation of selected events on the Catsop catchment by KINEROS2: A report for the GCTE conference on catchment scale erosion models, *Catena*, 37, 457–475.

Smith, R.E., Goodrich, D.C., Woolhiser, D.A. and Unkrich, C.L., KINEROS - A Kinematic Runoff and Erosion Model, in Singh, V.J. (ed.)(1995), Computer Models of Watershed Hydrology, Water Resources Publications, 697–732.

Smith, R.E., and Woolhiser, D.A. (1971), Overland flow on an infiltrating surface, *Water Resour. Res.*, 7, 899–913.

Soil Survey Staff (1998), Keys to Soil Taxonomy, 8th Edition, US Department of Agriculture Natural Resource Conservation Service, Washington DC, 326 p.

Soinne, H. (2002), Fosforin ja kiintoaineksen kulkeutuminen ja pidättyminen savimaaprofiilissa – kirjallisuuskatsaus, Soveltavan kemian ja mikrobiologian laitos, Helsingin yliopisto, 48 p.

Spitz, K. and Moreno, J. (1996), A practical guide to groundwater and solute transport modeling, John Wiley & Sons, 461 p.

Steenhuis, T.S., Parlange, J.-Y. and Andreini, M.S. (1990), A numerical model for preferential solute movement in structured soils, *Geoderma*, 46, 193–208.

Strecker, E.W. and Chu, W.-S. (1986), Parameter identification of a groundwater contaminant transport model, *Groundwater*, 24, 56–62.

Sudicky, E.A. (1990), The laplace transform Galerkin technique for efficient time-continuous solution of solute transport in double-porosity media, *Geoderma*, 46, 209–232.

Sun, N.-Z. (1994), Inverse problems in groundwater modeling (Theory and applications of transport in porous media), Springer, 352 p.

Tamm, T. (2002), Effect of meteorological conditions and water management on hydrological processes in agricultural fields, Doctoral dissertation, Helsinki University of Technology, 194 p.

Taskinen, A. (2002), Mathematical modelling of overland flow, erosion and transport of phosphorus, PhD thesis, University College Dublin.

Taskinen, A. and Bruen M. (2007a), Incremental distributed modelling investigation in a small agricultural catchment: 1. Overland flow with comparison with the unit hydrograph model, *Hydrol. Proc.*, 21, 80–91.

Taskinen, A. and Bruen M. (2007b), Incremental distributed modelling investigation in a small agricultural catchment: 2. Erosion and phosphorus transport, *Hydrol. Proc.*, 21, 92–102.

Tattari, S. and Bärlund, I. (2001), The concept of sensitivity in sediment yield modelling, *Phys. Chem. Earth (B)*, 26, 27–31.

Tattari, S. and Rekolainen, S., Finland, in Boardman, J. and Poesen, J. (ed.)(2006), Soil erosion in Europe, John Wiley & Sons, 27–32.

Tattari, S., Bärlund, I., Rekolainen, S., Posch, M., Siimes, K., Tuhkanen, H.-R. and Yli-Halla, M. (2001), Modeling sediment yield and phosphorus transport in Finnish Clayey soils, *Trans. ASAE*, 44, 297–307.

Tiihonen, T. (2007), Hydrological processes in urban watersheds; development and application of a distributed stormwater model, Master's thesis, Helsinki University of Technology, 111 p.

Tracy, F.T. (2007), Three-dimensional analytical solutions of Richards' equation for a box-shaped soil sample with a piecewise-constant head boundary conditions on the top, *J. Hydrol*, 336, 391–400.

Tracy, F.T. (2006), Clean two- and three-dimensional analytical solutions of Richards equation for testing numerical solvers, *Water Resour. Res.*, 42, W08503.

Tracy, F.T. (1995), 1-D, 2-D, and 3-D analytical solutions of unsaturated flow in groundwater, *J. Hydrol*, 170, 199–214.

Trancoso, A.R., Braunschweig, F., Leitão, P.C., Obermann, M. and Neves, R. (2009), An advanced modelling tool for simulating complex river systems, *Sci. Total Environ.*, 407, 3004-3016.

Turtola, E. and Paajanen A. (1995), Influence of improved subsurface drainage on phosphorus losses and nitrogen leaching from a heavy clay soil, *Agric. Wat. Man.*, 28, 295–310.

Turtola, E., Alakukku, L. and Uusitalo, R. (2007), Surface runoff, subsurface drainflow and soil erosion as affected by tillage in a clayey Finnish soil, *Agric. and Food Sci.*, 16, 332–351.

Turunen, M. (2011), Analysis of the water balance and subsurface drainage methods in an agricultural field, Master's thesis, Aalto University, 116 + 10 p.

Ulén, B. (1997), Nutrient losses by surface runoff from soils with winter cover crops and spring-ploughed soils in the south of Sweden, *Soil Till. Res.*, 44, 165–177.

Ulén, B. (1995), Episodic precipitation and discharge events and their influence on losses of phosphorus and nitrogen from tiledrained arable fields, *Swed. J. Agr. Res.*, 25, 25–31.

USDA (1972), National Engineering Handbook, Section 4, Hydrology, USDA, National Resources Conservation, Service, Washington DC.

USDA (1995), WEPP user summary, NSERL Report No. 11, National Soil Erosion Research Laboratory, USDA, 141 p.

Uusitalo, R., Turtola, E., Kauppila, T. and Lilja, T. (2001), Particulate phosphorus and sediment in surface runoff and drainflow from clayey soils, *J. Env. Qual.*, 30, 589–595.

Uusitalo, R., Turtola, E. and Lemola, R. (2007), Phosphorus losses from a subdrained clayey soil as affected by cultivation practices, *Agric. and Food Sci.*, 16, 352–365.

Uusitalo, R., Turtola, E., Puustinen, M., Paasonen-Kivekäs, M. and Uusi-Kämppä, J. (2003), Contribution of particulate phosphorus to runoff phosphorus bioavailability, *J. Env. Qual.*, 32, 2007–2016.

Vakkilainen, P. (1982), On the estimation of evapotranspiration, Doctoral dissertation, University of Oulu, 146 p.

Vakkilainen, P. (1980), Tutkimus pellon tiivistymisen vaikutuksesta salaojituksen toimintaan, *Vesitalous*, 2, 23–28.

Vakkilainen, P., Alakukku, L., Koskiaho, J., Myllys, M., Nurminen, J., Paasonen-Kivekäs, M., Peltomaa, R., Puustinen, M. and Äijö, H. (2010), Pellon vesitalouden optimointi, Loppuraportti 2010, Salaojituksen tutkimusyhdistys ry:n tiedote 30, Helsinki 2010, Salaojituksen tutkimusyhdistys ry, 114 p.

Vakkilainen, P. and Paasonen-Kivekäs, M. (2004), Savimaa, vesi ja ravinteet – salaojatutkimusta Kirkkonummela, in Työtä, tietoa ja tutkimusta, Salaojituksen Tukisäätiö, 135 p.

Van Beers, W.F.J. (1976), Computing drain spacings, Bull. 15, ILRI, Wageningen, The Netherlands.

van Genuchten, M.T. (1980), A closed form equation for predicting the hydraulic conductivity of unsaturated soils, *Soil Sci. Soc. Am. J.*, 44, 892–898.

van Genuchten, M.Th. and Dalton, F. N. (1986), Models for simulating salt movement in aggregated field soils, *Geoderma*, 38, 165–183.

van Genuchten, M.Th. and Wierenga, P.J. (1976), Mass transfer studies in sorbing porous media I: analytical solutions, *Soil Sci. Soc. Am. J.*, 40, 473–480.

van Keulen, H. and van Beek, C.G.M. (1971), Water movement in layered soils; A simulation model, *Neth. J. Agric. Sci.*, 19, 138–153.

van der Ploeg, R.R. and Benecke, P. (1974), Unsteady, unsaturated n-dimensional moisture flow in soil: A computer simulation program, *Soil Sci. Soc. Am. Proc.*, 38, 881–885.

Vanderborght, J., Jacques, D. and Feyen J. (2000), Deriving transport parameters from transient flow leaching experiments by approximate steady-state flow convection-dispersion models, *Soil Sci. Soc. Am. J.*, 64, 1317–1327.

Vassilev, D. and Yotov, I. (2010), Coupling Stokes - Darcy flow with transport, *SIAM J. Sci. Comput.*, 31, 3661–3684.

Versteeg, H.K. and Malalasekera, W. (2007), An introduction to computational fluid dynamics; The finite volume method, 2nd edition, Prentice Hall, 520 p.

Villholth, K.G., Jensen, K.H. (1998), Flow and transport processes in a macroporous subsurface-drained glacial till soil. II. Model analysis, *J. Hydrol*, 207, 121–135.

Vogel, T. and Cislerova, M. (1988), On the reliability of unsaturated hydraulic conductivity calculated from the moisture retention curve, *Transp. Porous. Med.*, 3, 1–15.

Vogel, T., Gerke, H., Zhang, R. and van Genuchten, M. (2000), Modeling flow and transport in a two-dimensional dual-permeability system with spatially variable hydraulic properties, *J. Hydrol*, 238, 78–89.

Vogel, T., Huang, K., Zhang, R. and van Genuchten, M.Th. (1996), The HYDRUS code for simulating one-dimensional water flow, solute transport, and heat movement in variably-saturated media (version 5.0), Research Report No. 140, US Salinity Laboratory, USDA-ARS, Riverside, CA.

Vuorenmaa, J., Rekolainen, S., Lepistö, A., Kenttämies, K. and Kauppila, P. (2002), Losses of nitrogen and phosphorus from agricultural and forest areas in Finland during the 1980s and 1990s, *Environ. Monit. Assess.*, 76, 213–248.

Väisänen, S. and Puustinen, M. (Ed.)(2010), Managing the agricultural load on water bodies, The Finnish Environment Institute, *Suomen Ympäristö*, 23, 134 p.

Warren, J.E. and Root, P.J. (1963), The behavior of naturally fractured reservoirs, *SPEJ*, 228, 245–255.

Warsta, L. (2007), Modelling overland and subsurface drainage runoffs at an agricultural field, Licentiate thesis, Helsinki University of Technology, 70 p.

Warsta, L. (2005), Exploitation of fly ash produced by the forest industry: transport of harmful substances, Master's thesis, Helsinki University of Technology, 95 p.

Warsta, L., Paasonen-Kivekäs, M., Karvonen, T. (2008a), Modelling runoff at an agricultural field, 10th International Drainage Workshop of ICID Working Group on Drainage, Helsinki-Tallinn, Finland-Estonia, 6.–11. July 2008, Conference proceedings, 209–217.

Warsta, L., Paasonen-Kivekäs, M., Karvonen, T. and Taskinen, A. (2009), Modelling surface and subsurface flow of water and erosion at clayey, subsurface drained agricultural field, 18th World IMACS/MODSIM Congress, Cairns, Australia, 13.–17. July 2009, Conference proceedings, 1901–1907.

Warsta, L., Paasonen-Kivekäs, M., Karvonen, T. and Taskinen, A. (2008b), Dual-permeability modelling of three-dimensional water flow at a clayey field, IASTED Symposium on Environmental Modelling and Simulation, Orlando, USA, 16.–18. November 2008, Conference proceedings, 326–332.

Weill, S., Mouche, E. and Patin, J. (2009), A generalized Richards equation for surface/subsurface flow modelling, *J. Hydrol*, 366, 9–20.

Werner, M.v. (1995), GIS-orientierte Methoden der digitalen Reliefanalyse zur Modellierung von Bodenerosion in kleinen Einzugsgebieten, Doctoral Dissertation, Freie Universität Berlin.

Wicks, J.M. and Bathurst, J.C. (1996), SHESED: a physically based, distributed erosion and sediment yield component for the SHE hydrological modelling systems, *J. Hydrol.*, 175, 213–238.

Wilson, G.V., Jardine, P.M. and Gwo, J.P. (1992), Modeling the hydraulic properties of a multiregion soil, *Soil. Sci. Soc. Am. J.*, 56, 1731–1737.

Wind, G.P. and Van Doorne, W. (1975), A numerical model for the simulation of unsaturated vertical flow of moisture in soils, *J. Hydrol*, 24, 1–20.

Woolhiser, D.A., Smith, R.E. and Goodrich, D.C. (1990), KINEROS, A Kinematic Runoff and Erosion Model: Documentation and User Manual, US. Department of Agriculture, Agricultural Research Service, ARS-77, 130 p.

Wyllie, M.R.J. and Gardner, G.H.F. (1958), The generalized Kozeney-Carman equation, *World Oil*, 146, 210–228.

Yalin, M.S. (1963), An expression for bed-load transportation, *Proc. Am. Civ. Eng., J. Hydraul. Div.*, 89, 221–250.

Yalin, M.S. (1977), Mechanics of sediment transport, Pergamon Press, Toronto, 298 p.

Yli-Halla, M., Mokma, L. Peltovuori, T. and Sippola, J. (2000), Suomalaisia maaprofiileja, Agricultural soil profiles in Finland and their classification, Publications of Agricultural Research Centre of Finland, Series A 78, 104 p.

Yli-Halla, M., Tattari, S., Bärlund, I., Tuhkanen H.-R., Posch, M., Siimes, K., Rekolainen, S. (2005), Simulating processes of soil phosphorus in geologically young acidic soils of Finland, *Trans. ASAE*, 48, 101–108.

Youngs, G.V. (1980), The analysis of groundwater seepage in heterogeneous aquifers, *Hydr. Sci. Bulletin*, 25, 155–154.

Zheng, C. and Bennet G.D. (2002), Applied Contaminant Transport Modelling, 2nd edition, Wiley, 621p.

Zienkiewicz, O.C. (1971), The finite element method in engineering science, McGraw – Hill, London, 521 p.

Zimmerman, R.W., Chen, G., Hadgu, T. and Bodvarsson, G. (1993), A numerical dual-porosity model with semianalytical treatment of fracture/matrix flow, *Water Resour. Res.*, 29, 2127–2137.

Zimmerman, R.W., Hadgu, T. and Bodvarsson, G.S. (1996), A new lumped-parameter model for flow in unsaturated dual-porosity media, *Adv. Water Resour.*, 19, 317–327.

Zinke, P., Olsen, N.R.B., Bogen, J. and Rüther, N. (2010), 3D modelling of the flow distribution in the delta of Lake Øyren, Norway, Hydr. Res., 41, 92-103.

Appendix A PDMA multipliers for subsurface flow

Macropore system multipliers:

$$\boldsymbol{A}[2k+1] = -A_{i,j,k-0.5}K^{\eta+1}_{FZ,i,j,k-0.5}/L_{i,j,k-1} \tag{97}$$

$$\boldsymbol{B}[2k+1] = -\alpha_W/w$$

$$\boldsymbol{C}[2k+1] =$$
$$\frac{C_{WF}}{\Delta t}V_{i,j,k} + A_{i-0.5,j,k}K^{\eta+1}_{FX,i-0.5,j,k}/L_{i-1,j,k} + A_{i+0.5,j,k}K^{\eta+1}_{FX,i+0.5,j,k}/L_{i+1,j,k} +$$
$$A_{i,j-0.5,k}K^{\eta+1}_{FY,i,j-0.5,k}/L_{i,j-1,k} + A_{i,j+0.5,k}K^{\eta+1}_{FY,i,j+0.5,k}/L_{i,j+1,k} +$$
$$A_{i,j,k-0.5}K^{\eta+1}_{FZ,i,j,k-0.5}/L_{i,j,k-1} + A_{i,j,k+0.5}K^{\eta+1}_{FX,i,j,k+0.5}/L_{i,j,k+1} + \alpha_W/w$$

$$\boldsymbol{D}[2k+1] = 0$$

$$\boldsymbol{E}[2k+1] = -A_{i,j,k+0.5}K^{\eta+1}_{FZ,i,j,k+0.5}/L_{i,j,k+1}$$

$$\boldsymbol{F}[2k+1] = C_{WF}\frac{H^{\eta}_{F,i,j,k}}{\Delta t}V_{i,j,k} + A_{i-0.5,j,k}K^{\eta+1}_{FX,i-0.5,j,k}H^{\eta+1}_{F,i-1,j,k}/L_{i-1,j,k} +$$
$$A_{i+0.5,j,k}K^{\eta+1}_{FX,i+0.5,j,k}H^{\eta+1}_{F,i+1,j,k}/L_{i+1,j,k} + A_{i,j-0.5,k}K^{\eta+1}_{FY,i,j-0.5,k}H^{\eta+1}_{F,i,j-1,k}/L_{i,j-1,k} +$$
$$A_{i,j+0.5,k}K^{\eta+1}_{FY,i,j+0.5,k}H^{\eta+1}_{F,i,j+1,k}/L_{i,j+1,k}$$

Matrix system multipliers:

$$\boldsymbol{A}[2k] = -A_{i,j,k-0.5}K^{\eta+1}_{MZ,i,j,k-0.5}/L_{i,j,k-1} \tag{98}$$

$$\boldsymbol{B}[2k] = 0$$

$$\boldsymbol{C}[2k] =$$
$$\frac{C_{WM}}{\Delta t}V_{i,j,k} + A_{i-0.5,j,k}K^{\eta+1}_{MX,i-0.5,j,k}/L_{i-1,j,k} + A_{i+0.5,j,k}K^{\eta+1}_{MX,i+0.5,j,k}/L_{i+1,j,k} +$$
$$A_{i,j-0.5,k}K^{\eta+1}_{MY,i,j-0.5,k}/L_{i,j-1,k} + A_{i,j+0.5,k}K^{\eta+1}_{MY,i,j+0.5,k}/L_{i,j+1,k} +$$
$$A_{i,j,k-0.5}K^{\eta+1}_{MZ,i,j,k-0.5}/L_{i,j,k-1} + A_{i,j,k+0.5}K^{\eta+1}_{MX,i,j,k+0.5}/L_{i,j,k+1} + \alpha_W/(1-w)$$

$$\boldsymbol{D}[2k] = -\alpha_W/(1-w)$$

$$\boldsymbol{E}[2k] = -A_{i,j,k+0.5}K^{\eta+1}_{MZ,i,j,k+0.5}/L_{i,j,k+1}$$

$$\boldsymbol{F}[2k] = C_{WM}\frac{H^{\eta}_{M,i,j,k}}{\Delta t}V_{i,j,k} + A_{i-0.5,j,k}K^{\eta+1}_{MX,i-0.5,j,k}H^{\eta+1}_{M,i-1,j,k}/L_{i-1,j,k} +$$
$$A_{i+0.5,j,k}K^{\eta+1}_{MX,i+0.5,j,k}H^{\eta+1}_{M,i+1,j,k}/L_{i+1,j,k} + A_{i,j-0.5,k}K^{\eta+1}_{MY,i,j-0.5,k}H^{\eta+1}_{M,i,j-1,k}/L_{i,j-1,k} +$$
$$A_{i,j+0.5,k}K^{\eta+1}_{MY,i,j+0.5,k}H^{\eta+1}_{M,i,j+1,k}/L_{i,j+1,k}$$

Appendix B TDMA multipliers for subsurface transport

Macropore system multipliers:

$$\boldsymbol{A}[2k] = \tag{99}$$
$$-A_{i,j,k-0.5}\theta^{\eta+1}_{F,i,j,k-0.5}D^{\eta+1}_{FZZ,i,j,k-0.5}/L_{i,j,k-1} - \left(1-\zeta_{F,i,j,k-0.5}\right)A_{i,j,k-0.5}v^{\eta+1}_{FZ,i,j,k-0.5}$$

$$\boldsymbol{B}[2k]$$
$$= \frac{V_{i,j,k}}{\Delta t} + A_{i-0.5,j,k}\theta^{\eta+1}_{F,i-0.5,j,k}D^{\eta+1}_{FXX,i-0.5,j,k}/L_{i-1,j,k}$$
$$+ A_{i+0.5,j,k}\theta^{\eta+1}_{F,i+0.5,j,k}D^{\eta+1}_{FXX,i+0.5,j,k}/L_{i+1,j,k}$$
$$+ A_{i,j-0.5,k}\theta^{\eta+1}_{F,i,j-0.5,k}D^{\eta+1}_{FYY,i,j-0.5,k}/L_{i,j-1,k}$$
$$+ A_{i,j+0.5,k}\theta^{\eta+1}_{F,i,j+0.5,k}D^{\eta+1}_{FYY,i,j+0.5,k}/L_{i,j+1,k} + A_{i,j,k-0.5}\theta^{\eta+1}_{F,i,j,k-0.5}D^{\eta+1}_{FZZ,i,j,k-0.5}/L_{i,j,k-1}$$
$$+ A_{i,j,k+0.5}\theta^{\eta+1}_{F,i,j,k+0.5}D^{\eta+1}_{FZZ,i,j,k+0.5}/L_{i,j,k-1} - \zeta_{F,i+0.5,j,k}A_{i+0.5,j,k}v^{\eta+1}_{FX,i+0.5,j,k}$$
$$- \zeta_{F,i-0.5,j,k}A_{i-0.5,j,k}v^{\eta+1}_{FX,i-0.5,j,k} - \zeta_{F,i,j+0.5,k}A_{i,j+0.5,k}v^{\eta+1}_{FY,i,j+0.5,k}$$
$$- \zeta_{F,i,j-0.5,k}A_{i,j-0.5,k}v^{\eta+1}_{FY,i,j-0.5,k} - \zeta_{F,i,j,k+0.5}A_{i,j,k+0.5}v^{\eta+1}_{FZ,i,j,k+0.5}$$
$$- \zeta_{F,i,j,k-0.5}A_{i,j,k-0.5}v^{\eta+1}_{FZ,i,j,k-0.5}$$

$$\boldsymbol{C}[2k] =$$
$$-A_{i,j,k+0.5}\theta^{\eta+1}_{F,i,j,k+0.5}D^{\eta+1}_{FZZ,i,j,k+0.5}/L_{i,j,k+1} - \left(1-\zeta_{F,i,j,k+0.5}\right)A_{i,j,k+0.5}v^{\eta+1}_{FZ,i,j,k+0.5}$$

$$\boldsymbol{D}[2k] = \frac{c^{\eta}_{F,i,j,k}}{\Delta t}V_{i,j,k} + A_{i-0.5,j,k}\theta^{\eta+1}_{F,i-0.5,j,k}D^{\eta+1}_{FXX,i-0.5,j,k}c^{\eta+1}_{F,i-1,j,k}/L_{i-1,j,k} +$$
$$A_{i+0.5,j,k}\theta^{\eta+1}_{F,i+0.5,j,k}D^{\eta+1}_{FXX,i+0.5,j,k}c^{\eta+1}_{F,i+1,j,k}/L_{i+1,j,k} +$$
$$A_{i,j-0.5,k}\theta^{\eta+1}_{F,i,j-0.5,k}D^{\eta+1}_{FYY,i,j-0.5,k}c^{\eta+1}_{F,i,j-1,k}/L_{i,j-1,k} +$$
$$A_{i,j+0.5,k}\theta^{\eta+1}_{F,i,j+0.5,k}D^{\eta+1}_{FYY,i,j+0.5,k}c^{\eta+1}_{F,i,j+1,k}/L_{i,j+1,k} +$$
$$\left(1-\zeta_{F,i+0.5,j,k}\right)A_{i+0.5,j,k}v^{\eta+1}_{FX,i+0.5,j,k}c^{\eta+1}_{F,i+1,j,k} +$$
$$\left(1-\zeta_{F,i-0.5,j,k}\right)A_{i-0.5,j,k}v^{\eta+1}_{FX,i-0.5,j,k}c^{\eta+1}_{F,i-1,j,k} +$$
$$\left(1-\zeta_{F,i,j+0.5,k}\right)A_{i,j+0.5,k}v^{\eta+1}_{FY,i,j+0.5,k}c^{\eta+1}_{F,i,j+1,k} +$$
$$\left(1-\zeta_{F,i,j-0.5,k}\right)A_{i,j-0.5,k}v^{\eta+1}_{FY,i,j-0.5,k}c^{\eta+1}_{F,i,j-1,k}$$

Appendix C Theoretical test case images

Water depths and flow velocities at the theoretical test plot at 205 h during a rainstorm event are presented in Fig. 82a. Precipitation sum immediately before the event was 54 mm. The highest flow velocity value at the time was 0.022 m s^{-1} and the deepest flow depth value was 0.0028 m. Distribution of overall net erosion after the simulation at the plot is presented in Fig. 82b. The maximum net erosion value was 0.21 kg m^{-2}. The erosion patterns in Fig. 82b are artefacts caused by the rectangular grid cells used to represent a circular hill and are not caused by the model parameterisation. Pressure head distribution in the grid after the simulation in macropores and soil matrix is presented in Fig. 83.

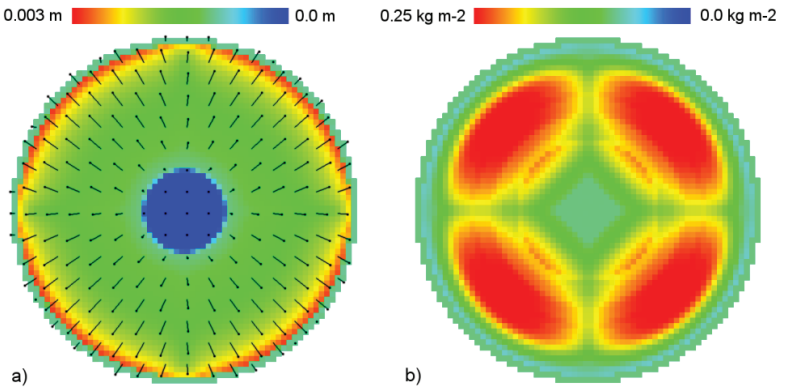

Figure 82. a) Simulated overland water depths and flow velocities at the theoretical plot during a rainstorm event. The color range from red to blue corresponds to water depths of 0.003 to 0.0 m, respectively. The vectors describe velocity and direction of the overland flow. The maximum flow velocity value was 0.022 m s^{-1}. b) Distribution of net soil erosion at the plot. The color range from red to blue corresponds to net soil erosion values of 0.025 to 0.0 kg m^{-2}, respectively.

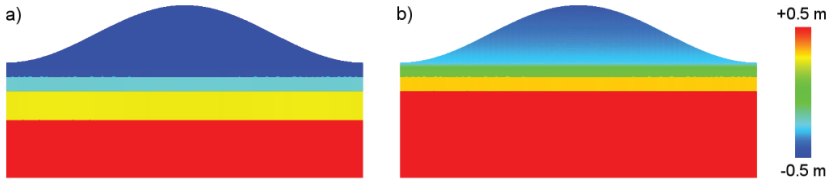

Figure 83. Pressure head distribution at the theoretical plot (*x*-*z* direction) in a) macropores and b) soil matrix. The color range from red to blue corresponds to pressure head values of +0.5 to -0.5 m, respectively. The vertical coordinates have been increased eightfold to accentuate the topography.

Appendix D Statistical model performance indicators

The Nash-Sutcliffe model efficiency coefficient E_{NS} [-] is defined as (Nash and Sutcliffe 1970):

$$E_{NS} = 1 - \frac{\sum_{t=1}^{T}(Q_O^t - Q_S^t)^2}{\sum_{t=1}^{T}\left(Q_O^t - \overline{Q_O}\right)^2} \tag{100}$$

where Q_O [L^3 T^{-1}] is the observed discharge, Q_S [L^3 T^{-1}] is the simulated discharge, and T is the number of time steps in the test. An efficiency of one is considered as a perfect match between the observed and simulated results. An efficiency of zero indicates that the model results are as accurate as the mean of the observed data. An efficiency value below zero means that the observed mean value is a better predictor than the simulated value. Bias of the predicted and observed values is calculated as follows:

$$BIAS = \frac{1}{T}\sum_{t=1}^{T}(Q_S - Q_O) \tag{101}$$

where P [L^3 T^{-1}] is the simulated discharge and O [L^3 T^{-1}] is the observed discharge. The bias value describes the measure of systematic difference between simulation results and observations. The mean absolute error between the predicted and observed values is as follows:

$$MAE = \frac{1}{T}\sum_{t=1}^{T}|Q_S - Q_O| \tag{102}$$

The mean absolute error is the average of the absolute errors between simulated and observed discharges.

Appendix E Overland flow and erosion images

Simulated overland flow conditions immediately after rain storm events in autumn at the Sjökulla (28 Oct. in 1998 and 13 Nov. in 1996) and Hovi (10 Oct. in 1988 and 21 Oct. in 1984) fields are presented in Figs. 84 and 86. Precipitation sums before the events at the Sjökulla field were 12.1 and 13.7 mm (4 hours) in 1998 and 1996, and at the Hovi field 14.9 and 10.3 mm (one hour) in 1988 and 1984, respectively. Overland net erosion results in the fields after the simulation periods are presented in Figs. 85 and 87.

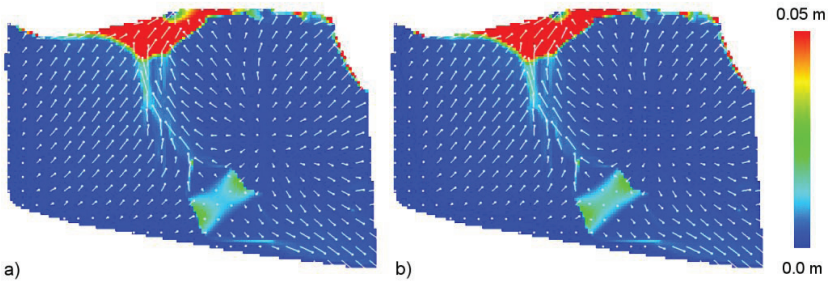

Figure 84. Simulated overland water depths and flow velocities in the Sjökulla field in a) 1998 and b) 1996 after rainstorm events. The color range from red to blue corresponds to water depths of 0.05 to 0.0 m, respectively. The vectors describe velocity and direction of the overland flow. The maximum flow velocities were 0.095 m s^{-1} and 0.102 m s^{-1} in 1998 and 1996, respectively.

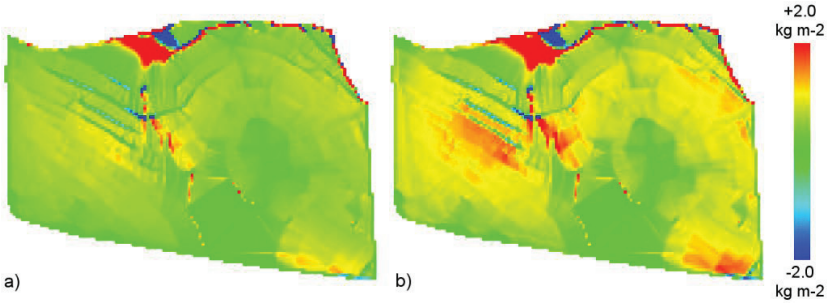

Figure 85. Simulated net erosion in the Sjökulla experimental field in a) 1998 and b) 1996. The color range from red to blue corresponds to net erosion results of +2.0 to -2.0 kg m^{-2}, respectively. Green color indicates zero net erosion.

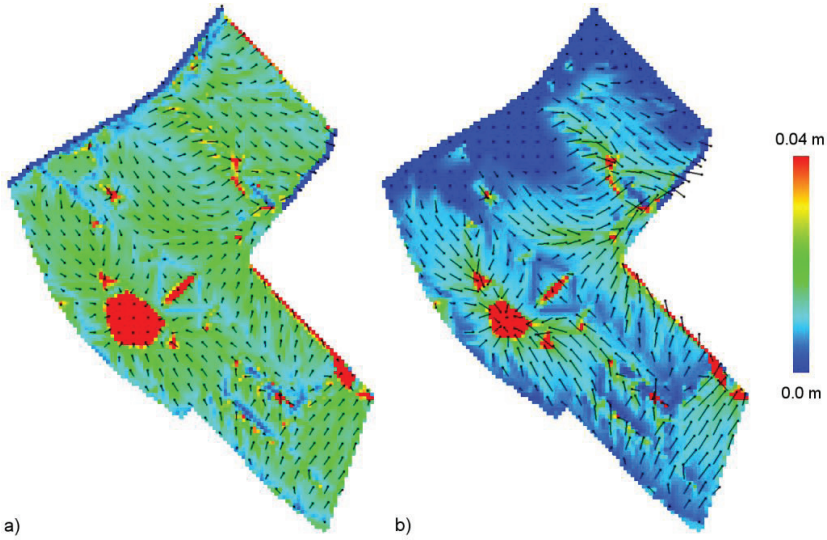

Figure 86. Simulated overland water depths and surface flow velocities in the Hovi field in a) 1988 and b) 1984 after rainstorm events. The color range from red to blue corresponds to water depths of 0.04 to 0.0 m, respectively. The vectors describe velocity and direction of the overland flow. The maximum flow velocities were 0.007 m s^{-1} and 0.022 m s^{-1} in 1988 and 1984, respectively.

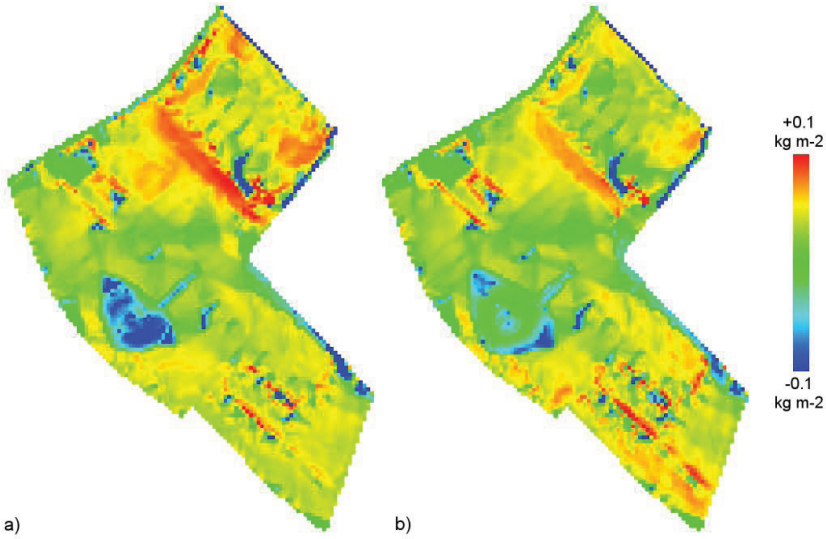

Figure 87. Simulated net erosion in the Hovi experimental field in a) 1988 and b) 1984. The color range from red to blue corresponds to net erosion results of +0.1 to -0.1 kg m^{-2}, respectively. Green indicates zero net erosion.

Water fluxes and sediment load from clayey, subsurface drained agricultural fields are potentially harmful to surface waters due to dissolved nutrients in water and adsorbed nutrients on sediment particles. Until now, only a few comprehensive tools existed that could be used to estimate water balance in a whole field section and sediment loads via surface runoff and drainflow. Simulation of water flow in clayey soils is difficult due to the preferential flow in macropores and the dynamic nature of the soil itself. A new numerical model called FLUSH is introduced in the thesis and tested with data from two clayey, subsurface drained agricultural fields in southern Finland. The most important new feature of the model is the possibility to simulate transport of suspended sediment from the field surface to subsurface drains via preferential flow pathways. Objectives of the thesis are to produce mechanistic descriptions for water flow and soil erosion phenomena and to develop efficient numerical solution algorithms.

Aalto-DD 82/2011

ISBN 978-952-60-4289-3 (pdf)
ISBN 978-952-60-4288-6
ISSN-L 1799-4934
ISSN 1799-4942 (pdf)
ISSN 1799-4934

Aalto University
School of Engineering
Department of Civil and Environmental Engineering
www.aalto.fi

BUSINESS + ECONOMY

ART + DESIGN + ARCHITECTURE

SCIENCE + TECHNOLOGY

CROSSOVER

DOCTORAL DISSERTATIONS